

**Montana Water Center  
Annual Technical Report  
FY 2017**

# Introduction

The Montana University System Water Center (MWC), located at Montana State University in Bozeman, was established by the Water Resources Research Act of 1964. In 2017, the Center's Director, Wyatt Cross, and the Assistant Director, Whitney Lonsdale, both at Montana State University, worked closely with the Associate Directors from Montana Tech of the University of Montana - Butte as well the University of Montana - Missoula, to coordinate statewide water research and information transfer activities. This is all in keeping with the Center's mission to investigate and resolve Montana's water problems by sponsoring research, fostering education of future water professionals and providing outreach to water professionals, water users and communities.

## Research Program Introduction

In addition to the goal of investigating and providing solutions for Montana's water problems, Montana Water Center 104b grants are aimed at training the next generation of water professionals through the training, support and mentorship of undergraduate and graduate students by Montana University System faculty. Funded faculty research projects are required to directly involve students in a variety of activities aimed at building students' expertise and experience, such as: collecting field or lab data, conducting data analysis, attending conferences and other outreach events, making presentations, writing articles for peer-reviewed publications and/or other research outlets. Graduate student research is supported through small grants aimed to help students complete a particular task or stage of their research and/or allow them to share their findings through avenues such as professional conferences or meetings. The graduate student program is also focused on addressing Montana's most critical water issues. Below is a brief description of faculty and student work that took place in 2017.

Three faculty seed grant projects that were funded and initiated in 2016 were continued in 2017 and completed in early 2018: 1. Robert Payn of Montana State University received an award of \$14,961 to study "Understanding how beaver mimicry restoration influences natural water storage in Missouri River headwater streams." A report from this project is presented in this annual report.

2. Lindsey Albertson of Montana State University received an award of \$15,000 to study "Impacts of river flow and temperature on salmonfly productivity and terrestrial subsidy." A report from this project is presented in this annual report.

3. Alysia Cox of Montana Tech - University of Montana received an award of \$15,000 to study "Characterizing Microbial Activity as Related to Water Quality in the Clark Fork Headwaters: A Baseline Study." A report from this project is presented in this annual report.

In 2017, four faculty seed grant projects were begun and five graduate student fellowship projects were completed with USGS 104(b) research program funds administered by the Montana Water Center.

The faculty grants funded in 2017 are:

1. Jia Hu at Montana State University received a \$17,220 grant to study "Rocky Mountain Juniper influences on Stream Flow Dynamics." An initial report on this project is presented in this annual report.

2. Benjamin Colman of MT Tech received a \$17,213 grant to study "Effects of floating treatment wetlands on the abundance and removal of dissolved and nanoparticulate contaminants in waste water lagoons." An initial report on this project is presented in this annual report.

3. W. Payton Gardner of MT Tech \$19,247 "Exploring Hydrologic Connectivity Between Shallow and Deep Groundwater Flow Systems in Upland Catchments." An initial report on this project is presented in this annual report.

4. Laurie Yung of MT Tech \$23,334 "Improving Climate Information to Enhance the Drought Preparedness of Montana Agricultural Producers." An initial report on this project is presented in this annual report.

The student projects completed in 2017 are:

1. Emily Stoick at Montana State University received \$2000 for Student Fellowship Project: "Microbially induced metal precipitation and co precipitation in mine influenced water." A final report on this project is

## Research Program Introduction

presented in this annual report.

2. Charles Shama at Montana Tech \$2000 for Student Fellowship Project: “Estimate Mountain Front Recharge in a Basin and Range Province in Southwest Montana.” A final report on this project is presented in this annual report.
3. Christine Brissette received \$2000 at University of Montana for Student Fellowship Project: “Science to inform restoration: Effects of channel reconstruction on hydraulic exchange and baseflow generation.” A final report on this project is presented in this annual report.
4. Jonathon Byers at University of Montana received \$2000 for Student Fellowship Project: “Remote Sensing of Snowpack in the Bitterroot Mountains of Montana Using Unmanned Aircraft Systems (UAS).” A final report on this project is presented in this annual report.
5. Caelan Simeone at University of Montana received \$2000 for Student Fellowship Project: “Leaf Water Potential as an Improved Predictor of Drought Induced Conifer Stress.” A final report on this project is presented in this annual report.
6. Robin Welling at University of Montana received \$769 for Student Fellowship Project: “Influence of wood on sediment storage in a low order stream in the northern Rocky Mountains.” A final report on this project is presented in this annual report.

In the fall of 2017, three faculty and six graduate students were selected for 104b funding in 2018.

The funded faculty are:

1. HongYi Li will receive \$14,998 to study “Deciphering the combined effects of artificial and natural water storage structures on late-season flows.”
2. Katherine Zodrow will receive \$15,000 to study “Reducing Acid Rock Drainage Volume using Passive Solar Evaporation Islands”
3. Jeremy Crowley will receive \$14,850 to study “Identifying seasonal spatial distribution of geothermal groundwater discharge to surface water using UAV-based thermal infrared imaging, LaDuke hot springs, MT.”

The funded students are: 1. Kristen Cook will receive \$2000 for Student Fellowship Project: “Are Montana’s Aquatic Ecosystems Becoming a ‘Hot Mess’ Due to Climate Change?”

2. Miranda Margetts will receive \$2000 for Student Fellowship Project: “Assessing pharmaceuticals in Montana’s waste water and drinking water to determine exposure risk, and inform targeted environmental and public health regulatory initiatives to protect Montanan communities.”
3. Hannah Koepnick will receive \$2000 for Student Fellowship Project: “Microbial reduction of selenium at the Colstrip power plant.”
4. Emma Raeside will receive \$2000 for Student Fellowship Project: “Student Research: Understanding root-microbe interactions in the rhizosphere.”
5. Isaiah Robertson will receive \$2000 for Student Fellowship Project: “Student Research: Limitations to Photosynthesis in Silver Bow Creek.”

## Research Program Introduction

6. Kaitlin Perkins will receive \$1610 for Student Fellowship Project: “Interactive effects of metal and nutrient cycling in the Upper Clark Fork River, Montana.”

# Understanding how beaver mimicry restoration influences natural water storage in Missouri River headwater streams

## Basic Information

<b>Title:</b>	Understanding how beaver mimicry restoration influences natural water storage in Missouri River headwater streams
<b>Project Number:</b>	2016MT300B
<b>Start Date:</b>	3/1/2016
<b>End Date:</b>	2/28/2018
<b>Funding Source:</b>	104B
<b>Congressional District:</b>	1
<b>Research Category:</b>	Climate and Hydrologic Processes
<b>Focus Categories:</b>	Hydrology, Ecology, Groundwater
<b>Descriptors:</b>	None
<b>Principal Investigators:</b>	Robert A Payn

## Publications

There are no publications.

# **Understanding how beaver mimicry restoration influences natural groundwater storage in Missouri River headwater streams**

**A Final Report for the Montana Water Center's Faculty Seed Grant Program,  
The Montana Department of Natural Resources and Conservation, and  
The Nature Conservancy - Montana**

Andrew L. Bobst and Robert A. Payn

March 30, 2018

## **Background**

Beaver-mimicry restoration (BMR) seeks to simulate the effects of beaver activity on stream ecosystems, and has become a popular approach to aggrade incised streams and reconnect stream channels to riparian systems (Pollock et al., 2015). Proponents of BMR suggest that it will improve stream and riparian habitat, improve water quality, reduce stream temperatures in the summer, increase water storage in ponds, wetlands and shallow alluvial aquifers, and increase late-summer stream flows. The ecological benefits of BMR have been well documented, and research has shown that increased overland flow and reactivation of secondary channels are often effective at increasing groundwater recharge. However, the effects of BMR on seasonal dynamics of natural water storage in shallow aquifers have yet to be tested directly, and the specific hydrologic mechanisms that would promote higher and cooler late-summer flows due to aquifer storage remain poorly understood.

To increase groundwater discharge to the stream in the late-summer due to increased water storage in the shallow aquifer, recharge of the connected aquifer must increase during high flow conditions. Then, a meaningful fraction of that water must be stored for months before discharging back to the stream. Simple conservation of mass dictates that any increase in recharge must be offset by an increase in water leaving the aquifer over the long term (Theis, 1940); however, this steady-state perspective tells us nothing about when or where the discharge will occur. In addition, components of the water balance other than recharge from and discharge to the stream must be considered to understand if stored water is actually returned to the stream. The site-specific hydrogeologic setting will determine how BMR will affect the components of the dynamic groundwater budget.

Lower late-summer stream temperatures could be achieved in two ways. First, increases in relatively cool late summer groundwater discharge would aid in cooling the stream. Second, an increase in vegetation (e.g. willow) could result in cooler stream temperatures by reducing inputs of solar (shortwave) radiation. Alternatively, BMR could increase stream temperatures if pools behind the structures are not shaded.

In order to assess the effects of BMR, we have been monitoring hydrologic characteristics of BMR restoration sites on Alkali Creek and Long Creek (fig. 1). Beaver mimicry structures (BMSs) were installed in the late-summer and fall of 2016. Monitoring began at Alkali Creek in the fall of 2015 and at Long Creek in the spring of 2016. Both sites include stream reaches with treatment, control, and reference conditions, allowing for before-after and control-treatment comparisons at each site. We plan to continue to monitor at these sites through November 2018. At each site, we are monitoring water table elevations, groundwater temperatures, surface-water stage, stream discharge, and stream temperature. The response of vegetation to the treatments is also being monitored through a combination of vegetation transects (TNC) and remote sensing (NDVI).

The Alkali Creek site has a drainage area of 9.5 km<sup>2</sup> above the treatment area, while the Long Creek site has a drainage area of 107.5 km<sup>2</sup>. As a result, Alkali Creek is a smaller stream, having a late summer low flow of about 10 Ls<sup>-1</sup> while Long Creek has a late summer flow of about 40 Ls<sup>-1</sup>. Since Alkali Creek was more deeply incised, the structures at Alkali Creek raised stream stages by up to 1 m, while at Long Creek the maximum stage increase was about 30 cm. At Alkali Creek, the density of BMSs was 6 structures installed over 774 m of stream (1 per 129 m), which about twice the density at Long Creek where the most dense treatment area had 6 structures installed over 1,544 m of stream (1 per 257 m). Also, while Alkali Creek will receive no additional treatment in 2018, additional modifications at Long Creek will be made to inundate more of the flood plain and to fill surface-water storage during high flows.

Generic groundwater flow models were developed to aid in understanding the fundamentals of the potential effects of BMR on seasonal groundwater storage. These models were developed to operate at the same scale as our study sites, but from a simple conceptual perspective to address a broader range of BMR goals and allow for testing the effects of different hydrologic settings on simplified BMR installation scenarios.

This report briefly summarizes the activities conducted for this project in 2017. This work was funded in part by the second year of support from a Montana Water Center Faculty Seed grant awarded to PI Robert Payn in April of 2016. Support for this project was also provided by the Nature Conservancy and the Montana Department of Natural Resources Conservation. Graduate student Andrew Bobst had primary responsibility for coordinating or executing these activities, as well as compiling this report.

### **Monitoring Activities - April 2017 to date**

At Alkali Creek we monitored 59 piezometers, 5 surface-water sites, 10 stream temperature stations, and 3 groundwater recharge stations (fig. 2). Groundwater recharge stations were vertical arrays of temperature and head measuring instruments collecting time series data. Data were also collected using fixed-wing unmanned aerial vehicles (UAVs) in mid-August. The UAV data included visible, near-IR, and thermal-IR images. Digital elevation models (DEMs) of the top of vegetation were developed from the RGB images using photogrammetry.

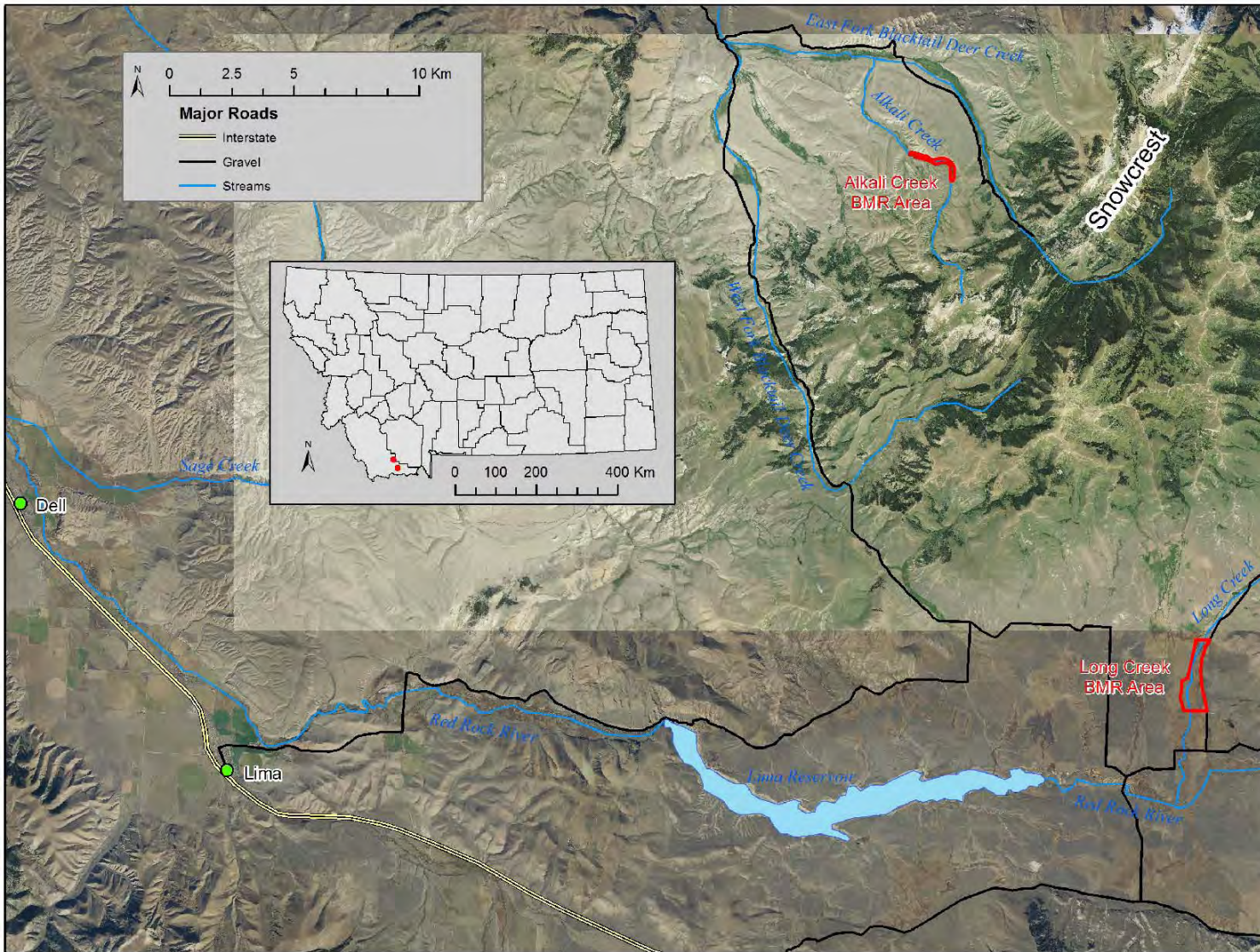


**Figure 1.** TNC installed BMR structures on Long Creek and Alkali Creek in the fall of 2016. These sites are located in Southwest Montana (USA), in the headwaters of the Beaverhead River.

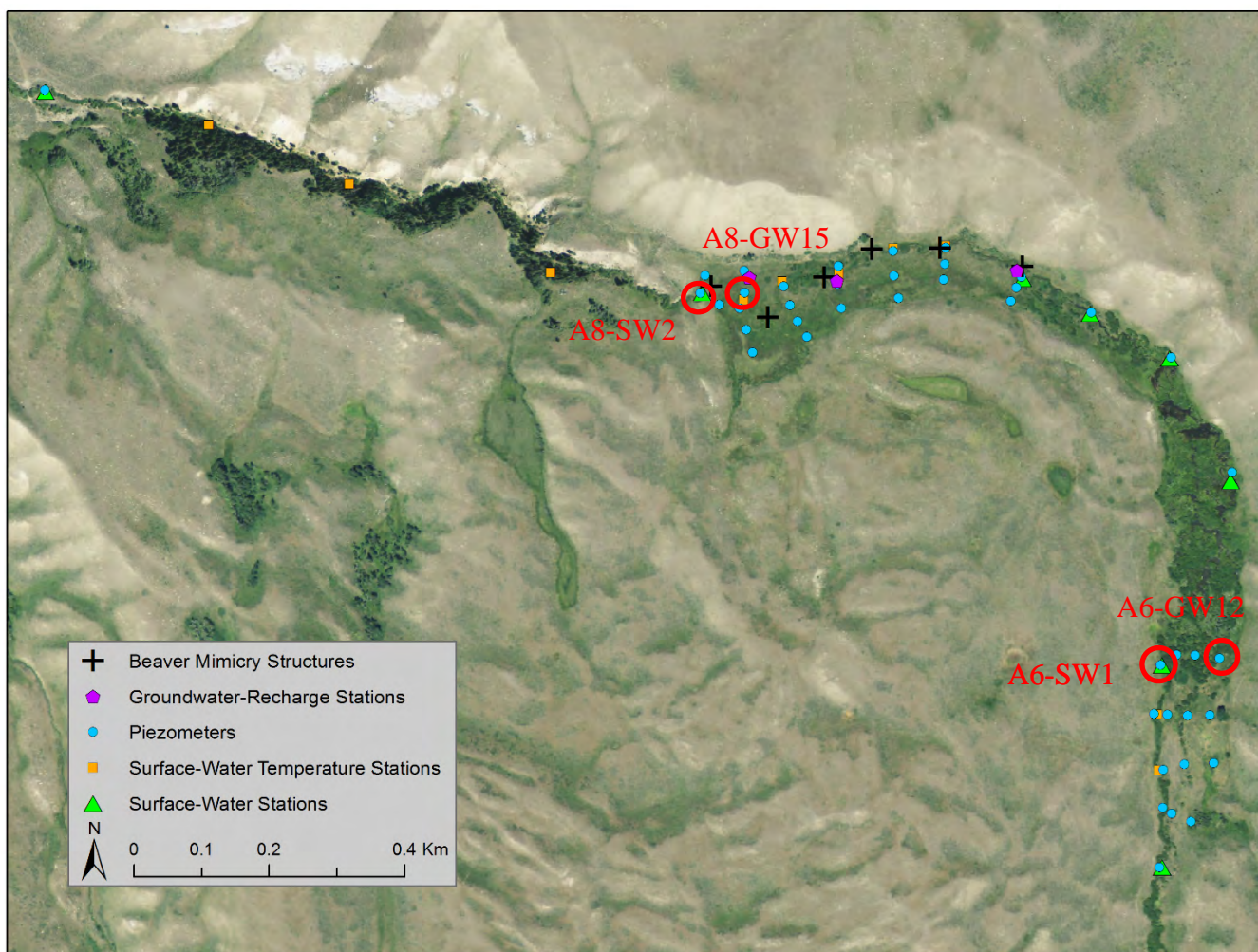


**Figure 2.** A total of 40 piezometers and 5 surface-water stations were installed at Alkali Creek in the late-summer of 2015. An additional 16 piezometers, 3 staff gauges, and 10 surface-water temperature sites were installed in the spring and early summer of 2016. TNC installed BMR structures on Alkali Creek mid-October 2016. Groundwater-recharge stations were installed in November 2016. Monitoring will occur twice per month from May to November through the fall of 2018.

At Long Creek (fig. 3) we monitored 42 piezometers and wells, 5 surface-water stations, 4 stream temperature stations, and 3 groundwater recharge stations. Visible, near-IR, and thermal-IR images were collected by UAV in mid-August. The RGB images were used to develop top of vegetation DEMs.

## **Summary of monitoring results**

### *Alkali Creek*

#### *Groundwater*

Water table elevations within the treatment reach at Alkali Creek increased by more than 30 cm from August 2016 to August 2017 in a contiguous area bordering the stream, and covering an area of 2.7 hectares (fig. 4). As a result, lateral groundwater gradients toward the stream became flatter while longitudinal gradients downstream of the treatment became much steeper. Hydrographs from piezometers near treated stream reaches show a noticeable increase in groundwater levels, while hydrographs from wells in the control area do not (figs. 5a and 5b). Wells in southern areas of the floodplain and further from the stream show less change in water levels before and after BMS installation (figs. 4 and 5c).

#### *Stream Flows*

Stream flows were measured at the surface-water monitoring stations (fig. 2). At the downstream end of the control reach (A6-SW1; figs. 2 and 6a) there was a slight decrease in the estimated mean August flow from 2016 to 2017. At the downstream end of the treatment reach (A8-SW2; figs. 2 and 6b) there was a slight increase in estimated mean August flow from 2016 to 2017. While these changes are calculable, they are smaller than the error inherent in measuring stage and flow, and fitting a rating curve.

#### *Stream Temperature*

Mean August stream temperature at the downstream end of the control reach increased by 0.3°C from 2016 to 2017, while mean August stream temperature at the downstream end of the treatment reach increased by 0.9°C (fig. 7). Therefore 0.6 C° of warming appears to be attributable to the BMR treatment. Because the pools created in the treatment reach are not shaded and the stream before treatment was highly incised, the temperature increase attributed to BMR treatment was likely due to increased insolation over increased water residence times behind the BMS. Since willow planting occurred with the treatment and groundwater levels are elevated, a long-term increase in shade from the willows may eventually mediate the short-term increase in insolation and therefore reduce the warming.

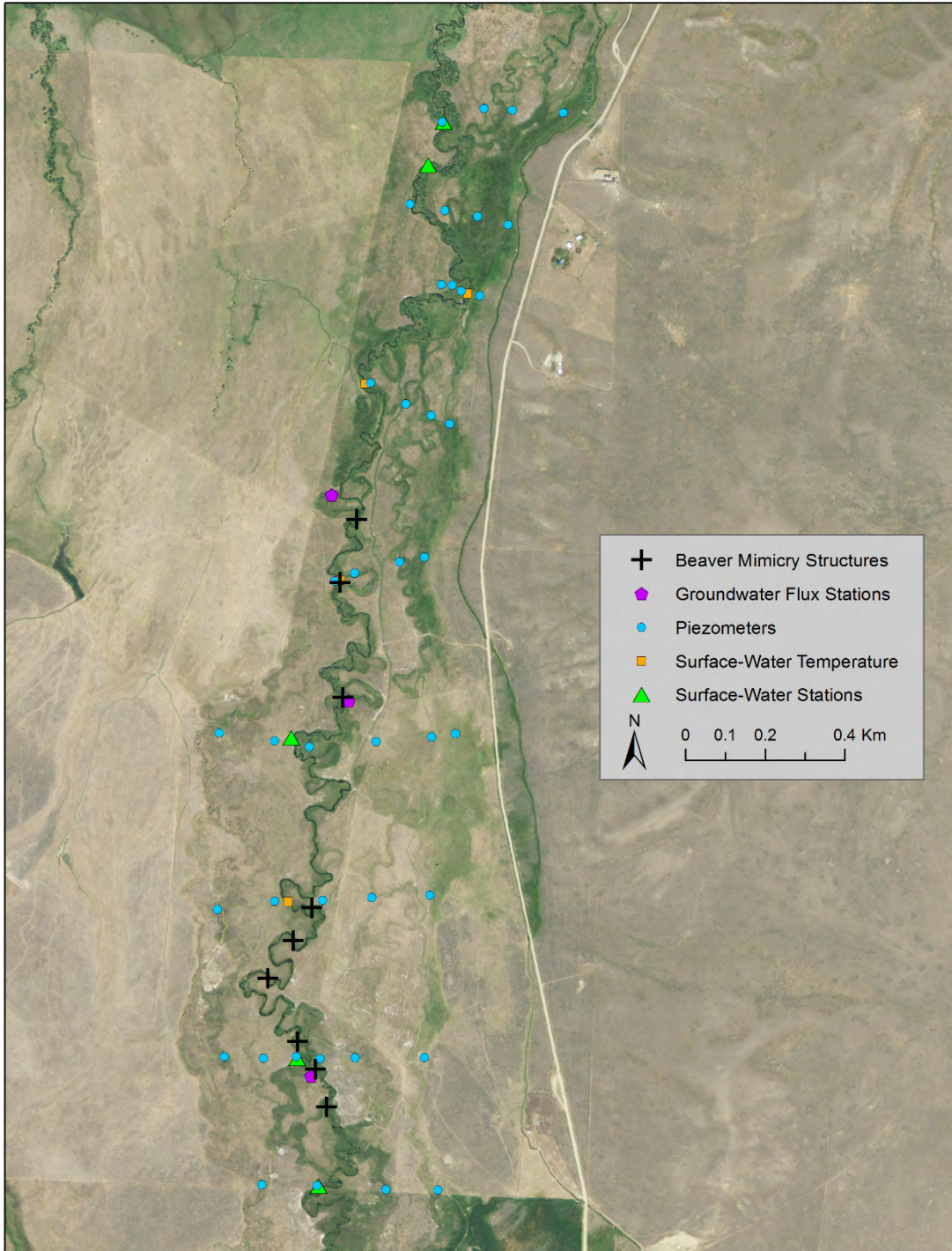


**Figure 3.** TNC has monitored 3 piezometers and 3 surface-water stations at the Long Creek site since 2012. An additional 39 piezometers, 2 surface-water monitoring stations, and 4 surface-water temperature stations were installed in the spring of 2016 (mostly in May). TNC installed BMR structures on Long Creek in late-August 2016. Groundwater-recharge stations were installed in November 2016. Monitoring will occur twice per month from April to November through the fall of 2018.

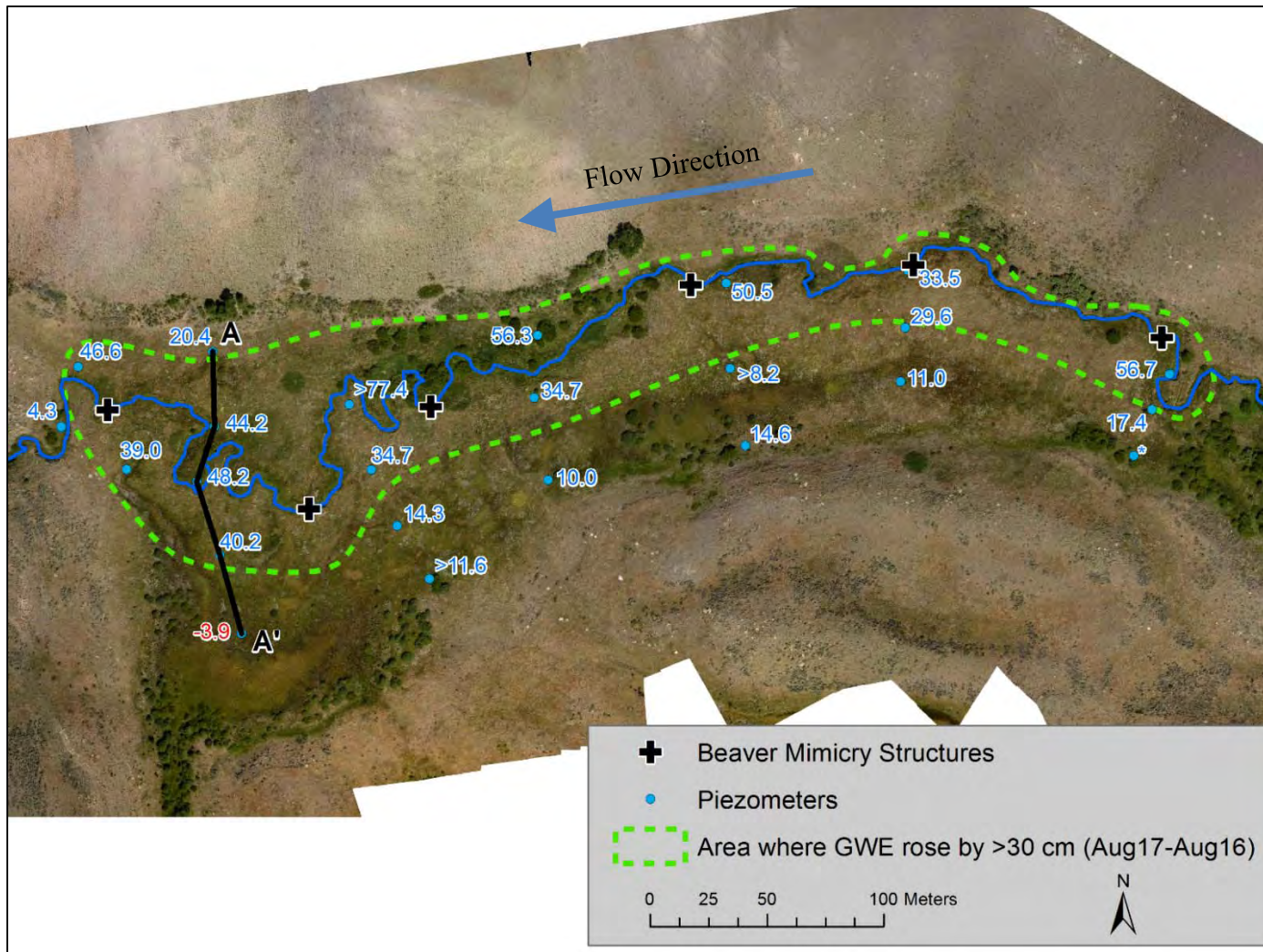


**Figure 4.** Groundwater monitoring shows that groundwater elevation (GWE) increased by 30 cm or more over 2.7 hectares adjacent to Alkali Creek. Labels show the increase in water table elevations between 2016 and 2017, in cm. Values denoted with ">" indicate that the piezometer was dry in 2016, and the piezometer labeled with "\*" indicates that the piezometer was dry in both 2016 and 2017. Cross section A-A' is shown on figure 5. Note the substantial increase in the longitudinal groundwater gradient at the downstream end of the treatment.

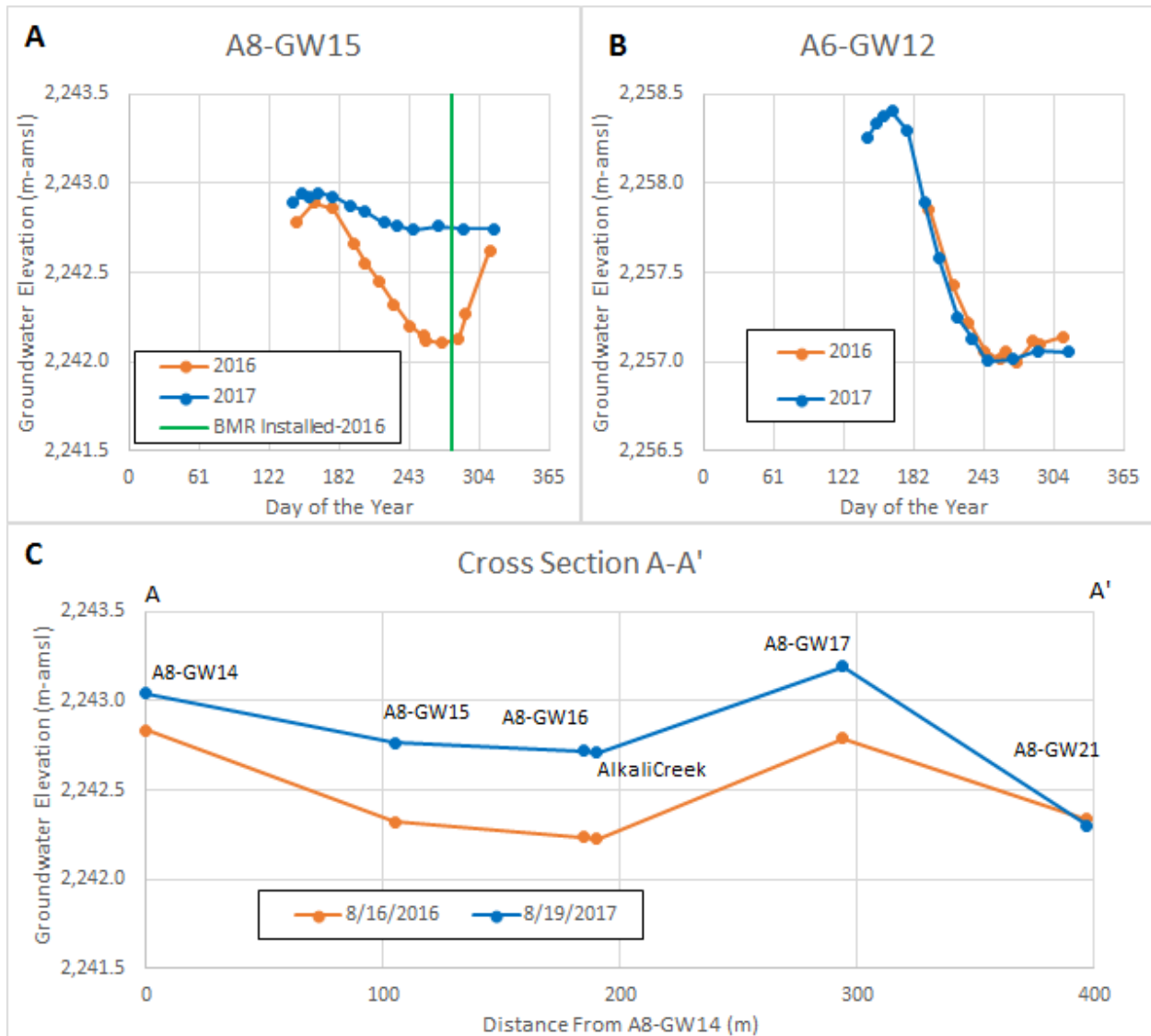


**Figure 5.** Groundwater monitoring shows a distinct increase in summer time groundwater elevations in the treated area (A) while groundwater levels in the control are unchanged (B). Along cross section A-A' (C; fig. 4) it is noticeable that the lateral gradients toward the stream decreased; however longitudinal gradients increased (fig. 4).

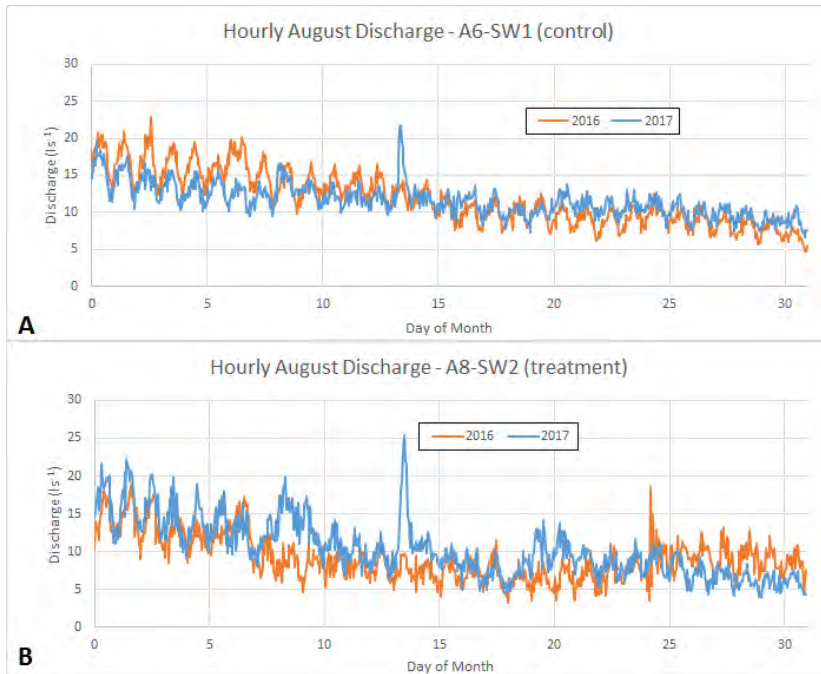


**Figure 6.** Stream discharge decreased slightly at the downstream end of the control reach (A) and increased slightly at the downstream end of the treatment reach. While these changes are calculable, they are smaller than the error inherent in measuring stage and flow, and fitting a rating curve.

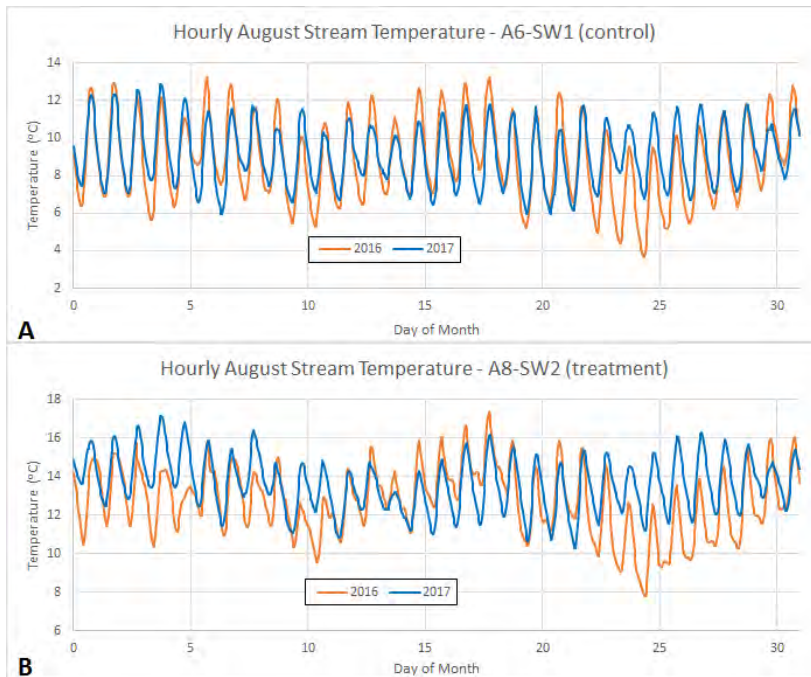


**Figure 7.** Hourly recorded stream temperatures show that the estimated mean August stream temperature in 2017 was  $0.3^{\circ}\text{C}$  warmer at the downstream end of the control reach than in 2016 (A). Estimated mean August stream temperature for the downstream end of the treatment reach was  $0.9^{\circ}\text{C}$  warmer in 2017 relative to 2016 (B).

### *UAV Data*

DEM differences suggest that vegetation was taller in 2017 than in 2016 for both the treatment and control areas (figs. 8b and 9b). The NIR images were used to calculate an index of photosynthesis (natural difference vegetation index; NDVI), and the change in NDVI shows that the vegetation in the treatment area was photosynthesizing more in 2017, while the control was unchanged (figs. 8c and 9c). Thermal imaging also suggests that the treatment and control areas were both cooler in 2017 than in 2016, but that the treatment area cooled by more. This cooling is a potential consequence of greater evapotranspiration in the treatment area. The resolution of the thermal images was not sufficient to identify any areas in the stream with increased groundwater/hyporheic inflow.

### *Long Creek*

#### *Groundwater*

BMSs and piezometers were further apart at Long Creek, and contiguous areas of increased groundwater levels could not be defined; however, observed water levels in piezometers near BMSs increased from August 2016 to August 2017 by up to 26 cm. Groundwater levels in the reference area increased by up to 90 cm from 2016 to 2017, while groundwater levels showed little change near the control reach. The increased groundwater levels in the reference area appear to be related to the addition of natural beaver dams.

#### *Stream Flows*

Stream flows were measured at the surface-water monitoring stations (fig. 3). At the upstream end of the site (L-SW7A) there was a slight increase in the estimated mean August flow from 2016 to 2017. There was also a slight increase in the estimated mean August flow at the downstream end of the site (L-SW12). While these changes are calculable, they are smaller than the error inherent in measuring stage and flow, and fitting a rating curve.

#### *Stream Temperature*

Mean August stream temperature at the upstream end of the site (L-SW7A) increased by 0.5°C from 2016 to 2017, while mean August stream temperature at the downstream end of the site (L-SW12) increased by 0.3°C. Therefore the estimated warming across the site was 0.2°C less following the treatment. While this change is slight, it is notable that the sign of the change is opposite from Alkali Creek, where the treatment reach warmed by 0.6 °C more than the control. This difference may be due to Long Creek being less incised before the treatment, and existing riparian vegetation being more mature than at Alkali Creek. As such, the change in insolation at Long Creek was likely less pronounced than at Alkali Creek. It appears that the balance between cooling due to increased hyporheic exchange and increased late-summer groundwater inflow, and warming due to increased insolation, favored warming at Alkali Creek and cooling at Long Creek.

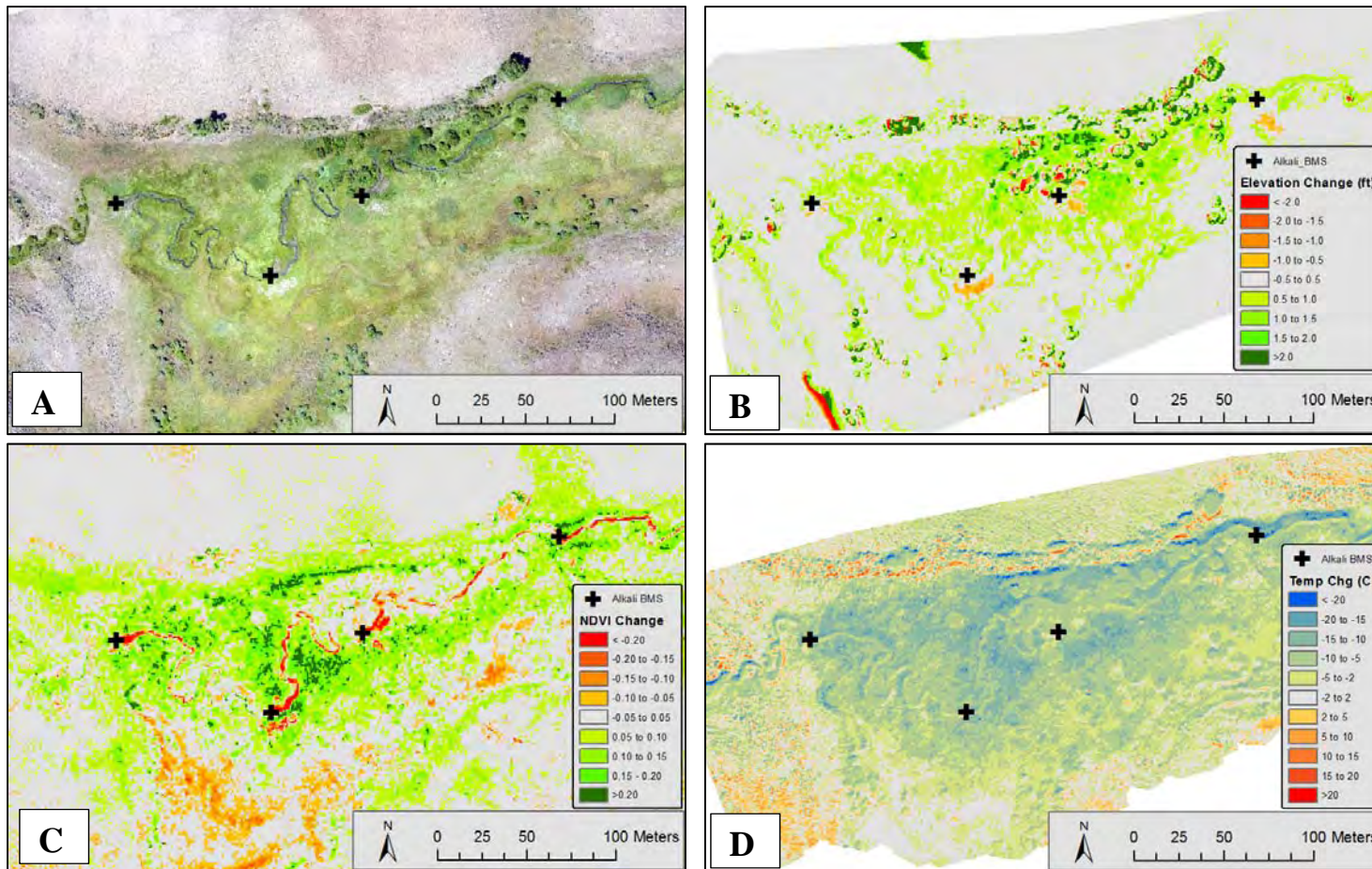


**Figure 8.** UAVs were used at Alkali Creek in August of 2016 and 2017 to evaluate changes in vegetation characteristics and temperature before and after beaver mimicry structures (BMSs) were installed. Visible imagery (RGB; A) shows the locations of BMSs, and the disturbance due to their construction. These RGB images were used to develop DEMs of the top of vegetation for each year. Comparison of the DEMs (B) shows that vegetation is taller near the BMSs, except for the disturbed areas, where it is shorter. NIR images were used to calculate NDVI values for 2016 and 2017, and comparing them shows that vegetation near the BMSs is more green following the treatment, except for in the disturbed areas. Thermal imagery also shows that the area near the BMSs is cooler after treatment (D); an indication of greater plant transpiration.

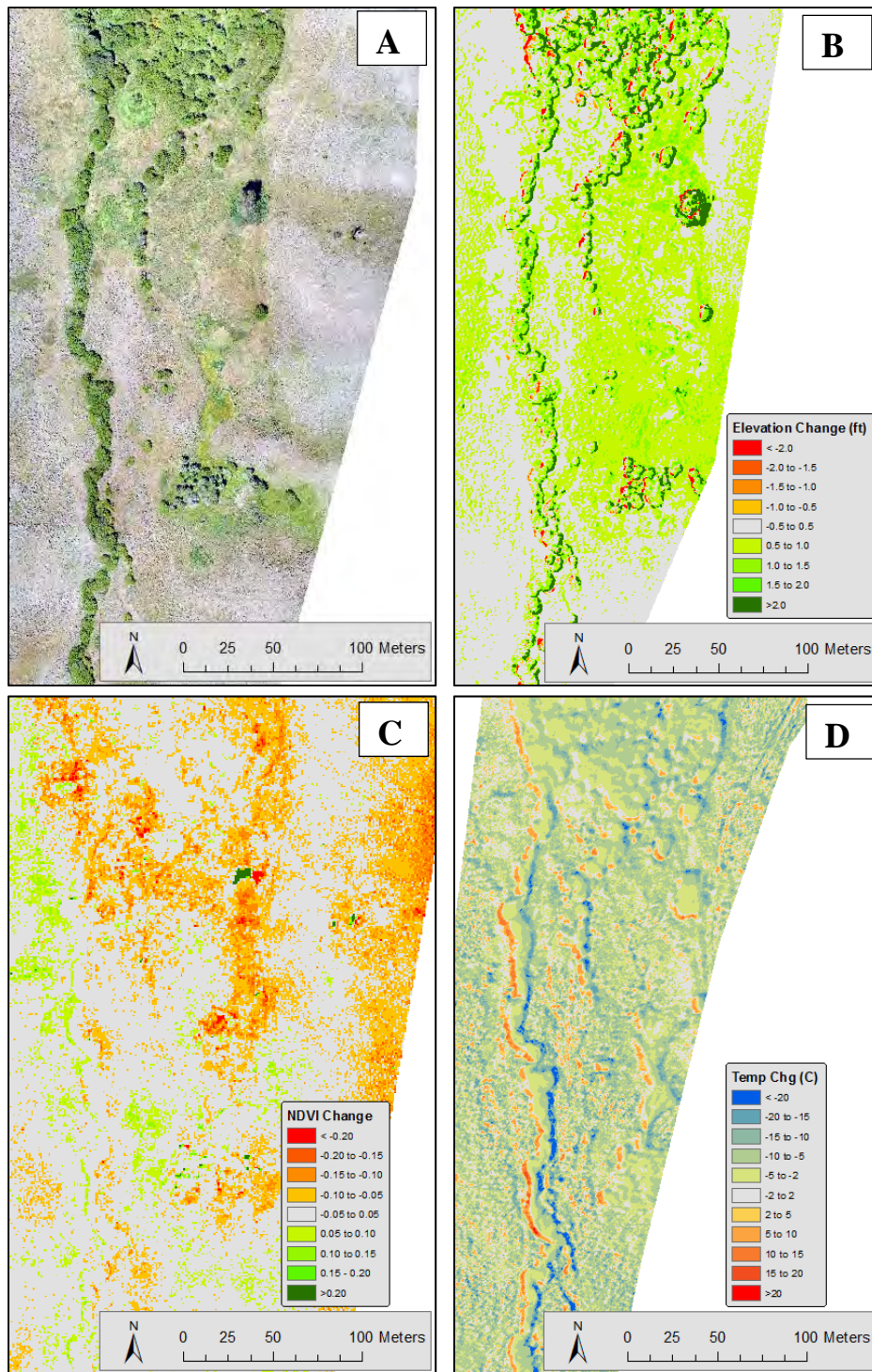


**Figure 9.** The control area at Alkali Creek was imaged using UAVs for comparison to the treatment area (fig. 8). The 2017 RGB image (A) does not appear to be any greener than the 2016 image. Similar to the treatment area the top of vegetation is higher in 2017 than it was in 2016 (B); however NDVI (C) shows that the vegetation is less green, and temperature show that while 2017 was cooler than 2016, it is not as much cooler as in the treatment area (D). Field observations indicate that the taller vegetation in the treatment is thistle and upland grasses, while in the treatment area it is wetland grasses. The overall cooler temperatures reflect that in 2017 imagery was obtained on a cooler day.

### *UAV Data*

NDVI from UAV imagery suggested that riparian photosynthesis in the treatment and reference areas was higher in 2017 after BMS installation, while riparian photosynthesis in the control reach was unchanged. The change in NDVI appeared to be associated with areas of increased groundwater levels due to BMS or natural beaver activity. Thermal imaging also showed that the treatment area and portions of the reference area were cooler in 2017 than in 2016, suggesting greater heat loss to evapotranspiration.

### **Modeling Activities - April 2017 to date**

Groundwater modeling was used to aid in understanding the mechanisms of water storage expected from different types of BMR in different hydrogeologic settings. Since the storage and release of water is critical to this analysis, models that allow for time-dependent water storage were used (“transient” or “dynamic storage” models). Models were used to simulate a 5 year period using a snowmelt driven seasonal hydrograph, and were developed for gaining (G), losing (L), and strongly losing (SL) streams by adjusting the elevation of groundwater drains. For each of these systems, 5 scenarios were modeled (table 1): 1) baseline (B), 2) in-stream structure (S), 3) in-stream structure with a near channel activated (NC), 4) in-stream structure with a far channel activated (FC), and 5) in-stream structure with floodplain inundation (several channels activated, I). Side channels received water only during high spring flows for scenarios 3, 4, and 5.

Differences between each treatment scenario (S, NC, FC, and I) from the baseline scenario (B) within the same hydrogeologic setting (G, L, or SL) were quantified in mid-August of the last modeled year (year 5). We used the mean change in groundwater elevations, and the change in net flux to streams as indicators of the potential for seasonally dynamic storage in the alluvial aquifer. Changes in groundwater flow out of the model domain through downvalley subsurface flow were also quantified during the last modeled year (year 5).

Sensitivity analyses were used to evaluate how late-summer net gain in stream flow within the model domain respond to variation in horizontal hydraulic conductivity ( $K_h$ , ease of water movement), specific yield ( $S_y$ , the available storage), streambed conductance, drain conductance, maximum evapotranspiration rate, and evapotranspiration extinction depth (table 2). The B (as a control) and FC (as a treatment) scenarios were used to test the sensitivity of model results to each parameter. Differences between the control and treatment in net flux to streams in mid-August of the 5<sup>th</sup> year were calculated to assess the effects the FC restoration strategies on late summer flows using different model parameters.

Table 1. Models developed to test the effects of different treatments in different settings

Setting	Baseline	In-Stream Structure	In-Stream Structure + Near Channel	In-Stream Structure + Far Channel	In-Stream Structure + Inundation
Gaining	Model G-B	Model G-S	Model G-NC	Model G-FC	Model G-I
Losing	Model L-B	Model L-S	Model L-NC	Model L-FC	Model L-I
Strongly Losing	Model SL-B	Model SL-S	Model SL-NC	Model SL-FC	Model SL-I

Table 2. Sensitivity Analysis Summary – Parameters and values tested

Parameter	Values Tested				
$K_h$ ( $\text{md}^{-1}$ )	0.025	0.25	2.5	<b>25*</b>	250
$S_y$	0.02	0.10	<b>0.20*</b>	0.30	0.40
Stream Conductance [ $(\text{m}^2\text{d}^{-1})\text{m}^{-1}$ ]	0.005	0.05	<b>0.5*</b>	5	50
Drain Conductance ( $\text{m}^2\text{d}^{-1}$ )	0.1	1	<b>10*</b>	100	1000
Maximum ET Rate ( $\text{cm yr}^{-1}$ )*	<b>0*</b>	15	30	60	120
ET Extinction Depth (m)**	<b>0*</b>	1	2	3	5

For Maximum ET Rate tests an extinction depth of 2 m was used.

For Extinction Depth tests a maximum ET rate of 60  $\text{cm yr}^{-1}$  was used.

**Bold\*** values used for model scenarios (table 1).

### Summary of modeling results

The model scenarios showed that for all treatment scenarios and in all hydrogeologic settings, BMR is expected to cause an increase in groundwater levels in the treatment area and increase the amount of water leaving the model domain as groundwater (table 3). For the gaining and losing scenarios BMR resulted in a higher mid-August net surface water gain through the treatment area relative to baseline scenario; however, in a strongly losing stream BMR causes a decrease in the mid-August net surface water gain. The simulated differences in groundwater levels between restoration and baselines scenarios were large enough to be measurable in the field (7.5 to 9.5 cm), but the subsequent influence on late-summer flow predicted by the model (max = 6.8  $\text{m}^3/\text{d}$ ; 0.08 L/s) would likely be too small to measure considering the uncertainties in differential stream gauging. Note that these simulations were only designed to test the effects of increased transient groundwater storage, so any changes caused by water stored on the surface (e.g. ponds connected by groundwater) would be in addition to those calculated by these models.

Table 3. Scenario Results – Change from Baseline – year 5.

Indicator	Setting	In-Stream Structure	In-Stream Structure + near Channel	In-Stream Structure + far Channel	In-Stream Structure + inundation
Change in Mid-August Net Flux to Streams ( $\text{m}^3/\text{d}$ )	Gaining	5.5	5.7	5.8	6.4
	Losing	5.9	6.0	6.2	6.8
	Strongly Losing	-1.6	-2.6	-1.2	-0.8
Change in Mean Mid-August Groundwater Elevation (cm)	Gaining	7.6	8.0	7.7	7.9
	Losing	7.5	7.8	7.6	7.8
	Strongly Losing	9.0	9.3	9.2	9.5
Change in Average Annual Groundwater Outflow ( $\text{m}^3/\text{d}$ )	Gaining	3.9	3.8	3.7	3.9
	Losing	3.7	3.8	3.8	3.8
	Strongly Losing	10.2	10.0	10.2	10.3

The sensitivity analysis suggested that properties of the substrate and evapotranspirative forcing influence the effects of BMR on seasonal storage (table 4).

- Lower to moderate values of  $K_h$ , resulted in a lower net stream gains, and high values of  $K_h$  resulted in negative net stream gains since groundwater was more likely to move down-valley through the subsurface than to the stream.
- Varying  $S_y$  values showed that higher available storage in subsurface pore space caused higher net stream gains in the late summer.
- Streambed conductance values lower than the 0.5 (m<sup>2</sup>/d)/m resulted in less net stream gain late in the summer because less stream water recharges the aquifer during high flows. Interestingly, when stream conductance values are high there is also a lower net stream gain late in the summer, due to greater hydrologic losses from the channel during low flow conditions.
- Lower drain conductance (potentially representing flow towards a constriction in the alluvium) results in higher net stream gains, because the water flows to the stream rather than the drain. Conversely, when drain conductance is high (potentially representing flow into expanding alluvium) water preferentially flows to the drains rather than the stream.
- Evapotranspiration (ET) directly competes with flow to the stream and the drains. Higher maximum ET rates (greater phreatophyte density or longer growing seasons) resulted in lower net stream gains. Maximum ET rates greater than 30 cm/yr caused a negative net stream gain. A dense willow stand in Montana is expected to have a maximum ET rate of about 60 cm/yr (Hackett et al., 1964).
- ET extinction depths (rooting depths) more than 2 m caused negative net stream gains due to the direct competition between plant use and groundwater flow to the stream. An extinction depth of 1 m caused ET to have little effect on the model since groundwater in most parts of the model was deeper than 1 m.

**Table 4.** Sensitivity Analysis – Losing Stream - Difference between treatment and control on Mid-August Net Stream Gain (m<sup>3</sup>/d) using different model parameter values.

$K_h$ (m/d)	Parameter Value	0.025	0.25	2.5	<b>25*</b>	250
	Result	2.6	6.8	8.8	6.2	-20.7
$S_y$	Parameter Value	0.02	0.10	<b>0.20*</b>	0.30	0.40
	Result	-3.7	0.9	6.2	9.1	10.7
Stream Conductance [(m <sup>2</sup> /d)/m]	Parameter Value	0.005	0.05	<b>0.5*</b>	5	50
	Result	-0.3	-1.6	6.2	1.6	-0.8
Drain Conductance (m <sup>2</sup> /d)	Parameter Value	0.1	1	<b>10*</b>	100	1000
	Result	10.3	8.9	6.2	5.1	5.1
Maximum ET Rate (cm/yr)	Parameter Value	<b>0*</b>	15	30	60	120
	Result	6.2	2.4	-1.1	-10.1	-26.3
ET Extinction Depth (m)	Parameter Value	<b>0*</b>	1	2	3	5
	Result	6.2	6.2	-10.1	-14.0	-5.8

**Bold\*** values used for the model scenarios (table 3).

## **Planned continued activities after funding expiration**

We will monitor at Alkali Creek and Long Creek while roads are passable in 2018. This will include continued monitoring of the existing sites, and collection of post-treatment remote sensing data in August (funded by TNC).

At Alkali Creek, the existing structures will remain in place with no further modifications at the site.

At Long Creek, water will be applied on the east side of the creek during high flows. This will include flood irrigation, and filling surface water features (reservoirs and abandoned channels). These activities will be undertaken so that there is a single point of surface-water inflow, and a single point of surface-water outflow. We will install surface-water monitoring stations at each of these points to quantify the net amount of water stored.

The theoretical groundwater flow models will be finalized, and a manuscript prepared for publication.

## **Project benefits**

The data collected during this study is publicly available from MBMG's GWIC database at <http://mbmggwic.mtech.edu/sqlserver/v111/data/dataProject.asp?project=BMS&datatype=well&>

We anticipate developing at least three peer-reviewed publications from this work. The anticipated topics are:

- 1) *Using simplified hydrologic models to explore how different strategies for Beaver Mimicry Restoration influence dynamic groundwater storage.*

This publication would focus on the changes in dynamic groundwater storage that would be anticipated from different types of beaver mimicry restoration in different hydrogeologic settings. These effects will be modeled based on changes in groundwater recharge from surface waters, changes in groundwater discharge to surface waters, changes in groundwater elevations, changes in groundwater outflow, and changes in evapotranspiration. This analysis will include sensitivity analyses to aid in determining the site characteristics that most strongly control changes in seasonally dynamic groundwater storage.

- 2) *Changes in late-summer groundwater discharge to streams due to beaver-mimicry stream restoration*

A typical goal of BMR is to increase late-summer stream flow using water storage in the shallow aquifer. This paper would assess the potential for recharged water to return to streams at an appropriate place and time. The recharged water could be removed from the shallow aquifer by a variety of pathways (e.g. evapotranspiration or groundwater

outflow), so it is necessary to understand the potential magnitude of these alternative pathways. To assess when, where, and how much of the recharged water returns to the stream we will use observed changes in stream flow, observed changes in groundwater gradients, changes in vegetation patterns (NDVI), changes in temperature patterns (thermal imaging), and groundwater flow modeling (including sensitivity analysis). This manuscript may also include an evaluation of the changes in water storage, and late-summer stream flows caused by BMR related surface water storage.

3) *Effects of beaver mimicry stream restoration on late-summer stream temperatures at two sites in Southwest Montana*

BMR has been suggested to decrease late-summer stream temperatures; however, this has not been clearly demonstrated. Monitoring for this study shows that BMR may cause warming or cooling depending on the balance between cooling caused by increased hyporheic flow and groundwater discharge, and warming caused by changes in insolation. This paper will focus on the empirical effects of BMR on stream temperature changes over the study reaches at Alkali Creek and Long Creek, and statistical or mechanistic models of stream temperature.

## **Synthesis of Findings**

Monitoring at Alkali Creek and Long Creek and modeling of fundamental BMS installation scenarios show that BMR causes late-summer groundwater elevations to be higher in treatment areas. These increases in groundwater elevations are due to both the increase in the stage of the stream caused by the structure and the increase in recharge obtained by reactivating dry channels and inundating the floodplain. Changing groundwater elevations also causes flow paths to and from the stream to be altered. Patterns of exchange between the stream and the aquifer become more heterogeneous, potentially resulting in the creation of more diverse aquatic habitat. The increased groundwater elevations also cause the vegetation near the structures to be greener, and taller. This increase in the vigor of riparian plants likely results in greater transpiration. Modeling suggests that when moderately dense riparian vegetation becomes established, the plants may consume more water than is recharged, resulting in a slight decrease in net late-summer stream gains.

Modeling indicates that BMR can increase late-summer stream flows; however, the changes caused by a small group of structures will likely be too small to measure. Monitoring confirms this conclusion, as any changes in stream flow at Alkali Creek and Long Creek are smaller than the uncertainty in the gauging methods.

When the treatment is in a gaining or weakly losing stream, modeling indicates that BMR will be most successful at increasing seasonally dynamic groundwater storage, and therefore increasing late-summer flows. BMR in streams that are strongly losing or disconnected will result in recharge to groundwater, but the water is less likely to flow back to the stream in proximity to

the restoration. Instead the water flows down-valley out of the treatment area as groundwater, but it will eventually resurface where the alluvium is constrained or the system becomes gaining by some other mechanism. In these strongly losing settings there would be an increase in inter-annual or longer-term dynamic storage rather than seasonally dynamic storage.

For gaining and weakly losing streams, modeling indicates that the type of BMR treatment is less important than the fact that there is a treatment. While BMR treatments that inundate the most area cause the greatest increase in late-summer stream flows, the differences between these treatment types are much less than the difference between any level of treatment and the baseline (table 3).

Sensitivity analysis indicates that BMR will be most effective at increasing late-summer stream flows in gaining or weakly losing streams where the aquifer permeability is moderate ( $K_h$  0.25 to 25 m/d; silty sand to coarse sand). From a storage ( $S_y$ ) perspective, unconsolidated sediments that are silt sized or larger work well. Streambed materials should be silt to gravel sized. If the treatment occurs up gradient from an obstruction, which forces alluvial water to the stream (e.g. a bedrock notch), more of the water will flow back to the stream. If the treatment occurs in a region of expanding alluvium, which causes the stream to become more strongly losing (e.g. a tributary alluvium joining with a larger system), the water will not flow back to the stream. As noted above, high rates of ET (dense riparian plants) would result in less groundwater being discharged to surface waters.

Monitoring data shows that stream temperatures may increase or decrease following BMR implementation. It appears that this is due to the balance between heating caused by increased unshaded area, and cooling from increased hyporheic exchange and late-summer groundwater inflow. If riparian vegetation increases in response to BMR, more shade would be expected to develop in treatment areas over time, which would shift this balance towards cooling.

## References

Hackett, O.M., Stermitz, F., Boner, F.C. and Krieger, R.A., 1960, Geology and ground-water resources of the Gallatin Valley, Gallatin County, Montana: US Government Printing Office (No. 1482).

Pollock, M.M., Lewallen, G., Woodruff, K., Jordan, C.E., and Castro, J.M. (Editors), 2015, The beaver restoration guidebook, working with beaver to restore streams, wetlands and floodplains, version 1.02: United States Fish and Wildlife Service, Portland Oregon, 189 pgs.

Theis, C.V., 1940, The source of water derived from wells: essential factors controlling the response of an aquifer to development: Civil Engineer, v. 10, pgs. 277-280.

Appendix A – GWIC IDs for Monitored sites

Monitoring data is available from <http://mbmggwic.mtech.edu/>

GWIC ID numbers for Alkali Creek Monitoring Sites					
A5-SW1	285834	A7-GW1	288278	A8-SW1	286976
A5-GW1	285835	A7-SW1	288279	A8-GW1	286977
		A7-GW2	288280	A8-GW1A	287986
A6-GW1	285837	A7-SW2	288281	A8-GW2	286978
A6-GW2	285838	A7-GW3	288282	A8-GW3	286979
A6-GW2A	287997	A7-SW3	288283	A8-SWT1	287983
A6-GW3	285839			A8-GW4	286980
A6-GW3A	287996	A9-SWT1	287977	A8-GW5	286981
A6-GW4	285840	A9-SWT2	287978	A8-GW6	286982
A6-GW5	285841	A9-SWT3	287976	A8-SWT2	287982
A6-GW5A	287995	A9-GW1	285858	A8-GW22	287021
A6-GW6	285842	A9-SW1	285859	A8-GW23	287022
A6-GW6A	287994			A8-GW24	287023
A6-SWT1	287999	AF1P	290216	A8-GW7	286989
A6-GW8	285844	AF1LowT	295241	A8-SWT3	287981
A6-GW8A	287993	AF1UpT	295242	A8-GW8	286990
A6-GW9	285847	AF1SG	290217	A8-GW9	286991
A6-GW9A	287992	AF2P	290219	A8-SWT4	287980
A6-GW10	285848	AF2LowT	295244	A8-GW10	286992
A6-GW10A	287991	AF2UpT	295245	A8-GW11	286993
A6-SWT2	287998	AF2SG	290221	A8-GW12	286994
A6-GW11	285849	AF3P	290222	A8-GW13	286995
A6-GW11A	287990	AF3LowT	295246	A8-GW14	286996
A6-GW12	285850	AF3UpT	295247	A8-GW15	286997
A6-GW12A	287989	AF3SG	290223	A8-SWT5	287979
A6-GW13	285851			A8-GW16	286998
A6-GW14	285853			A8-GW17	286999
A6-GW14A	287988			A8-GW21	287020
A6-GW15	285856			A8-GW18	287000
A6-GW15A	287987			A8-GW19	287001
A6-SW1	285857			A8-GW19A	287984
				A8-GW20	287019
				A8-SW2	287024

GWIC ID numbers for Long Creek Monitoring Sites

L-GW7A	287434
L-SW7A	287975
L-P1	287435
L-P2	287436
L-P3	287438
L-SW7	287484
L-P4	287439
L-P5	287440
L-P6	287442
L-P7	287443
L-P8	287445
L-P9	287446
L-P10	287447
L-SWT1	287486
L-P11	287448
L-SWT2	287487
L-P12	287449
L-P13	287450
L-P14	287451
L-P15	287452
L-P16	287453
L-SWT3	287488
L-P17	287454
L-P18	287455
L-P19	287457

L-P20	287458
L-GW6	287459
L-SW6	287490
L-P21	287460
L-P22	287463
L-P23	287464
L-P24	287465
L-P25	287466
L-P26	287467
L-SWT4	287973
L-P27	287468
L-P28	287469
L-P29	287470
L-P30	287471
L-GW8	287472
L-P31	287473
L-SW8	287974
L-P37	287509
L-P32	287474
L-P33	287475
L-P34	287476
L-GW12	287477
L-SW12	287972
L-P35	287478
L-P36	287479

LF1P	290202
LF1LowT	295740
LF1UpT	295738
LF1SG	290206
LF2P	290208
LF2LowT	295743
LF2UpT	295741
LF2SG	290210
LF3P	290212
LF3LowT	295745
LF3UpT	295744
LF3SG	290214

# Impacts of river flow and temperature on salmonfly productivity and terrestrial subsidy

## Basic Information

<b>Title:</b>	Impacts of river flow and temperature on salmonfly productivity and terrestrial subsidy
<b>Project Number:</b>	2016MT301B
<b>Start Date:</b>	3/1/2016
<b>End Date:</b>	2/28/2018
<b>Funding Source:</b>	104B
<b>Congressional District:</b>	1
<b>Research Category:</b>	Biological Sciences
<b>Focus Categories:</b>	Ecology, Drought, Climatological Processes
<b>Descriptors:</b>	None
<b>Principal Investigators:</b>	Lindsey Albertson

## Publication

1. Anderson, H. E., L. K. Albertson, and D. Walters. In review. Temperature-driven range contraction and body size reduction of an iconic river macroinvertebrate. *Freshwater Science*.

## **Impacts of river flow and temperature on salmonfly productivity and terrestrial subsidy**

**Overview:** In this project, we tracked emergence of the iconic salmonfly *Pteronarcys californica* on two rivers in southwestern Montana, the Gallatin and Madison Rivers, over two consecutive years and have used rare historical datasets available only for the Madison River to evaluate changes in salmonfly population sizes over time. Funds for this award have been used to support PI Albertson and MS student Heidi Anderson. Additional funds provided by the undergraduate scholars program at MSU have helped Anderson work with two undergraduate research assistants (Niall Clancy and Cailey Philmon), and Albertson's startup funds supported a technician that worked on this project (Charlotte Hoover). Data have been included in 8 presentations, 1 manuscript in review, and 1 manuscript in preparation. This final report stems from Anderson's thesis (which will be defended in August 2018) and draws from the two manuscripts that contribute to the bulk of her thesis document.

**Major data collection efforts and summary of results:** In summer 2016 and 2017, we collected field data to identify relative densities of *P. californica* larvae in the Madison and Gallatin Rivers. Quantitative sampling showed that on the Madison River, *P. californica* are present in low densities above Hebgen Reservoir, abundant between Hebgen and Ennis Reservoirs, and are functionally extinct below Ennis Reservoir. Warm August temperatures appear to be driving the extirpation of salmonflies on the lower Madison River below Ennis Reservoir. Our modeling of future temperature scenarios suggests that additional habitat is likely to be lost if warming trends continue. On the Gallatin River, *P. californica* are extremely rare above Taylor's Fork, and common throughout the Gallatin canyon between Taylor's Fork and Spanish Creek. Densities decrease rapidly in the downstream direction after the river empties out onto the wide valley floor. For both rivers, spring water temperature is a primary driver of salmonfly emergence timing. Below, we detail the findings from the two projects that resulted from the USGS 104b grant.

**Background:** Increased temperature stress and fine sediment inputs are important mechanisms of ecological degradation in fluvial ecosystems (Jones et al., 2012; Poff et al., 2010), and are the two main hypothesized mechanisms for the decline of salmonflies in the Lower Madison River, Montana (Stagliano, 2010). Limited long-term datasets provide some evidence that conditions on the lower Madison River have changed over the past forty years. Spring and summer water temperatures on the lower Madison River have increased an average of 0.25 and 0.29° C per decade, respectively, since USGS monitoring began in 1977 (Anderson et al. in review). Similarly, days of extreme heat are increasing along the lower Madison. In the last 4 years, water temperatures exceeded 20°C an average of 46 days/year, and the number of days over 20°C has increased a rate of ~6 days/decade at a long-term monitoring site below Madison Dam (Anderson et al. personal communication).

Consistent monitoring of substrate type is limited, but available data indicates that fine sediment and embeddedness is increasing on the lower Madison River. Increased sedimentation is a widespread phenomenon in western Montanan rivers: in a 2015 survey of Montanan fishery biologists, fishing guides, and general fisherman, 100% of guides and fishery biologists and 50% of general fisherman reported an increase of sediment and silt (Stagliano, 2010). On the lower

Madison River, two earlier reports (Fraley, 1978; Hauer, 1991) do not mention highly embedded substrate or vascular plants in their descriptions of the lower Madison below Beartrap Canyon, both of which are now common on this section of the river.

Long-term datasets monitoring water temperature, substratum characteristics, and benthic macroinvertebrate population are uncommon. There is rising concern that salmonfly populations are in decline throughout the American West (e.g., Nehring et al., 2011; Stagliano, 2010), but in the absence of long-term data, quantifying the presence and/or extent of a population decline is difficult and often based on qualitative or anecdotal evidence. We established baseline data regarding the status of *P. californica* on the Madison and Gallatin Rivers that can be used to document the future of these at-risk populations. Additionally, we quantified how fine sediment and warm water temperatures affect *P. californica* by determining how these controls correlate with current *P. californica* distribution. Given our findings,

**Project 1 (Anderson et al. in review):** We compared current surveys with several long-term datasets documenting physical (water temperature, discharge, substrate characterization) and ecological (salmonfly larval density, salmonfly adult body size, salmonfly emergence timing) parameters to determine how environmental change has impacted salmonfly distribution, abundance, body size, and emergence phenology. We hypothesized that increased water temperatures and deposition of fine sediment would correspond with lower salmonfly abundance over time and space, predicting that current abundances will be lower than historical abundances and lower at sites with relatively warm water temperatures or relatively high proportions of fine bed sediments. We also predicted that water temperatures would be the primary control on salmonfly body size and emergence timing, with body size and emergence timing negatively correlated with water temperatures across both space and time and emergence timing advancing since records began in 1973. We provide further context for how these changes in salmonfly populations may continue throughout the 21<sup>st</sup> century by using predictive models of temperature change and extrapolated historic water temperature trends.

**Project 1 findings:**

5 figures, 2 tables

**Table 1.** Mean water temperature at each site from April – September, 2017. Site numbers increase in the upstream direction. Dotted lines represent reservoir locations: Ennis Reservoir is located between Sites 3 and 4, and Hebgen Reservoir is located between sites 9 and 10.

Site	Water Temperature (°C)
1	15.92
2	15.52
3	15.02
4	13.34
5	12.79
6	12.47
7	11.84
8	11.94
9	12.99
10	15.63
11	15.78

**Table 2.** Results of model selection used to predict salmonfly larval density from temperature and substrate quality variables.

Model variables	R <sup>2</sup>	AICc	ΔAICc	AIC wt.
Mean August Temperature	0.71	60.6	0.00	0.486
Mean August Temperature + % Particles highly embedded	0.78	63.0	2.42	0.145
Mean August Temperature + Mean July Temperature	0.77	63.2	2.66	0.128
Mean August Temperature + % Particles embedded	0.77	63.5	2.94	0.112
Mean July Temperature	0.60	64.3	3.67	0.078
Mean August Temperature + MWMT <sup>†</sup>	0.73	65.1	4.49	0.052

<sup>†</sup>Maximum weekly maximum temperature

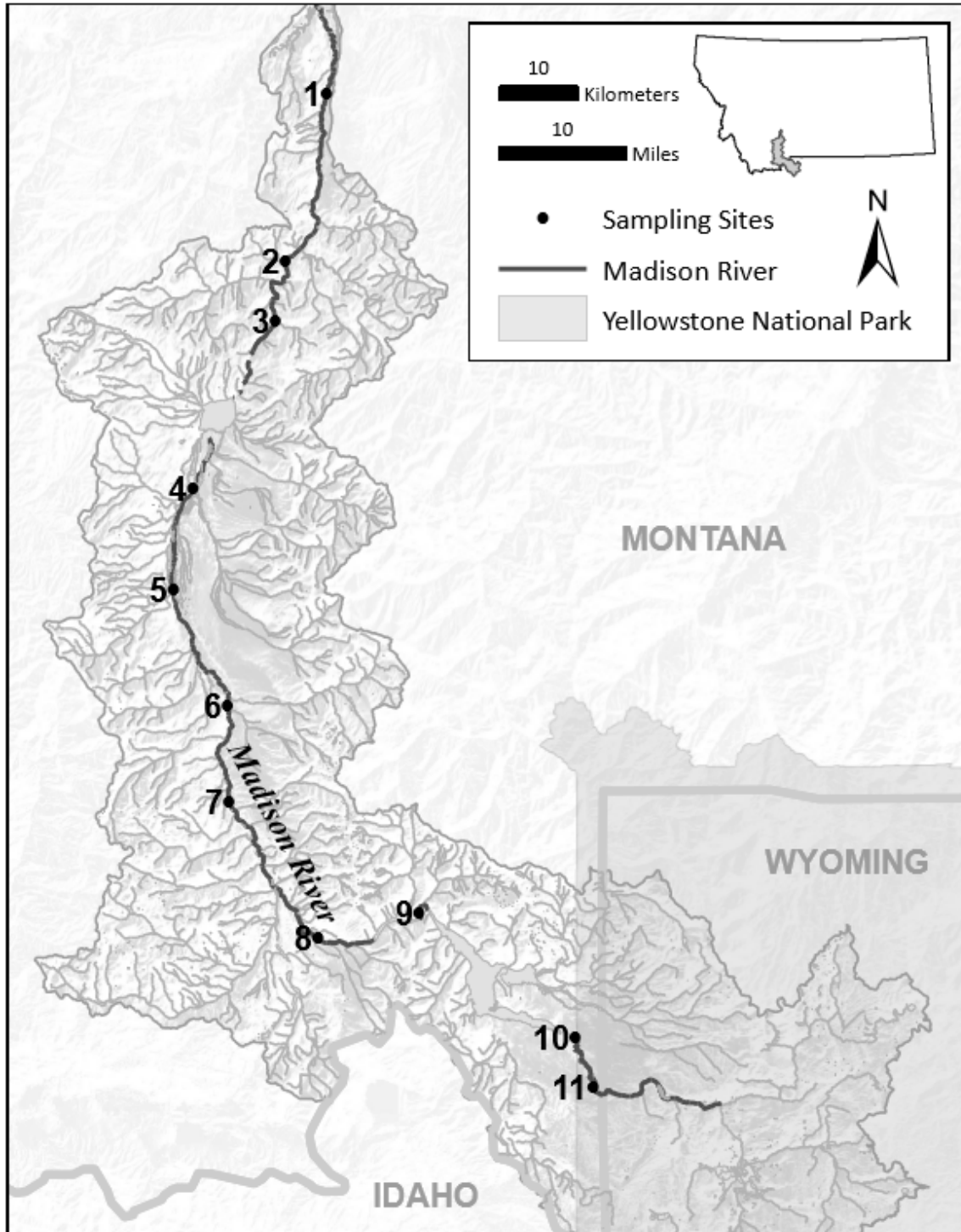


**Figure 1.** Study sites along the Madison River, which flows northwards, in southwest Montana. Historical data were collected at sites 1 – 5 in 1977 (Fralely 1978). Physical variables and salmonfly larval densities were quantified at all eleven sites in 2017.

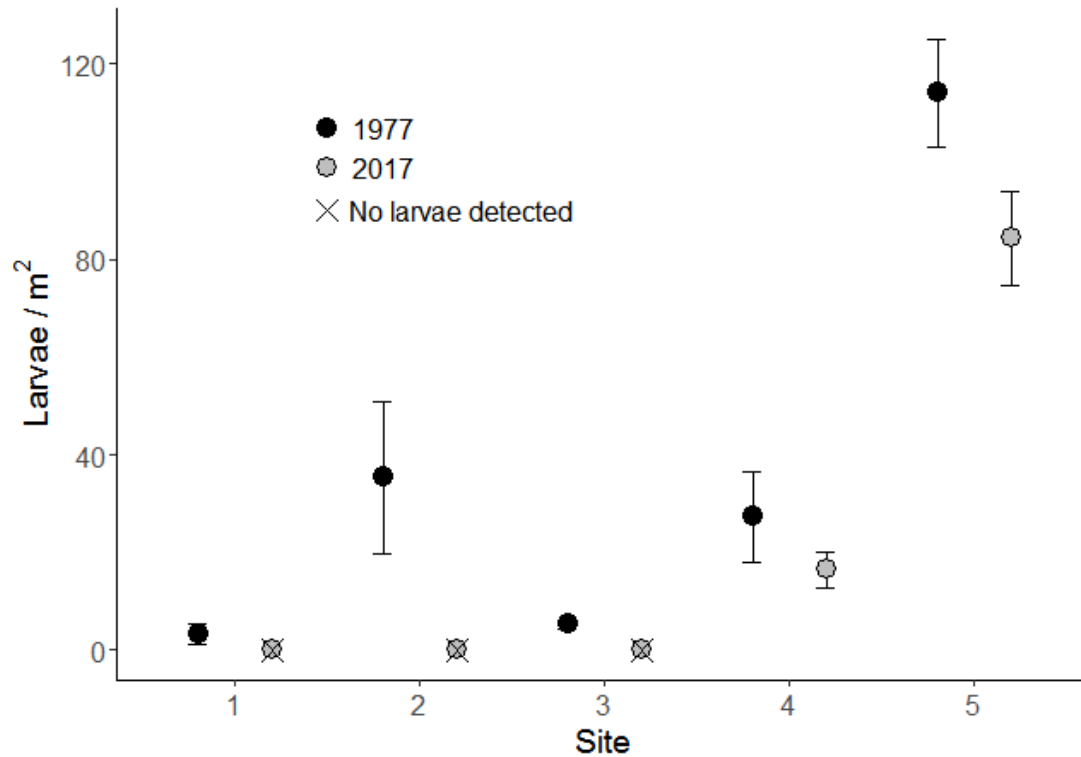


**Figure 2.** Salmonfly larval densities for five sites on the Madison River in 1977 and 2017. Salmonfly larvae were present at all sites in 1977, but were not detected at sites 1-3 below Ennis Reservoir in 2017. Values are means  $\pm$  1 SE of N=6 in 1977 and N=12 in 2017. Black circles indicate sampling in 1977, grey circles indicate sampling in 2017, and an X overlaying these circles represents a site where no larvae were detected in the sampling efforts.

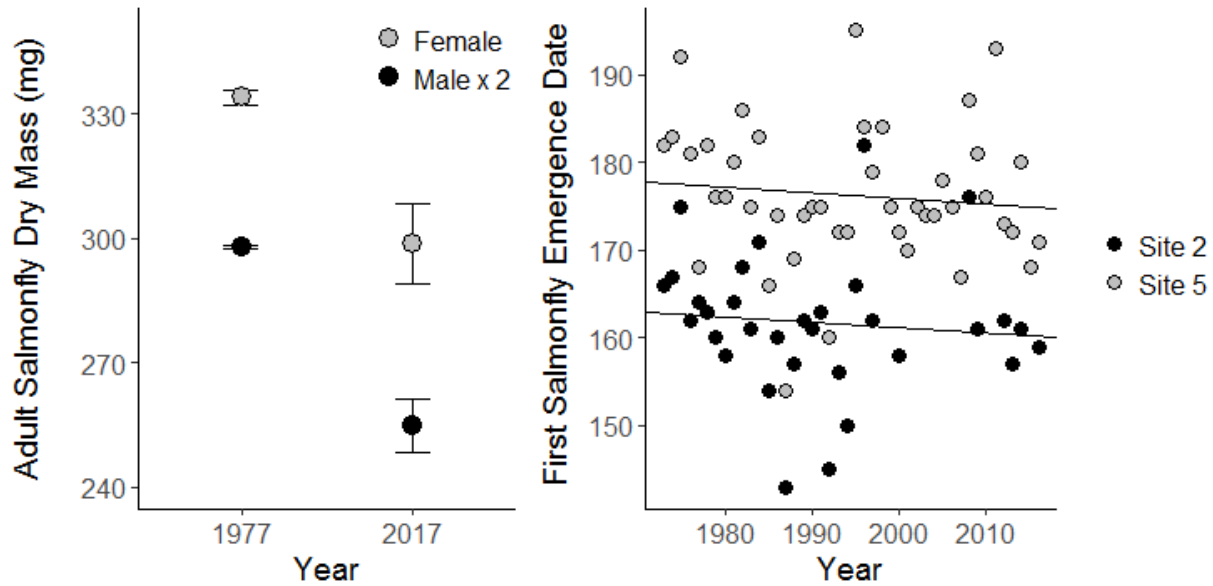


**Figure 3. (a)** Adult salmonfly dry mass (mg) above Ennis Reservoir in 1977 and 2017. Salmonfly dry mass across both sexes was an average of 11.8 % smaller in 2017 compared to adult salmonfly dry mass at the same location 40 years previous ( $p = 0.043$ ). Average female dry weight was 2.3x more than males, so adult male dry mass was doubled for ease of graphical viewing. Values are means  $\pm$  1 SE. **(b)** First date (day of year) of salmonfly emergence from 1973 to 2017 for two sites along the Madison River where long-term monitoring data were available. Emergence timing between years varied up to 39 days at site 2 and 41 days at site 5. Emergence date did not change over time ( $p = 0.392$ ).

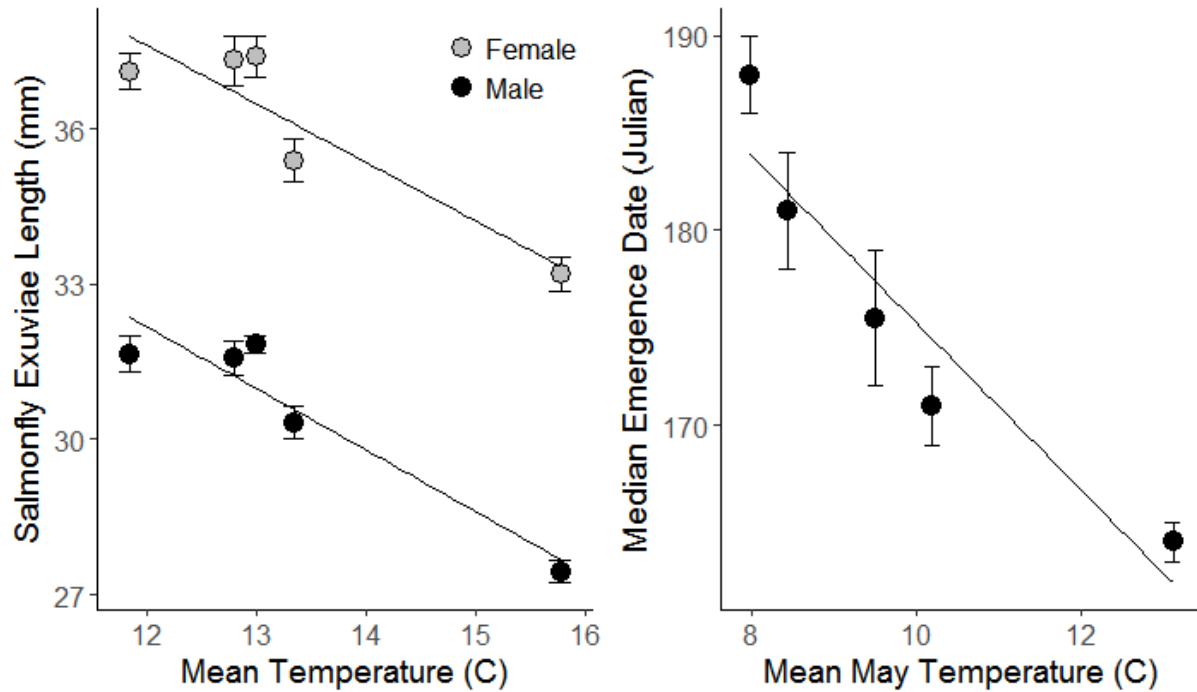


**Figure 4. (a)** Male and female salmonfly exuviae lengths (mm) from five sites that vary in water temperature on the Madison River. Mean April – September water temperature was negatively correlated with salmonfly exuviae length ( $p < 0.001$ ,  $R^2 = 0.72$ ). Values are means  $\pm$  1 SE. **(b)** Median salmonfly emergence date (Julian day) from five sites that vary in water temperature on the Madison River. Mean May water temperature, the month prior to emergence, was negatively correlated with salmonfly emergence date ( $p = 0.016$ ,  $R^2 = 0.85$ ). Error bars represent duration of emergence at each site, defined as the first day of  $>$  5% cumulative emergence through the first day of  $>$  95% cumulative emergence.

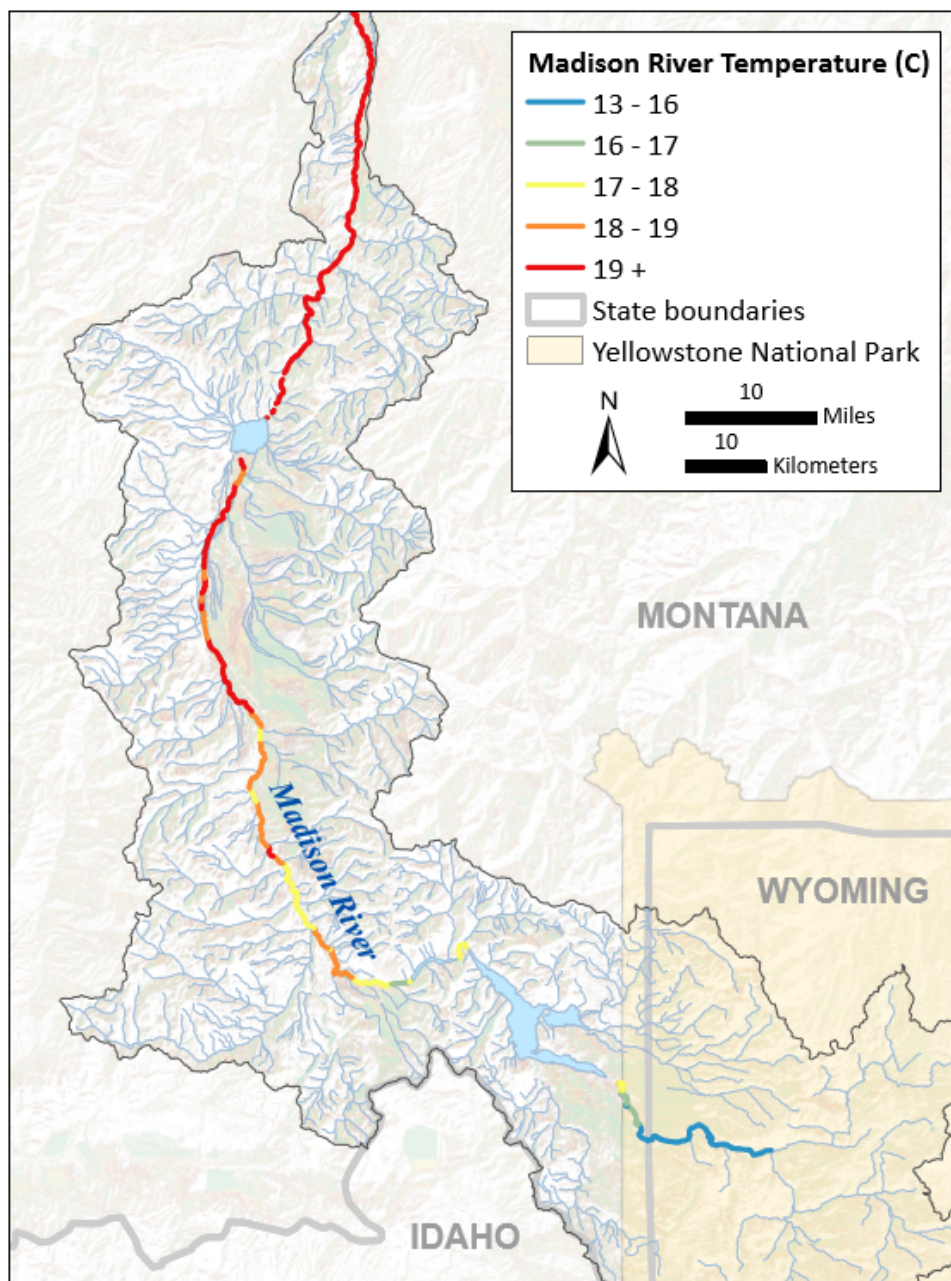


**Figure 5.** Mean August water temperatures projected for the Madison River mainstem in 2100 assuming an increase of 2°C from present. This increase is based linear extrapolations of observed warming trends from 1977 to 2017 (USGS gage 2017). Red lines indicate areas where mean August water temperatures are expected to exceed 19° C and where salmonfly populations will likely be unable to persist. This model predicts a loss of 30 river kilometers of currently occupied salmonfly habitat.

**Project 2 (Anderson et al. in preparation):** We quantified longitudinal patterns and duration of emergence for the pteronarcyid stonefly *Pteronarcys californica* (common name: salmonfly) along two rivers of differing topographic complexity in southwest Montana. Salmonflies provide a significant food resource to a variety of aquatic and terrestrial consumers, including birds, fish, ants, and spiders (Rockwell and Newell 2009), and can dominate subsidies to terrestrial ecosystems (Walters et al. 2017). Salmonfly emergence events are brief at any one location (2-7 days), but can last over a month on a single river (Anderson et al., in review). Thus, variation in the spatial patterning and duration of salmonfly emergence at a landscape scale could have important implications for mobile consumers able to track this high-quality resource pulse over space and time or for the duration of site-specific static consumers.

We hypothesized that longitudinal patterns of water temperature and total temperature gradients drive large-scale patterns and duration of aquatic insect emergence. Specifically, we predicted that salmonfly emergence would move upstream in a predictable wave along the Madison River, a river with relatively simple catchment topography and correspondingly few thermal discontinuities along the study length. Additionally, we predicted that emergence duration would be extended along the Madison River due to a large water temperature gradient caused by dewatered tributaries and irrigation inputs warming temperatures along the downstream extent of our study length and cooled water temperatures at the most upstream extent of our study length at a reservoir output. We predicted that salmonfly emergence would be discontinuous and relatively synchronous at an entire-river scale along the Gallatin River, a river with more complex catchment topography and frequent cold-water tributary inputs, and a correspondingly complex thermal profile and reduced water temperature gradient. This study provides insight into how catchment topography can alter spatiotemporal dynamics of aquatic-terrestrial subsidies, furthering our understanding of linkages between physical structure and ecological function in fluvial ecosystems.

**Project 2 findings:**

5 figures, 0 tables

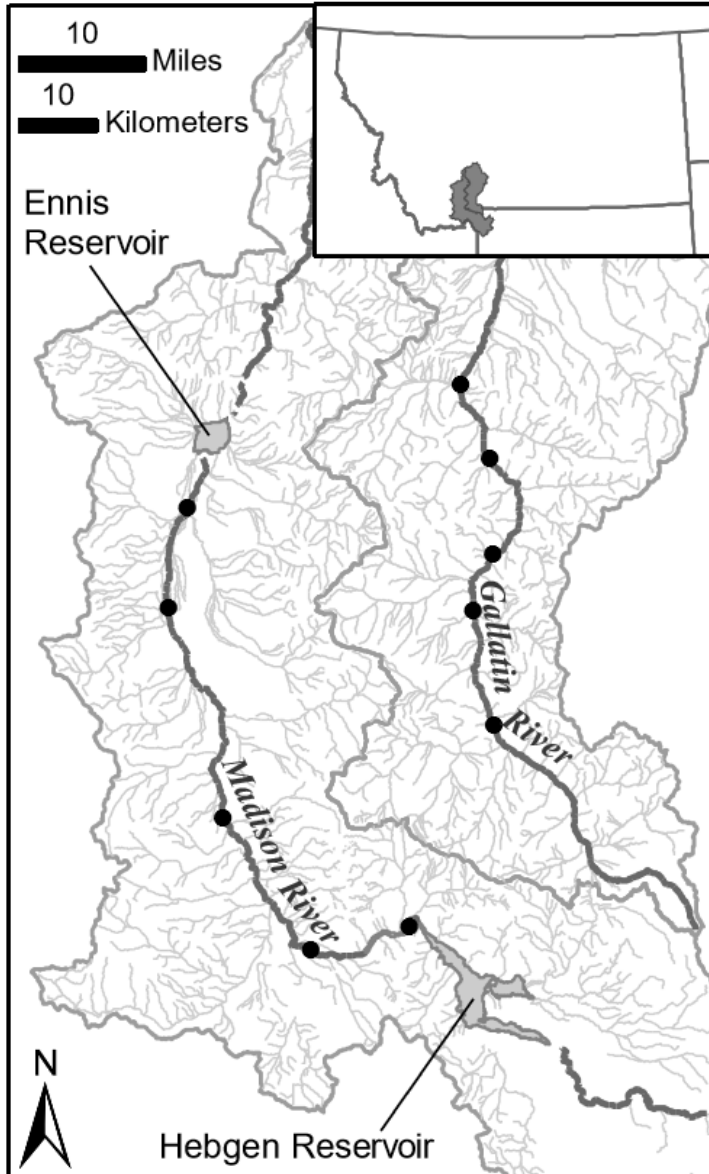


**Figure 1.** Study sites along the Madison and Gallatin Rivers, which flow northwards, in southwest Montana. Salmonfly (*Pteronarcys californica*) emergence phenology and water temperature were measured at five sites on each river (solid circles). Emergence phenology was quantified in both 2016 and 2017. Water temperature was measured in 2017.

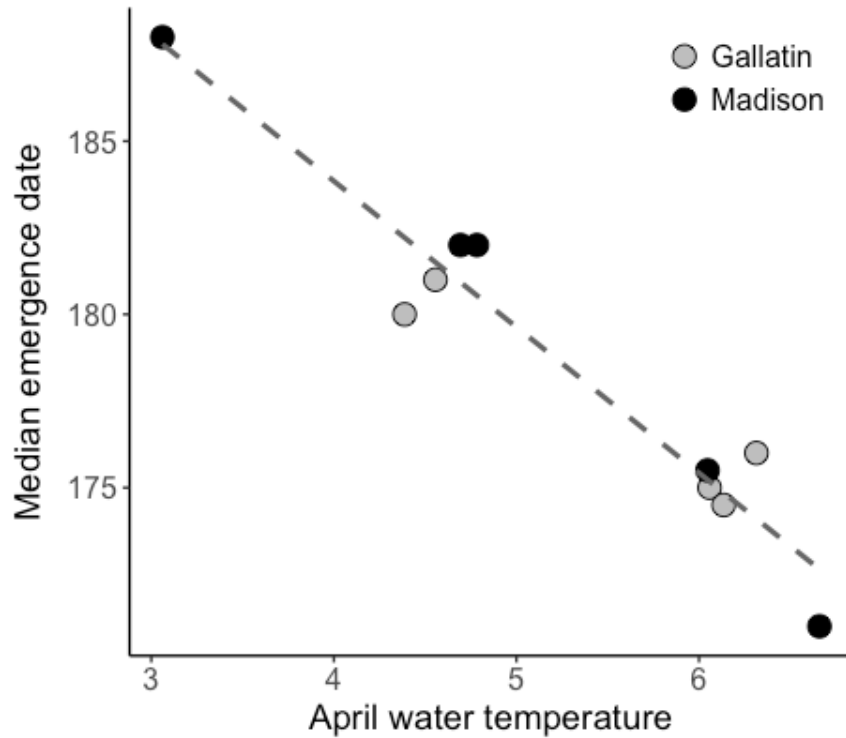


**Figure 2.** Median salmonfly emergence date was strongly correlated with mean April water temperature (lm:  $R^2 = 0.93$ ,  $p < 0.001$ ) on both the Gallatin (grey circles) and Madison (black circles) Rivers in 2017. We found no evidence of an interactive effect between rivers (ANCOVA:  $F = 5.02$ ,  $p = 0.066$ ).

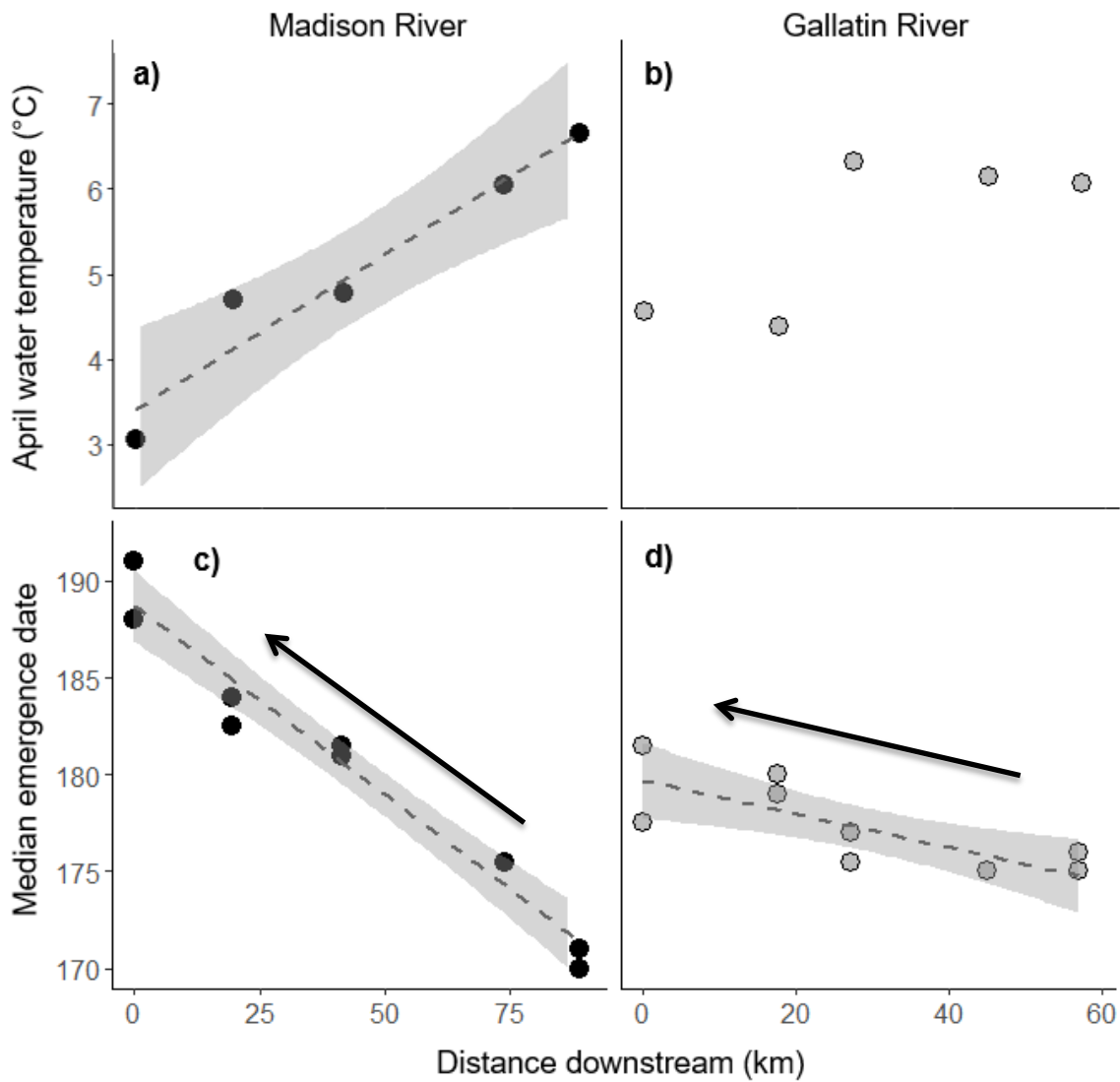


**Figure 3.** Spatial patterns of mean April water temperatures and salmonfly emergence. Water temperature in 2017 was correlated with longitudinal distance (0 = most upstream) on **a)** the Madison River (lm:  $R^2 = 0.92$ ,  $p = 0.0065$ ) but not on **b)** the Gallatin River (lm:  $R^2 = 0.45$ ,  $p = 0.13$ ). Salmonfly emergence moved from downstream to upstream in both rivers: median salmonfly emergence date in both 2016 and 2017 was tightly correlated with longitudinal distance on both the **c)** Madison River (lm:  $R^2=0.95$ ,  $p < 0.001$ ) and **d)** Gallatin River (lm:  $R^2=0.57$ ,  $p = 0.007$ ), but on the Gallatin River, salmonfly emergence moved in a less-predictable wave, occurring at some upstream sites simultaneously or before emergence at downstream sites. Arrows represent the general direction of movement of salmonfly emergence over time. Dashed lines represent significant linear fits with grey shading displaying the 95% CIs.

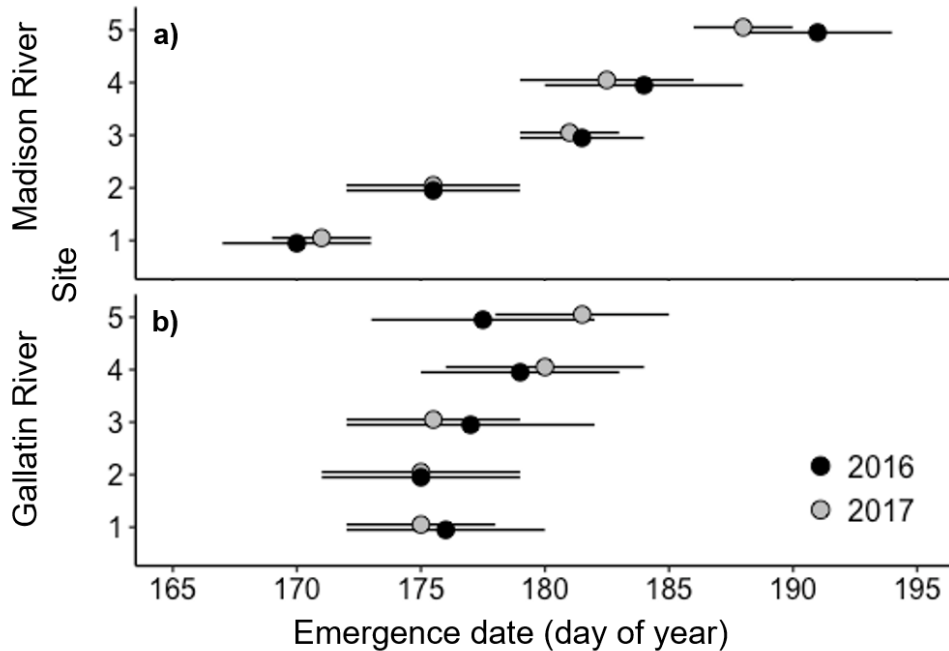


**Figure 4.** Temporal patterns of salmonfly emergence. Salmonfly emergence was asynchronous along the **a)** Madison River: the difference in median emergence date among sites was 21 days in 2016 and 24 days in 2017. Salmonfly emergence was relatively synchronous along the **b)** Gallatin River: the difference in median emergence date among sites was 4 days in 2016 and 6.5 days in 2017. Black circles represent median emergence date in 2016 and grey circles represent median emergence date in 2017. Error bars represent duration of emergence at each site averaged over both years, defined as the first day of > 5% cumulative emergence through the first day of > 95% cumulative emergence at any given site.

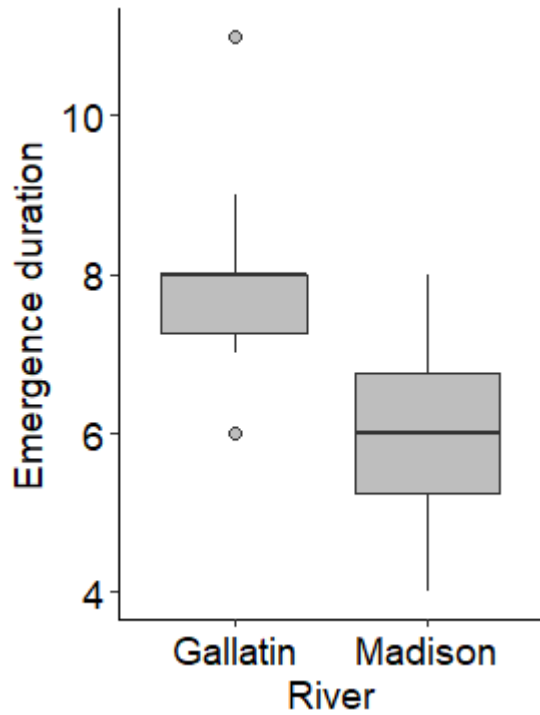


**Figure 5.** Site-specific duration of salmonfly emergence on the Gallatin and Madison Rivers. Emergence duration was quantified for five sites on each river in both 2016 and 2017, for N = 10 on each river. The horizontal line within the box and whisker plots represents the sample median, and the outer margins represent the 25th and 75th percentiles. The whiskers extend to the farthest value no further than 1.5x the inter-quartile range from the box. Grey circles represent outliers.

**Literature Cited:**

- Anderson, H.E., L.K. Albertson, and D. Walters. In review. Temperature-driven range contraction and body size reduction of an iconic river macroinvertebrate. Submitted to Freshwater Science.
- Anderson, H.E., L.K. Albertson, D. Walters, L. Burkle and W.F. Cross. In preparation. Longitudinal temperature profiles determine patterns and duration of aquatic insect emergence. To be submitted to Freshwater Biology.
- Fraley, J.J. (1978). Effects of elevated summer water temperature below Ennis Reservoir on the macroinvertebrates of the Madison River, MT. M.S. Thesis. MT State University. 120 p.
- Gustafson D. (1990) Ecology of Aquatic Insects in the Gallatin River Drainage. PhD Thesis. Montana State University.
- Hauer, F.R., J. A. Stanford, and J. T. Gangemi, 1991. Effects of stream regulation in the upper Missouri River. Report 116-91. Flathead Biological Station. Report to MT Power Co.
- Jones, J.I., J.F. Murphy, A.L. Collins, D.A. Sear, P.S. Naden, & P.D. Armitage, (2012). The impact of fine sediment on macroinvertebrates. *River Research and Applications*. 28:8, 1055-1071.
- Nehring, B.R., B. Heinold, & J. Pomeranz (2011). Colorado River Aquatic Resources Investigations Federal Aid Project F-237R-18. Colorado Division of Wildlife.
- Poff, N. L., M.I. Pyne, B.P. Bledsoe, C.C. Cuhaciyan, & D.M. Carlisle (2010). Developing linkages between species traits and multiscaled environmental variation to explore vulnerability of stream benthic communities to climate change.
- Stagliano, D., (2010). Evaluation of Salmonflies in Montana's Rivers: Are Statewide Populations Really Declining? Montana Natural Heritage Program.
- Rockwell, I. P., & Newell, R. L. (2009) Note on mortality of the emerging stonefly *Pteronarcys californica* on the Jocko River, Montana, USA. *Western North American Naturalist*, 69:264-266. doi: 10.3398/064.069.0218
- Walters, D. M., Wesner, J. S., Zuellig, R. E., Kowalski, D. A. and Kondratieff, M. C. (2017) Holy flux: spatial and temporal variation in massive pulses of emerging insect biomass from western U.S. rivers. *Ecology* doi:10.1002/ecy.2023

### **Lindsey Albertson – Publications and presentations**

Albertson, L.K., H.E. Anderson, and D. Walters. 2018. (Pending acceptance). An iconic macroinvertebrate in peril? Salmonfly emergence patterns and climate-driven range contraction. Scientific Conference of the Greater Yellowstone Ecosystem. Big Sky, MT. Oral presentation

Albertson, L.K. 2018. Small aquatic insects can teach us big things: Ecological indicators and community facilitators in streams. University of Montana Seminar Series, Missoula, MT. Invited oral presentation.

Anderson, H., and L.K. Albertson. 2018. Large-scale drivers of resource pulse phenology: Salmonfly emergence patterns differ between human dominated and natural rivers. Society for Freshwater Science Annual Meeting, Detroit, MI. Oral presentation  
Philmon, C., H.E. Anderson, and L. K. Albertson. 2017. Relating Non-Destructive Measurements of Growth to Biomass of Salmonfly Larvae (*Pteronarcys californica*). Undergraduate Research Celebration, Montana State University, Bozeman, MT. Poster presentation.

Clancy, N., H.E. Anderson, and L.K. Albertson. 2017. Unique emergence of salmonflies on the Gallatin and Madison Rivers of Montana. Undergraduate Research Celebration, Montana State University, Bozeman, MT. Poster presentation.

Anderson, H.E., and L.K. Albertson. 2017. An iconic macroinvertebrate in peril: Impacts of increasing water temperatures on *Pteronarcys californica* in southwestern Montana. Society for Freshwater Science Annual Meeting, Raleigh, NC. Poster presentation

Albertson, L. K. 2017. Animals and sediment disturbance in streams. Montana Aquatic Research Colloquium, Polson, MT. Oral presentation

Albertson, L. K. 2017. Animals and sediment disturbance: Linking macroinvertebrate ecology and fluvial geomorphology. Idaho State University Seminar Series, Pocatello, ID. Invited oral presentation

Albertson, L. K. 2017. Animals and sediment disturbance: Linking macroinvertebrate ecology and fluvial geomorphology. Idaho State University Seminar Series, Pocatello, ID. Invited oral presentation

# Characterizing Microbial Activity as Related to Water Quality in the Clark Fork Headwaters: A Baseline Study

## Basic Information

<b>Title:</b>	Characterizing Microbial Activity as Related to Water Quality in the Clark Fork Headwaters: A Baseline Study
<b>Project Number:</b>	2016MT302B
<b>Start Date:</b>	3/1/2016
<b>End Date:</b>	2/28/2018
<b>Funding Source:</b>	104B
<b>Congressional District:</b>	1
<b>Research Category:</b>	Biological Sciences
<b>Focus Categories:</b>	Ecology, Water Quality, Surface Water
<b>Descriptors:</b>	None
<b>Principal Investigators:</b>	Alysia Cox

## Publications

1. Schmidt, R., 2017, Biogeochemical Interactions in Flooded Underground Mines, MS Thesis, Department of Geosciences, Montana Tech of The University of Montana, Butte, Montana, 24pp.
2. Cox, A. D., Schmidt, R., Dahlquist, G. R., Foster, J., & Dillard, M. (2016, February). Habitability from the Surface to the Deep. In AGU Fall Meeting Abstracts.

# **Characterizing Microbial Activity as Related to Water Quality in the Clark Fork Headwaters: A Baseline Study**

Final Report for the Montana Water Center

Dr. Alysia Cox

Laboratory Exploring Geobiochemical Engineering and Natural Dynamics (LEGEND)

Chemistry and Geochemistry Department

Montana Tech

## **Project Overview**

This project aims to link microbial identity and activity with water quality data on the Upper Fork in order to provide both an indication of metal contamination from past mining on the overall health of the system and serving as a baseline for evaluating the effects of future climate change on microbial and chemical processes in this ecosystem. This research addresses the following basic questions: What is the baseline microbial community and activity in the headwaters of the Clark Fork and how do they relate to the water chemistry? What is the level of metal contamination reached in these headwaters and does the microbial community reflect that? How will microbial activity change with the climate (lower water flow, higher CO<sub>2</sub> available for photosynthesis)? The microbial community and activity is expected to correlate with the water chemistry and reflect the level of metal concentrations in these waters. These results will contribute to water quality and remediation solutions now and in the future.

## **Preliminary Results**

Fourteen sites on Silver Bow and Blacktail Creeks, German Gulch, and the Upper Clark Fork were sampled every three months beginning in May 2016 (Figure 1). Preliminary data for this project were collected at five locations on Silver Bow and Blacktail Creeks in August 2015 and February 2016. At each site, time sensitive parameters were measured with a hydrolab (temperature, pH, conductivity, dissolved oxygen); field spectrophotometry was performed for dissolved silica, ferrous iron, and sulfide; water samples were collected and filtered for immediate analyses in the lab (hydrogen and oxygen isotopes in water, dissolved inorganic carbon (DIC), dissolved organic carbon (DOC), major cations and anions, and trace elements), and biological samples, both sediment and planktonic biomass, were collected and frozen on dry ice for lab extraction and analyses.

We found that the headwaters of the Upper Clark Fork range in pH from 6.2 to 9.4 and in temperature from 0 to 20°C, with higher pH values and temperatures in August (Figure 2). This means that the water is outside the range of EPA aquatic life pH standards at some times and locations. The temperatures reached in August tend to be above the 15°C recommended for inland freshwater fish.

Zn concentrations vary from less than 10<sup>-7</sup> to 10<sup>-5</sup> molal in the Upper Clark Fork and Silver Bow and Blacktail Creeks (Figure 3). These concentrations are somewhat elevated for the pH values measured. A few sampling times and locations exceeded EPA aquatic life limits for dissolved zinc.

More connections will be made between the geochemistry of the Upper Clark Fork and the microbial life when already extracted DNA samples are sent for sequencing. The geochemical analyses are already performed on samples through May 2016, the samples after that are preserved and stored until analysis. Analysis of DNA will reveal the metabolic potential

of the system as well as provide a baseline for ecosystem health. Protein extractions to be performed this summer will show microbial activity, allowing us to link metabolic activity with concurrent geochemistry. Protein extractions are now routine and in house protein analyses using our LC-MS/MS are nearly operational at Montana Tech.



Figure 1: 14 sampling locations on the Upper Clark Fork and Silver Bow and Blacktail Creeks (map done in DataBasin).

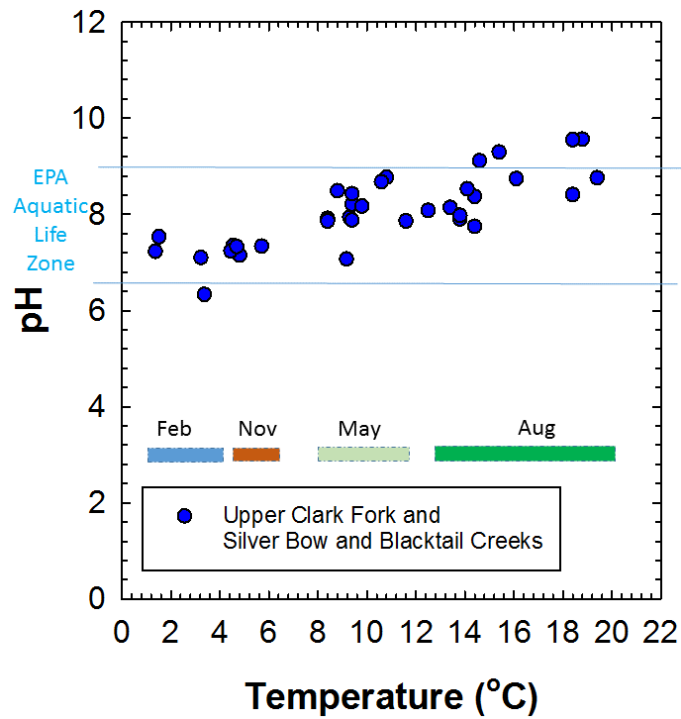


Figure 2: pH vs. Temperature on the Upper Clark Fork and Silver Bow and Blacktail Creeks.

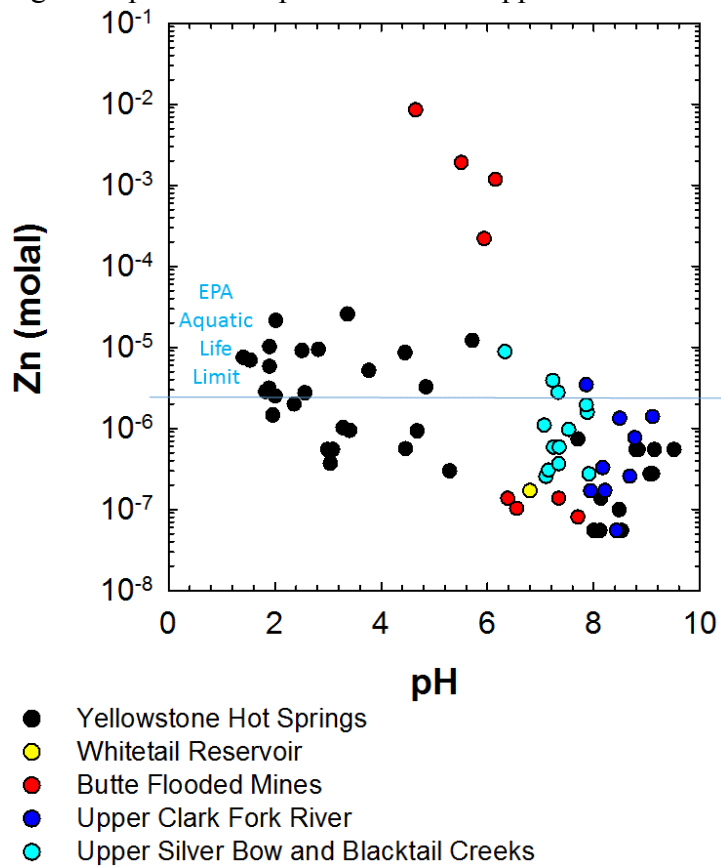


Figure 3: Zn vs. pH for a wide variety of sampling locations including the Upper Clark Fork and Silver Bow and Blacktail Creeks.

### **Ongoing Work**

DNA extractions have been successfully performed on one set of the sediment samples, PCR for universal, Bacterial, Archaeal, and Eukaryotic 16S and 18S rRNA genes performed, and DNA preserved. Plans are underway to send pure DNA extracts off for metagenomic sequencing. This is the focus of the lab in summer 2018.

This work is a part of Jordan Foster's undergraduate thesis. He has been interested in this project since his freshman year and will be starting his senior year this fall. We will be writing up geochemical and microbial results for publication in *Frontiers*.

Also, we plan to continue sampling every three months so we can observe how and why the system is changing over time. Samples will be preserved for later geochemical and biological analysis pending more funding.

### **Budget**

This grant provided partial summer funding for three female scientists: one undergraduate (1.5 months), one graduate (1.5 months), and one assistant professor (0.5 months). It also provided field sampling supplies to help support 4 sampling expeditions, as well as lab supplies for LEGEND to be fully capable of environmental DNA extractions. In addition, funds were used to pay the Montana Bureau of Mines and Geology for major anions and trace elemental analyses.

### **Budget Match**

The majority of the match was provided by my time. Joe Griffin, our consultant, also donated his time by helping us plan our sampling scheme and going out sampling with us.

### **Field Research Expeditions**

Students involved (7 masters, 5 undergraduate): Jordan Foster, McKenzie Dillard, Renee Schmidt, Georgia Dahlquist, Shanna Law, Mallory Nelson, James Foltz, Cynthia Cree, Johnathan Feldman, Isaiah Roberston, McKenzie Joseph, Bob Radar. Others involved: Joe Griffin, Cathy Cree.

May 2018, Upper Clark Fork/Silver Bow and Blacktail Creeks, (3 days), S Law and J Foster, field leaders.

February 2018, Upper Clark Fork/Silver Bow and Blacktail Creeks, (3 days), S Law and J Foster, field leaders.

November 2017, Upper Clark Fork/Silver Bow and Blacktail Creeks, (2 days), S Law and J Foster, field leaders.

September 2017, Upper Clark Fork/Silver Bow and Blacktail Creeks, (2 days), S Law and J Foster, field leaders.

May 2017, Upper Clark Fork/Silver Bow and Blacktail Creeks, (3 days), S Law and J Foster, field leaders.

February 2017, Upper Clark Fork/Silver Bow and Blacktail Creeks, (3 days), A Cox, field leader.

November 2016, Upper Clark Fork/Silver Bow and Blacktail Creeks, (2 days), A Cox, field leader.

August 2016, Upper Clark Fork/Silver Bow and Blacktail Creeks, (2 days), A Cox, field leader.

May 2016, Upper Clark Fork/Silver Bow and Blacktail Creeks, (3 days), A Cox, field leader.

### **Related Grant Activity**

I received a grant from the Butte Area One Butte Natural Resource Defense Council (BNRC) entitled “Microbial Activity in Silver Bow and Blacktail Creeks” in the amount of \$77,225, starting September 2017-2019.

I also used some of the data collected for this grant in an NSF CAREER proposal that was not funded in 2016.

Undergraduate researcher Jordan Foster was supported the summer of 2016 on an Institute on Ecosystems Summer Fellowship for \$4,000. His work was directly related to this grant.

MS in Geochemistry student Isaiah Robertson was selected for a graduate research fellowship from the Montana Water Center for \$2,000.

### **Publications**

\* indicates MS student MTech author, \*\* indicates undergraduate MTech author

Cox AD, Schmidt R\*, Dahlquist GR\*, Foster J\*\*, Dillard M\*\* 2016. Habitability from the surface to the deep. American Geophysical Union (AGU) Fall Meeting Abstract B51K-07.

Schmidt R\*. 2017. Biogeochemical interactions in flooded underground mines. Montana Tech Graduate Thesis 129.

### **Invited Talks**

Cox A. Schmidt R\*, Foster J\*\*, Dahlquist G\*. How healthy is our ecosystem? Check the microbes and geochemistry! Citizens Technical Environmental Committee (CTEC) Meeting, Butte, MT, April 13<sup>th</sup>, 2017.

Cox A. Microbial Activity in Silver Bow and Blacktail Creeks. Butte Area One Butte Natural Resource Defense Council Meeting, Butte, MT, April 5<sup>th</sup>, 2017.

Cox A. LEGEND at Montana Tech. Butte High School Science National Honor Society, Butte, MT, February 15th, 2017.

Cox A. Environmental Dynamics in Geobiochemical Engineering: From Supervolcanoes to Silver Bow Creek. Montana Tech Public Lecture Series, Butte, MT, September 8th, 2016.

Cox A. Environmental Dynamics in Geobiochemical Engineering: From Supervolcanoes to Silver Bow Creek, NIH Bringing Research Into the Classroom (BRIC) Teacher Academy, Helena, MT, June 12<sup>th</sup>, 2016.

### **LEGEND Presentations**

\* indicates MS student MTEch author, \*\* indicates undergraduate MTEch author

Feldman J\*, Cox A. 2018. Mineralogical influences on aqueous metal speciation in Silver Bow Creek and the Upper Clark Fork. Techxpo poster, April 26th.

Foster J\*\*, Cox A. 2018. Metal-microbe interactions in Silver Bow Creek. Techxpo poster, April 26th.

Robertson I\*, Cox A. 2018. Limitations to photosynthesis in Silver Bow Creek. Techxpo poster, April 26th.

Foster J\*\*, Law S\*, Robertson I\*, Feldman J\*. 2018. LEGEND - Laboratory Exploring Geobiochemical Engineering and Natural Dynamics. Techxpo booth, April 26th. Best Booth - Department of Chemistry and Geochemistry.

Foster J\*\*, Cameron D, Graff J, Cox A. 2018. Metal-microbe interactions in Silver Bow Creek. Montana Academy of Sciences Meeting Butte, MT, talk, April 7th.

Schmidt R, Dahlquist G, Law S, Foster J, Foltz J. 2017. LEGEND - Laboratory Exploring Geobiochemical Engineering and Natural Dynamics. Techxpo booth, April 27th. Best Booth - Department of Chemistry and Geochemistry

Cox A, Schmidt R\*, Dahlquist G\*, Foster J\*\*, Dillard M\*\*, Law S\*, Nelson M\*, Cree C\*\*, Foltz J\*. Aquatic Habitats from Hot Springs to Silver Bow Creek. Montana Aquatic Research Colloquium Flathead Lake Biological Research Station, MT, Talk, April 8<sup>th</sup>, 2017.

Cox A, Foster J\*\*, Schmidt R\*, Dahlquist G\*, Dillard M\*\*. Defining Microbial Habitats in Mining Impacted Watersheds. Montana American Water Resources Association Conference, Fairmont Hot Springs, MT, Talk, October 14th, 2016.

Foster J\*\*, Cox A. 2016. Stormwater in Silver Bow and Blacktail Creeks: Implications for the microbial community. Techxpo poster, April 3rd. Best Poster Department of Chemistry and Geochemistry.

Foster J\*\*, Cox A, 2016. Stormwater in Silver Bow and Blacktail Creeks: Implications for the microbial community. Montana Academy of Sciences Meeting talk, April 9th. \*Laurie Henneman Outstanding Student Presentation Award for Best Undergraduate Student Oral Presentation.

# Using weathering geochemistry to understand the sources of base flow water supply in rivers across mountain-basin transitions in the Upper Missouri Watershed

## Basic Information

<b>Title:</b>	Using weathering geochemistry to understand the sources of base flow water supply in rivers across mountain-basin transitions in the Upper Missouri Watershed
<b>Project Number:</b>	2016MT308G
<b>USGS Grant Number:</b>	G16AP00193
<b>Start Date:</b>	9/1/2016
<b>End Date:</b>	8/30/2019
<b>Funding Source:</b>	104G
<b>Congressional District:</b>	MT-001
<b>Research Category:</b>	Ground-water Flow and Transport
<b>Focus Categories:</b>	Hydrogeochemistry, Hydrology, Water Quality
<b>Descriptors:</b>	None
<b>Principal Investigators:</b>	Stephanie Ewing, Robert A Payn, James B Paces, Rob Striegl

## Publications

There are no publications.

## Annual report - May 2018

### **Using weathering geochemistry to understand the sources of base flow water supply in rivers across mountain-basin transitions in the Upper Missouri Watershed**

**Principle Investigator** Stephanie A. Ewing, Ph.D., Associate Professor, Dept. of Land Resources & Environmental Sciences, Montana State University, Bozeman, MT 59717, [stephanie.ewing@montana.edu](mailto:stephanie.ewing@montana.edu), 406-994-5247

**Graduate Student** Florence Miller, MS student (expected completion July 2018), Dept. of Land Resources & Environmental Sciences, Montana State University, Bozeman, MT 59717

**Undergraduate/Post-graduate Researcher** Samuel Leuthold, BS (completed December 2017), Dept. of Land Resources & Environmental Sciences, Montana State University, Bozeman, MT 59717

#### **Co-Investigators**

Robert A. Payn, Ph.D., Assistant Professor, Dept. of Land Resources & Environmental Sciences, Montana State University, Bozeman, MT 59717, [rpayn@montana.edu](mailto:rpayn@montana.edu), 406-994-7197

James B. Paces, Ph.D., Research Geologist, U.S. Geological Survey – Denver Radiogenic Isotope Lab, Box 25046, MS963, Denver Federal Center, Denver, CO 80225-0046, United States, [jbpaces@usgs.gov](mailto:jbpaces@usgs.gov), 303-236-0533

Robert Striegl, Ph.D., Research Hydrologist and Biogeochemist, U.S. Geological Survey, 3215 Marine St., Suite E-127, Boulder, CO 80303, United States, [rstriegl@usgs.gov](mailto:rstriegl@usgs.gov), 303-541-3091

#### **Key Collaborators**

Tom Michalek, Montana Bureau of Mines and Geology

Steve Custer, Montana State University (emeritus)

## 1 Introduction

A repeated landscape pattern in the intermountain west is relatively steep, actively eroding mountainous headwater streams draining to more depositional sedimentary environments in intermountain basins. Little is understood about how hydrologic storage and weathering change across this dramatic transition between hydro-geomorphological process domains. This limits our ability to make informed management decisions regarding baseflow water supply, because human infrastructure typically becomes more directly coupled to the hydrosystem within

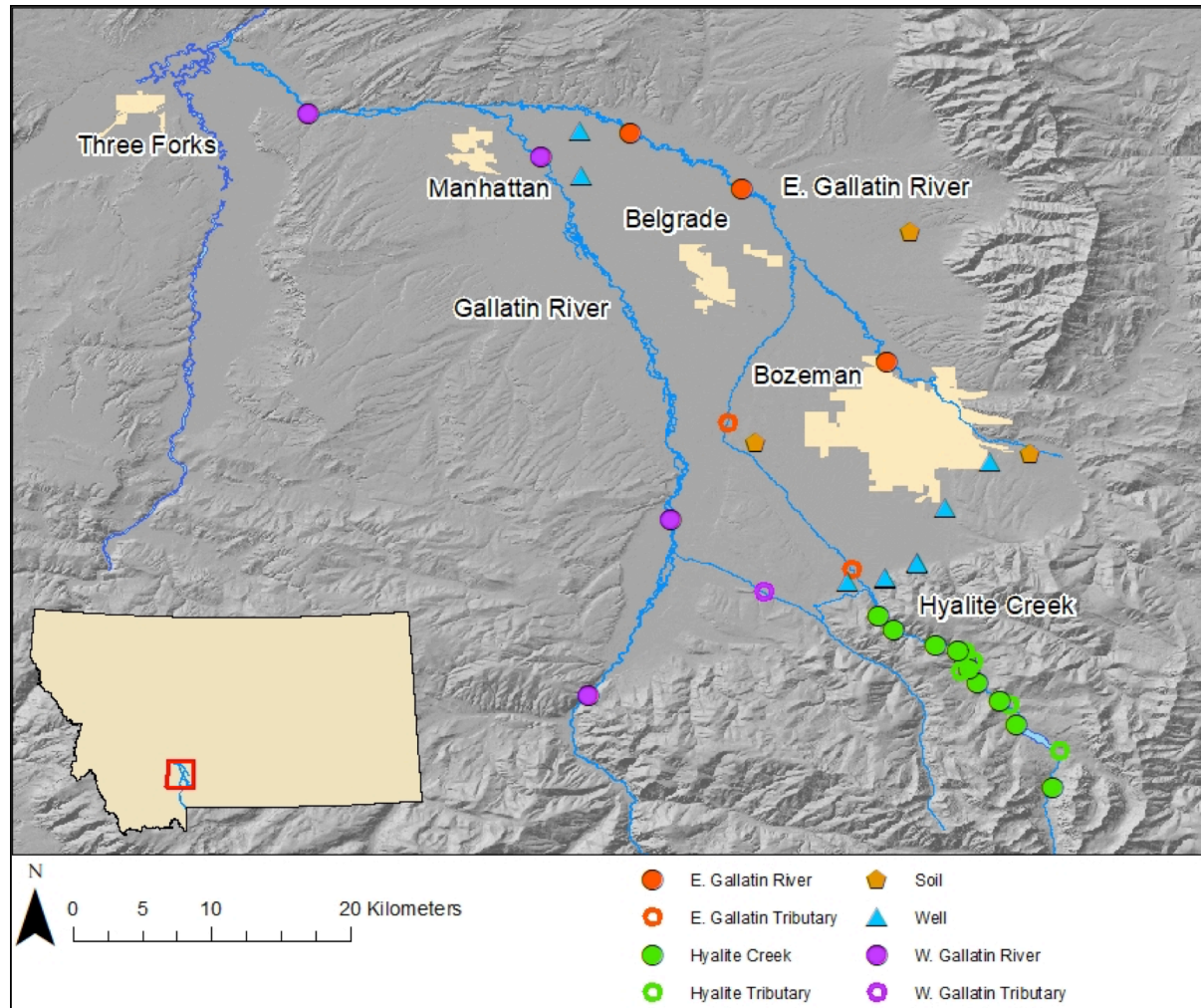


**Figure 1a.** Water sample locations in Hyalite Canyon, the East and West Gallatin River, and valley wells; soil sample locations on Gallatin Valley alluvial fan surfaces.

intermountain basins. In summer 2016, we were funded by USGS to evaluate the Gallatin River watershed as a case study in the continuum of watershed hydrologic storage and the coupling between human and natural systems that are typical for the region. Geochemical weathering imparts a chemical signal on water that is an underutilized source of information about the nature of base flow storage along the mountain-basin continuum. Therefore, we are exploring spatial and temporal patterns of weathering products dissolved in base flow of the Gallatin River and its network, with the purpose of gaining new insight into the patterns of aquifer storage contributing to surface-water base flow across the mountain-basin continuum.

Our **goal** for this research is to apply emerging geochemical methods to improve understanding of hydrologic storage dynamics that are characteristic of the inter-mountain region, in order to improve the ability to detect and predict how climate and land use change influences water supply quantity and quality. By examining the mountain-to-basin transition in the Gallatin Valley (Figure 1a, 1b; see compiled figures following references), we seek to address a key gap in our understanding of inputs from the headwaters that drives river biogeochemistry and may influence observations downstream. A longer term goal is to link these Missouri Headwaters chemistries with downstream results, including a time series of Sr isotope data on the middle Missouri (Yankton Gage; Paces unpublished data), and dissolved inorganic and organic carbon loads (DIC and DOC loads) suggesting land use effects on productivity (Stets *et al* 2014, Stackpoole *et al* 2014).

## 2 Activities to date

*Field sampling.* Surface water samples were collected from Hyalite Canyon (six to seventeen sites) and Gallatin Valley (seven to nine sites) on four dates in 2016 (February, May, July, August; three of these prior to this award), three dates in 2017 (February, May, August), and two dates in 2018 (February, May) (Table 1, Figure 1). These sites reflect the mountain-basin transition from the alpine catchment of Hyalite Creek (a tributary of the East Gallatin River) to sites traversing the Gallatin Valley along the main stem and tributaries of the Gallatin River to its lowest elevation site at Logan, MT (HY7). To represent the endmember geochemistry of the oldest rocks in the lower canyon and at the mountain front, well samples were collected in Hodgeman Canyon (GW2, GW3) just east of Hyalite Canyon on 18 May 2017. Inflows of groundwater to Hyalite Creek from the Madison Group limestones (HY16, HY17) at 1936 m in Hyalite Canyon were sampled in December-January 2017-2018 (K. Kirk MS thesis, MSU 2002). Additional valley wells (GW4-GW9) were sampled in summer 2017 and summer 2018. Final sampling during the coming year in Hyalite Creek and the Gallatin Valley will occur in summer 2018.

During field sampling, water samples were filtered (0.45 µm) and analyzed at sample collection points for temperature, pH, electrical conductivity (EC), specific conductivity (SC), dissolved oxygen (DO), and alkalinity (colorimetric titration). When conditions allowed, discharge measurements were taken using the area velocity method with stream velocities measured using a Marsh McBirney flow meter (Hach). At sites located near a USGS gage, discharge measurements were compared to USGS values and generally taken from the USGS database for a given date. For wells, three well volumes were pumped using home well pumps or a submersible impeller pump prior to sampling. In May 2018 we also sampled at select wells for noble gas and tritium analysis to determine recharge elevations and groundwater age.

*Laboratory Analysis.* Solute concentrations in water samples were determined at Montana State University Environmental Analytical Laboratory (MSU-EAL). Water samples are analyzed for total carbon (TC), inorganic carbon (IC), and total nitrogen (TN) using a Shimadzu combustion analyzer. Major anions ( $\text{NO}_3^-$ ,  $\text{SO}_4^{2-}$ , and  $\text{Cl}^-$ ) were determined by ion chromatography (Dionex 2100). Major ions and trace metals were analyzed by inductively coupled plasma mass spectroscopy (ICP-MS) or optical emission spectroscopy (ICP-OES) at MSU-EAL and at the Montana Bureau of Mines and Geology (MBMG) in Butte, MT. Isotopes of the water molecule were analyzed by undergraduate/post-graduate research assistant Sam Leuthold in 2017-2018, with additional funding from an Montana University System Institute on Ecosystems undergraduate fellowship. Mr. Leuthold is currently working to complete a manuscript on these data by July 2018.

Based on U concentrations, 40 water samples collected during baseflow conditions in February 2016/2017 and August 2016 were prepared for U and Sr isotopic analysis in the MSU Soil Biogeochemistry laboratory as previously described (Ewing *et al* 2015, Paces and Wurster 2014): samples were spiked with  $^{236}\text{U}$ , dried down on a hotplate in a total exhaust clean hood, subject to U and Sr purification using standard ion exchange, and carried to the USGS Southwest Isotope Research Lab (SWIRL) at the Denver Federal Center in Denver, CO. At SWIRL, purified samples were analyzed by thermal ionization mass spectrometry (ThermoFinnegan Triton) to determine the U and Sr isotopic composition and the precise U concentrations of the samples (Ewing *et al* 2015, Paces and Wurster 2014).

MS student Florence Miller led sampling in 2017-2018, along with sample handling and preparation for solute analysis. Ms. Miller also undertook U and Sr isotope analysis preparation prior to mass spectrometric analysis at the Federal Center, and plans to complete her thesis work with submission of one to two manuscripts for publication in July 2018. Post-graduate research assistant Sam Leuthold, post-graduate research assistant Joe Capella and MS student Ethan Wologo continue to support sampling efforts in 2018-2019.

**Table 1. Sample locations and elevations**

Site ID	Location	Elevation (m)	Latitude	Longitude
HY1	Hyalite Creek above reservoir	2087	45.452	-110.959
HY2	Emerald Creek	2063	45.475	-110.954
HY7	Hyalite Creek below reservoir at DNRC gauge 41H 2000	1962	45.501	-110.986
HY3	Lick Creek	1960	45.505	-110.988
HY9	Hyalite Creek below Lick Creek	1941	45.506	-110.993
HY16	Madison limestone spring channel	1936	45.508	-110.998
HY17	Madison limestone spring seep	1931	45.509	-110.997
HY10	Middle Hyalite Creek	1909	45.517	-111.007
HY11	Hyalite Creek at Langohr Logging Road Unnamed creek in terminal glacial moraine	1882	45.527	-111.013
HY13	Meadow Creek	1898	45.524	-111.017
HY12	Buckskin Creek	1889	45.530	-111.013
HY4	Hyalite Creek at Langohr's Campground	1861	45.535	-111.017
HY8	Moser Creek	1871	45.537	-111.016
HY14	Hyalite Creek below Moser Creek	1854	45.539	-111.020
HY15	Hyalite Creek above Practice Rock	1729	45.554	-111.062
HY5	Hyalite Creek at Practice Rock	1807	45.542	-111.034
HY6	Hyalite Creek at USGS gauge 06050000	1690	45.563	-111.072
SD1	Sourdough Creek	1926	45.524	-110.926
GV1	Hyalite/Middle Creek at S. 19th	1618	45.453	-110.958
GV2	S. Cottonwood Creek	1596	45.577	-111.145
GV3	Gallatin River at USGS gauge 06043500	1580	45.510	-111.259
GV4	Gallatin River at Axtell Bridge	1473	45.624	-111.211
GV5	Hyalite/Middle Creek at Monforton School Rd.	1428	45.686	-111.169
GV6	E. Gallatin River at USGS gauge 06048650	1405	45.726	-111.066

GV9	E. Gallatin River at Belgrade	1321	45.838	-111.160
GV10	E. Gallatin River at Dry Creek Rd.	1296	45.874	-111.233
GV8	Gallatin River at Manhattan	1294	45.859	-111.229
GV7	Gallatin River at USGS gauge 06052500	1246	45.886	-111.441
GW2	Hodgman Canyon - gneiss spring	1704	45.585	-111.067
GW3	Hodgman Canyon - gneiss well	1692	45.586	-111.067
GW4	Hyalite Creek alluvial fan well	1641	45.583	-111.091
GW7	Mystic Heights subdivision well #2	1630	45.594	-111.046
GW6	Mystic Heights subdivision well #3	1622	45.596	-111.046
GW5	Hitching Post subdivision well	1543	45.631	-111.028
GW1	Bozeman Trail Rd. well	1517	46.661	-111.000
GW8	MBMG Monitoring well GWIC ID: 266832	1303	45.846	-111.264
GW9	MBMG Monitoring well GWIC ID: 266803	1288	45.875	-111.265
EF	Ellis Farm soil sample	1522	45.657	-111.974
PF	Post Farm soil sample	1465	45.673	-111.151
LF	Lutz Farm soil sample	1414	45.818	-111.052

### 3 Results to date – Hyalite Canyon

#### 3.1 Elemental composition

Concentrations of Sr, U, and Ca, along with Ca/Sr ratios, generally increased moving downstream Hyalite Creek (Tables 2 and 4, Figures 5 and 6). The upper Hyalite Creek tributaries Hyalite Creek (HY1) and Emerald Creek (HY2) had Sr concentrations of below detection at 0.01 (mean  $0.01 \pm 0.01$ ) and 0.03 (mean  $0.03 \pm 0.02$ ) ppm respectively. Hyalite Creek below Hyalite Reservoir had slightly increased Sr concentrations at HY7 of 0.04 to 0.03 (mean  $0.03 \pm 0.01$ ) and HY9 0.04 ppm. Samples taken from sedimentary tributary Lick Creek had a high Sr concentration of 0.08 to 0.15 (mean  $0.12 \pm 0.03$ ) ppm. Sample sites in the middle elevations of Hyalite Creek reflected the confluence of tributaries draining sedimentary rocks with possible groundwater discharge; in this zone we saw increased average Sr concentrations for HY10, HY11, and HY4 of 0.04, 0.04, and 0.04 to 0.06 (mean  $0.05 \pm 0.01$ ) ppm respectively. Tributaries Buckskin Creek, 'Meadow Creek', and Moser Creek (HY12, HY13, HY8) had relatively high Sr concentrations of 0.14, 0.08, and 0.14 to 0.16 (mean  $0.15 \pm 0.02$ ) ppm respectively. Sample sites in the lower reaches of Hyalite Creek where Archean gneiss is mapped at the surface (Figure 4) had an average Sr concentration that remained steady with distance downstream to the mouth of the canyon, with values of 0.04 to 0.05 (mean  $0.04 \pm 0.02$ ) ppm for sites HY14, HY15, HY5, and HY6. The Hodgeman Canyon groundwater samples in the Archean gneiss revealed similar Sr concentrations of 0.05 and 0.06 ppm for GW2 and GW3 respectively. The alluvial fan well (GW4) at the mouth of Hyalite Canyon had increased Sr concentration values of 0.11 ppm. Overall, Sr concentration increased moving through the middle elevations of Hyalite Creek, but remained relatively constant or the middle and lower elevations of Hyalite Creek. Overall, variation in Sr concentration did not follow seasonal trends.

Similar to Sr, U concentrations trended to increase moving downstream in Hyalite Creek (Tables 2 and 4, Figure 5b). Sites sampling the upper Hyalite Creek tributaries (HY1 and HY2) had U concentrations of 0.005 to 0.015 (mean  $0.01 \pm 0.006$ ) and 0.011 to 0.014 (mean  $0.03 \pm 0.001$ ) ppb respectively. Below Hyalite Reservoir U concentrations increased to 0.023 to 0.242 (mean  $0.13 \pm 0.154$ ) and 0.039 to 0.080 (mean  $0.06 \pm 0.029$ ) ppb at HY7 and HY9 respectively.

Lick Creek (HY3), draining rocks mapped as Cretaceous sedimentary units, had a higher U concentration of 0.160 to 0.713 (mean  $0.40 \pm 0.266$ ) ppb. Variation in U concentration did not follow any seasonal trends. Water draining the Madison Group limestones had U concentrations ranging from 0.04 to 0.42 ppb at HY16 and HY17. The variation is likely due to snowmelt dilution due to sampling on above freezing winter days in December, January, and March. Downstream of the Madison Group, samples taken in the middle elevations of Hyalite Creek had U concentrations of 0.079 to 0.114 (mean  $0.10 \pm 0.025$ ), 0.11, and 0.069 to 0.186 (mean  $0.13 \pm 0.057$ ) at HY10, HY11, and HY4 respectively. Tributaries draining sedimentary units based on surficial geologic mapping in the middle elevations of Hyalite Canyon (Buckskin and Moser Creeks, HY12 and HY8) had higher U concentrations of 0.59 and 0.542 to 0.596 (mean  $0.57 \pm 0.038$ ) ppb respectively, with the exception of 'Meadow' Creek (HY13) which had a lower U concentration of 0.02 ppb, likely due to the reducing conditions of the meadow's peat bog environment. Moving into the lower canyon with surficial geology of Archean gneiss, sample sites HY14 and HY15 had U concentrations of 0.077 and 0.083, respectively. Below the shear zone in the Archean gneiss in the lower elevations of Hyalite Canyon, average U concentrations increased to 0.152 to 0.554 (mean  $0.29 \pm 0.227$ ) and 0.121 to 0.791 (mean  $0.52 \pm 0.351$ ) ppb at sample sites HY5 and HY6 respectively, with higher U concentrations associated with February sampling dates and lower concentrations associated with August sampling dates. The Hodgeman Canyon cistern and well (GW2 and GW3), hosted in the Archean gneiss, had U concentrations of 0.353 and 0.364 ppb. The upper alluvial fan well (GW4) at the mouth of Hyalite Canyon had a U concentration of 0.233 ppb.

### 3.2 $^{87}\text{Sr}/^{86}\text{Sr}$ Ratios

#### 3.2.1 $^{87}\text{Sr}/^{86}\text{Sr}$ ratios in regional rocks and waters

Many representative local rock units and streams have already been analyzed for  $^{87}\text{Sr}/^{86}\text{Sr}$  values, with a partial list of available  $^{87}\text{Sr}/^{86}\text{Sr}$  values presented in Table 4. The same Absaroka volcanics rock unit that is present in Hyalite Canyon was found to have  $^{87}\text{Sr}/^{86}\text{Sr}$  values ranging from 0.70433-0.70826 (Feeley and Cosca 2003, Lindsay and Feeley 2003, Hiza 1999). Waters draining Eocene age Absaroka Volcanics in the nearby Clark's Fork drainage have been measured to have  $^{87}\text{Sr}/^{86}\text{Sr}$  values ranging from 0.704-0.705 (Horton *et al* 1999). Carbonates in the greater Yellowstone National Park region were found to have an average  $^{87}\text{Sr}/^{86}\text{Sr}$  isotope ratio of 0.71062 (Kharaka *et al* 1991), with the Madison limestone formation having an average  $^{87}\text{Sr}/^{86}\text{Sr}$  isotope ratio of 0.708834 (Moore-Nall, 2016). Paleozoic sedimentary catchments in the Clark's Fork drainage yield waters with  $^{87}\text{Sr}/^{86}\text{Sr}$  values ranging from 0.704-0.7075 ( exact values not provided; Horton *et al.* 1999). Archean age granitics, including the neighboring Beartooth mountains, had  $^{87}\text{Sr}/^{86}\text{Sr}$  values ranging from 0.70617-0.78304 with a median of 0.73558 and average of 0.71200 (Wooden and Mueller 1988). Precambrian granitic gneiss rock units in the Clark's Fork yielded water  $^{87}\text{Sr}/^{86}\text{Sr}$  values of 0.721-0.732 ( exact values not provided; Horton *et al.* 1999). The average  $^{87}\text{Sr}/^{86}\text{Sr}$  ratio for all river water is 0.712, ranging from 0.704 to 0.922, illustrating predicted range of  $^{87}\text{Sr}/^{86}\text{Sr}$  values in natural waters (Capo *et al* 1998).

#### 3.2.2 Measured $^{87}\text{Sr}/^{86}\text{Sr}$ values in Hyalite Canyon water samples

Overall,  $^{87}\text{Sr}/^{86}\text{Sr}$  ratios increased moving downstream Hyalite Creek, with a slight decrease in the vicinity of the Madison Group; seasonal variation was limited (Tables 2 and 4, Figure 7). Samples from the upper tributaries of Hyalite Creek (HY1, HY2) had  $^{87}\text{Sr}/^{86}\text{Sr}$  values of 0.70883 – 0.70921 (mean  $0.70895 \pm 0.00018$ ) and 0.70890 – 0.70895 (mean  $0.70891 \pm 0.00003$ ) respectively. Sample sites from Hyalite Creek below Hyalite Reservoir (HY7 and HY9) had slightly lower  $^{87}\text{Sr}/^{86}\text{Sr}$  values of 0.70871 – 0.70870 (mean  $0.70871 \pm 0.00001$ ) and 0.70853 – 0.70859 (mean  $0.70856 \pm 0.00004$ ) respectively. Lick Creek (HY3), had  $^{87}\text{Sr}/^{86}\text{Sr}$

ratio of 0.70846 – 0.70859 (mean 0.70849 ± 0.00006). The Madison aquifer water samples (HY16 and HY17) both had  $^{87}\text{Sr}/^{86}\text{Sr}$  values of 0.70835. The mean  $^{87}\text{Sr}/^{86}\text{Sr}$  ratios of samples taken from the middle elevations of Hyalite Creek, below the confluence the Madison aquifer increased slightly to 0.70857 – 0.70860 (mean 0.70859 ± 0.00002), 0.70861, and 0.70866 – 0.70879 (mean 0.70870 ± 0.00006  $\sigma$ ) at HY10, HY11, and HY4 respectively. Middle elevation tributaries Buckskin (HY12) and Moser Creeks (HY8), had elevated  $^{87}\text{Sr}/^{86}\text{Sr}$  ratios of 0.71146 and 0.71143 – 0.71181 (mean 0.71146 ± 0.00027) respectively. ‘Meadow’ Creek had a  $^{87}\text{Sr}/^{86}\text{Sr}$  ratio of 0.70893. Entering lower Hyalite Creek with surficial geology of Archean gneiss, HY14 and HY15 had  $^{87}\text{Sr}/^{86}\text{Sr}$  ratios of 0.70874 and 0.70885. Below the shear zone in the Archean gneiss mean  $^{87}\text{Sr}/^{86}\text{Sr}$  ratios increased to 0.70973 – 0.72242 (mean 0.71031 ± 0.00095) and 0.70998 – 0.71202 (mean 0.71080 ± 0.00097) at HY5 and HY6 respectively. Groundwater samples from the Archean gneiss (GW2 and GW3) had high  $^{87}\text{Sr}/^{86}\text{Sr}$  ratios of 0.73687 and 0.74497. The alluvial well at the mouth of Hyalite Canyon had a  $^{87}\text{Sr}/^{86}\text{Sr}$  ratio of 0.71121, similar to the main stem of Hyalite Creek at the mountain front sample sites. Overall there was no trend in seasonal variation in  $^{87}\text{Sr}/^{86}\text{Sr}$ , except for sample sites downstream of the Archean gneiss shear zone (HY5 and HY6), which consistently displayed higher  $^{87}\text{Sr}/^{86}\text{Sr}$  for February sample dates than for August sample dates.

### 3.3 UAR values

UAR values varied from 1.497 to 5.285 across our sample locations in Hyalite Canyon and showed limited variation seasonally (Table 5, Figure 9). In samples from the upper Hyalite Creek tributaries (HY1, HY2) there was a relatively low UAR of 1.616 – 1.722 (mean 1.67 ± 0.05) and 1.629 – 1.691 (mean 1.66 ± 0.03) respectively (Tables 3 and 5, Figure 9). In Hyalite Creek sample sites below Hyalite Reservoir the UAR remained relatively low with values of 1.591 – 1.621 (mean 1.61 ± 0.02) and 1.598 – 2.121 (mean 1.86 ± 0.37  $\sigma$ ) for HY7 and HY9 respectively. Sedimentary derived tributary Lick Creek (HY3) had a UAR of 1.497 – 1.570 (mean 1.61 ± 0.03). The Madison aquifer (HY16, HY17) had high UAR’s of 5.23 and 5.29, values indicative of ground water. Below the contribution zone of the Madison aquifer, samples taken in the middle reaches of Hyalite Creek had increased UARs of 2.957 – 2.958 (mean 2.96 ± 0.0004), 2.970, and 2.977 – 3.195 (mean 3.06 ± 0.10) at HY10, HY11, and HY4 respectively, indicating the of mixing Madison aquifer groundwater with Hyalite Creek. Sedimentary tributaries Buckskin Creek, ‘Meadow Creek’, and Moser Creek (HY12, HY13, and HY8) had slightly elevated UAR values of 2.69, 1.96, and 2.236 – 2.241 (mean 2.24 ± 0.003) respectively. Moving into the Archean gneiss basement geology in the lower reaches of Hyalite Creek, the UAR values remained high, measured at 3.05 and 2.94 at HY14 and HY15 respectively. Below the shear zone in the Archean gneiss, there was a decrease in UAR to 1.788 – 2.128 (mean 2.00 ± 0.19) and 1.691 – 1.966 (mean 1.80 ± 0.15) at HY5 and HY6. Groundwater samples (GW2 and GW3) from the Archean gneiss end member sample site in Hodgman canyon had UAR values of 1.85 and 1.49, similar to the lower, Archean gneiss hosted reaches of Hyalite Creek. Groundwater found in the alluvial aquifer at the mouth of Hyalite Canyon had a UAR of 1.78, remaining consistent with surface water samples from the lower reaches of Hyalite Creek. Overall there was no consistent seasonal variation in UAR, except for with site HY4, HY5, and HY6. Sample site HY4 displayed slightly higher UAR in February sample dates than in August sample dates, while sites HY5 and HY6 displayed slightly lower UAR in February sample dates compared to August sample dates.

## 4 Results to date – Gallatin Valley

Please see Figures 12-18 for preliminary results from the Gallatin Valley samples. Generally, a correlation between increasing chloride and nitrate concentrations with distance down valley suggests influence of septic waste in local surface waters and groundwater (Figure 12).

Concentrations of U and Sr, along with  $^{87}\text{Sr}/^{86}\text{Sr}$  ratios, increase down valley, suggesting influence of infiltration through soils and possible dissolution of aquifer material (Figures 13, 15, 16). Consistent with this, Ca/Sr ratios plateau at a value of  $\sim 200$  (Figure 14) and UAR values do not increase, remaining under 2.0 (Figure 17).

## 5 Testing hypotheses – discussion of results and next steps

In the Upper Missouri River watershed, mountain-basin transitions commonly transform seasonal discharge patterns and are likely to strongly influence river geochemistry. These transitions have not been well characterized in previous studies, though the importance of similar gradients in watershed dynamics has been documented (Capell *et al* 2011, Covino and McGlynn 2007).

Accordingly we asked: *How does streamflow chemistry reflect fundamental changes in groundwater dynamics between upland catchments and distributive fluvial systems in intermountain basins of the upper Missouri River watershed?*

In our proposal, we identified four specific hypotheses developed to address this broader question. Our initial work addresses two of these and leads us to follow-up work in 2018-2019.

**Hypothesis 1.** *The configuration of rock units in Hyalite Canyon will determine geochemistry of baseflow waters in the mountain headwater section of Hyalite Creek, resulting in increasing limestone influence with distance downstream, and a distinctive geochemical progression reflecting increasing rock age and changing rock character.*

Our results support the resulting prediction that as limestone dissolution increasingly affects solute loads with distance downstream, waters will show increasing Ca/Sr, alkalinity, and conductivity. In addition, our isotope results support the prediction that distinct Sr and U isotopic patterns will be evident in these samples based on previous results for host lithologies and associated waters in the region (Horton *et al* 1999, Paces *et al* 2015, Frost and Toner 2004); however our data to date do not resolve whether deeper weathering zones would dominate solute fluxes (Brooks *et al* 2015). We demonstrated that the previously suggested influx of longer flowpath water at Langhor's Campground (HY4) actually extends from the Madison inflows (HY16-HY17), and the suggested exchange of water revealed by isotopic and concentration data in lower Hyalite Canyon can be quantified as inmixing of water resembling the Hodgeman's Canyon well water. Thus our results provide novel insight regarding the hydrology of this system. We successfully tested our understanding of the processes at play in Hyalite Canyon using longitudinal sampling in Hyalite Creek during summer 2017, as well as further exploration for springs and wells capturing endmember waters. Water isotope values additionally revealed seasonal, elevational and soil dynamics that influence streamflow character.

**Hypothesis 2.** *Across the mountain-basin transition, controls on geochemical mixing will exhibit a fundamental change from convergent flow through bedrock derived sources to divergent flow through alluvial/soil sources.*

Our results support our prediction of strong contrast in  $^{87}\text{Sr}/^{86}\text{Sr}$  values but not  $^{234}\text{U}/^{238}\text{U}$  activity ratios from crystalline basement sources compared to Mesozoic to Cambrian limestone sources, both by virtue of their geochemical character and their likely contrasting flow character (fracture flow vs. karst) (Horton *et al* 1999, Paces *et al* 2015). However, the variation in UAR values within Hyalite Canyon reveals flowpath length variation consistent with groundwater inflows from the Madison Group limestones (UAR $\sim$ 5).

Within the Gallatin Valley depositional basin, we expected that divergent hydrologic pathways would become more important, as infiltration through carbonate-rich soils at lower elevations and flow through aquifers containing limestone alluvium influence shallow groundwater. We thought that geochemical indication of weathering effects would be enhanced in irrigation return-flow to adjacent rivers. We therefore expected the following trends with elevation in the Gallatin Valley: an increase in Ca/Sr ratios accompanied by more uniform, intermediate  $^{87}\text{Sr}/^{86}\text{Sr}$  ratios reflecting this mixture of sources, and  $^{234}\text{U}/^{238}\text{U}$  activity ratios that mix limestone dissolution values approaching unity (secular equilibrium) with soil infiltration values of  $\sim 1.5$  as observed in similar semiarid soil environments (Sharp *et al* 2003). Instead, we observed that UAR values were steady through the valley (Figure 17), suggesting mixing of mountain front sources, while U concentrations and  $^{87}\text{Sr}/^{86}\text{Sr}$  values rose, suggesting inmixing of recharge from Archean rocks and/or recharge from Tertiary sediments lower in the valley (Michalek & Custer, personal communication). At the same time, our targeted sampling of wells in the valley and longitudinal sampling in the Gallatin River and tributaries during 2017-2018 has revealed that these trends likely also reflect influence of mixing in the valley system through irrigation and infiltration through soils.

Generally, we expected the combination of Sr and U isotope values to be an effective tool for parsing the relative influence of infiltration and storage in the basin hydrologic system on altering the original chemistry of recharge delivered from the mountain system. Increases in U concentration and  $^{87}\text{Sr}/^{86}\text{Sr}$  values with flow through the valley may support this prediction. This idea was further tested through direct examination of U and Sr isotope values in soil carbonate from variable age fans and substrate (loess vs. alluvium) in the valley during summer 2017 (Figure 18), supporting the interpretation of an infiltration component. Water isotope measures in soils revealed influence of evaporation (Orlowski *et al* 2016, Oerter *et al* 2014) and will be used to evaluate seasonal water dynamics in soils that may be influenced by differential mobility with soil development (Brooks 2015, Brooks *et al* 2015, Evaristo *et al* 2015).

**Hypothesis 3.** *Upland runoff will more directly reflect surficial geology and dominate upland surface waters in the mountain headwaters as well as during snowmelt and major rainfall events.* Our initial results for the runoff period of May 2016 suggest that in Hyalite Canyon, the baseflow signal is diluted but relatively consistent with other sampling dates, with the exception of lower Hyalite Canyon where the local Archean rock signal was strengthened. We interpret this as increase flow through fractured Archean rocks and soils with snowmelt. In addition, water isotope results revealed that proximal snowmelt waters reflecting local elevation were most influential in late winter (February) samples.

**Hypothesis 4.** *In the basin, infiltration through soils will strongly influence the character of water in the shallow aquifer, such that fall-winter flows (primarily baseflow) are enhanced by infiltration geochemistry associated with summer irrigation.* Our Sr isotope analysis of pedogenic carbonate in valley soils (Figure 18) reveals that down-valley waters could be influenced by infiltration through soils. In order to trace water movement through soils in the valley, we measured the strontium isotopic composition ( $^{87}\text{Sr}/^{86}\text{Sr}$  ratios) of pedogenic carbonate in three soil profiles on MSU properties that traverse loess-derived soils across the Gallatin Valley (Post Farm, Ft. Ellis Farm, Lutz Farm; Figure 1). These samples were collected with a Giddings probe and prepared using 1M acetic acid extraction. To our knowledge, these measures are the first  $^{87}\text{Sr}/^{86}\text{Sr}$  values for pedogenic carbonate in soils of the Gallatin Valley.

Two important interpretations emerge from these data. First, the distinct Sr isotopic composition of the Fort Ellis pedogenic carbonate (weighted average  $^{87}\text{Sr}/^{86}\text{Sr} = 0.71002$ ), along with higher total carbon content, correspond to greater carbonate accumulation from a distinct loess mixture

with longer duration of weathering on this older fan surface. On the younger Lutz and Post Farm surfaces, Sr isotopic ratios are higher and similar (weighted average  $^{87}\text{Sr}/^{86}\text{Sr} = 0.71128$  and  $0.71122$ , respectively). Second, these  $^{87}\text{Sr}/^{86}\text{Sr}$  values correspond to trends in Gallatin Valley groundwater; with distance down-valley in surface waters and groundwaters, increasing Sr concentrations and  $^{87}\text{Sr}/^{86}\text{Sr}$  values that approach  $0.71183$  suggest that water movement through these calcareous loess soils may contribute to the geochemistry and water balance of groundwater in the valley aquifer.

## 6 Products

### Manuscripts in preparation

Miller, F.R., Ewing, S.A., Payn, R.A., Paces, J.B., and Custer, S. (in preparation). Sr and U isotopes reveal the influence of lithologic structure on surface-groundwater interaction along a mountain stream (Hyalite Canyon, MT). Manuscript in preparation for *Water Resources Research*.

Miller, F.R., Ewing, S.A., Payn, R.A., Paces, J.B., and Custer, S. (in preparation). Sr and U isotopes suggest the influence of water recharge along the mountain front and infiltration through soils on surface and groundwater composition of intermountain basins (Gallatin Valley, MT). Manuscript in preparation.

Leuthold, S., Ewing, S.A., Payn, R., Miller, F., Klassen, J., Paces, J. (In preparation) Late winter connectivity of soils and streamflow in Hyalite Canyon, Montana. In preparation for *Journal of Hydrology*.

### Thesis in preparation

Miller, F.R. (expected completion July 2018). Sr and U isotopes reveal the influence of lithologic structure on surface-groundwater interaction along the mountain headwaters and intermountain basin process domains (Hyalite Canyon and Gallatin Valley, MT). Thesis in preparation.

### Presentations (\*presenting author)

\*Ewing, S.A., Miller, F.R., Payn, R.A., Leuthold, S., and Paces, J.B. (2017). Using weathering and solute geochemistry to water sources of base flow water supply across mountain-basin transitions in the Upper Missouri watershed. Poster presentation at 2017 Gordon Research Conference, Catchment Science: Interactions of Hydrology, Biology, and Geochemistry, Lewiston, ME, 25-30 Jun.

\*Miller, F.R., Ewing, S.A., Paces, J.B., Sturn, E., Custer, S., Michalek, T., and Payn, R. (2017). Strontium and uranium isotopes suggest changing water storage and groundwater exchange along a mountain stream (Hyalite Canyon, Montana). Oral presentation at 2017 annual meeting, AWRA Montana section, Helena, MT, 19-20 Oct.

Miller, F.R., \*Ewing, S.A., Payn, R.A., Paces, J.B., and Custer, S. (2018). Strontium and uranium isotopes reveal surface water-groundwater interaction as a function of lithology along a mountain stream (Hyalite Canyon, Montana). Oral presentation at 2018 European Geochemical Union, Vienna, Austria, 8-13 Apr.

\*Miller, F.R., Ewing, S.A., Payn, R.A., Paces, J.B., Leuthold, S., Michalek, T., and Custer, S. (2018). Sr and U isotopes reveal the influence of lithologic structure on surface-groundwater interaction along a mountain stream (Hyalite Canyon, MT). Oral presentation at 2018 Goldschmidt conference, Boston, MA, 12-17 Aug.

## 7 References

- Brooks J R 2015 Water, bound and mobile *Science* (80-. ). **349** 138–9 Online:  
<http://www.sciencemag.org/cgi/doi/10.1126/science.aac4742>
- Brooks P D, Chorover J, Fan Y, Godsey S E, Maxwell R M, McNamara J P and Tague C 2015 Hydrological partitioning in the critical zone: Recent advances and opportunities for developing transferable understanding of water cycle dynamics *Water Resour. Res.* **51** 6973–87
- Capell R, Tetzlaff D, Malcolm I A, Hartley A J and Soulsby C 2011 Using hydrochemical tracers to conceptualise hydrological function in a larger scale catchment draining contrasting geologic provinces *J. Hydrol.* **408** 164–77 Online:  
<http://dx.doi.org/10.1016/j.jhydrol.2011.07.034>
- Capo R C, Stewart B W and Chadwick O A 1998 Strontium isotopes as tracers of ecosystem processes : Theory and methods processes : theory and methods *Geoderma* **82** 197–225
- Covino T P and McGlynn B L 2007 Stream gains and losses across a mountain-to-valley transition: Impacts on watershed hydrology and stream water chemistry *Water Resour. Res.* **43** 1–14
- Evaristo J, Jasechko S and McDonnell J J 2015 Global separation of plant transpiration from groundwater and streamflow *Nature* **525** 91–4 Online:  
<http://www.nature.com/doi/10.1038/nature14983>
- Ewing S A, Paces J B, O'Donnell J A, Jorgenson M T, Kanevskiy M Z, Aiken G R, Shur Y L, Harden J W, Striegl R G, O'Donnell J A, Jorgenson M T, Kanevskiy M Z, Aiken G R, Shur Y L, Harden J W and Striegl R G 2015 Uranium isotopes and dissolved organic carbon in loess permafrost: modeling the age of ancient ice *Geochim. Cosmochim. Acta* **152** 143–65
- Feeley T C and Cosca M A 2003 Time vs . composition trends of magmatism at Sunlight volcano , Absaroka volcanic province , Wyoming *Geol. Soc. Am. Bull.* 714–28
- Frost C D and Toner R N 2004 Strontium isotopic identification of water-rock interaction *Ground Water* **42** 418–32
- Hiza M M 1999 *The geochemistry and geochronology of the Eocene Absaroka volcanic province, northern Wyoming and southwest Montana, USA* (Oregon State University)
- Horton T W, Chamberlain C P, Fantle M and Blum J D 1999 Chemical weathering and lithologic controls of water chemistry in a high-elevation river system: Clark's Fork of the Yellowstone river, Wyoming and Montana *Water Resour. Res.* **35** 1643–55
- Kharaka Y K, Mariner R H, Bulled R D, Kennedy B M and Sturchio N C 1991 *Geochemical Investigations of Hydraulic connections between the Corwin Springs Know Geothermal Resources Area and Adjacent Parts of Yellowstone National Park, in Sorrey, M.L., Effects of potential geothermal development in the Corwin Springs Known Geother*
- Lindsay C R and Feeley T C 2003 Magmagenesis at the Eocene Electric Peak – Sepulcher Mountain complex , Absaroka Volcanic Province , USA **67** 53–76
- Oerter E, Finstad K, Schaefer J, Goldsmith G R, Dawson T and Amundson R 2014 Oxygen isotope fractionation effects in soil water via interaction with cations (Mg, Ca, K, Na) adsorbed to phyllosilicate clay minerals *J. Hydrol.* **515** 1–9 Online:  
<http://dx.doi.org/10.1016/j.jhydrol.2014.04.029>

- Orlowski N, Breuer L and McDonnell J J 2016 Critical issues with cryogenic extraction of soil water for stable isotope analysis *Ecohydrology* **9** 3–10
- Paces J B, Long A J and Koth K 2015 *Potential Application of Radiogenic Isotopes and Geophysical Methods to Understand the Hydrothermal System of the Upper Geyser Basin , Yellowstone National Park*
- Paces J B and Wurster F C 2014 Natural uranium and strontium isotope tracers of water sources and surface water-groundwater interactions in arid wetlands - Pahrnagat Valley, Nevada, USA *J. Hydrol.* **517** 213–25
- Sharp W D, Ludwig K R, Chadwick O A, Amundson R and Glaser L L 2003 Dating fluvial terraces by  $^{230}\text{Th}/\text{U}$  on pedogenic carbonate, Wind River Basin, Wyoming *Quat. Res.* **59** 139–50 Online: <http://linkinghub.elsevier.com/retrieve/pii/S0033589403000036>
- Stackpole S M, Stets E G and Striegl R G 2014 The impact of climate and reservoirs on longitudinal riverine carbon fluxes from two major watersheds in the Central and Intermontane West *J. Geophys. Res. Biogeosciences* 1–16
- Stets E G, Kelly V J and Crawford C G 2014 Science of the Total Environment Long-term trends in alkalinity in large rivers of the conterminous US in relation to acidification , agriculture , and hydrologic modification **489** 280–9
- Wooden J L and Mueller P A 1988 Pb, Sr, and Nd isotopic compositions of a suite of Late Archean, igneous rocks, eastern Beartooth Mountains: implications for crust-mantle evolution *Earth Planet. Sci. Lett.* **87** 59–72

## Hyalite Canyon Tables and Figures

Table 2. Geologic unit descriptions of Hyalite Canyon (Vuke et al. 2007; Vuke et al. 2003).

Geologic Unit	Name	Description
Tav	Absoraka Volcanics (Eocene)	Slightly porphyritic andesite with plagioclase, augite, and hypersthene phenocrysts in individual flows interlayered with stratified flow breccias.
Kcof	Cody Shale and Frontier Formation, undivided (Upper Cretaceous)	Cody Shale—Mudstone interbedded with siltstone and very fine grained sandstone. Frontier Formation—thick-bedded to massive sandstone with subordinate siltstone.
Kmfr	Mowry Shale through Fall River Sandstone, Undivided (Upper Cretaceous)	Mowry Shale: Interbedded, siliceous, very fine to fine-grained sandstone, siltstone, shale. Thermopolis Shale: Bentonitic shale and several beds of bentonite. Fall River Sandstone: Brownish-gray, thin bedded, argillaceous; fine-grained, quartz sandstone.
Kk	Kootenai Formation (Lower Cretaceous)	Upper: Light gray gastropod-rich limestone. Middle: Shale and mudstone interbedded with sandstone. Basal: conglomeratic, chert-rich sandstone or conglomerate.
Jme	Morrison Formation and Ellis Group, undivided (Middle and Upper Jurassic)	Morrison Formation (Jurassic)— mudstone, shale, and siltstone with thin sandstone, siltstone, and limestone beds. Ellis Group (Jurassic) - Swift Sandstone— calcareous quartz sandstone. Rierdon Limestone— limestone and calcareous shale. Some quartz and chert grains. Sawtooth Formation—Upper: Fossiliferous mudstone; thin-bedded carbonaceous siltstone, limestone, and dolomite. Lower: Conglomeratic quartz and chert sandstone
IPMqa	Quadrant Sandstone and Amsden Formation, undivided (Upper Mississippian and Pennsylvanian)	Quadrant Sandstone (Pennsylvanian): Quartzite, well sorted quartzose, sandstone, and dolomite. Amsden formation: Interbedded grayish pink to light-red mudstone, limestone, and siltstone.
Mm	Madison Group, undivided (Upper Mississippian)	Limestone and dolomitic limestone.
MDtj	Three Forks Formation and Jefferson Formation, undivided (Mississippian and Upper Devonian)	Dolomite
Cgf		
Aqfg	Quartzofeldspathic gneiss (Paleoprotozoic and Archean)	Includes plagioclase-microcline-quartz biotite gneiss, plagioclase-quartz-biotite gneiss, banded biotite gneiss, aluminous gneiss and schist, gedrite gneiss, and garnet gneiss
XAah	Amphibolite and hornblende gneiss (Paleoprotozoic and Archean)	Paleoprotozoic and Archean age; Gray to black, medium-grained, hypidiomorphic, equigranular, moderately foliated to well-foliated hornblende-plagioclase gneiss and amphibolite.

**Table 3.** Average chemical composition of each site. For Individual measurements see Table 5

Site ID	Description	Ca (mg/L)	1SD	Sr (mg/L)	1SD	Ca/Sr	$\sigma$	U (ng/g)	1SD	$^{87}\text{Sr}/^{86}\text{Sr}$	2 $\sigma$	$^{234}\text{U}/^{238}\text{U}$	2 $\sigma$	Alkalinity (mg CaCO <sub>3</sub> /L)	1SD
HY1	Hyalite Creek above reservoir	3.60	0.35	0.01	0.010	181	6	0.01	0.006	0.70895	0.00018	1.67	0.05	17	2
HY2	Emerald Creek	5.43	0.56	0.03	0.002	183	10	0.01	0.001	0.70891	0.00003	1.66	0.03	27	3
HY7	Hyalite Creek below reservoir at DNRC gauge 41H 2000	8.17	1.65	0.03	0.005	240	13	0.13	0.154	0.70871	0.00001	1.61	0.02	23	16
HY3	Lick Creek	36.94	11.54	0.12	0.032	306	20	0.40	0.266	0.70849	0.00006	1.52	0.03	183	56
HY9	Hyalite Creek below Lick Creek	8.52		0.04		243		0.06	0.029	0.70856	0.00004	1.86	0.37	45	
HY16	Madison limestone spring channel							0.42		0.70835		5.23			
HY17	Madison limestone spring seep							0.26	0.196	0.70835		5.26	0.04		
HY10	Middle Hyalite Creek	11.00		0.04		259		0.10	0.025	0.70859	0.00002	2.96	0.00	46	
HY11	Hyalite Creek at Langohr Logging Road	11.00		0.04		259		0.09		0.70861		2.97		49	
HY13	Unnamed creek in terminal glacial moraine meadow	14.60		0.08		192		0.02		0.70893		1.96		88	
HY12	Buckskin Creek	68.60		0.14		504		0.59		0.71146		2.69		212	
HY4	Hyalite Creek at Langohr's Campground	13.76	2.71	0.05	0.007	277	17	0.13	0.057	0.70870	0.00006	3.06	0.10	39	12
HY8	Moser Creek	42.10	7.07	0.15	0.018	285	14	0.57	0.038	0.71162	0.00027	2.24	0.00	137	43
HY14	Hyalite Creek below Moser Creek	11.60		0.04		267		0.08		0.70874		3.05		45	
HY15	Hyalite Creek above Practice Rock	11.60		0.04		270		0.08		0.70885		2.94		73	
HY5	Hyalite Creek at Practice Rock	11.45	1.42	0.04	0.003	265	17	0.29	0.227	0.71031	0.00095	2.00	0.19	61	26
HY6	Hyalite Creek at USGS gage 06050000	12.24	1.81	0.05	0.004	270	16	0.52	0.351	0.71080	0.00097	1.80	0.15	57	6
SD1	Sourdough Creek							0.02		0.70862		2.05			
GW2	Hodgman Canyon - gneiss spring	15.30		0.05		321		0.35		0.73687		1.85		37	
GW3	Hodgman Canyon - gneiss well	27.00		0.06		467		0.36		0.74497		1.49		146	
GW4	Hyalite Creek alluvial fan well	42.90		0.11		383		0.23		0.71221		1.78		139	

Table 4. Compilation of strontium isotope ratios in literature on associated or surrounding rock units and catchments.

Unit Description	$^{87}\text{Sr}/^{86}\text{Sr}$	Source
Absaroka Volcanic rock units (WY)	0.70433 - 0.70826	Feeley & Cosca, 2003; Lindsay & Feeley, 2003
Absaroka Volcanics (MT and WY)	0.70543	Hiza, 1999
Continental volcanic rock units (average)	0.702 - 0.714	Capo et al., 1998
Carbonates (average, Yellowstone National Park)	0.71062	Khraka et al., 1991
Madison Limestone Formation (Bighorn Basin, MT)	0.70883	Moore-Nall, 2016
Archean age granitics (Beartooth Mountains, MT)	0.70617 - 0.78304 (mean 0.73267)	Wooden & Mueller, 1988
Average river water	0.704 - 0.922 (average 0.712)	Capo et al., 1998
Catchments draining Eocene Absaroka volcanics (Clark's Fork, MT)	0.704 - 0.705	Horton et al., 1999
Catchments draining paleozoic sedimentary units (Clark's Fork, MT)	0.704 - 0.708	Horton et al., 1999
Catchments draining precambrian granitic gneiss units (Clark's Fork, MT)	0.721 - 0.732	Horton et al., 1999

**Table 5. Complete chemical data**

Site ID	Description	Sample Date	Ca (mg/L)	Sr (mg/L)	U (ng/g)	±2σ	Ca/Sr	<sup>87</sup> Sr/ <sup>86</sup> Sr	±2σ	<sup>234</sup> U/ <sup>238</sup> U	±2σ	Alkalinity (mg CaCO <sub>3</sub> /L)
HY1	Hyalite Creek above reservoir	2/19/2016	3.07	0.02	0.005	0.00005	176	0.70883	0.000009	1.722	0.022	
		8/25/2016	3.75	0.02	0.014	0.00014	188	0.70885	0.000010	1.695	0.013	18
		2/4/2017	3.79	0.00	0.015	0.00015		0.70890	0.000009	1.642	0.012	15
		8/23/2017	3.78	0.02	0.005	0.00005	179	0.70921	0.000010	1.616	0.025	
HY2	Emerald Creek	2/19/2016	4.60	0.03	0.014	0.00014	172	0.70890	0.000009	1.629	0.006	
		8/25/2016	5.67	0.03	0.012	0.00012	186	0.70890	0.000009	1.691	0.012	29
		2/4/2017	5.87	0.03	0.012	0.00012	196	0.70890	0.000009	1.645	0.006	24
		8/23/2017	5.56	0.03	0.011	0.00011	178	0.70895	0.000009	1.671	0.010	28
HY7	Hyalite Creek below reservoir at DNRC gauge 41H 2000	2/4/2017	9.33	0.04	0.242	0.00242	249	0.70871	0.000010	1.591	0.006	35
		8/23/2017	7.00	0.03	0.023	0.00023	231	0.70870	0.000009	1.621	0.007	12
HY3	Lick Creek	2/19/2016	21.65	0.08	0.536	0.00536	277	0.70846	0.000010	1.570	0.004	
		8/25/2016	44.60	0.14	0.203	0.00203	321	0.70847	0.000010	1.506	0.006	190
		2/4/2017	34.50	0.11	0.160	0.00160	314	0.70859	0.000009	1.497	0.004	123
		8/23/2017	47.00	0.15	0.713	0.00713	313	0.70846	0.000010	1.499	0.005	235
HY9	Hyalite Creek below Lick Creek	8/23/2017	8.52	0.04	0.039	0.00039	243	0.70859	0.000009	1.598	0.007	45
		12/14/2017			0.080	0.00080		0.70853	0.000009	2.121	0.006	
HY16	Madison limestone spring channel	12/14/2017			0.424	0.00424		0.70835	0.000009	5.226	0.017	
HY17	Madison limestone spring seep	12/14/2017			0.038	0.00038		0.70835	0.000009	5.285	0.013	
		1/29/2018			0.382	0.00382				5.282	0.032	
		3/27/2018			0.372	0.00372				5.215	0.015	
HY10	Middle Hyalite Creek	8/23/2017	11.00	0.04	0.079	0.00079	259	0.70860	0.000010	2.958	0.010	46
		12/14/2017			0.114	0.00114		0.70857	0.000009	2.957	0.016	
HY11	Hyalite Creek at Langohr Logging Road	8/23/2017	11.00	0.04	0.085	0.00085	259	0.70861	0.000009	2.966	0.008	49
HY13	Unnamed creek in glacial meadow	8/24/2017	14.60	0.08	0.017	0.00017	192	0.70893	0.000009	1.961	0.058	88
HY12	Buckskin Creek	8/23/2017	68.60	0.14	0.592	0.00592	504	0.71146	0.000009	2.695	0.228	212
HY4	Hyalite Creek at Langohr's Campground	2/19/2016	13.52	0.05	0.164	0.00164	261	0.70868	0.000009	3.195	0.009	

		8/25/2016	12.50	0.05	0.069	0.00069	277	0.70866	0.000009	2.977	0.011	37
		2/4/2017	17.60	0.06	0.186	0.00186	301	0.70868	0.000010	3.100	0.010	52
		8/23/2017	11.40	0.04	0.088	0.00088	268	0.70879	0.000009	2.983	0.022	28
HY8	Moser Creek	2/4/2017	37.10	0.14	0.596	0.00596	275	0.71143	0.000010	2.236	0.006	106
		8/23/2017	47.10	0.16	0.542	0.00542	294	0.71181	0.000009	2.241	0.008	167
HY14	Hyalite Creek below Moser Creek	8/24/2017	11.60	0.04	0.077	0.00077	267	0.70874	0.000009	3.047	0.012	45
HY15	Hyalite Creek above Practice Rock	8/24/2017	11.60	0.04	0.083	0.00083	270	0.70885	0.000009	2.944	0.013	73
HY5	Hyalite Creek at Practice Rock	2/19/2016	9.86	0.04	0.554	0.00554	246	0.71141	0.000010	1.788	0.005	
		8/25/2016	12.60	0.05	0.170	0.00170	278	0.70979	0.000009	2.086	0.006	43
		8/24/2017	11.90	0.04	0.152	0.00152	272	0.70973	0.000009	2.128	0.008	79
HY6	Hyalite Creek at USGS gage 06050000	2/19/2016	10.05	0.04	0.638	0.00638	249	0.71202	0.000010	1.691	0.005	
		8/25/2016	12.70	0.05	0.121	0.00121	270	0.71007	0.000010	1.966	0.005	
		2/4/2017	14.40	0.05	0.791	0.00791	287	0.71112	0.000009	1.747	0.004	52
		8/24/2017	11.80	0.04			274	0.70998	0.000009			61
SD1	Sourdough Creek	12/13/2017			0.024	0.00024		0.70862	0.000009	2.047	0.018	
GW2	Gneiss spring	5/18/2017	15.30	0.05	0.353	0.00353	321	0.73687	0.000010	1.849	0.084	37
GW3	Gneiss well	5/18/2017	27.00	0.06	0.364	0.00364	467	0.74497	0.000010	1.489	0.022	146
GW4	Hyalite Creek alluvial fan well	6/20/2017	42.90	0.11	0.233	0.00233	383	0.71221	0.000010	1.784	0.006	139

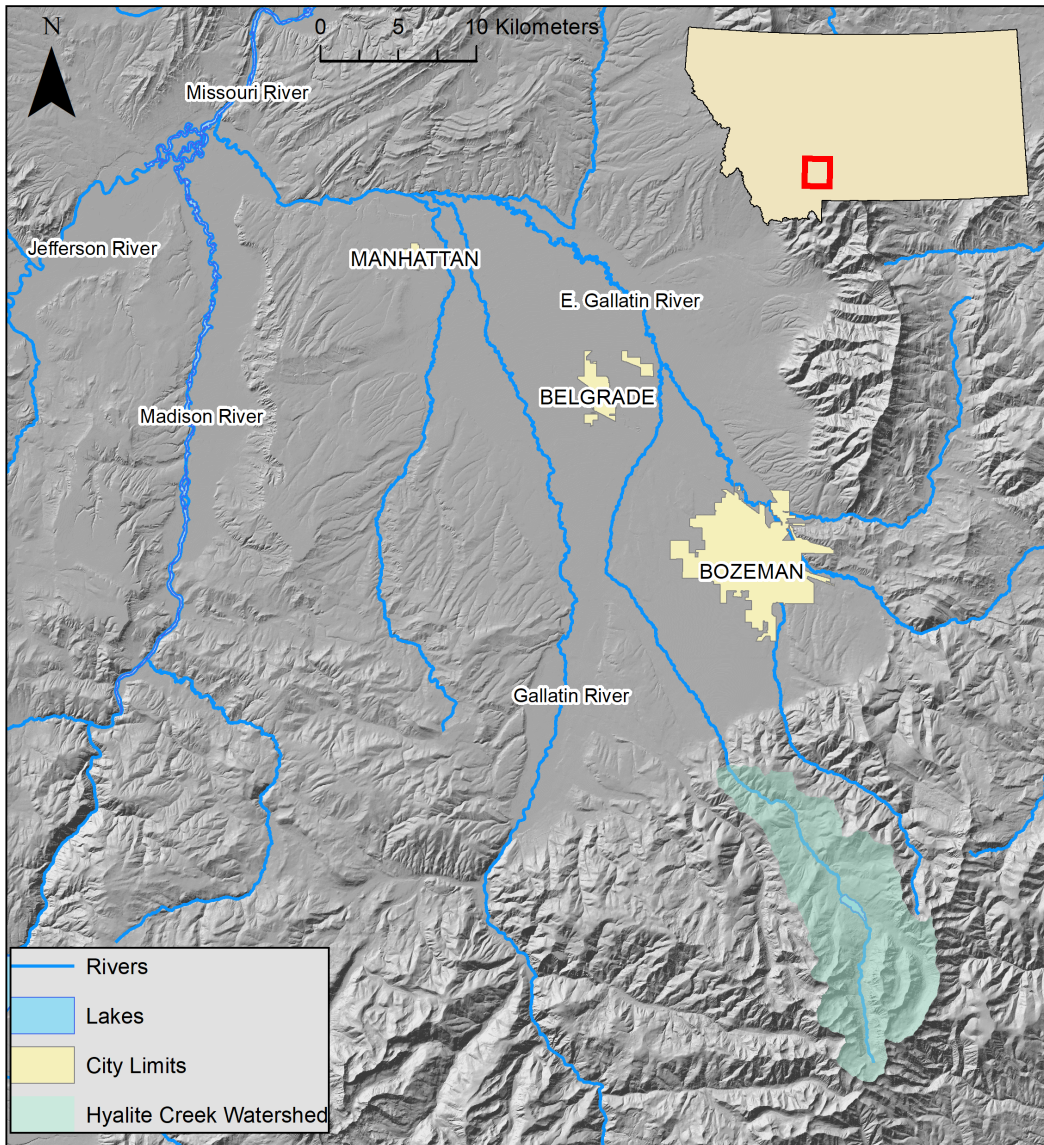


Figure 1b. Location map of Hyalite Creek watershed (green shading) and the Gallatin Valley within the state of Montana (inset).

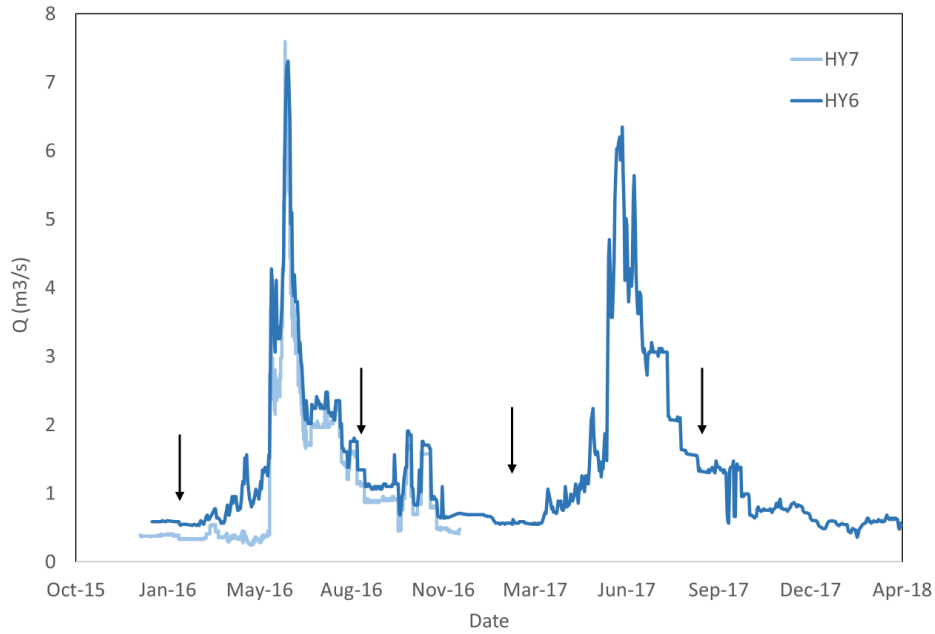


Figure 2. Hyalite Creek discharge from 1/1/2016 to 4/9/2018 at the HY7 DNRC gauge (light blue) and HY6 USGS gauge (dark blue). Black arrows indicate sample dates. Gauge locations shown on Figure 3.

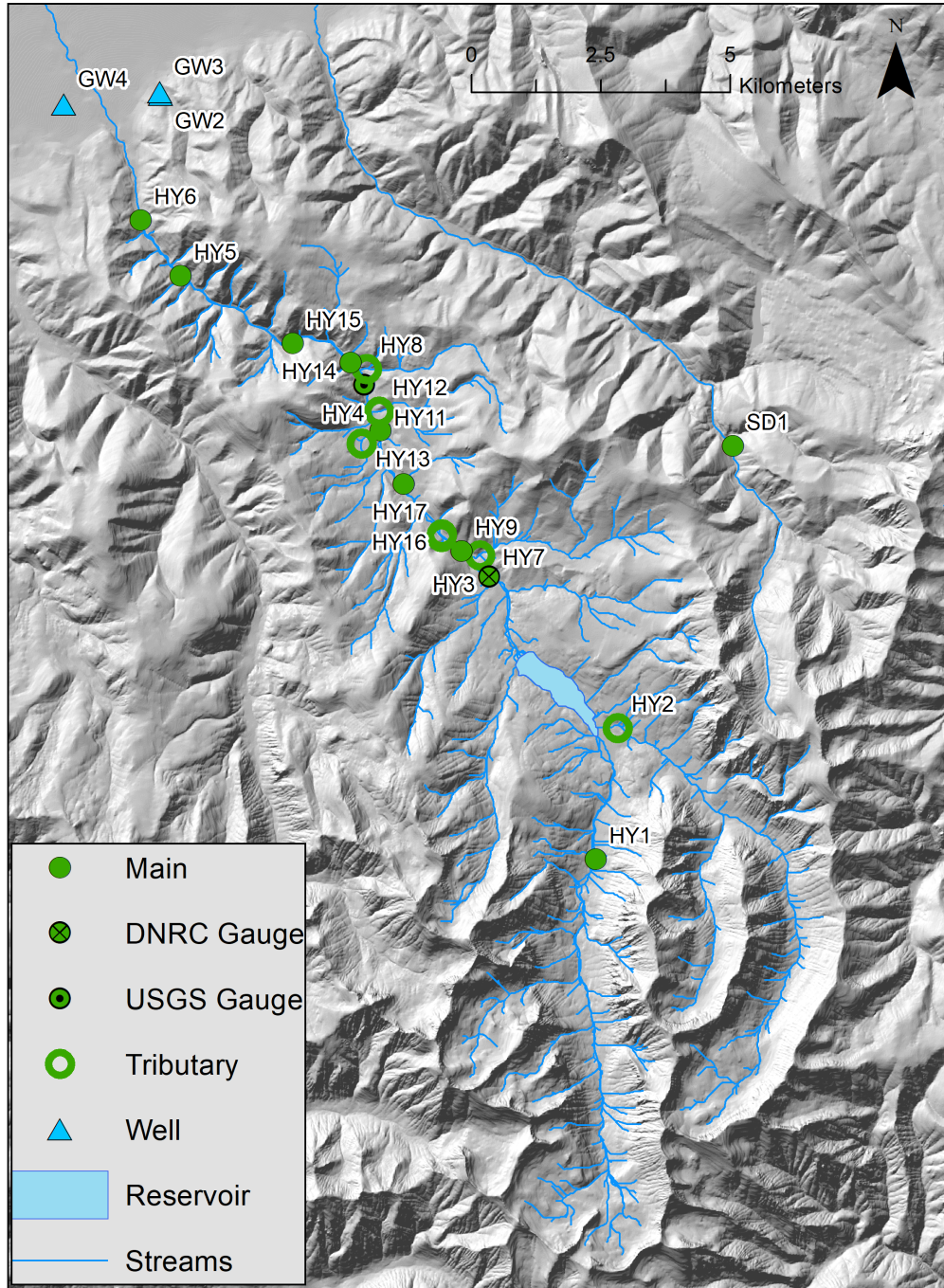


Figure 3. Location of sample sites and gauge locations along Hyalite Creek and its tributaries (HY1-HY17, GW4), in Hodgman Canyon (GW2, GW3), and in Sourdough Canyon (SD1).

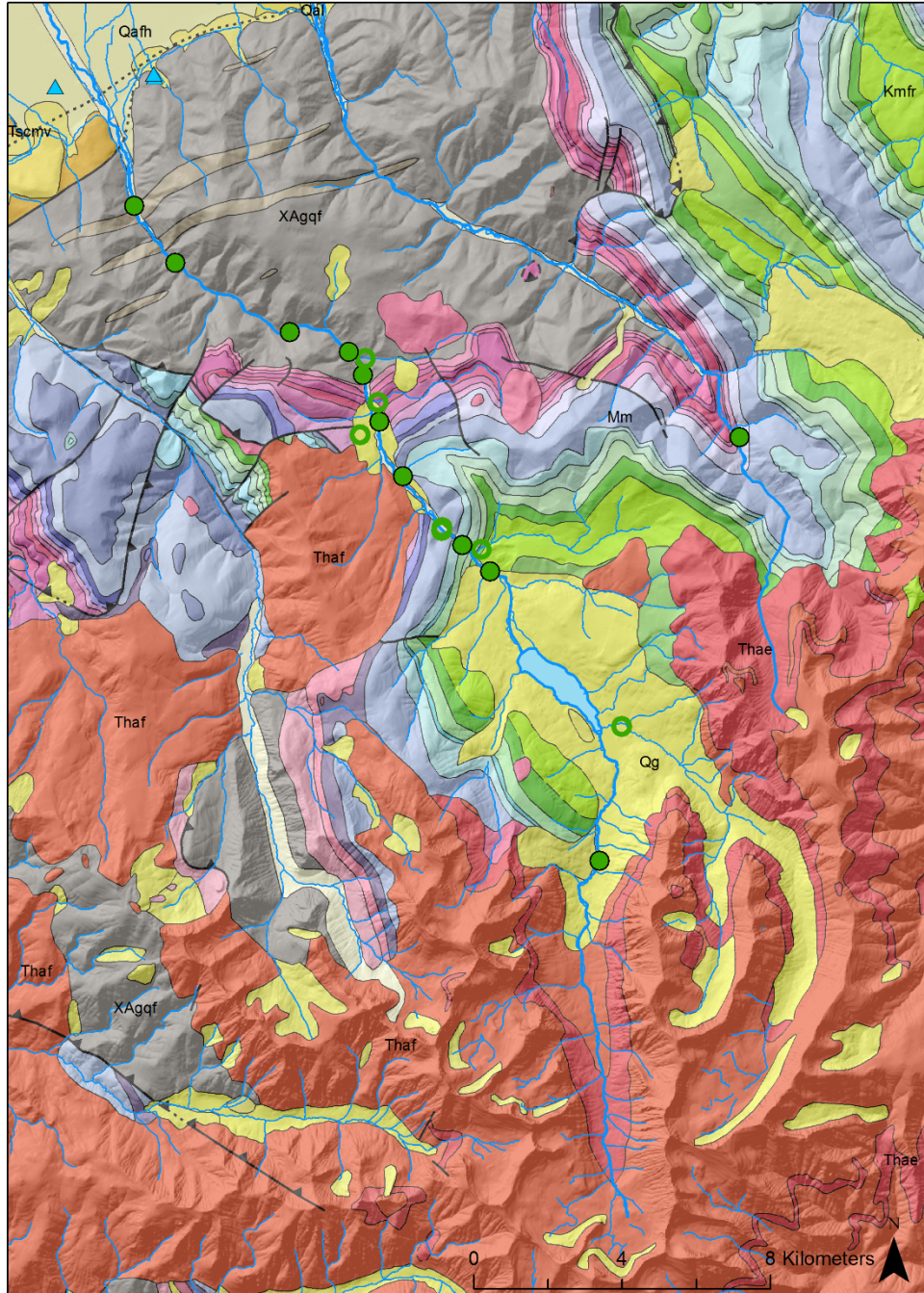


Figure 4. Geologic map showing sample sites along Hyalite Creek and its tributaries (HY1-HY17, GW4), in Hodgman Canyon (GW2, GW3), and in Sourdough Canyon (SD1). Rock units described in Table 2.

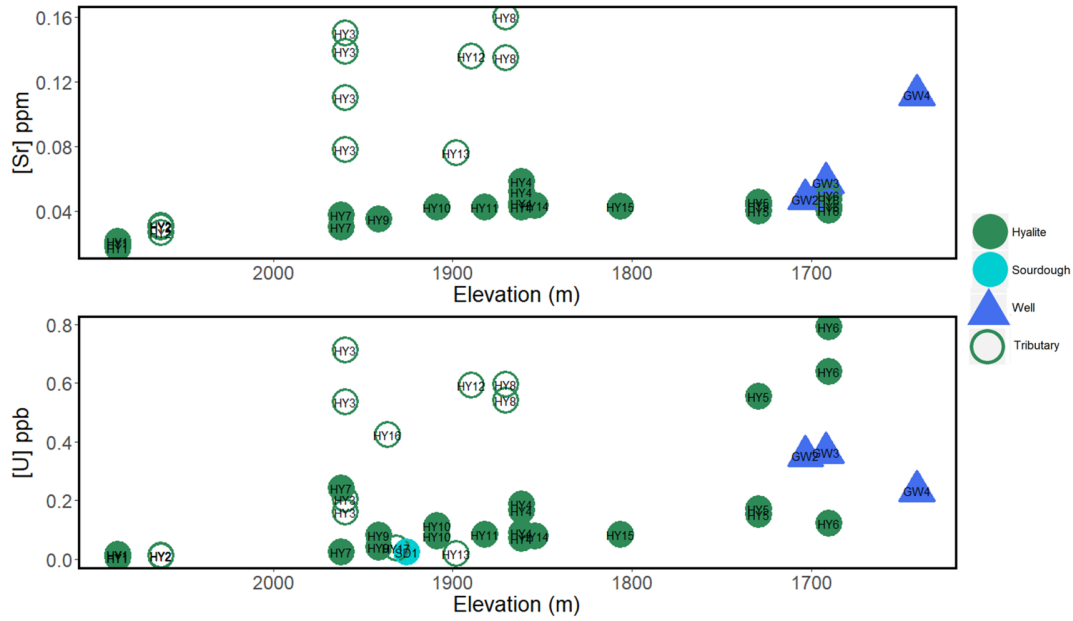


Figure 5. Strontium and Uranium concentration with elevation along Hyalite Creek (green filled circles), its tributaries (green open circles), and connected wells (blue triangles).

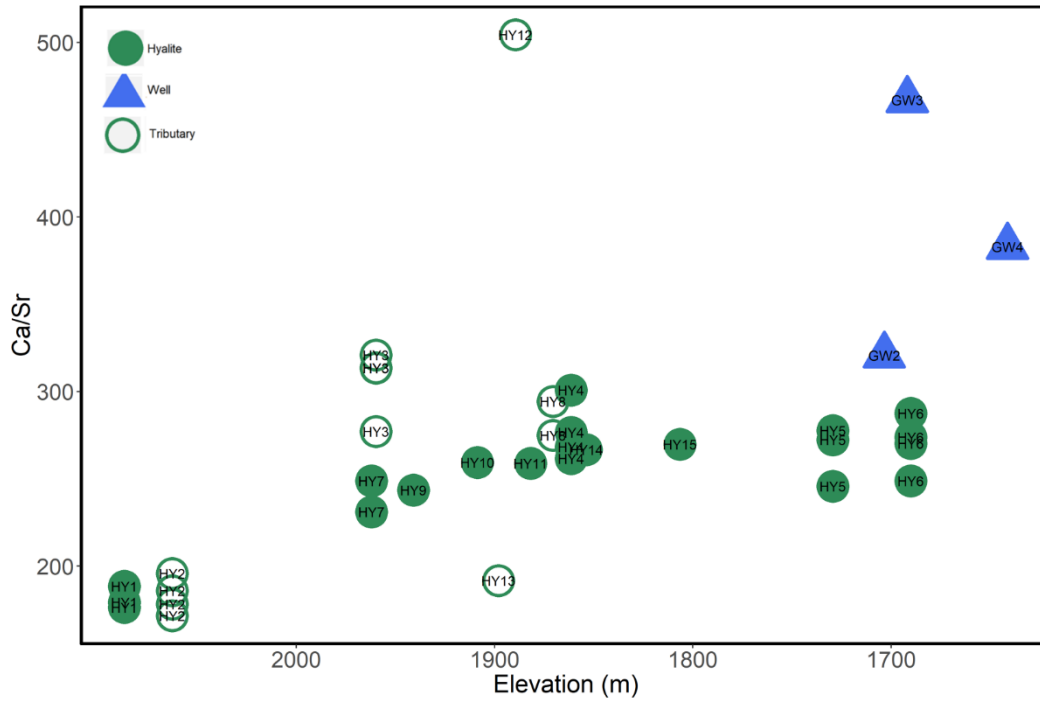


Figure 6. Ca/Sr ratio versus elevation along Hyalite Creek (closed green circles), its tributaries (open green circles), and connected wells (blue triangles).

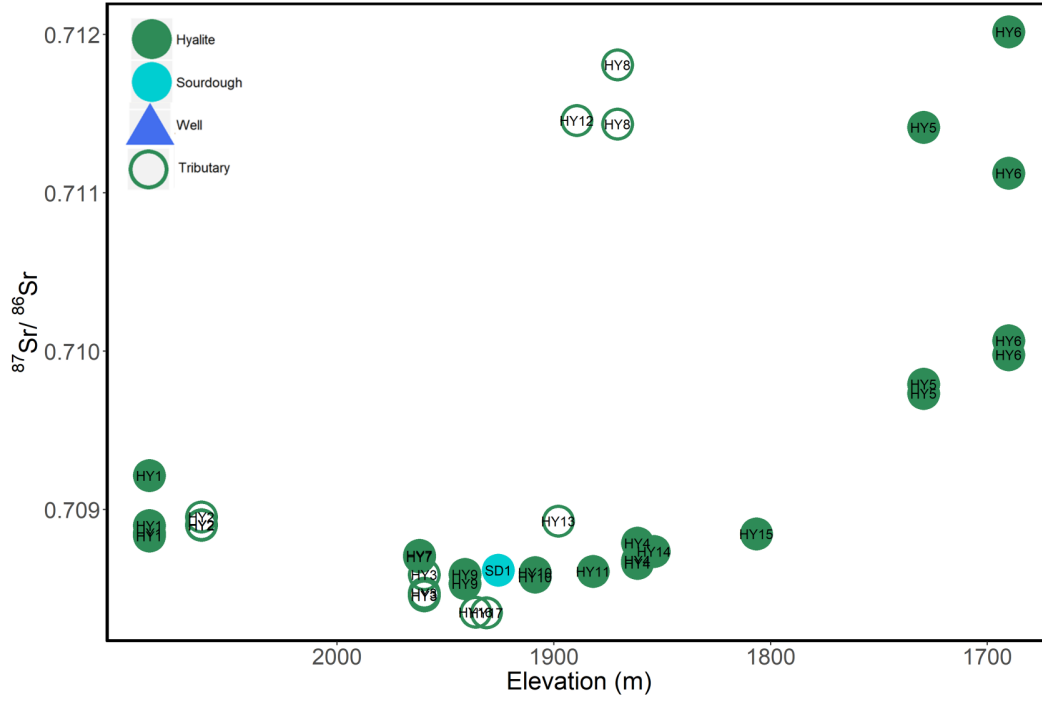


Figure 7.  $^{87}\text{Sr}/^{86}\text{Sr}$  isotope ratio versus elevation along Hyalite Creek (closed green circles), its tributaries (open green circles).

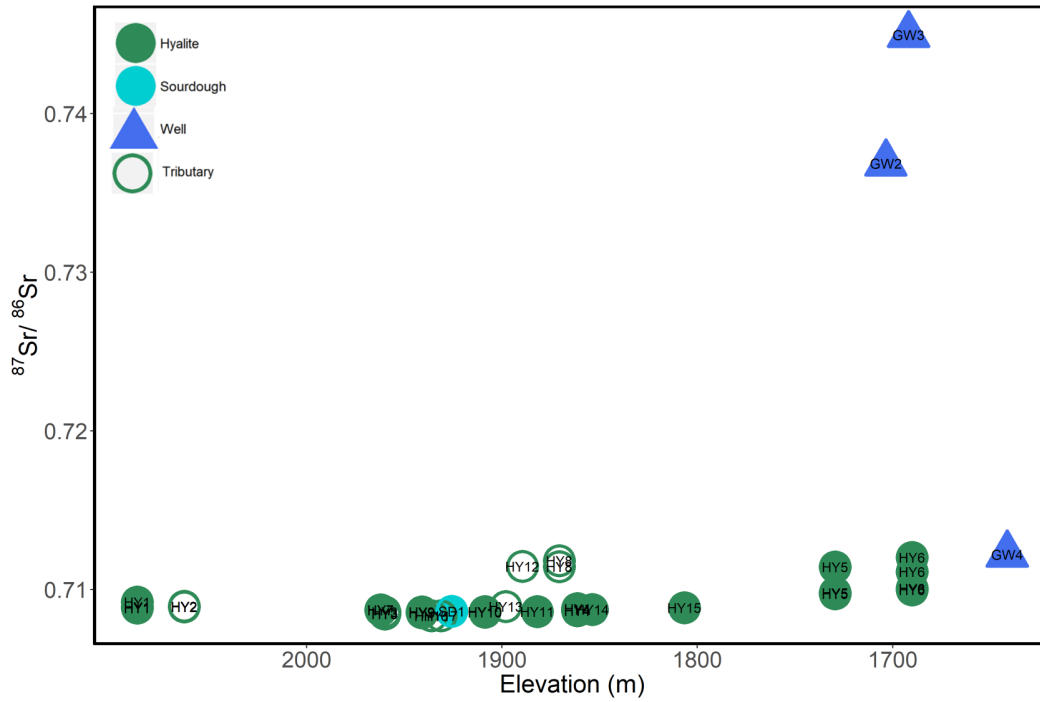


Figure 8.  $^{87}\text{Sr}/^{86}\text{Sr}$  versus elevation along Hyalite Creek (closed green circles), its tributaries (open green circles), and connected wells (blue triangles).

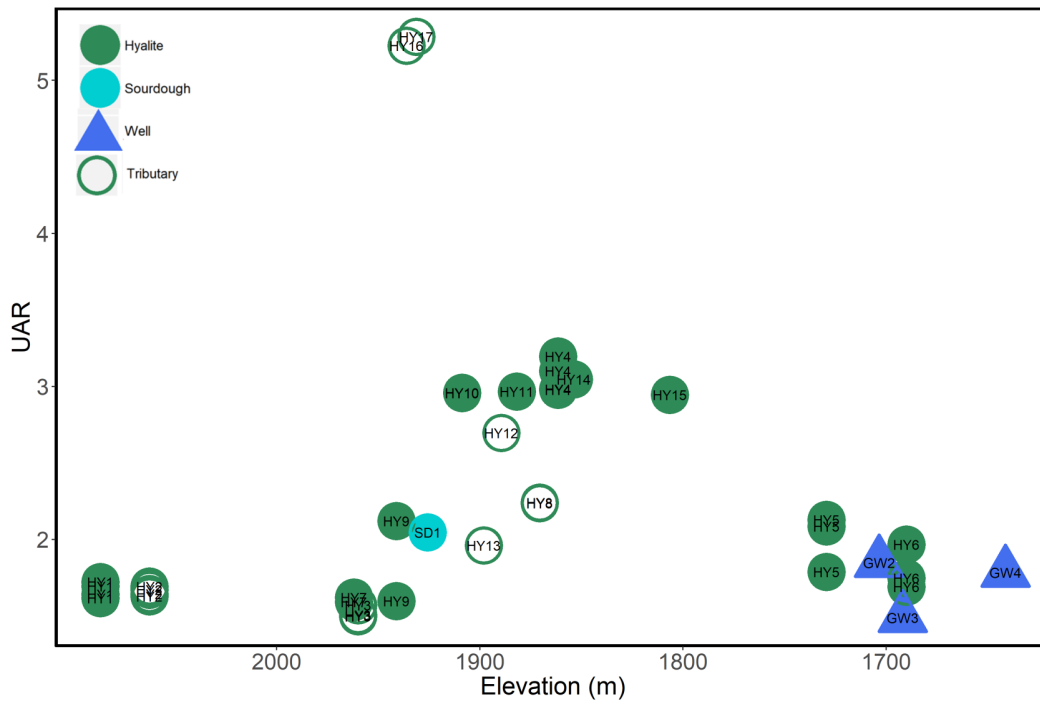


Figure 9. UAR versus elevation along Hyalite Creek (closed green circles), its tributaries (open green circles), and connected wells (blue triangles).

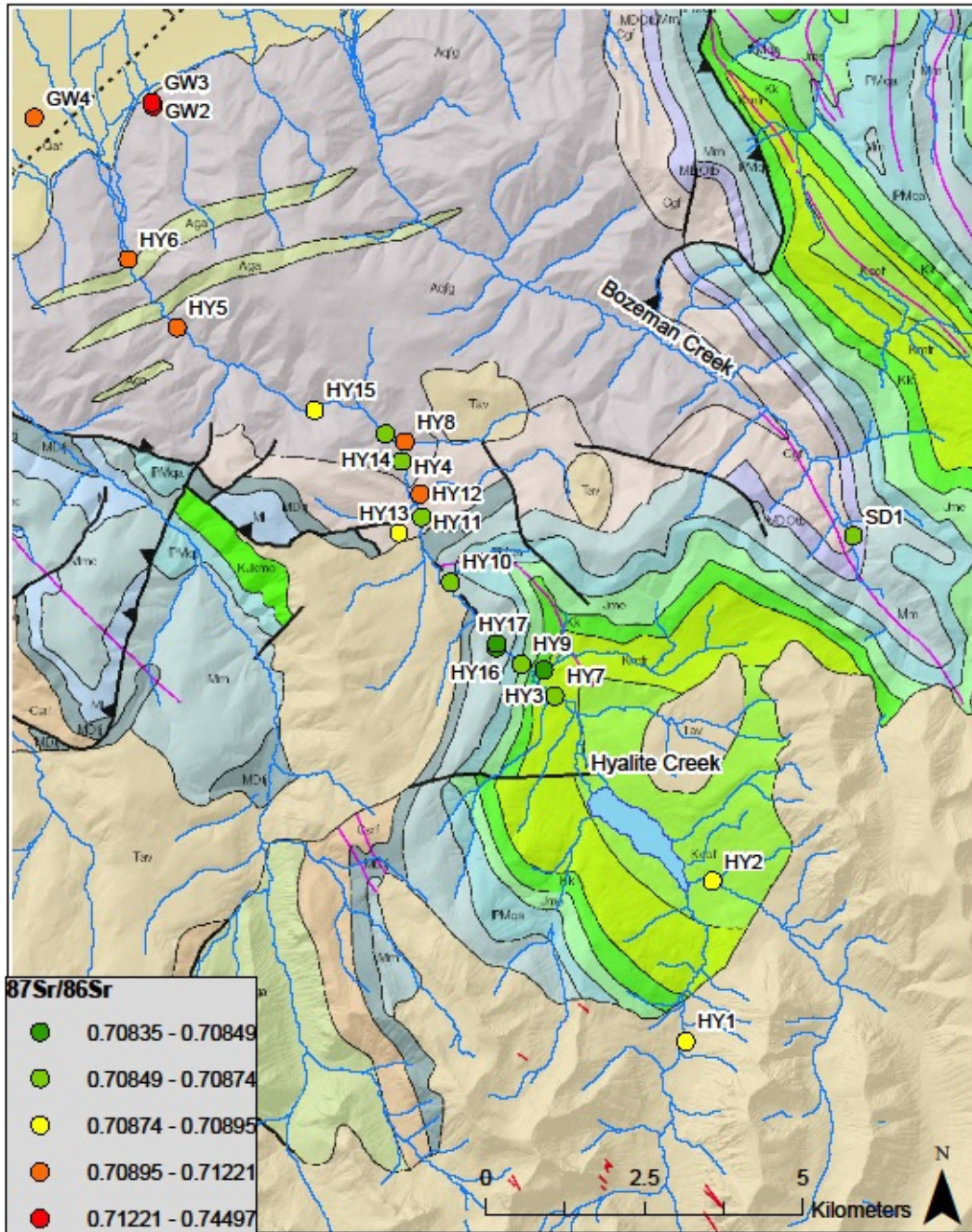


Figure 10. Strontium isotope ratio along Hyalite Creek in relation to lithology. Separated by natural breaks with a green-yellow-red gradient with green circles representing sample sites with comparatively low strontium isotope ratio and red circles representing sample sites with comparatively high strontium isotope ratio.

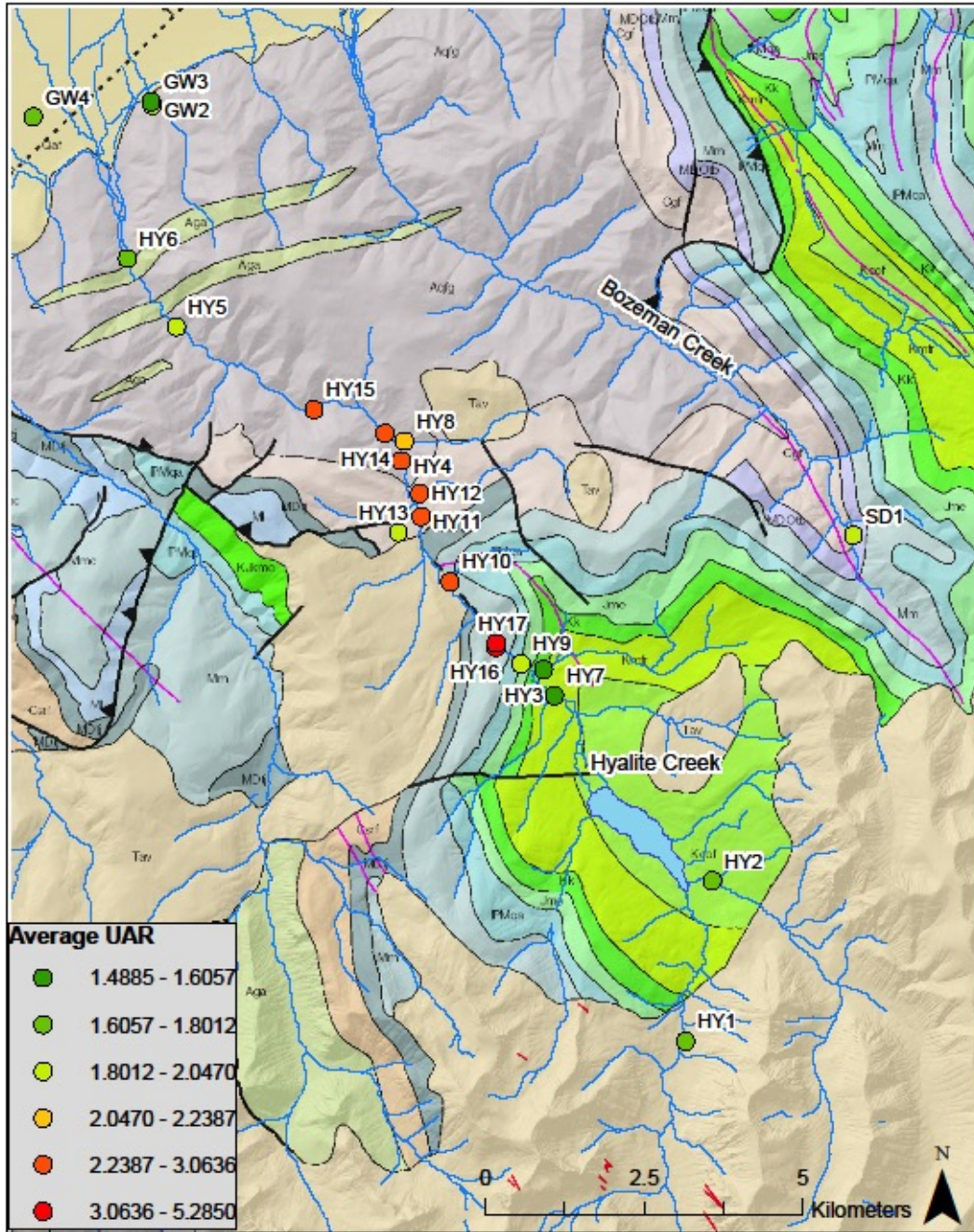


Figure 11. UAR along Hyalite Creek in relation to lithology. Separated by natural breaks with a green-yellow-red gradient with green circles representing sample sites with comparatively low UAR and red circles representing sample sites with comparatively high UAR. Notice increase in UAR values coinciding with the Madison Limestone (Mm) formation.

Gallatin Valley Figures

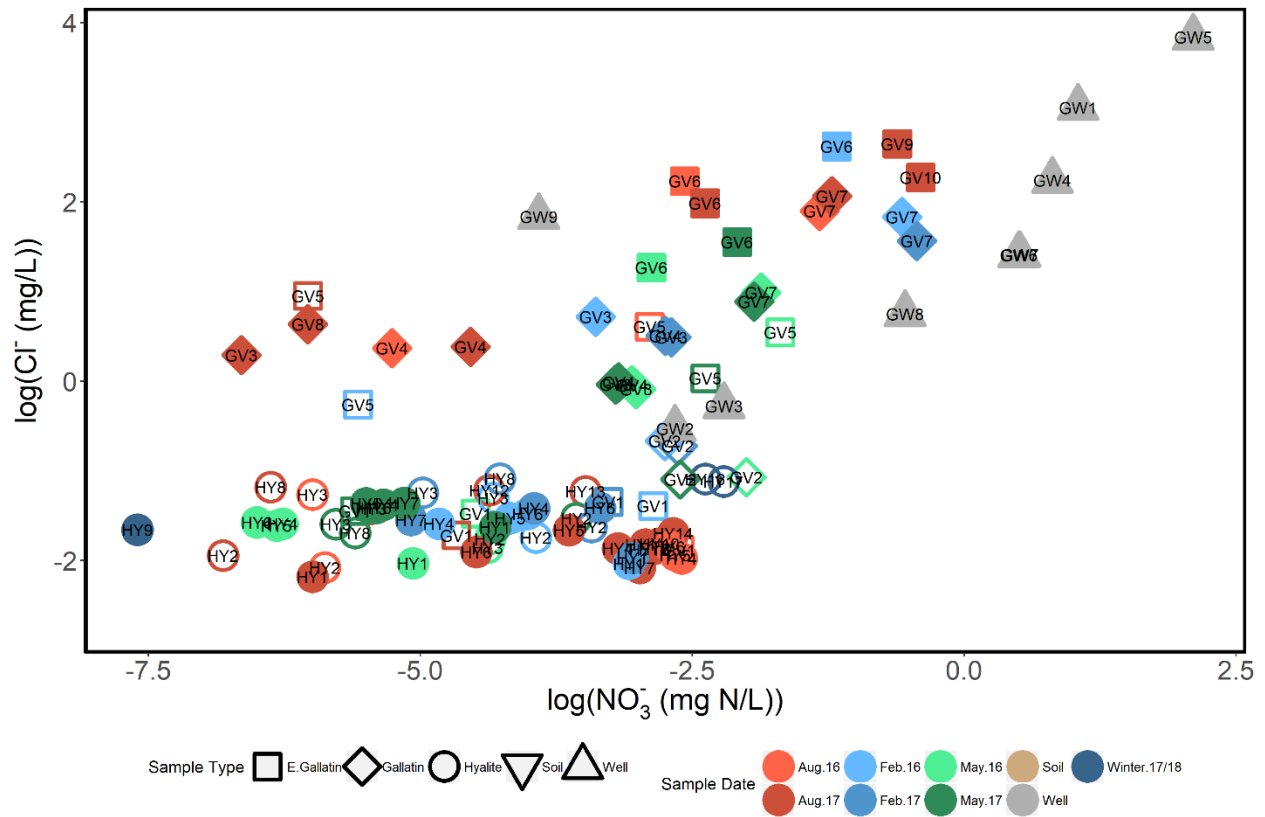
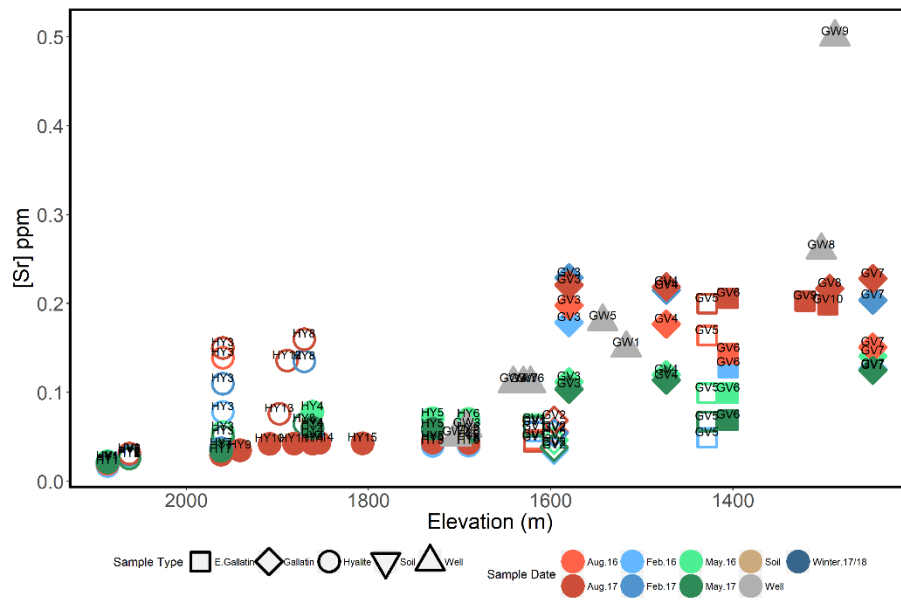


Figure 12. Log-log plot of  $\text{NO}_3^-$  versus  $\text{Cl}^-$ . Hyalite Creek and its tributaries are represented by circles, the Gallatin River and its tributaries are represented by diamonds, the East Gallatin River and its tributaries are represented by squares, wells are represented by gray triangles, and tributaries are characterized by open circles. For surface waters (Hyalite Creek, Gallatin River, East Gallatin River and tributaries) sample date is represented by color with light blue representing February 2016, medium blue representing February 2017, dark blue representing winter of 2017-2018, light green representing May 2016, dark green representing May 2017, light orange representing August 2016, and dark orange representing August 2017.

a.



b.

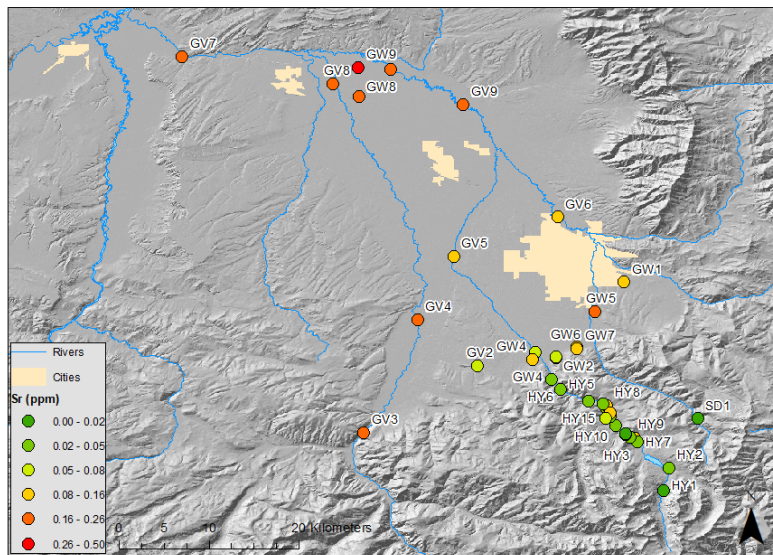
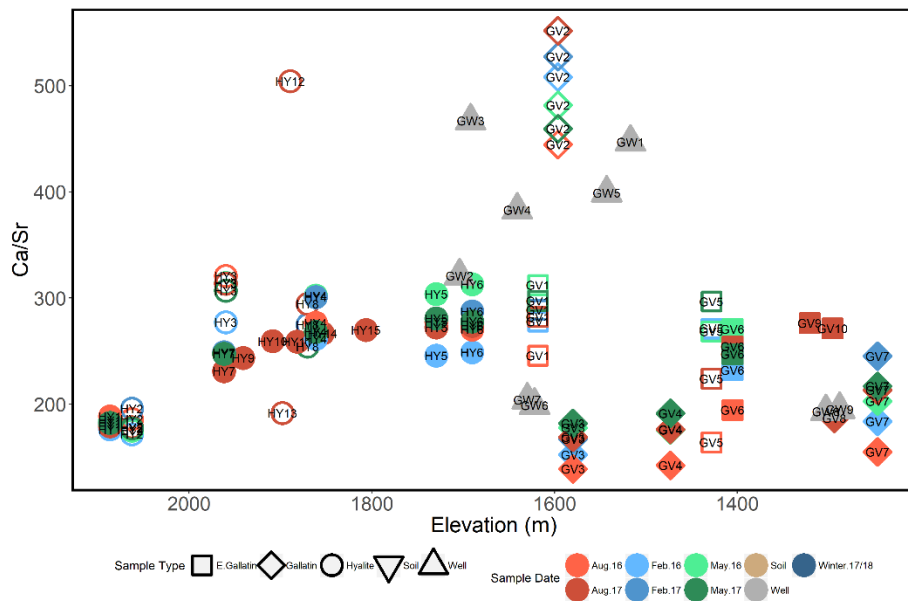


Figure 13. Strontium concentration distribution in the Gallatin Valley, a) Sr concentration trends with elevation, b) spatial distribution of Sr concentrations. Hyalite Creek and its tributaries are represented by circles, the Gallatin River and its tributaries are represented by diamonds, the East Gallatin River and its tributaries are represented by squares, wells are represented by gray triangles, and tributaries are characterized by open circles. For surface waters (Hyalite Creek, Gallatin River, East Gallatin River and tributaries) sample date is represented by color with light blue representing February 2016, medium blue representing February 2017, dark blue representing winter of 2017-2018, light green representing May 2016, dark green representing May 2017, light orange representing August 2016, and dark orange representing August 2017.



a.



b.

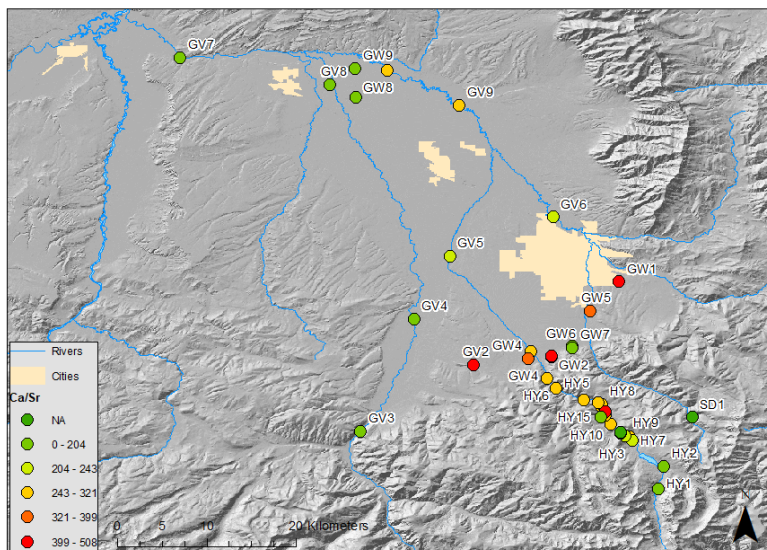
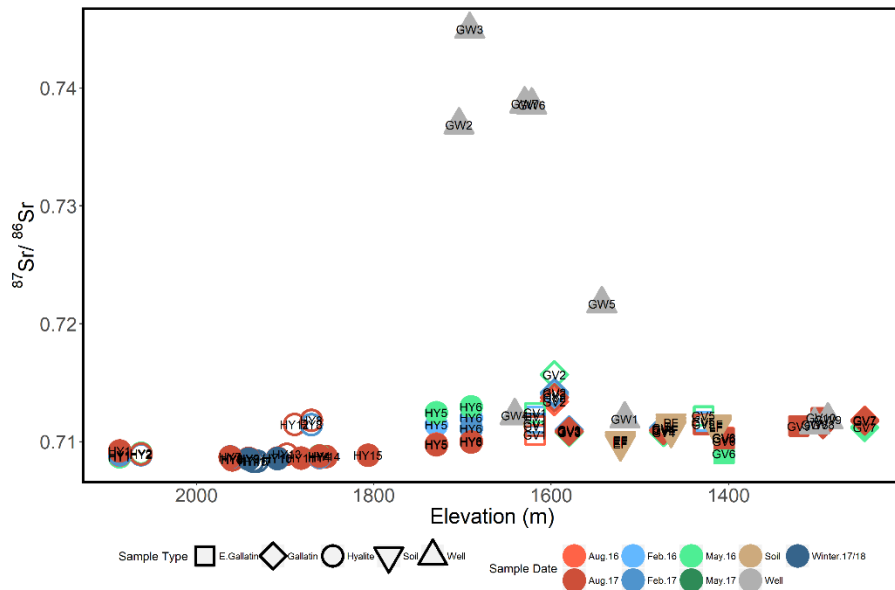


Figure 14. Ca/Sr ratio distribution in the Gallatin Valley, a) Ca/Sr trends with elevation, b) spatial distribution of Ca/Sr ratios. Hyalite Creek and its tributaries are represented by circles, the Gallatin River and its tributaries are represented by diamonds, the East Gallatin River and its tributaries are represented by squares, wells are represented by gray triangles, and tributaries are characterized by open circles. For surface waters (Hyalite Creek, Gallatin River, East Gallatin River and tributaries) sample date is represented by color with light blue representing February 2016, medium blue representing February 2017, dark blue representing winter of 2017-2018, light green representing May 2016, dark green representing May 2017, light orange representing August 2016, and dark orange representing August 2017.

a.



b.

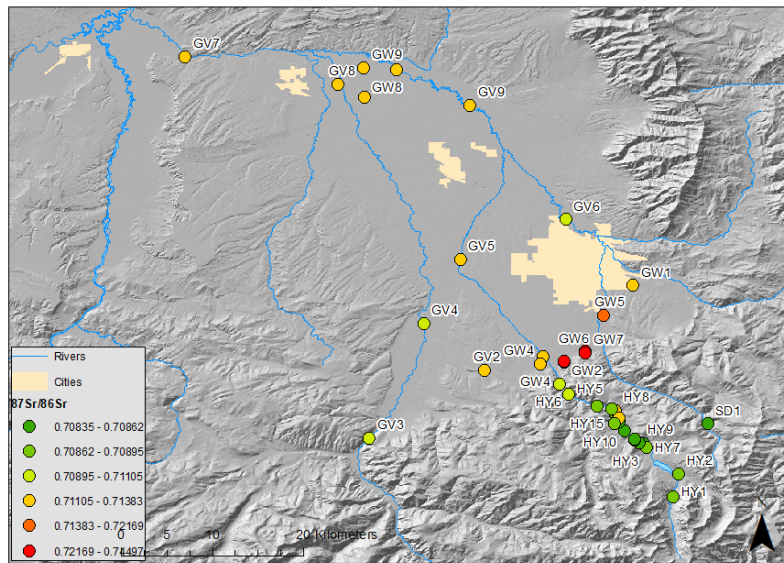
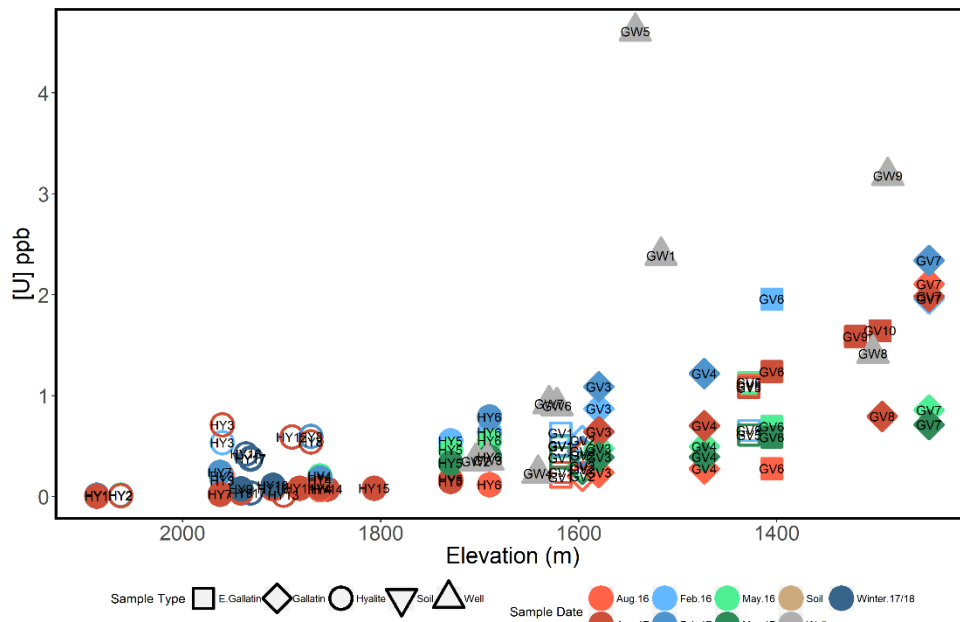


Figure 15.  $^{87}\text{Sr}/^{86}\text{Sr}$  isotope ratio distribution in the Gallatin Valley, a)  $^{87}\text{Sr}/^{86}\text{Sr}$  isotope ratio trends with elevation, b) spatial distribution of  $^{87}\text{Sr}/^{86}\text{Sr}$  isotope ratio. Hyalite Creek and its tributaries are represented by circles, the Gallatin River and its tributaries are represented by diamonds, the East Gallatin River and its tributaries are represented by squares, wells are represented by gray triangles, soils are represented by brown downwards pointing triangles, and tributaries are characterized by open circles. For surface waters (Hyalite Creek, Gallatin River, East Gallatin River and tributaries) sample date is represented by color with light blue representing February 2016, medium blue representing February 2017, dark blue representing winter of 2017-2018, light green representing May 2016, dark green representing May 2017, light orange representing August 2016, and dark orange representing August 2017.

a.



b.

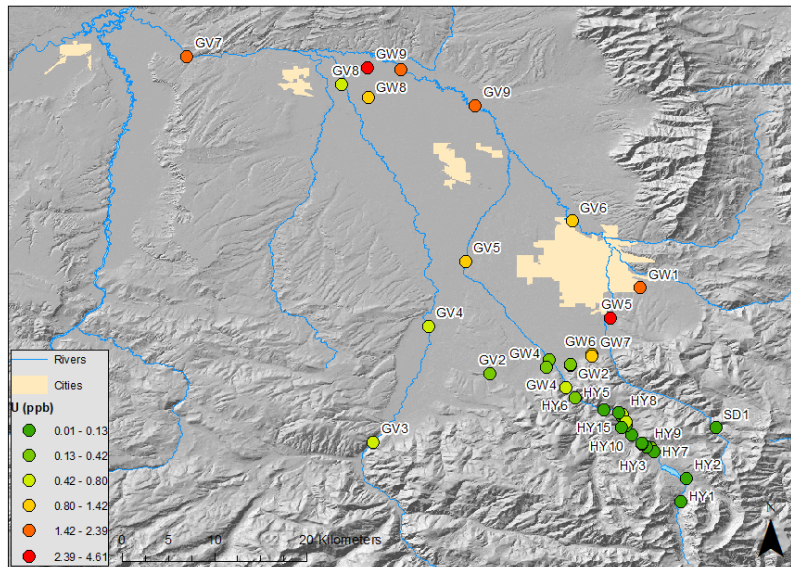
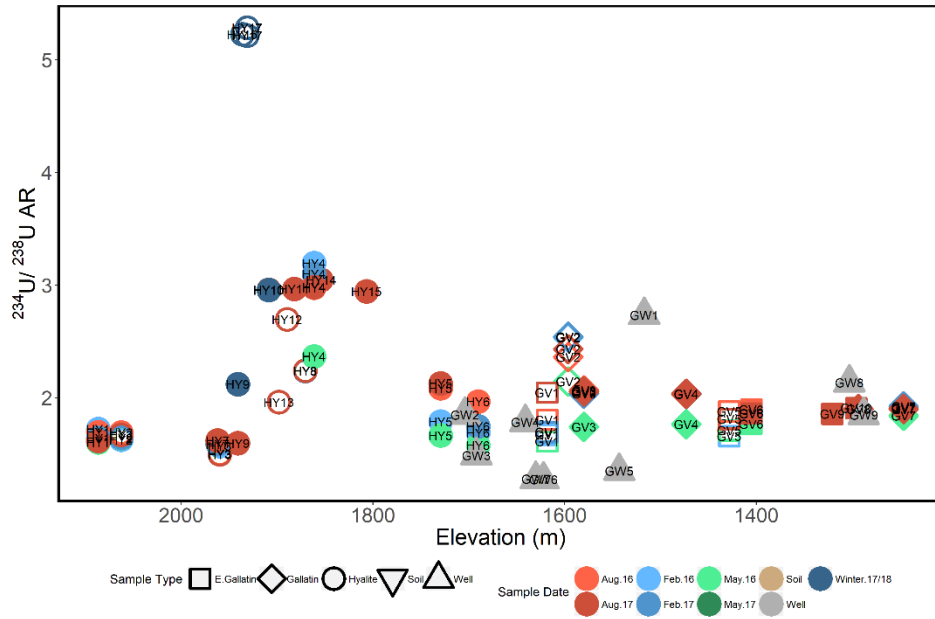


Figure 16. U concentration distribution in the Gallatin Valley, a) U concentration trends with elevation, b) spatial distribution of U concentration. Hyalite Creek and its tributaries are represented by circles, the Gallatin River and its tributaries are represented by diamonds, the East Gallatin River and its tributaries are represented by squares, wells are represented by gray triangles, and tributaries are characterized by open circles. For surface waters (Hyalite Creek, Gallatin River, East Gallatin River and tributaries) sample date is represented by color with light blue representing February 2016, medium blue representing February 2017, dark blue representing winter of 2017-2018, light green representing May 2016, dark green representing May 2017, light orange representing August 2016, and dark orange representing August 2017.

a.



b.

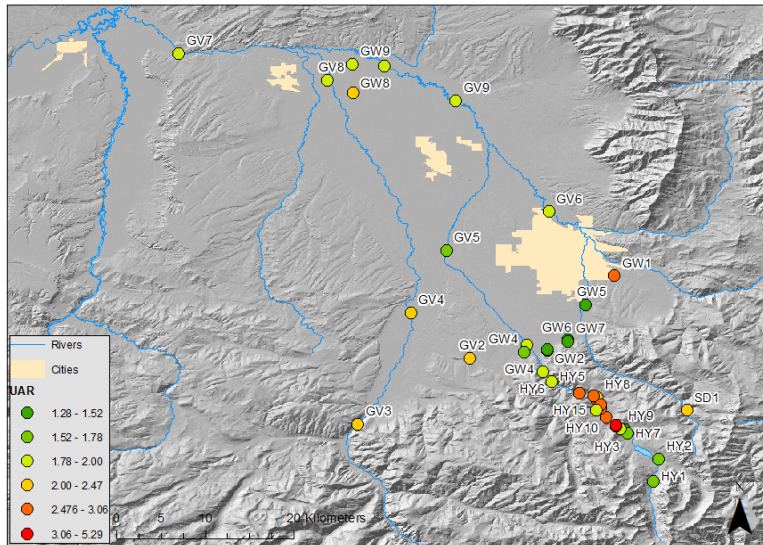
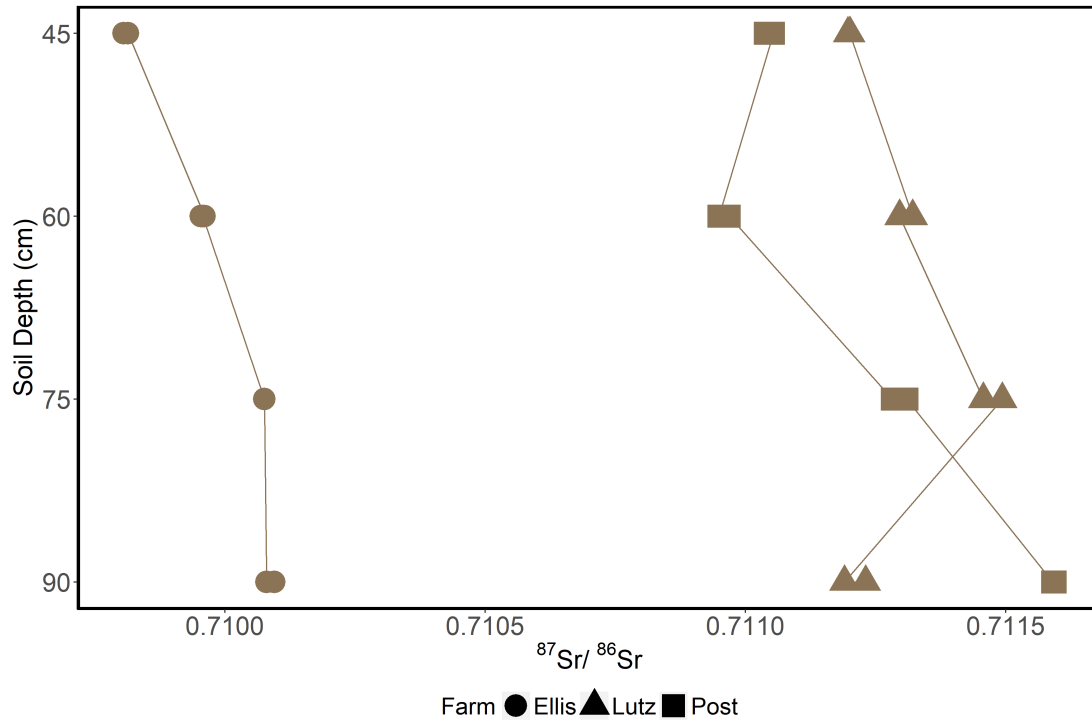


Figure 17.  $^{234}\text{U}/^{238}\text{U}$  AR distribution in the Gallatin Valley, a)  $^{234}\text{U}/^{238}\text{U}$  AR trends with elevation, b) spatial distribution of  $^{234}\text{U}/^{238}\text{U}$  AR. Hyalite Creek and its tributaries are represented by circles, the Gallatin River and its tributaries are represented by diamonds, the East Gallatin River and its tributaries are represented by squares, wells are represented by gray triangles, and tributaries are characterized by open circles. For surface waters (Hyalite Creek, Gallatin River, East Gallatin River and tributaries) sample date is represented by color with light blue representing February 2016, medium blue representing February 2017, dark blue representing winter of 2017-2018, light green representing May 2016, dark green representing May 2017, light orange representing August 2016, and dark orange representing August 2017.

a.



b.

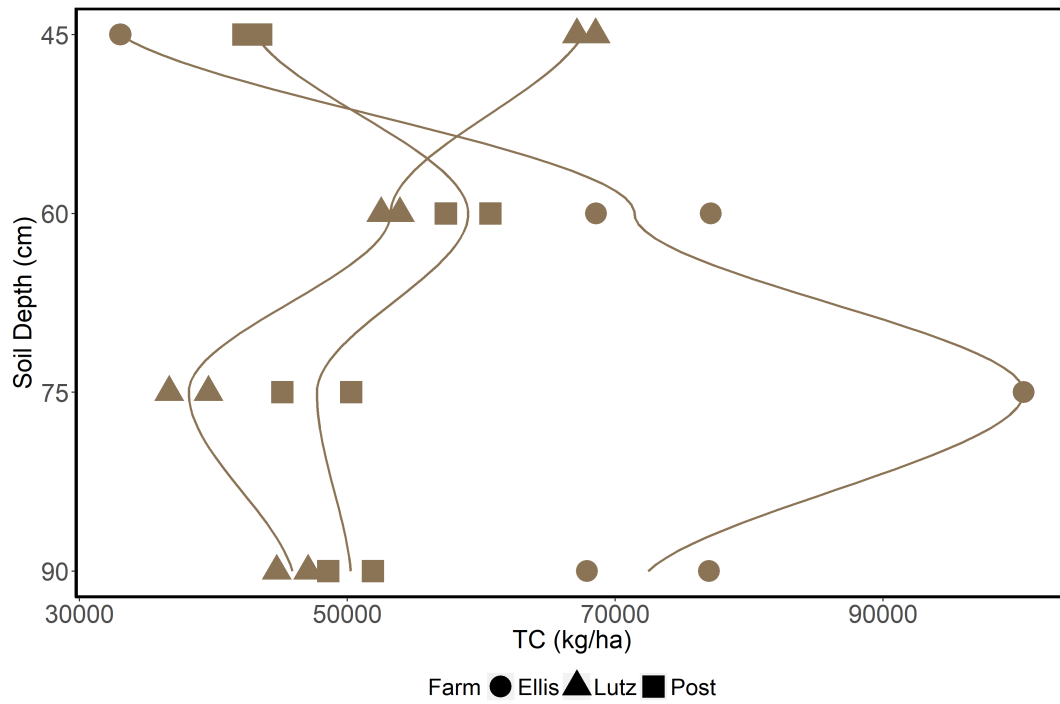


Figure 18. a)  $^{87}\text{Sr}/^{86}\text{Sr}$  isotope composition and b) total carbon % of soils from Ellis (circle), Lutz (triangle), and Post (square) Farms in the Gallatin Valley at 15 cm depth intervals.

# Rocky Mountain Juniper influences on Stream Flow Dynamics

## Basic Information

<b>Title:</b>	Rocky Mountain Juniper influences on Stream Flow Dynamics
<b>Project Number:</b>	2017MT310B
<b>Start Date:</b>	3/1/2017
<b>End Date:</b>	2/28/2019
<b>Funding Source:</b>	104B
<b>Congressional District:</b>	1
<b>Research Category:</b>	Climate and Hydrologic Processes
<b>Focus Categories:</b>	Ecology, Hydrology, Water Quantity
<b>Descriptors:</b>	None
<b>Principal Investigators:</b>	Jia Hu

## Publications

There are no publications.

## **Rocky Mountain Juniper influences on Stream Flow Dynamics**

Keywords: *Rocky Mountain Juniper, willow, hydrology, water source use, transpiration, stable isotopes*

**Start Date:** June 1, 2017

**End Date:** February 28, 2019

**Principle Investigator:** Jia Hu, Assistant Professor, Montana State University, 310 Lewis Hall, Bozeman, MT 59717, phone: 406-551-5437, email: [jia.hu02@montana.edu](mailto:jia.hu02@montana.edu)

**Project Partners:**

- 1) Nathan Korb, Freshwater Director, The Nature Conservancy, 32 S. Ewing, Suite 215, Helena, MT 59601, phone: 406-495-2261, email: [nkorb@tnc.org](mailto:nkorb@tnc.org)
- 2) Carter Kruse, Turner Enterprises, Inc., 901 Technology Blvd, Bozeman, MT 59718, phone: 406-556-8508, email: [Carter.Kruse@retranches.com](mailto:Carter.Kruse@retranches.com)

## Introduction

The expansion of *Juniperus* spp. across the western U.S. has lasting ecological and economic impacts. One main concern of juniper expansion is the alternation of ecosystem hydrology. Because junipers have deep roots, they can often access a pool of water unavailable to shallow rooted species. As junipers deplete this deep soil water, less water might be available to recharge streams and groundwater. Although some studies have documented an increase in groundwater and spring recharge after juniper removal at the watershed scale, these studies have primarily focused on invasion of junipers in areas once dominated by non-woody species. Less well understood is how conversion from one woody species to another (in this case willow to juniper) influences hydrology. However, in order to begin assessing the impacts of this species transition on watershed hydrology, we must first quantify total water use and seasonal patterns of water use between juniper and willow. In this research project, we address four main questions:

- 1) Are junipers growing in riparian areas using water from streams?
- 2) Are junipers using more water than other riparian woody plants, such as willow?
- 3) Are the seasonal patterns of water use between juniper and willow different?
- 4) After juniper removal, do willow have access to more water (i.e. do they transpire more)?

## Activities/data collected to date

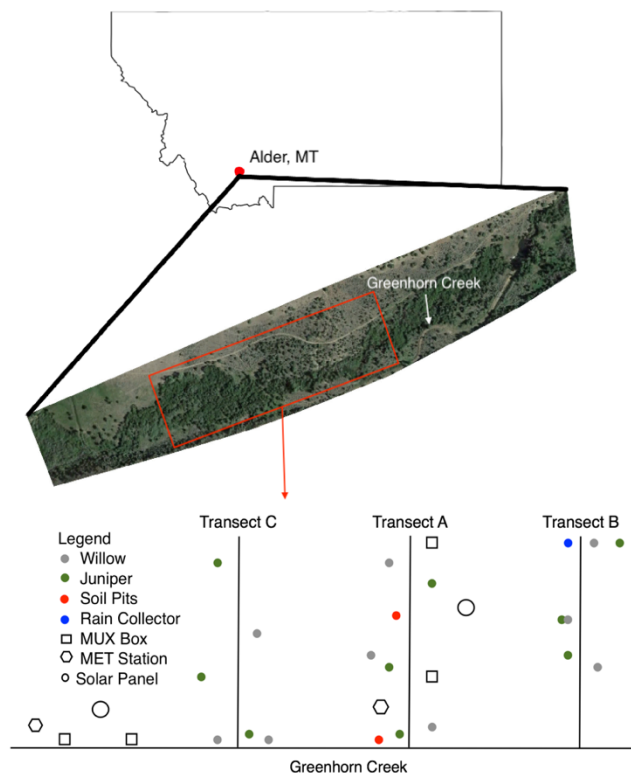


**Figure 1.** Greenhorn Creek with the three established transects, A, B, and C. All meteorological stations are mapped.

In 2017, we established three transects along the Greenhorn River at the Snow Crest Ranch, located in Central Montana near the city of Alder. Along the river, we established one control transect (A) and one juniper removal transect (C). After one year of field measurements (from June 2017- June 2018), we will remove juniper from the riparian areas in transect C and then measure willow responses to juniper removal (removal is planned for end of June 2018) (Figure 1). We have been measuring site meteorology, including air temperature, relative humidity, precipitation, and soil moisture and temperature from three depths (10, 40, 60cm).

To examine potentially differences in source water use (e.g. deep or shallow soil water, stream water, ground water), we used stable isotope analysis of oxygen and hydrogen. We also measured transpiration rates in both species throughout the growing season. These transpiration rates along with measurements of tree sapwood area will be used to quantify total water loss per tree per year and eventually scaled up to estimate transpiration rates at the catchment scale (fall 2018).

## Results to Date

### *Meteorological Data*

Since instrumenting the site early July, we have been monitoring air temperature, relative humidity, soil temperature and moisture. All measurements show strong seasonality at the site, with fall arriving abruptly in late September following a large rain storm.

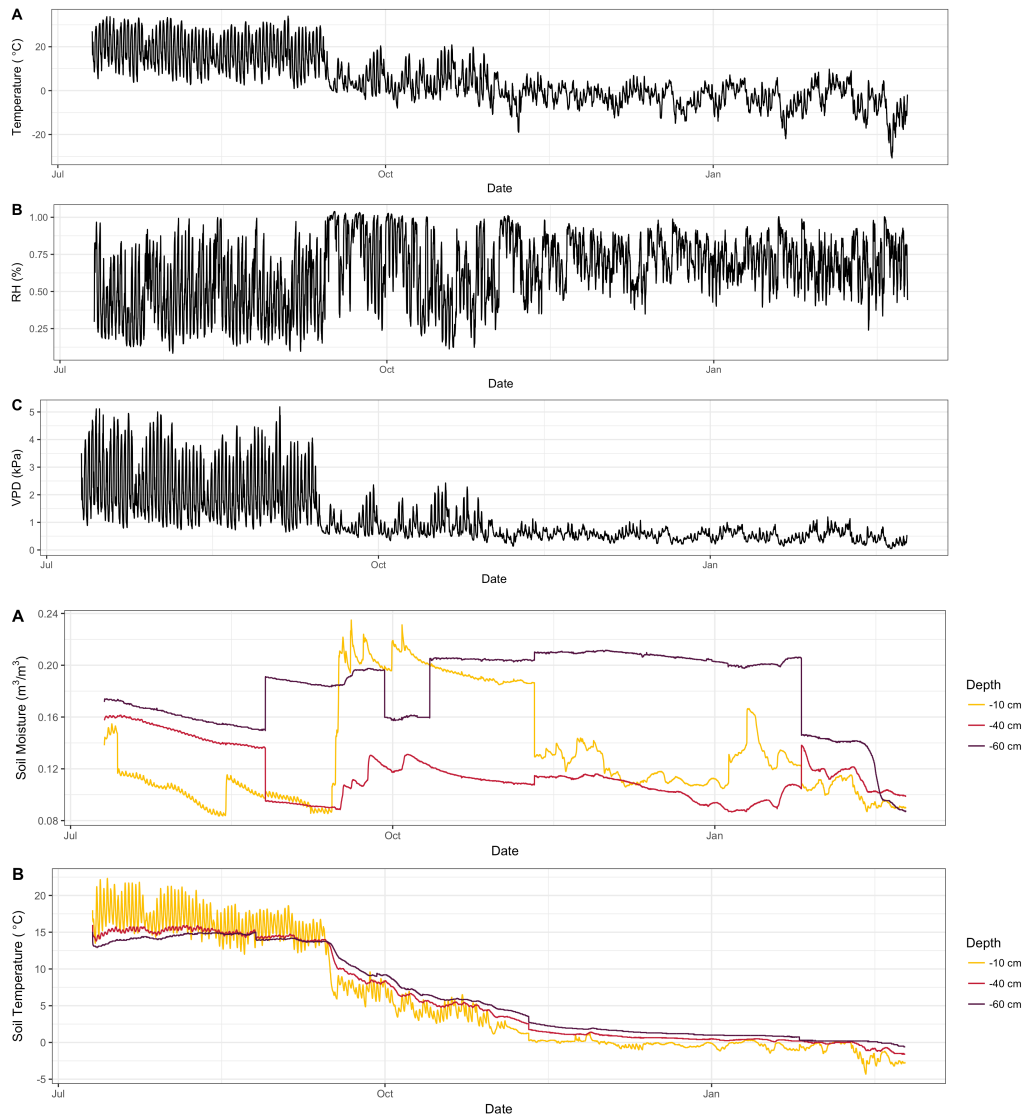


**Figure 2.** Site level meteorological measurements.

*Question 1: Are Junipers growing in riparian areas using water from streams?*

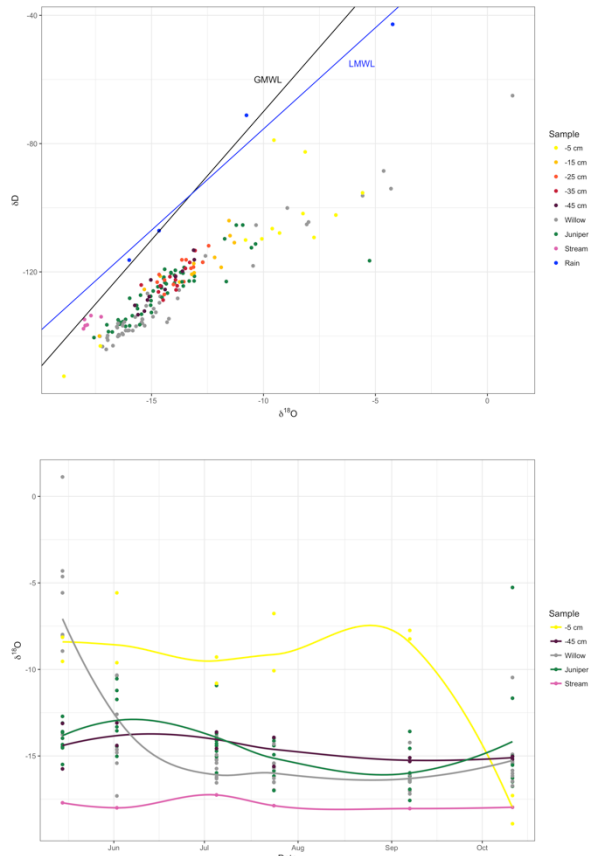


**Figure 3** a) soil, xylem, stream and rain water plotted in dual isotope space, b) soil, xylem, and stream water isotopes plotted through time.

contributed from ground water because ground water integrates a large land area and is a mixture of different precipitation sources. Because the stream water was isotopically negative, this isotope signal suggests that the stream water is mainly snowmelt derived (not surprising given the location of this site). The second interesting result was the gradient in soil water values (represented as -5 to -45cm depths, yellow to brown dots). The deeper soil water isotope values were more negative than the shallower soil water values, suggesting that water was evaporating from the upper soils (5 to 15 cm depth), but very little evaporation was occurring at soil depths below 25cm. The xylem water for the willow (gray dots) and juniper (green dots) plot closely to one another and tend to cluster together. The data show that the xylem water isotope values were similar between the two species, suggesting that these two species were using similar sources of water. However, we found that neither species were directly using stream water, since the xylem water values did not overlap with the stream water.

When we plotted the isotope data through time (May – October) (Figure 3b), we found a similar result as previously described. However, this figure better demonstrates that neither willow nor juniper changed water sources throughout the growing season. The xylem water isotope data for both species suggest that willow and juniper are using deeper water than 45cm, but neither are tapping directly into stream water.

An additional metric that supports our findings that willow and juniper were using similar sources of moisture are seasonal measurements of plant water potential (WP). Water potential measurements indicate the hydraulic tension of water within plants, with more negative WP values over time indicating

The goal of increasing streamflow through juniper removal in riparian areas hinges on the assumption that junipers are removing water from soils that would otherwise contribute to stream flow recharge. There are two ways in which this could occur: 1) junipers are directly using stream water and 2) junipers do not directly use stream water, but instead tap into deeper unsaturated soil water that can contribute to streamflow. However, studies have also found that streamside trees do not necessarily use stream water. To address Question 1, we characterized the oxygen and hydrogen isotopic composition ( $\delta^{18}\text{O}$ ,  $\delta\text{D}$ ) of various water sources (snowmelt, rain, ground water, soil water, stream) and ecosystem pools (tree xylem) to partition plant water use between these different water sources across three growing seasons and between the two species. We present the data below, plotted in dual isotope space (Figure 3a, x-axis  $\delta^{18}\text{O}$ , y-axis  $\delta\text{D}$ ). Two lines are plotted for orientation: 1) the global meteoric water line (GMWL) represents where precipitation tends to fall globally, with precipitation from warmer regions plotting in less negative areas and precipitation from colder areas plotting in more negative areas, 2) the local meteoric water line (LMWL), which represents the local precipitation and which can differ from the GMWL because of local climate processes. There are several interesting features from this figure. First, the stream water (pink dots) clustered towards the lower left hand corner and did not change over time. This suggests that stream water was most likely

plants experiencing water stress. However, because juniper and willow are different plant functional types (willow is a deciduous angiosperm and willow is an evergreen gymnosperm), baseline differences in WP will exist due to differences in xylem morphology and leaf area. We found that as the growing season progressed and the site became more dry, WP for both species became more negative (Figure 4), indicating an increase in water stress. However, both species recovered (e.g. WP became less negative) after the large rain even in late September. Furthermore, although the two species had different WP values (most likely due to morphology), the seasonal response from both species were similar, suggesting that they were both accessing the same, reliable water source throughout the season.

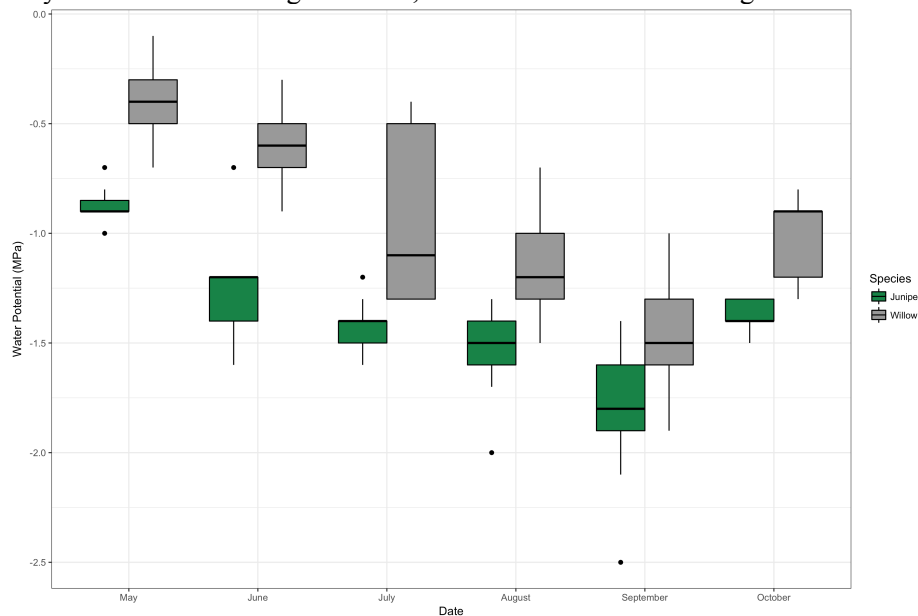


**Figure 3.** Water potential (MPa) of willow and juniper across the growing season.

*Question 2: Are Junipers using more water than other riparian woody plants, such as willow?*

*Question 3: Are the seasonal patterns of water use between juniper and willow different?*

One of the main ecohydrological concerns of juniper encroachment is that juniper will use more stream water for transpiration, leading to low late season stream flows. Willows are deciduous angiosperms while junipers are evergreen gymnosperms, resulting in large differences in both physiology and morphology. Willows tend to have higher stomatal conductance and photosynthetic rates (and therefore higher transpiration rates) while junipers have lower stomatal conductance and photosynthetic rates (and lower transpiration rates). Junipers are also adapted to dry environmental conditions and have evolved water saving strategies. On the same day under the same environmental conditions, junipers transpire less water than willows. However, because junipers are evergreen, they have the ability to transpire for longer. So despite the water saving strategies of junipers, their evergreen nature might result in overall higher annual transpiration rates than willow. We measured transpiration rates across the growing season in 2018, but present only a fraction of the processed data (Figure 4). We found that per tree, juniper did transpire more water than willow, but that this was largely due to the great water conducting tissue per tree species; in other words, juniper trees transpired more water than willow because juniper have greater sapwood (for conducting water) than willow trees. We are still currently analyzing the remaining data to assess the seasonal patterns of water use.

### Future activities

While our transpiration measurements demonstrate that per tree, juniper use more water, it remains unclear if this pattern holds true across the catchment. We are using allometric relationships between stem diameter at breast height (DBH) and crown diameter (data collected from a collaboration with Dr. Scott Powell from Montana State University) to scale up individual tree transpiration to transpiration across a 100m reach of the Greenhorn River.

In June, 2018, we will also begin juniper removal along Transect C and we assess if willow change their water source after juniper are removed. These results can be used by managers to evaluate if, when, and where junipers should be removed along a riparian area.

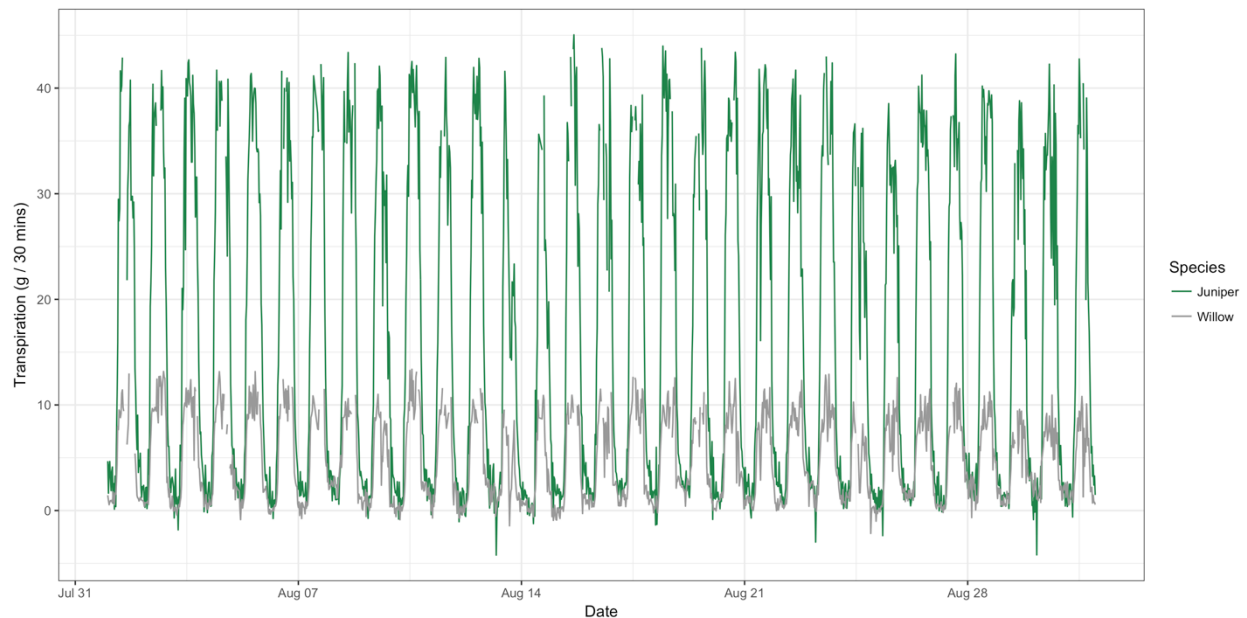


**Figure 4.** Whole tree transpiration rates (g H<sub>2</sub>O/ 30min) for one representative juniper and willow tree.

### Project outputs

We anticipate two manuscripts from this project:

- 1) Ecohydrology of two co-occurring riparian species, *Juniperus scopulorum* and *Salix amygdaloides* pre- and post- *Juniperus scopulorum* removal.
- 2) Disentangling the mechanism of riparian encroachment by *Juniperus scopulorum*: management legacies, climate changes, or both?

### Grad student work

This project has supported one graduate student from the Ecology Department at Montana State University, Kinzie Bailey. Kinzie will be starting her second year of the Master's degree in fall 2018.

# Improving Climate Information to Enhance the Drought Preparedness of Montana Agricultural Producers

## Basic Information

<b>Title:</b>	Improving Climate Information to Enhance the Drought Preparedness of Montana Agricultural Producers
<b>Project Number:</b>	2017MT311B
<b>Start Date:</b>	3/1/2017
<b>End Date:</b>	6/30/2018
<b>Funding Source:</b>	104B
<b>Congressional District:</b>	1
<b>Research Category:</b>	Climate and Hydrologic Processes
<b>Focus Categories:</b>	Drought, Agriculture, Water Use
<b>Descriptors:</b>	None
<b>Principal Investigators:</b>	Laurie Yung

## Publications

There are no publications.

# **Improving Climate Information to Enhance the Drought Preparedness of Montana Agricultural Producers: The Montana Drought and Climate Project**

Progress Report for the Montana Water Center, 5.11.18

## Principal Investigators

*Laurie Yung*, Professor, Natural Resource Social Science, University of Montana  
[laurie.yung@umontana.edu](mailto:laurie.yung@umontana.edu), (406) 243-6934

*Kelsey Jencso*, Associate Professor, Hydrology and Director, Montana Climate Office, University of Montana; [kelsey.jencso@umontana.edu](mailto:kelsey.jencso@umontana.edu), (406) 243-6793

*Libby Metcalf*, Associate Professor, Human Dimensions of Natural Resources, University of Montana; [libby.metcalf@umontana.edu](mailto:libby.metcalf@umontana.edu), (406) 243-6673

*Kyle Bocinsky*, Research Associate, Montana Climate Office, University of Montana  
[kyle.bocinsky@umontana.edu](mailto:kyle.bocinsky@umontana.edu), (770) 362-6659

*Michael Sweet*, Research and Information Systems Specialist, Montana Climate Office, University of Montana; [michael.sweet@umontana.edu](mailto:michael.sweet@umontana.edu), (406) 243-5265

## **Project Summary/Abstract**

Growing demand for water resources coupled with climate-driven water scarcity and variability present critical challenges to agriculture and food production. One of the priorities outlined in the State Water Plan (2015) is to increase Montana's drought preparedness. Extensive resources are being allocated to downscaling climate projections and climate scientists have made important advances in understanding past, current, and future climatic conditions. However, despite expected benefits, climate information is rarely used by agricultural producers and therefore has little impact on drought preparedness (Mase and Prokopy 2014). Thus, there is a critical need for research focused on improving climate information and effectively integrating that information into producer decision-making. To fill this gap, we propose an interdisciplinary research project that transforms existing climate and forecast data through new analyses and more effective science communication to produce prototypes that better meet the needs of agricultural producers in Montana. These prototypes will then be field tested with end-users to examine how producers trade-off different aspects of climate information, such as accuracy, uncertainty, and spatial and temporal scale, to determine usefulness. Research results will

inform revision of prototypes so that climate information is relevant to producers' decision context and more likely to be integrated into decision-making.

This research is particularly important because: (1) demands on Montana's limited water resources are growing and water conservation is more important than ever (State Water Plan 2015), (2) drought and water variability are predicted to worsen in Montana due to climate change, (3) agricultural producers are incredibly vulnerable to changes in water resources, (4) impacts to agricultural production effects producer livelihoods, rural communities, local economies, and food security, and (5) climate information is rapidly improving but is rarely used by producers to adapt to drought or reduce vulnerability (Dilling and Lemos 2011, Mase and Prokopy 2014, Davis et al. 2015, Soares and Dessai 2016).

### Activities to Date

Climate information is hard to access—even for domain specialists—and even when accessible it is often difficult to visualize and interpret. A key objective of the *MT Drought & Climate* project is to develop innovative technologies (in the form of web-applications and other computer software) to transform existing forecasts and projections into tools (e.g. newsletter) that meet producer needs and communicate relevant details in compelling and useful formats. This project is innovative in that we are not only producing such tools, but also are using social science methods to evaluate and refine the delivery of climate information in order to maximize utility for farmers and ranchers in Montana and beyond. Focus groups with farmers and ranchers will be conducted during summer of 2018 to gain knowledge about how producers interpret and utilize climate information, and obtain specific feedback regarding how to effectively display and communicate climate information in newsletter formats.

While our ultimate goal is to enhance understanding and utility of climate information for producers, we are also developing tools for all stakeholders in Montana agriculture, including researchers, land managers, and extension officers. The accomplishments listed below focus on the tangible and publically available outcomes of the *MT Drought & Climate* project thus far, as well as the plan for conducting focus groups with farmers and ranchers this summer.

- Developed three open-source *R* packages for downloading, analyzing, and visualizing climate data.
  - **mcor** — the base package for the Montana Climate Office.
    - 38 code commits (large code revisions)
    - Downloaded and installed by 31 individuals
    - Starred and watched by 3 developers
    - Used in a Short Course on Environmental Modeling in *R*
  - **thredds** — querying and downloading from THREDDS servers into *R*
    - 13 code commits (large code revisions)

- **mtdrought** — data and code supporting the development of the *MT Drought & Climate* seasonal newsletters; Includes all code, scripts, and functions for mapping and graphing relevant climate data in both print and web formats.
    - 3 newsletters
    - 51 code commits (large code revisions)
- Developed three *MT Drought & Climate* seasonal newsletters that transform existing forecasts and projections into tools that meet producer needs and communicate relevant details in compelling and useful formats. The newsletters form the starting point for the remaining two years of the project which will focus on refining and enhancing the presentation of climate data. Newsletter drafts were reviewed by subject matter experts and by local producers; feedback was integrated into a revision.
  - **Winter 2018** — Published January 1, 2018, and including a year-in-review; print and web
  - **Spring 2018** — Published April 1, 2018; print and web
  - **Summer 2018** — Published June 1, 2018; print and web
- Developed detailed plan for focus groups.
  - Selected focus groups sites to represent a range of agricultural operations in the state, including dryland farming, ranching, and irrigated farming. Focus group sites include Choteau (ranching), Fairfield (irrigated farming), Chester (dryland farming), and Harlowton (a mix of ranching and farming).
  - Developed interview guide to ensure systematic and comparable focus group data. Focus group questions examine challenges related to water availability and decision-making; the perceived salience, credibility, and legitimacy of climate information; how climate information is (or is not) integrated into farm decision-making; information needs (including seasonal forecasts, mid-century projections, timing of information, and relevant spatial and temporal scales); needs relative to accuracy and certainty; and barriers to using climate information.
- Leveraged our Montana Water Center proposal/project into an USDA NIFA Water for Agriculture grant.
  - After developing our proposal for the Montana Water Center, we were able to build on preliminary findings and submit a proposal to the USDA for an expanded research project.
  - USDA NIFA funds will enable us to conduct a long-term, mixed methods research project to test the efficacy of climate information for preparing farmers and ranchers for drought and water variability. This expanded project will employ a multi-year experimental design using surveys and panels to examine

how climate information effects the actual behaviors and decisions of Montana producers.

- Leveraged our Montana Water Center proposal/project into a NOAA NIDIS grant in collaboration with MT DNRC and the US Forest Service. This team will contribute to key areas of the NIDIS mandate under its 2014 Public Law 113– 86. Specifically our project team will:
  - Collect, assess and integrate information on the key indicators of drought in the Upper Missouri River Basin (UMRB) and drought impacts in order to make usable, reliable and timely forecasts of drought.
  - Continue ongoing research and monitoring activities related to predicting drought in its varying durations and magnitudes across the UMRB.
  - Build the technical capacity of the MT State Drought Task Force through the development of automated drought mapping and summarization tools.
  - Provide timely drought information and products from watershed to regional scales across the UMRB.
  - Communicate drought conditions and impacts on a regular basis to public and private entities engaged in drought planning and preparedness.

## **Project Outputs/Products**

### *MT Drought & Climate project website*

We developed a website detailing the goals and accomplishments of the *MT Drought & Climate* project that is now hosted as a section of the Montana Climate Office website:

<https://climate.umt.edu/mtdrought>. The website:

- Provides an overview of the project objectives, potential impacts, and project timeline;
- Introduces the key personnel on the project and all collaborating institutions;
- Acknowledges USDA NIFA funding;
- Presents links to the *MT Drought & Climate* seasonal newsletters.

Throughout the project, the website will be updated with new newsletters and content as it is developed.

### *MT Drought & Climate newsletter*

Effort during Year 1 was focused on developing the *MT Drought and Climate* seasonal newsletter. The newsletter has both a print and a web version; the first newsletter was published in January 2018, with subsequent issues in April and June. Each newsletter has three primary sections:

- An overview of **current conditions** and a review of how the past three months relates to historical “normal” conditions;
- A **seasonal forecast** projecting relevant conditions over the next three months;

- A mid-century outlook, presenting data from global climate models for 2040–2069, and how those conditions relate to conditions experienced in the recent past.

Each section includes maps and interpretations of climate conditions most relevant to agricultural producers in Montana. Subsections are included as seasonally relevant; for example, summer issues focus on drought metrics like evapotranspiration and soil moisture, while winter newsletters include details about snowpack.

Each newsletter is *scripted*—the newsletters are written in the *R* computer language as *RMarkdown* notebooks (<https://rmarkdown.rstudio.com/>) and can be re-compiled as conditions change. In essence, the notebooks are templates for producing such newsletters for other states and regions. All of the code necessary to re-compile the newsletters is currently being held in a publically available repository to facilitate re-use: <https://github.com/mt-climate-office/mtdrought>. We hope that other state climate offices and NIFA projects will be able to take advantage of these free and publicly available tools for communicating agriculturally-relevant climate science.

The seasonal newsletters are available for viewing (on the web) or download (pdf) on the project website, and are publicly hosted on Github. Please go to <https://climate.umt.edu/mtdrought/newsletters.php> to view and download the *MT Drought and Climate* seasonal newsletters.

#### Open-source computational tools for downloading, analyzing, and visualizing climate data

As part of developing the *MT Drought & Climate* seasonal newsletters, we have developed several *R* packages (software) and repositories of *R* code supporting the development of the newsletters and more general functions of the Montana Climate Office. Each of these is available in a public repository on Github, and we've made particular effort to document and test the code as it is developed (see links below):

- **mcor** (<https://github.com/mt-climate-office/mcor>) — The core Montana Climate Office *R* package. It contains useful data such as county and climate division maps, data download tools for commonly used datasets (including state, county, climate division, and tribal land boundaries), and convenience functions including standard web and print map templates. Of particular interest are access functions for:
  - the NOAA climate division dataset,
  - the GridMet gridded weather dataset,
  - the MACAv2 downscaled global climate model data,
  - the NASA Soil Moisture Active Passive (SMAP) soil moisture data, and
  - Snow Water Equivalent data from the SNOTEL network.
- **thredds** (<https://github.com/mt-climate-office/thredds>) — Access to THREDDS Servers. THREDDS data servers (<https://www.unidata.ucar.edu/software/thredds/current/tds/>) are web-servers that provide software-based access to gridded data. THREDDS servers not only serve data, but provide tools for subsetting gridded data in space and time on the

server, reducing the amount of data the end user must download. **thredds** is an *R* front end to THREDDS servers designed to make exploration, subsetting, and download of THREDDS data into *R* as simple as possible. Datasets available through **thredds** salient to the *MT Drought & Climate* seasonal newsletters include the GridMet gridded weather data and the MACAv2 downscaled global climate models, though **thredds** can be used to access any publically available THREDDS server.

- **mtdrought** (<https://github.com/mt-climate-office/mtdrought>) — The *MT Drought & Climate* seasonal newsletters. This repository contains functions and *RMarkdown* notebooks necessary to build each of the seasonal newsletters. A new sub-directory of the project is added for each newsletter.

Additionally, several *MT Drought & Climate* products—including the seasonal newsletters and **mcor** and **thredds** *R* packages—were highlighted in a short course in environmental analysis in *R* held at Salish Kootenai College in early May (Co-PI Bocinsky was an instructor in the course). While the course itself was sponsored under a different project (*Native Waters on Arid Lands*, funded by USDA NIFA), the *R* packages developed as part of *MT Drought & Climate* was presented as a new useful tool for land management and environmental analysis in Montana. Course participants downloaded the **mcor** and **thredds** packages and used datasets and functions from them throughout the three-day course.

### Graduate and Undergraduate Student Work

During spring 2018, M.S. student Adam Snitker was supported on a Research Assistantship to design and conduct focus groups. Adam reviewed and synthesized relevant literature on agricultural decision-making in the context of drought, and examined the literature focus group methods. He worked with the project team on study site selection and characterizing the study sites, and developed lists of initial contacts in each site. He also developed interview questions and assisted with focus group logistics. During summer 2018, Adam will code and analyze all focus group data, and summarize findings for the project team.

Also during spring 2018, undergraduate intern Carly Kuske also worked on this project (although she was funded from a different grant). Carly developed the local agricultural basis for the initial timing of the seasonal newsletters (i.e., delivering them in time for farmers and ranchers to make effective decisions); drafted the year-in-review for the Winter 2018 newsletter; and led the development of a section highlighting the Montana CoCoRaHS network—Community Collaborative Rain, Hail, and Snow network (<https://www.cocorahs.org/>)—for the Summer 2018 newsletter. Under the guidance of Co-PI Bocinsky, Carly has been learning the *R* statistical language so that she can begin developing data-driven content for future newsletters.

Both Carly and Adam attend all project meetings and are fully integrated into the project team, providing them an opportunity to participate in this innovative, interdisciplinary project, and understand how different parts of the project fit together.

## Future Activities

Over the next six months, we plan to conduct focus group, analyze focus group data, and use findings to improve climate information provided online and in newsletters. We are also working with MSU Extension to translate climate information into more specific recommendations for agricultural produces. A timeline of future activities is provided below.

May 29, 2018	Conduct focus group pilot test in St. Ignatius
June 11-13, 2018	Conduct focus groups in Choteau, Fairfield, Chester, and Harlowton
June 2018	Focus group recordings professionally transcribed
June-July 2018	Analyze focus group data in NVivo 10
August 2018	Integrate focus group findings into revised climate information
Fall 2018	Develop and submit manuscript
Winter 2018/19	Submit final report to Montana Water Center

## Literature Cited

Davis, M. et al. 2015. Barriers to using climate information: Challenges in communicating probabilistic forecasts to decision makers. *Seasonal-to-decadal climate Prediction for the improvement of European Climate Services (SPECS) Technical Note 4*. 20 pp.

Dilling, L. and Lemos, M.C. 2011. Creating usable science. *Global Environ Chng* 21:680–689.

Mase, A.S. and Prokopy, L.S. 2014. Unrealized potential: A review of perceptions and use of climate information in agricultural decision making. *Weather, Clim, and Soc* 6:47-61.

Montana State Water Plan. 2015. Department of Natural Resources and Conservation. Helena, MT.

Soares, M.B. and Dessai, S. 2016. Barriers and enablers to the use of seasonal climate forecasts amongst organisations in Europe. *Climatic Change* 137:89–103.

# Effects of floating treatment wetlands on the abundance and removal of dissolved and nanoparticulate contaminants in waste water lagoons

## Basic Information

<b>Title:</b>	Effects of floating treatment wetlands on the abundance and removal of dissolved and nanoparticulate contaminants in waste water lagoons
<b>Project Number:</b>	2017MT312B
<b>Start Date:</b>	3/1/2017
<b>End Date:</b>	2/28/2019
<b>Funding Source:</b>	104B
<b>Congressional District:</b>	1
<b>Research Category:</b>	Water Quality
<b>Focus Categories:</b>	Water Quality, Water Use, Wetlands
<b>Descriptors:</b>	None
<b>Principal Investigators:</b>	Benjamin Colman

## Publications

There are no publications.

# Effects of floating treatment wetlands on the abundance and removal of dissolved and nanoparticulate contaminants in waste water lagoons

## Introduction/background:

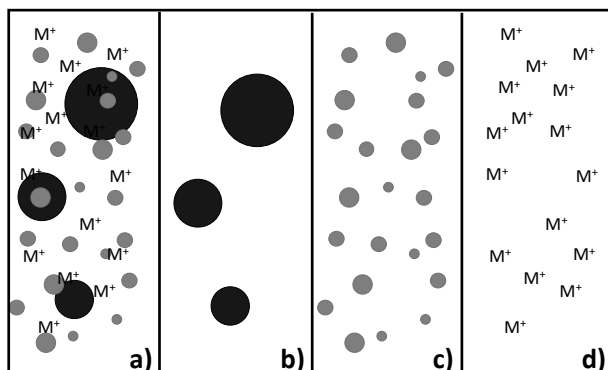
Even in sparsely populated Montana, aquatic ecosystems are exposed to an ever increasing variety of contaminants from wastewater. A majority of wastewater treatment facilities in Montana use storage lagoons as a passive treatment technology. While this approach has a reduced cost and is suitable for areas with low population density, the efficacy of contaminant removal by these wastewater lagoons is much lower than other technologies. As such, 30 out of Montana's 79 lagoon-style wastewater treatment facilities have been cited over eight times in the past twelve quarters for releasing discharge containing contaminant levels that exceed concentrations permissible by the Clean Water Act (CWA; "Enforcement and Compliance History Online" 2016). These facilities represent an important source of 'dissolved' metals and nutrients (operationally defined as passing through a 0.7 or 0.45  $\mu\text{m}$  filter) and total suspended solids (operationally defined as particulates retained by those same filters) in the surface waters into which they discharge. The resulting impairment of surface waters can change the abundance and biodiversity of organisms, ranging from the periphyton (consisting of algae, bacteria, archaea, and protists) at the base of the food web up through benthic invertebrates, fish, and terrestrial predators such as songbirds (Scheuhammer et al. 2007). This chemical impairment may also limit the resistance and resilience of ecosystems to additional stressors, including future warming and changes in the timing and magnitude of river flows (Ormerod et al. 2010).

As with all wastewater treatment facilities, the use of lagoons relies on a combination of physical and biological processes to remove excess carbon, nitrogen, phosphorous, and metals. While other technologies use a variety of actively managed biological, physical, and chemical purification steps, wastewater lagoons are largely passive and are characterized as either facultative (non-aerated) or aerated. In these lagoons, suspended solids that are sufficiently large and/or dense will settle out on their own. Dissolved solutes in lagoons are typically removed from the water column following uptake by algae and/or bacteria and subsequent deposition of the algal and/or bacterial biomass/necromass into the sediment. Bacterial activity is also essential for the removal of excess organic matter, often measured as biochemical oxygen demand. To maximize their efficiency, wastewater lagoons in Montana have a long residence time of at least 180 days. Efficiency can be further augmented by the use of aeration to increase biological oxidation of organic matter and inorganic nitrogen and by the use of multiple lagoons run in series, which to some extent spatially segregates settling and anaerobic-dominated processes from aerobic processes, thereby yielding higher rates of nutrient and metal removal overall.

While contaminants discharged from lagoons are a mixture of particles of varying size and dissolved solutes (Fig. 1a), they are operationally defined as either 'total suspended solids' (Fig. 1b) or 'dissolved'. The operational definition of dissolved includes nanoparticles and small colloids (1 – 450 nm, hereafter 'small colloids'; Fig. 1c) along with truly dissolved solutes (<1 nm; Fig. 1d). Small colloids do not settle readily from the water column, as their settling velocity is lower than their diffusion rate. This stability leads to concentrations of contaminants in excess of what would be expected based on thermodynamics and solubility alone. Yet, despite this stability, a growing body of literature on engineered particles in this

size range has shown them to be very efficiently removed by sorption and even taken up by periphyton and vascular plants (Colman et al. Manuscript in prep).

Figure 1: Schematic of water column particulates. (a) An unfiltered water sample can be separated into (b) suspended particulate matter (> 450 nm), (c) small



colloids (1-450 nm), and (d) truly dissolved solutes (<1 nm) represented by “M<sup>+</sup>” with the appropriate filters.

One technique proposed as a cost effective way of augmenting the efficacy of lagoon-style wastewater treatment facilities is the use of ‘floating treatment wetlands’ (Stewart et al. 2008). These floating islands are constructed out of recycled plastic fiber mats with foam for flotation on which a diverse assemblage of plants is grown. The plant roots extend into the water column where they create a large surface area through which nutrients and metals are taken up and sequestered by plants. The hydroponically-grown plants also serve as a source of labile carbon (food for microorganisms in the periphyton) in the form of root exudates and also provide extensive surface area for periphyton colonization. The periphyton then contributes to sequestration or removal of excess nitrogen (N), phosphorous (P), and metals by taking up contaminants as they grow and carrying N, P, and metals into the sediment with them as the slough off. Finally, the plants release oxygen via radial oxygen loss from the roots, which can help remove metals like zinc and arsenic that are susceptible to binding on iron and manganese oxide precipitates formed under oxic conditions (Brick and Moore 1996).

### **Research questions and hypotheses:**

We are using both observational and manipulative experimental approaches to address the following three questions:

1. What is the relative distribution of metals and nutrients in different size fractions in wastewater lagoons?
2. What is the role of size fraction in determining how metals and nutrients cycle between the water column, periphyton, plants, and sediments?
3. How effective are floating treatment wetlands in enhancing nutrient and metal removal from different size fractions in wastewater lagoons?

We hypothesize that much of the load of heavy metals and nutrients in wastewater lagoons are associated with the small colloidal fraction and nanoparticles as the result of their high surface area to volume ratio. Furthermore, we hypothesize that much of what has previously been thought to be leaving wastewater treatment lagoons as dissolved forms (i.e., less than 0.45  $\mu\text{m}$ ) is actually leaving as small colloids. Finally, we hypothesize that floating treatment wetlands will be effective for reducing contaminants in lagoon discharge due to their ability to remove these small particles in addition to dissolved solutes.

### **Activities/data collected to date:**

To answer Question 1, we conducted an observational study surveying wastewater treatment lagoons. To answer Questions 2 & 3, we conducted a mesocosm experiment using scaled down ecosystems with the addition of wastewater lagoon water. Below, both experiments are described and updates are provided on progress in data acquisition. Data acquisition should be complete by the end of June, and data analysis should be complete by the end of July.

**Observational study:** To examine the distribution of N, P, and metal(loid)s in different size fractions in wastewater treatment lagoons, we conducted an observational study of a set of six Montana wastewater treatment lagoons (Table 1). These six different lagoon systems varied in terms of the number of lagoons in the series, size, configuration, and whether they were aerated. As such, all the lagoons at each facility were sampled individually. Four of the lagoon systems either directly discharge into the Clark Fork River or into its tributaries while two were evaporation ponds.

**Table 1.** Wastewater facilities sampled for observational study:

Location	Lagoon Type	No. Lagoon	Quarters in Non Compliance	Reason for Violation
Drummond	Evaporation	1	3	Significant violations of improper management and not meeting compliance schedule
Ramsay	Evaporation	1	1	Inadequate information provided on safe drinking water
Philipsburg	Non-Aerated	2	12	Significant violations of BOD, E. Coli, TSS, metals, and inorganic toxins
MT State Hospital	Non-Aerated	3	7	BOD, pH, E. Coli, and TSS
Alberton	Aerated	3	8	BOD, pH, monitoring violations, algal growth, and metals
Anaconda	Aerated	2	NA	NA

Water samples were collected from three locations around each lagoon at each facility. Water samples were fractionated using filtration into three size fractions: whole (unfiltered), <450 nm fraction (small colloids, nanoparticles, and dissolved solutes), and <1 nm fraction (truly dissolved solutes). From these fractions, we will then calculate by difference the distribution of elements in the >450 nm fraction (suspended particulate matter) and the 1-450 nm fraction (small colloids and nanoparticles). Filtration was done by syringe for the <450 nm fraction (part, vendor, location), and by centrifugal ultrafiltration with a 1 kDa cutoff for the <1 nm fraction (Microrosep, Pall Corporation, Port Washington, USA). Lagoons were also characterized in the field in terms of their dissolved oxygen, pH, conductivity, and temperature using a YSI Professional Series Probe (YSI, Yellow Springs, USA) due to the influence these environmental conditions may have on the biogeochemical processes driving the distribution of elements among size fractions.

Separated fractions have been or are soon to be characterized in terms of their N, P, and metal(loid) content. Subsamples of all fractions have been measured for ammonium, nitrate, soluble reactive phosphorous (SRP), and will be analyzed this summer for total N and P as well as organic carbon. For metal(loid)s, the major focus will be on the six that are the largest contributors to river impairment in Montana, namely lead, arsenic, copper, iron, cadmium, and zinc. Manganese will also be examined, given the potential importance of this contaminant to cycling of other metals. All metal concentrations have been or will be measured using inductively coupled plasma mass spectrometry (ICP-MS).

**Manipulative Study (Q2 & Q3):** To examine the ability of FTWs to remove N, P, and metal(loid)s from wastewater, an experiment was established using mesocosms with and without FTWs receiving either high or low addition rates of lagoon-wastewater. Twelve mesocosms were established with six mesocosms having FTWs and six without (Figure 1). Mesocosms consisted of 300 gallon cattle troughs (Rubbermaid, Atlanta, USA) with liners made of 12 mil black Dura Skrim polyethylene sheeting (Americover, Escondido, USA). All mesocosms were filled with groundwater first filtered through a carbon block filter to remove dissolved and particulate matter (CFB-PLUS20BB, Pentek, Pittsburgh, PA). Islands were 63.5 x 175.26 x 160.5 cm, and were sized to give 20% coverage of the mesocosms (C.P. Edward, personal communication, March 27, 2017). Bareroot emergent macrophytes were selected for either their success in a previous experiment or their hyper accumulation capabilities, and were transplanted into the islands. Transplanted bareroot species installed were: *Sium suave*, *Equisetum hymale*, *Juncus arcticus*, *Carex aquatilis*, and *Schoenoplectus acutus* (Fourth Corner Nursery, Bellingham, USA). Islands were seeded with equal amounts of *Calamagrostis canadensis*, *Mentha arvensis*, and *Helianthus annuus* (Figure 2; Prairie Moon Nursery, Winona, USA). The planting medium consisted of a mix of 1/3 rockwool and 2/3 peat in each pre drilled 3 inch deep planting hole.

FTWs were established for 2.5 months with daily watering and with weekly cycling of water between mesocosms in order to maintain similar water chemistry between all mesocosms.

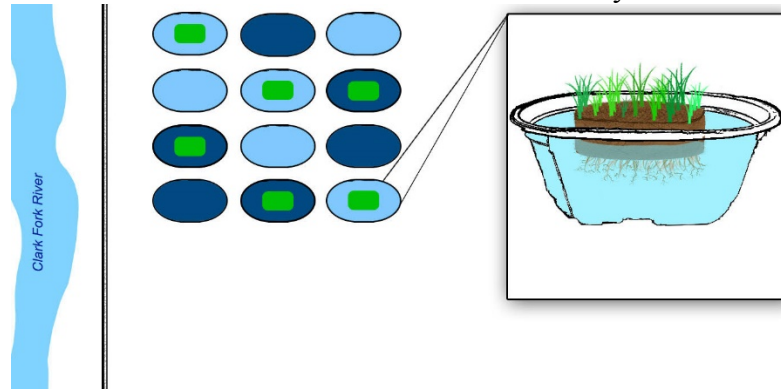


**Figure 1.** Schematic of experimental design for manipulative study. Light blue tanks represent low concentration wastewater and dark blue tanks represent high concentration wastewater.

- ✦ - *Equisetum hyemale*
- ✦ - *Sium suave*
- ✦ - *Juncus articus*
- ✦ - *Carex aquatilis*
- ✦ - *Schoenoplectus acutus*
- - Seed Mix (*Calamagrostis candensis*, *Mentha arvensis*, *Helianthus annuus*)

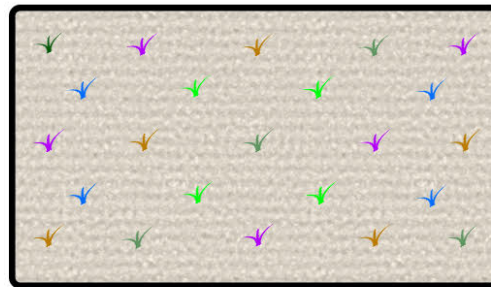


**Figure 2.** Schematic of planting design for all FTWs in Experiment 2.

To test the efficacy of FTWs in removing N, P, and metal(loid)s under high or low concentrations of these contaminants, water from Philipsburg’s terminal wastewater lagoon was brought to the mesocosm facility. Six high concentration mesocosms and six low concentration mesocosms were established, with three of each concentration with each cover type (FTW or open). Mesocosms were first drawn down to either 93 gallons of or 195 gallons and then received either 195 gallons or 93 gallons of wastewater for the high and low concentration mesocosms, respectively (Figure 1). After wastewater was added, the experiment was run for five weeks.

To examine the kinetics of changes in water chemistry over time, water samples were collected four times on day one, once per day for the first four days, and every five days thereafter over the course of a five week experiment. In order to determine the distribution of metal(loid)s, N, and P among size fractions, water samples were fractionated in the lab into the same three sizes fractions: whole (unfiltered), <450 nm fraction (small colloids, nanoparticles, and truly dissolved solutes), and a < 1 nm fraction (truly dissolved). Tower filtration was used for the < 450 nm fraction and centrifugal filtration with 1 kda ultrafiltration centrifuge filters (Microsep,

Pall Corporation, Port Washington, USA) was used to obtain the <1 nm fraction. A small volume of sample water was filtered through both the 450 nm and 1 kDa filter and then discarded prior to collecting sample filtrate in order to allow the most representative samples through the filters. Filtrates for each size fraction were then split into two aliquots, one for metal(loid)s and the other for nutrient analysis. All samples were kept on ice until processing (< 1 day). Nutrient samples were frozen while metal(loid) samples were acidified to 1% concentrated nitric acid for preservation. Given the possible role of environmental conditions on driving N, P, and metal(loid) biogeochemistry, a range of environmental parameters were measured at each sampling time point using a YSI Professional Series Probe including pH, conductivity, temperature, and dissolved oxygen.

To examine the fate of N, P, and metal(loid)s at the close of the five week experiment, all components of the mesocosms were harvested and processed for subsequent analyses including the roots, shoots, island material, periphyton, plankton, algae, and benthic organic matter at the bottom of the tanks. The roots, shoots, periphyton, plankton, and benthic organic matter were dried at 60 degrees Celsius for four days. The periphyton and benthic organic matter were combusted at 550 degrees Celsius to calculate ash free dry mass (AFDM) of the organic matter in each of these pools. Macroinvertebrates in the water column and benthic organic matter were dominated by the family *Culicidae* (mosquito), and so only *Culicidae* were collected to look at potential trophic transfer of metals. Analyses for N and P will be as described in Experiment 1, above. Subsamples from each ecosystem compartment will be analyzed to look for partitioning of metals using digestion by EPA Method 3050B (US EPA, 1996), followed by ICP-MS.

#### **Future activities, outputs, and graduate student work:**

This work is being led by Master's student, Lauren Sullivan, and will make up the majority of her thesis. Lauren has completed all of the field work, the majority of the lab work, and is starting the data analysis as she finishes the final pieces of lab work. A portion of this work will be presented at either the American Water Resources Association's Montana meeting or the Society for Ecological Restoration's Northwest Chapter meeting depending on which meeting is a better fit for the story that emerges. Lauren will also be writing this work up for her thesis and as manuscripts to submit for consideration at peer-reviewed journals in the Fall 2018/Winter 2019.

## References:

- Brick, C. M., & Moore, J. N. (1996). Diel Variation of Trace Metals in the Upper Clark Fork River, Montana. *Environmental Science & Technology*, 30(6), 1953–1960. <https://doi.org/10.1021/es9506465>
- Colman, B. P., Baker, L. F., Matson, C. W., King, R. S., Unrine, J. M., Marinakos, S. M., ... Bernhardt, E. S. (In revision). Dosing, not the dose: comparing chronic and pulsed silver nanoparticle exposures. *Environmental Science & Technology*.
- Enforcement and Compliance History Online. (n.d.). [Data & Tools]. Retrieved November 29, 2016, from <https://echo.epa.gov/>
- Ormerod, S. J., Dobson, M., Hildrew, A. G., & Townsend, C. R. (2010). Multiple stressors in freshwater ecosystems. *Freshwater Biology*, 55, 1–4. <https://doi.org/10.1111/j.1365-2427.2009.02395.x>
- Scheuhammer, A. M., Meyer, M. W., Sandheinrich, M. B., & Murray, M. W. (2007). Effects of Environmental Methylmercury on the Health of Wild Birds, Mammals, and Fish. *AMBIO: A Journal of the Human Environment*, 36(1), 12–19. [https://doi.org/10.1579/0044-7447\(2007\)36\[12:EOEMOT\]2.0.CO;2](https://doi.org/10.1579/0044-7447(2007)36[12:EOEMOT]2.0.CO;2)
- Stewart, F. M., Mulholland, T., Cunningham, A. B., Kania, B. G., & Osterlund, M. T. (2008). Floating islands as an alternative to constructed wetlands for treatment of excess nutrients from agricultural and municipal wastes - results of laboratory-scale tests. *Land Contamination & Reclamation*, 16(1), 25–33. <https://doi.org/10.2462/09670513.874>
- US EPA. (1996). *Method 3050B: acid digestion of sediments, sludges, and soils*. Retrieved from <https://www.epa.gov/sites/production/files/2015-06/documents/epa-3050b.pdf>
- Yang, Y., Colman, B. P., Bernhardt, E. S., & Hochella, M. F. (2015). Importance of a Nanoscience Approach in the Understanding of Major Aqueous Contamination Scenarios: Case Study from a Recent Coal Ash Spill. *Environmental Science & Technology*, 49(6), 3375–3382. <https://doi.org/10.1021/es505662q>

# Exploring Hydrologic Connectivity Between Shallow and Deep Groundwater Flow Systems in Upland Catchments

## Basic Information

<b>Title:</b>	Exploring Hydrologic Connectivity Between Shallow and Deep Groundwater Flow Systems in Upland Catchments
<b>Project Number:</b>	2017MT313B
<b>Start Date:</b>	3/1/2017
<b>End Date:</b>	10/1/2018
<b>Funding Source:</b>	104B
<b>Congressional District:</b>	1
<b>Research Category:</b>	Ground-water Flow and Transport
<b>Focus Categories:</b>	Hydrology, Geomorphological Processes, Climatological Processes
<b>Descriptors:</b>	None
<b>Principal Investigators:</b>	Payton Gardner

## Publications

There are no publications.

# Investigating Bedrock Hydrology in Upland Catchments

Progress report for the Montana Water Center

W. Payton Gardner  
Kelsey Jensco

## Overview:

The partitioning of water between surface, soil and groundwater reservoirs, determines the volume of storage and the rate of transmission of water through a watershed. Surface water and shallow soil water reservoirs have lower storage volumes and faster response times than groundwater reservoirs, and the partitioning of water between these reservoirs will exert primary control on watershed response to weather and climate. Little is known about the connection of soil flow and deep bedrock groundwater systems in mountainous areas where interaction is complicated by high slope angle and complex topography and geology. *In this project, the primary goal is to investigate the interaction between shallow soil flow and deep bedrock groundwater in upland catchments, and to determine the of dominant physical processes controlling the level of interaction between these reservoirs.* The final products will include: 1) the workflow and technological expertise for drilling deep groundwater wells on rugged, remote hillslopes 2) the establishment of a long-term hydrologic monitoring location and a seed dataset for increasingly complex investigation and interpretation of soil water-deep groundwater connection and 3) an outdoor laboratory to bring students and classes to learn about hillslope hydrology, streamflow generation and groundwater recharge.

## Project Findings Update:

### **Fieldwork:**

Project funds were not available until December 2017. However, initial field work started utilizing UM Departmental and Faculty start-up resources. We began drilling bedrock wells in Cap Wallace and N. Fork Elk Creek last summer. In addition, we began monitoring stream levels, flows and stream chemistry in Cap Wallace drainage. The installed monitoring network for Cap Wallace and N. Fk are shown in Figure 1. All four groundwater wells were installed as part of the cost match for this project. Stilling wells have been synoptically sampled throughout the year as part of this project and all shallow soil wells have been sampled as part of a Master's thesis, which is associated with this project.

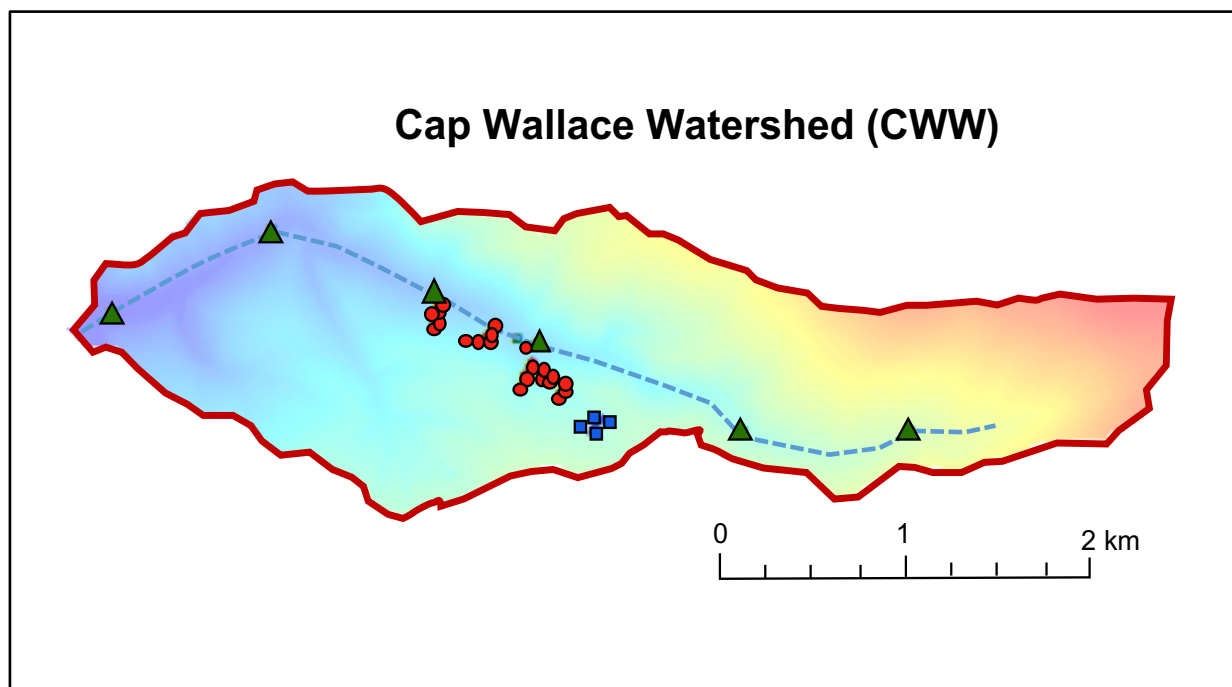
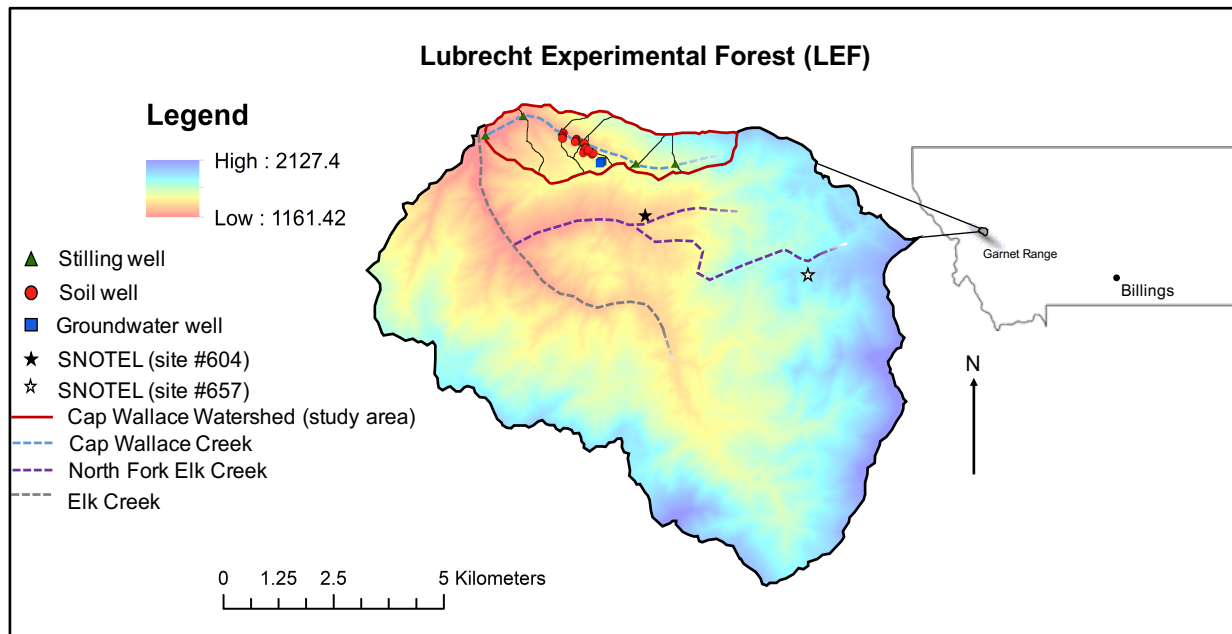


Figure 1. A regional map of Lubrecht Experimental Forest (LEF) showing its relative location on the north slope of the Garnet Range in west-central Montana. Outlined in red, Cap Wallace Watershed (CWW) was the primary area of focus in this study.

## Numerical Modeling Progress:

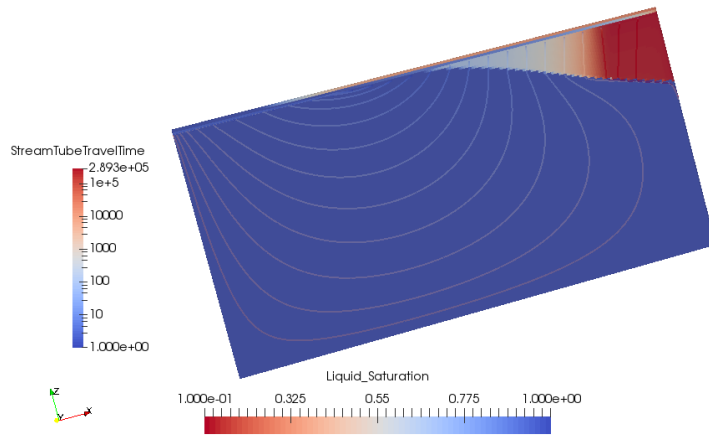


Figure 2 - The steady state saturation distribution. Streamlines originate in the first row of bedrock cells are colored according to advective travel time, with red indicating long residence times and blue indicating short residence times.

and 2 m of Columbia Sand Loam (CSL) overlying bedrock (Figure 2). Van Genuchten - Mualem capillary pressure and relative permeability curves were parameterized for the standard CSL and for fractured bedrock from (Reitsma 1994). Representative permeability values of  $10^{-13}$  m<sup>2</sup> for soil and  $10^{-17}$  m<sup>2</sup> for bedrock were used as a base case. Uniform, constant infiltration, equal to roughly 50% of precipitation at the proposed study site was applied across the top boundary. A hydrostatic seepage boundary was applied to the top 2 m of the left-hand side (upper left-hand corner) to simulate discharge to a perennial stream. Discussion of steady-state results allows for analysis of long-term average processes, suitable for the purposes of this proposal. Transient infiltration boundaries, derived from measured precipitation during the study will be used for project modeling.

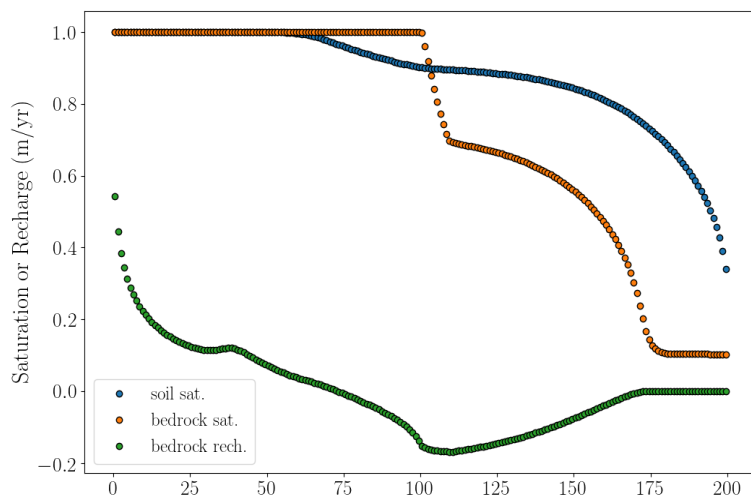


Figure 3 - Steady state soil saturation in the first row of cells above (blue), and the bedrock saturation in the first row cell below the bedrock-soil interface (orange) along with the darcy flux normal to the bedrock interface (green) plotted as a function of distance upslope.

## *Evaluating the coupling between soil moisture and groundwater*

As part of the cost share portion of the project, Dr. Gardner developed numerical models for evaluating the coupling between soil and groundwater on hillslopes. We explored the relationship between soil moisture and groundwater, with a model of a 200 m long and 100 m deep slab having a 15 degree slope

Modeled soil moisture indicates lateral redistribution with increasing soil moisture downslope (Figure 3). Underlying bedrock saturation remains and recharge flux are near zero until  $\sim 175$  m from the slope toe (roughly coincident with the groundwater ridge in Figure 2). At this location, soil moisture is  $\sim 0.7$ , and bedrock saturation rises as recharge is initiated (Figure 3). From 175 m to 100 m bedrock saturation and recharge steadily increase. After

90 m the bedrock is fully saturated and the groundwater now discharges to the soil zone (positive recharge flux).

Recharge occurs only when the soil saturation is high enough for the vertical gravity drainage to overcome the lateral slope parallel capillary flow in the soil. The point at which this critical soil moisture is achieved is a function of the upslope accumulated area lateral soil flow, thus is controlled by the watershed topography and the antecedent soil moisture conditions (OBJ1). Long term saturated soils occur where groundwater discharge is subsidizing the lateral soil flow. ***The location of recharge and groundwater discharge are critically coupled to the soil moisture distribution and landscape position.***

A sensitivity analysis of the basic parameters controlling recharge amount shows that the total amount of groundwater recharge over the hillslope changes as a function of the hill slope angle (Figure 4 a), ratio of bedrock and soil permeability (Figure 4 b), and ratio of soil to bedrock capillary pressure curves (Figure 4 c). The location and amount of recharge is clearly coupled to soil moisture and lateral flow as well as soil and bedrock hydraulic properties.

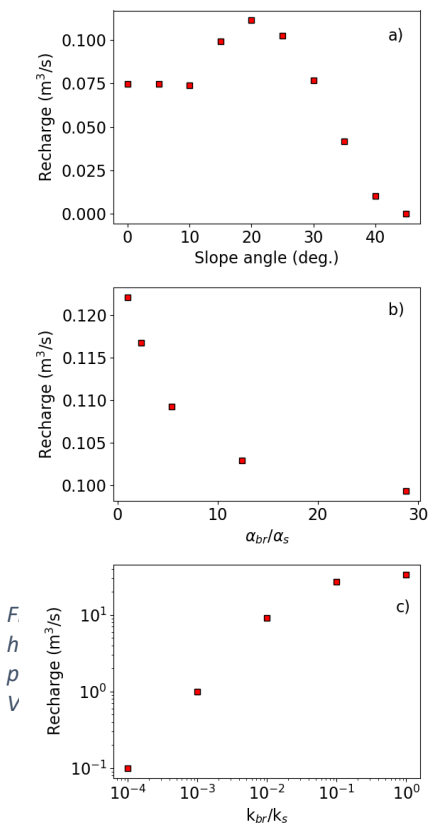


Figure 4 - Total groundwater recharge vs a) hillslope angle, b) ratio of soil to bedrock permeability and c) ratio of soil to bedrock Van Genuchten air entry pressure.

installed by a combination of soil auger and driving to the saprolite layer. Soil wells will be fully screened over the length of the soil column. Saturated soil hydraulic conductivity will be measured using an Amoozemeter.

At each sampling location we will measure hydraulic pressure response and sample for environmental tracers to understand fluid flux and residence time. In each well, we will install temperature, pressure and electrical conductivity loggers. Wells will be sampled for environmental tracers at seasonally strategic times including: spring snowmelt rising (March), spring snowmelt peak (April), spring snowmelt falling (May), baseflow transition (June) and late baseflow (August). Tracers analyzed will include major and minor elemental chemistry, stable isotopes of water, dissolved CFCs, light noble gases ( $^4\text{He}$ ,  $^{20}\text{Ne}$ ,  $^{40}\text{Ar}$ ),  $\text{SF}_6$  and radon. This tracer suite will provide information on recharge flux and a range of residence times, from days to thousands of years, recharge timing, mechanics and provenance will be investigated through the light noble gases and stable isotopes of water. Thus, we will be able to constrain the volume and rate of groundwater storage and release mechanisms over residence times rarely investigated in watershed studies.

#### Project Outputs:

Since funding was only received in winter of last year, the project is still just getting going. However, we have been working on related research funded as part of the cost share for this project, and which the project will leverage. Outputs so far include: 2 AWRA presentations, 1 presentation at AGU, 1 presentation at the MSU Rough Cut seminar, and 2 draft journal articles.

#### Project Outputs in Detail:

- Student poster 2017 Fall MT AWRA – awarded 1st prize for hydrology posters.
- Student presentation 2017 fall AGU meeting – awarded Outstanding Student Presentation – Hydrology Section.
- Faculty Presentation 2017 Fall MT AWRA
- Rough Cut Series Seminar 2017 – Dr. Gardner

# Student Fellowship Project: Science to inform restoration: Effects of channel reconstruction on hydraulic exchange and baseflow generation

## Basic Information

<b>Title:</b>	Student Fellowship Project: Science to inform restoration: Effects of channel reconstruction on hydraulic exchange and baseflow generation
<b>Project Number:</b>	2017MT314B
<b>Start Date:</b>	3/1/2017
<b>End Date:</b>	2/28/2018
<b>Funding Source:</b>	104B
<b>Congressional District:</b>	1
<b>Research Category:</b>	Ground-water Flow and Transport
<b>Focus Categories:</b>	Groundwater, Hydrology, Ecology
<b>Descriptors:</b>	None
<b>Principal Investigators:</b>	Christine Brissette

## Publication

1. Brissette, Christine M., 2017, Stream restoration effects on hydraulic exchange, storage and alluvial aquifer discharge, MS Thesis, Department of Forest Management, University of Montana, Missoula, Montana, 45pp.

# Stream restoration effects on hydraulic exchange, storage, and alluvial aquifer discharge

Christine Brissette

## ABSTRACT:

Stream restoration is increasingly being considered as a climate change mitigation tool, altering the storage and exchange capacities of streams and their adjacent alluvial aquifers. While previous research has shown that added geomorphic complexity and increased width-to-depth ratios can enhance hydraulic exchange and alluvial aquifer recharge, few studies have used field data to link these changes in form to baseflow generation. In this paper, we quantify the effect of stream restoration on nested scales of hydraulic exchange and temporal patterns of alluvial aquifer recharge and discharge. Our work compares a newly restored and adjacent degraded reach on Ninemile Creek, Montana following extensive placer mining in the mid- 1800's. Using a combination of topographic and morphologic surveys, well transects, piezometers and chemical tracers, we monitored hydraulic exchange processes across multiple spatial scales and six flow stages. We then used synoptic  $^{222}\text{Rn}$  surveys and discharge measurements to estimate reach-scale alluvial aquifer recharge and discharge over the 2016 hydrograph recession. We found that changes in channel form increased transient storage and induced feature-scale vertical exchange not observed in the degraded reach. However, vertical exchange flux and depth in the restored reach were limited by reduced subsurface hydraulic conductivity. Lateral gradients indicated increased alluvial aquifer recharge and underflow in the restored reach, in contrast to persistent alluvial aquifer drainage seen in the degraded reach. The cumulative impact of restoration resulted in a longer period of alluvial aquifer recharge early in the season, and higher volumetric groundwater discharge at baseflow. Our results suggest that restoration can increase storage and baseflow discharge, but also highlight that site-specific characteristics such as substrate hydraulic conductivity can counteract the intended effects of restoration. This work is a critical step towards understanding the efficacy of restoration in improving late season flows in the context of a changing climate and increased demands for mountain basin water resources.

## 1. INTRODUCTION

In response to climate change predictions for watersheds of the Northern Rocky Mountains, U.S.A, there is a growing interest across academic, policy and management communities in stream restoration techniques that may promote natural water storage and buffer stream flow variation. One of the most consistent climate change forecasts for these snowmelt dominated watersheds is a shift in spring snowmelt timing, resulting in earlier, more variable runoff (Barnett et al. 2005; Green et al. 2011; Huntington and Niswonger, 2012; IPCC, 2014). This shift will likely affect groundwater recharge-discharge dynamics, with earlier drainage of alluvial aquifer reservoirs and amplified water shortages in mid-to-late-summer (Barnett et al., 2008; Huntington and Niswonger, 2012). Stream discharge in this region already shows patterns of reduced summer flow (Kim and Jain, 2010; Moore et al. 2007) with the most dramatic reductions occurring in the driest years (Luce and Holden, 2009).

Stream restoration physically manipulates channel and floodplain form to increase the volumetric storage capacity of the shallow alluvial aquifer and alter the hydraulic exchange processes that affect retention and discharge within storage zones. While many studies have linked channel

geomorphic form to individual hydraulic exchange processes (e.g. hyporheic exchange or transient storage), few evaluate the net impact of multiple forms of exchange, nor their influence on seasonal trends of alluvial aquifer recharge and discharge. Furthermore, the efficacy of restoration for increasing alluvial aquifer discharge at base flow has not been well quantified. In their review of “River corridor science,” Harvey and Gooseff (2015) emphasize the challenge of - and need for - research linking small-scale mechanistic drivers of hydrologic exchange with large-scale fluvial and ecologic responses. Here, we quantify the effect of restoration on nested scales of hydraulic exchange and temporal patterns of alluvial aquifer recharge and discharge.

Streams gain and lose water across a range of spatial scales, from centimeters in the near-bed hyporheic zone, to kilometers across groundwater systems and from upland environments. Our research focuses on the river corridor (*sensu* Harvey and Gooseff, 2015), encompassing both the channel and the alluvial aquifer adjacent to, and beneath the stream, that connects the stream, groundwater, and hillslope hydrologic systems. Exchange between these systems is often referred to as “hydrologic connectivity,” with high levels of connectivity associated with ecosystem buffering (EPA, 2015; Harvey and Gooseff, 2015; Hauer et al. 2016; Jencso et al., 2010; Standford & Ward, 1993). Human impacts on the landscape such as mining, roads and development can disrupt natural patterns of hydrologic exchange and inhibit physical and biotic processes (Kasahara et al. 2009; Kondolf et al., 2006). In turn, restoration can alter, reinstate or amplify desired flowpaths and their associated hydrologic and ecosystemic functions.

Hydrologic exchange forms an essential connection between terrestrial, subterranean and aquatic systems and often follows a nested, hierarchical pattern initiated by variability in channel and floodplain topography (Berkowitz et al. 2006; Cardenas 2007; Gooseff et al. 2006; Poole et al., 2008; Stonedahl et al. 2010). The scale of the feature inducing exchange (wavelength and amplitude) positively correlates with the depth and residence time of subsurface flow (Marzadri et al., 2014; Stonedahl et al. 2010; Tonina & Buffington 2011). This results in residence times that often follow a power-law distribution, with numerous short-scale, rapid flow paths contained within increasingly larger-scale, longer-duration subsurface flows (Cardenas, 2007; Cardenas, 2008; Poole et al., 2008). While the concept of nested scales of exchange is well accepted, previous restoration research has generally focused on the response of a single metric of exchange (e.g. bedform-induced vertical exchange, or transient storage analyses). Our work, instead, evaluates exchange at three scales: 1) Transient storage, 2) Vertical hydraulic exchange, 3) Lateral and down-valley flow. These processes are then linked to seasonal patterns of alluvial aquifer recharge and discharge to better understand the broad hydrologic impact of stream restoration.

Transient storage represents streamflow moving slower than the mean advective velocity, often associated with eddies and short-term hyporheic exchange. It has been shown to increase with channel sinuosity (Patil et al., 2013; Gooseff et al. 2007), bed roughness (Gooseff et al. 2007; Wondzell, 2006) woody debris (Harvey et al., 2003; Salehin et al., 2003) and decreased channel slope (Patil et al., 2013; Gooseff et al. 2007), all of which are often enhanced through stream restoration. Vertical hydraulic exchange is driven by pressure gradients created by channel topography (e.g. bed roughness, riffles) and modulated by the hydraulic conductivity of the

substrate (Harvey and Bencala, 1993; Kasahara and Wondzell, 2003; Tonina and Buffington, 2009; Tonina et al. 2016; Woessner, 2000). Increased bed complexity through restoration may, thus, enhance the variability and scale of vertical exchange due to more variable hydraulic gradients around bed features. Finally, lateral and down-valley flow is driven by the relative elevations of the stream and adjacent water table (Woessner 2000) and strongly impacted by basin and aquifer characteristics such as valley slope, hydraulic conductivity, aquifer volume (Larkin and Sharp, 1992; Woessner, 2000) and the hydrologic connection to upland environments (Jencso et al 2010; Payn et al. 2012). While restoration will not likely affect basin-scale characteristics, previous work has shown that changes in channel geometry can increase the duration of aquifer storage (e.g. Hammersmark et al. 2008; Schilling et al. 2004; Schilling et al. 2006), or promote down-valley subsurface flow through bars and banks (Boano et al. 2009).

Cumulatively, these nested exchange processes affect temporal patterns of alluvial aquifer recharge and discharge, with longer hydraulic exchange flowpaths inherently resulting in longer subsurface residence times. Water leaving the stream and entering the subsurface is slowed by its interaction with the substrate and can be drawn away from the stream towards areas of lower hydraulic potential in the alluvial aquifer. These exchange processes, along with groundwater and hillslope contributions, fill the alluvial aquifer, which functionally “stores” water until it is discharged as streamflow down-gradient minutes, hours, days, months or years later (Cardenas, 2007; Helton et al. 2014). In this sense, the promotion of longer-duration flowpaths may have substantial impacts on later-season in-stream flows.

Our research evaluates a common stream restoration approach that simultaneously impacts multiple scales of exchange, and thus temporal trends of water storage and discharge dynamics (Figure 1). This approach includes 1) Increasing the complexity of stream bed topography to enhance deeper vertical exchange flowpaths; 2) Increasing sinuosity to activate transient storage zones and enhance exchange through banks and bars; and 3) Raising the channel bed elevation to neutralize the lateral gradient, promoting a longer bank storage period, a prolonged release of stored water and increased volumetric alluvial aquifer discharge at low flows. Using a combination of wells, piezometers, discharge measurements and groundwater tracers, we quantified the effects of restoration on nested scales of exchange and the resulting temporal patterns of alluvial aquifer recharge and discharge.

## **2. STUDY AREA**

### **2.1. Climate, Soils and Lithology**

Ninemile Creek is a tributary to the Middle Clark Fork River in Northwest Montana, USA (Figure 2a). The research site is located approximately 30 km upstream from the Clark Fork River confluence at approximately 1200 meters elevation. The basin contributing area from the downstream-most point of the study area is 60.5 km<sup>2</sup> and is primarily coniferous forest, managed by Lolo National Forest. Watersheds in this region are snowmelt-dominated, with peak discharge in May-June. Following snowmelt, the hydrograph recedes towards a base flow period in August-September with small increases in flow that are associated with fall precipitation in the form of rain and snow. Discharge at the project site ranged from approximately 100-900 liters sec<sup>-1</sup> in

2016. There are no perennial surface flows into the study area, though small ephemeral return flows occur at the break in slope between the valley and convergent uplands during snowmelt runoff. The Missoula Group of the Precambrian Belt Supergroup comprises the underlying lithology of the Ninemile basin, consisting of metasedimentary argillites, quartzites, and limestones. Valley alluvium is composed of weathered Belt, tertiary colluvial sediments and glacial lacustrine deposits from Glacial Lake Missoula. The river flows down the strike of the Ninemile fault, a regional normal fault, which was likely the source of gold deposits extracted from the region.

## **2.2 Mining and Restoration History**

Gold placer deposits were discovered in the late 1800's and were mined through the 1950's primarily through dry-land dredging. This resulted in a straightened, incised channel (Figure 2c) with 10-meter tall overburden piles and dredge ponds throughout the floodplain extent. In 2014, Trout Unlimited initiated restoration of Ninemile Creek, removing overburden piles, filling dredge ponds and establishing a new, single-thread meandering stream channel (Figure 2c) with adjacent floodplain wetlands. Restoration designs included raising the channel bed elevation to increase lateral connectivity between the stream and floodplain and adding sinuosity and riffle-pool sequences (typical of a Pool-Riffle channel sensu Montgomery and Buffington, 1997). The new channel was constructed using sorted alluvial fill from the project site.

This research compares a portion of the 2014 restoration site (351 m reach length) to a downstream reach still in post-mining condition (224 m reach length, with a 200-meter break between reaches) (Figures 2b-d ). The valley and floodplain width in both reaches (disregarding channel incision) are approximately 125 meters and 35 meters wide respectively, with a valley slope of 0.015. One important anomalous feature in the degraded reach is a channel-spanning beaver dam approximately 80 meters from the top of the reach.

## **3.0 METHODS**

### **3.1 Sampling Design**

We selected the restored and degraded reaches based upon restoration-induced differences in topographic and morphologic characteristics known to influence surface and subsurface water movement. These included channel width-to-depth ratios, slope, sinuosity and bedform complexity. The restored and degraded reaches had similar soil, geology, upslope topography and basin land cover. Valley slope and valley width were also consistent among the restored and degraded reaches. The hillslope area contributing to the restored and degraded reaches were 0.54 km<sup>2</sup> and 0.33 km<sup>2</sup> respectively.

Stream reaches were instrumented in March and April 2016. Figures 2c and 2d illustrate the locations of well transects and piezometers. We equipped shallow groundwater wells and stilling wells with pressure transducers (Solinst 3001 Levelogger Junior Edge M10, Georgetown, ON, Canada) to measure hourly groundwater and stream heights from April – November 2016. We also completed synoptic surveys of piezometers and discharge, and collected water samples for

<sup>222</sup>Radon analysis six times from May 24-November 11, 2016, with the goal of evenly characterizing the hydrograph recession.

### **3.2 Hydrometeorology**

Precipitation and snowmelt data were collected from the nearest USDA SNOTEL site, Sleeping Woman (#783) at 1875 m. elevation. This site is 600 meters above and 25 km. east-southeast of the project area, with similar characteristics to the upper basin that drains towards Ninemile Creek. These data were included in our analysis to represent the timing (not magnitude) of precipitation events in the area and to evaluate the seasonal snowmelt trends that contributed to hydrologic responses measured at our project site.

### **3.3 Characterization of channel and floodplain topography and geomorphology**

We conducted geomorphic and topographic surveys to quantify differences in the physical form of the channel and floodplain in restored and degraded reaches. Using a total station, we surveyed 1-meter resolution longitudinal profiles of each reach, and interpolated a 10 cm resolution spline to that profile for more detailed feature analyses. We also surveyed cross-sections (9 in degraded and 10 in restored) to calculate width-to-depth ratios. Survey points were georeferenced and transformed using benchmark points collected with a high resolution GPS unit (Trimble Nomad with GPS Pathfinder ProXRT receiver, Trimble Navigation Limited, Westminster, CO, USA). From these survey data, we calculated average streambed slope (upstream riffle to downstream riffle), bankfull stage, width-to-depth ratios and sinuosity (valley length/stream length). We described streambed topographic complexity by calculating thalweg variation, following the methods of Walters et al. (2003). We fit a linear regression to the longitudinal profile using the upstream and downstream-most elevations. Large residuals around the trendline correspond to prominent bed features, so a lower  $r^2$  value and larger standard deviation of residuals indicate more complex streambed topography.

A modified Wolman Pebble Count (Wolman, 1954) was used to characterize grain size distributions. Bed surface textural patches were visually assessed and mapped to estimate percent cover of each patch, and transect locations for pebble counts were stratified based on these textural patches. In the degraded reach, we identified 3 textural patches, with 105-172 total grains measured per patch. In the restored reach, we evaluated 2 patches with 208-210 grains measured per patch.

Subsurface saturated hydraulic conductivity was estimated at baseflow (August 24<sup>th</sup> and 29<sup>th</sup>) using a falling head test following Horslev (1951) in all wells (n=12) and piezometers (n=82). The Horslev method estimates the decay of the drawdown ratio of an elevated water height to baseline water height, described by the following equation from Schwartz & Zhang (2003):

$$H_t = H_0 * \exp(-KF/A * t) \tag{1}$$

Where  $A$  is the cross-sectional area of the well,  $K$  is the hydraulic conductivity and  $F$  is a shape factor describing the well or piezometer design (here,  $F = \frac{11R}{2}$  for a cased hole of radius  $R$  with soil flush with the bottom), and  $H_t$  and  $H_0$  are the drawdown ratios at times  $t_o$  and  $t_2$  (Schwartz & Zhang, 2003). We estimated  $K$  by fitting the observed drawdown ratio at all times with equation (1) using a Marquart-Levenberg technique.

### 3.4 Quantification of lateral and vertical exchange

To quantify lateral exchange dynamics, each reach was instrumented with three well transects consisting of two shallow groundwater wells, manually driven into riparian zones to approximately 1.5-meters depth and one in-stream stilling well, mounted on a T-post and sited 1-2-meters downstream of the groundwater wells. Wells were constructed from 3.81 cm PVC pipe, horizontally screened along the entire subsurface length. The total potential in the wells was measured as the water surface elevation and was characterized hourly, from spring runoff to base flow, using continuously recording water level meters (Solinst 3001 Levelogger Junior Edge M10, Georgetown, ON, Canada). We calculated lateral hydraulic gradients ( $\frac{dh}{dl}$ ) and specific discharge ( $q$ ) between groundwater and stilling wells to determine the direction (towards or away from the stream) and flux of groundwater flow:

$$q = -k_{sat} \left( \frac{dh}{dl} \right) \quad (2)$$

Where  $K_{sat}$  is saturated hydraulic conductivity  $dh$  is the change in total potential measured in the groundwater and stilling wells,  $dl$  is the distance between points.

To estimate vertical exchange between the channel and the hyporheic zone, we instrumented the reaches with 41 nested pairs of in-stream piezometers (degraded=18 pairs, restored n=23 pairs). Piezometers were constructed from 2.54 cm PVC, screened along the bottom 1 cm, and manually driven into the bed using a steel driving rod and post pounder. Piezometer nests were sited in the thalweg at 5-10 meter intervals that captured transitions between bed features (e.g. pools, riffles) expected to induce upwelling or downwelling (and later characterized by local slope). Each piezometer nest was comprised of a piezometer driven to 20 cm and 50 cm below the bed surface. We purged the piezometers of fine sediments using a drill pump at low speed, and they were allowed to equilibrate for one week before sampling. Head within the piezometers and relative stream stage were synoptically sampled six times during the study period with a water level meter (Solinst Mini Water Level Meter, Model 102M, Solinst Canada Ltd. Georgetown, ON, USA). Similar to the wells, total head in piezometers was measured as the water surface elevation within the piezometer. We calculated the vertical hydraulic gradient and specific discharge for shallow flowpaths (20 cm to the bed surface, measured as the height of the stream water surface) and deep flowpaths (50 cm to 20 cm below the bed) using **Eq. 2** above, where  $dl$  is the vertical distance between points, measured from the base of the paired piezometers.

To evaluate the influence of feature scale (e.g. cobble vs. large riffle) on patterns of vertical, subsurface exchange, we plotted piezometric vertical hydraulic gradients to the local slope of the

channel upstream of the piezometer nest. We varied the length across which slope was calculated to account for different scales of topography inducing vertical exchange, from small bed undulations (0.5 meters) to large bedforms (5-15 meters). We plotted vertical hydraulic gradients against this range of local bed slopes and fit regression lines to each relationship. All regressions were tested for significance ( $p < 0.05$ ) and significant results were compared in terms of their resulting  $r^2$  values. The length scale resulting in the best fit (highest  $r^2$ ), was interpreted as being the feature scale driving vertical exchange.

### 3.5 Well, Piezometer and Stream Specific Conductance

Environmental tracers can be used to determine the sources, fractions and residence times of water flowing along different subsurface paths. We used specific conductance (SC) as a simple tool to evaluate relative residence time and flushing behavior in the subsurface. As water travels through the subsurface, dissolved ions are accumulated, generally resulting in increased SC with increased contact time (Pilgrim et al. 1979). SC measurements were collected using a handheld YSI EC 300 probe (YSI Environmental, YSI Incorporated, Yellow Springs, OH, USA) from wells ( $n=12$ ), in-stream piezometers ( $n=82$ ) and stream sources ( $n=42$ ) during each of the six synoptic surveys. We also identified four groundwater seeps which were measured 2-3 times over the study period. Prior to measurement, wells and piezometers were slowly pumped with a drill-powered, peristaltic pump until 2x the water volume had been purged.

### 3.6 Stream Tracer Experiments: Net Change in Discharge and Transient Storage

We used dilution gauging to measure discharge ( $Q$ ) and transient storage at the reach and sub-reach scales (Day, 1976). The net change in discharge ( $dQ$ ) represents the net flux of water (gains plus losses) between the surface and subsurface systems over a given stream or valley length ( $dx$ ):

$$\text{Net change in discharge} = \frac{dQ}{dx} \tag{3}$$

A positive net change in flow indicates a net gaining stream, where more water is discharging to the stream from the adjacent valley bottom and hyporheic zone than is being lost from the stream. We divided each reach into three consecutive sub-reaches (53-120m length) and collected discharge measurements at each sub-reach boundary, six times over the study period.

Dilution gauging methods utilize conservation of mass principles to measure instantaneous discharge at a given location. A known mass of NaCl was injected upstream of a sub-reach boundary. At the downstream measurement location, an electrical conductivity probe, attached to a datalogger, measured the SC breakthrough curve (BTC) as the salt solution passed (Campbell CR1000 data logger and CS-547A temperature/conductivity probe, Campbell Scientific, Inc., Logan, Utah, United States). By integrating under the breakthrough curve, we calculate discharge (Eq. 4, from Covino et al., 2011) at each measurement location using a previously quantified linear relationship between SC and CI (1  $\mu\text{S cm}^{-1}$  increase in SC relates to 0.5 g liter<sup>-1</sup> NaCl):

$$Q = \frac{T_{MA}}{\int_0^1 T_c(t) dt}$$

(4)

where  $Q$  is discharge,  $T_{MA}$  is the tracer mass (NaCl) added and  $T_c$  is the background corrected tracer concentration. Even mixing of the salt solution throughout the water column is imperative for reliable measurements, so a mixing length (variable length, dependent on discharge) was included upstream of the reach boundary and Rhodamine dye was co-injected to visually assess mixing. To calculate precision error in our discharge measurements, we performed two replicate injections per flow stage, injecting a second NaCl slug after the first injection had passed and baseline SC had been maintained for at least 10 minutes. We then compared the resulting discharge estimates. The repeatability of our dilution gauging measurement was 4.3% of discharge (maximum error 7.6%, minimum error 0.2% of discharge).

Tracer BTC's were also used to quantify average velocity and transient storage based on the rising and tailing behavior of curves (Harvey et al. 1996). We collected three measurements per reach (along each sub-reach) at 6 flow stages. Average velocity was calculated as the injection mixing length divided by the elapsed time from injection to peak concentration ( $t_p$ ). To quantify transient storage, we normalized each curve by peak concentration (to account for different masses of NaCl injected) and evaluated the tailing behavior from peak concentration to background. A nonlinear least squared method was used to fit each BTC tail to an exponential function:

$$C = C_0 e^{-rt} \quad (5)$$

where ( $C_0$ ) is the peak concentration,  $t$  is time and  $r$  is the exponential decay coefficient that represents tailing behavior. In this case, an  $r$  value closer to zero represents more extended tailing behavior, thus higher transient storage. Mean storage residence time was evaluated as  $1/r$  (Gooseff et al. 2007) .

### 3.7 <sup>222</sup>Radon: Groundwater discharge modeling

<sup>222</sup>Radon (hereafter referred to as radon) is commonly used as a tracer for estimating groundwater discharge to surface water systems. Radon is naturally produced through the uranium decay series with a 3.82-day half-life. Radon is produced in aquifer sediments and its concentration is regionally variable. As groundwater moves through the aquifer, radon is rapidly accumulated until a maximum concentration is reached and maintained at secular equilibrium (where the rate of production equals the rate of radioactive decay) in approximately two weeks. Because radon is not present in the atmosphere, any contact with the atmosphere initiates degassing from the water body. These properties allow us to distinguish groundwater and stream water end members and approximate groundwater discharge into a stream based on the change in radon concentration over a given stream length.

#### 3.7.1 Radon sampling methods

Synoptic sampling of stream water occurred five times from May-November 2016 at the upstream and downstream extent of degraded and restored reaches. Samples were collected in 250 mL, sample-rinsed glass bottles. Alluvial aquifer samples were collected from floodplain wells and in-stream piezometers three times over the same period using a peristaltic pump. Prior

to sample collection, wells and piezometers were pumped at a low rate until 2x the initial volume had been purged.

Radon concentration was measured using a solid state alpha detector (RAD7 with RADH<sub>2</sub>O accessory unit, Durrige Company Inc, Billerica, MA, USA). To quantify instrument counting error (the largest potential source of error in estimating radon concentrations), we collected five replicate samples each at high and low flow periods. At average radon concentrations of 127 Bq m<sup>-3</sup> and 570 Bq m<sup>-3</sup>, the percent error associated with one standard deviation from the mean was 42% and 5% respectively. We assumed a linear relationship between concentration and error to estimate error at interim radon concentrations.

### 3.7.2 Radon modeling theory

To estimate groundwater seepage into Ninemile Creek, we applied a one-dimensional advective transport model adapted from Cook et al. (2006). The discharge mass balance over a given length is the sum of inflows ( $I$ ), outflows ( $O$ ) and evaporative loss ( $E$ ) over stream length  $x$ :

$$\frac{dQ}{dx} = I(x) - O(x) - E(x) \quad (7)$$

. The change in radon concentration ( $c$ ) over distance ( $x$ ) is given by (Cook et al. 2006):

$$Q \frac{dc}{dx} = I(c_i - \underline{c}) + wE\underline{c} - kw\underline{c} - dw\lambda\underline{c} + \frac{yhw\theta}{1 + \lambda t_h} - \frac{\lambda hw\theta}{1 + \lambda t_h} \underline{c} \quad (8)$$

where  $c_i$  is the radon concentration in groundwater [Bq m<sup>-3</sup>],  $\underline{c}$  is the mean concentration between upstream and downstream measurement points [Bq m<sup>-3</sup>],  $w$  is channel width [m],  $d$  is the channel depth [m],  $k$  is the gas transfer velocity [m day<sup>-1</sup>],  $\lambda$  is the decay coefficient [day<sup>-1</sup>],  $y$  is production of radon in the hyporheic zone [Bq m<sup>-3</sup> day<sup>-1</sup>],  $h$  is the depth of the hyporheic zone [m] and  $\theta$  is the porosity of the hyporheic zone.

The measured change in radon concentration over that reach was used to calculate groundwater inflows ( $I$ , in m<sup>3</sup> day<sup>-1</sup>meter stream<sup>-1</sup>). We assumed spatial homogeneity for each of our parameters, and steady-state flow conditions at each synoptic measurement time. By using  $\underline{c}$  to represent in-stream radon concentrations, we adopt a mixing model approach, assuming that the change in radon over the reach length is linear. It is important to note that the “groundwater” signature of radon at secular equilibrium is present in any water with a subsurface residence time greater than approximately two weeks. This means that regional groundwater is indistinguishable from most bank storage or parafluvial sources. “Groundwater,” in this model, is therefore defined as alluvial aquifer water that has reached secular equilibrium. This is in contrast to short, hyporheic flow paths. Hyporheic exchange can affect in-stream radon concentrations, as seen in the final two terms of **Eq. (8)**.

### 3.7.3 Parameterization and radon modeling methods

To evaluate temporal trends in groundwater discharge on restored and degraded reaches of Ninemile Creek, we approximated Eq. (8) with a mixing model approach, discretizing our model over the full reach length and applying the selected parameter values (Table 1). We then matched observed upstream and downstream radon concentrations by changing  $I$ . Groundwater discharge flux was modeled for each reach, at each of the five time intervals from May-November 2016.

Direct measurements of stream radon concentrations, stream discharge and stream channel dimensions provided reliable estimates of these parameters and their associated errors. Table 1 outlines the methods used to estimate other parameters. A series of sensitivity analyses were conducted to evaluate model response to any parameter that was not measured directly, allowing the parameter to vary over its estimated range. We modeled each equation independently, manually adjusting  $I$  to match measured  $dc/dx$  values. The range in  $I$  resulting from this variation provides insight into the sensitivity of the model to that parameter.

Accurate estimates for gas exchange velocity is especially difficult in low-order streams with highly variable geometry, velocity and temperature. Because  $k$  was not measured in the field, we used four common equations (Table 2) to approximate  $k$  and applied the mean of the results for each sampling period to our final model. All equations rely on physical measurements of velocity ( $V$ ), slope ( $S$ ) and depth ( $D$ ) which were measured at the project site throughout the season.

## 4. RESULTS

### 4.1 Seasonal streamflow and precipitation response

Precipitation and discharge trends followed a pattern typical of snowmelt-dominated mountainous regions, with peak flows associated with basin snowmelt in April and May, and rain events (June, July and October) that contributed to coincident rises in stream discharge (Figure 3). Baseflow occurred in September and was preceded by a period of 6-weeks with minimal precipitation. Average stream discharge measured on our sampling dates (dashed lines in Figure 3) were 666, 411, 292, 156, 112 and 149  $\text{l sec}^{-1}$  for May 24th, June 9th, July 7th, August 17th, September 14th and November 4th respectively.

Regional snow water equivalent reached 34 cm, 86% of the median for the period of record (measured at the Sleeping Woman SNOTEL site). The date of peak snow water equivalent was consistent with the historic record (first week of April), but the last day of recorded snowpack was May 4th, 23 days before the median historic date of full melt. Precipitation accumulation was at, or slightly above, the historic median throughout the study period.

### 4.2 Physical characterization of restored and degraded sites

Analysis of topographic and geomorphic survey data revealed notable differences between the restored and degraded reaches (Figures 4 and 5, Table 3). Sinuosity increased from 1.05 in the degraded reach to 1.33 in the restored reach. This added stream length resulted in a 50% decrease in stream slope, from 0.015 to 0.010. Width-to-depth ratios increased from 12 in the degraded

reach to 18 in the restored reach. Bed complexity was higher in the restored reach, with a lower  $r^2$  value (0.927 vs. 0.978) and higher standard deviation of residuals (32.4 vs. 10.3) when a regression line was fit to the surveyed longitudinal profiles.

Textural analysis of the stream bed (Figure 5a) revealed that the restored reach had a coarser composition overall, most notably in the large cobble-small boulder size classes (>128mm) which comprised 49% of grains sampled in the restored reach and only 30% in the degraded reach. The restored reach median grain size was 90 mm (cobble) in contrast with 64 mm (large pebble) in the degraded reach. Finer grain size classes were similar between reaches. Grains 2.0-5.6 mm (sand-granule) made up of 7% of the total grains sampled in both reaches. The degraded reach had 4% more silt and sand (< 2 mm), but most of these samples occurred in the pool upstream of the beaver dam. Discounting the beaver dam, silt and sand comprised only 1% of the total grain size distribution of the bed surface in both reaches.

Analysis of the saturated hydraulic conductivity of subsurface stream sediments from piezometers (Figure 5b) showed that the restored reach had a lower median conductivity and lower variability at both 20 and 50 cm depths. Median hydraulic conductivities in the restored reach were 8.6 cm hr<sup>-1</sup> (50 cm depth) and 52.2 cm hr<sup>-1</sup> (20 cm depth), in contrast to 14.5 (50cm depth) and 367.6 cm hr<sup>-1</sup> (20 cm depth) in the degraded reach. The interquartile range of conductivities at 20 cm and 50 cm depth were 58.7 and 137.6 cm hr<sup>-1</sup> in the restored reach and 308.2 and 462.8 cm hr<sup>-1</sup> in the degraded reach. There was also a clear differentiation between hydraulic conductivities at 20 and 50 cm for both treatments, with higher conductivity at shallower depths. This stratification was particularly evident in the degraded reach (difference between median values = 353.1 cm hr<sup>-1</sup> in degraded and 43.6 cm hr<sup>-1</sup> in restored).

### **4.3 Exchange**

#### *4.3.1 Advective velocity and transient storage*

Analyses of dilution gauging breakthrough curves showed 5-34% lower mean velocity for the restored reach at moderate to low flows. At the highest measured flows (May), the velocity in the restored reach was 11% higher than in the degraded reach (Restored monthly mean velocity: 0.89, 0.68, 0.45, 0.26, 0.29, 0.39 m sec<sup>-1</sup>; Degraded monthly mean velocity: 0.80, 0.72, 0.57, 0.39, 0.39, 0.48 m sec<sup>-1</sup>).

Mean transient storage residence time in the restored reach was 153-211% longer than the degraded reach (Figure 6) (mean of sub-reaches May-November: Restored: 1.39, 2.01, 4.03, 4.87, 3.95, 3.47 minutes; Degraded: 0.78, 1.29, 1.91, 2.46, 2.58, 1.96 minutes). In both reaches, transient storage residence time increased as streamflow and velocity decreased.

#### *4.3.2 Vertical exchange*

Vertical hydraulic gradients were similar between the restored and degraded reaches (Figure 7a). In both reaches, there was a clear separation of gradients by flowpath depth, with deeper flowpaths dominantly downwelling (median gradient degraded: -0.15; median gradient restored:-

.23), and shallow flowpaths generally exhibiting an even distribution of upwelling and downwelling (median gradient degraded: 0.11 ; median gradient restored:0.04).

The length scale of feature inducing vertical exchange differed between reaches. Regardless of the length-scale used to calculate the slope (0-15 meters), the degraded reach showed no significant relationship between vertical hydraulic gradient and local bed slope. In the restored reach, and at shallow depths (0-20 cm), there were significant negative relationships ( $p > 0.05$ ) in four of six months and at several length scales (Table 4). We also sought to represent the variable length of constructed bedforms. Because piezometers were intentionally sited to capture changes in bed slope associated with vertical exchange, we used the average slope between piezometers as our variable length scale for analysis. This variable length scale predicted vertical hydraulic gradients best (highest  $r^2$  value of all significant relationships) in May, July and September ( $r^2$  of 0.20, 0.26 and 0.19 respectively). In November, a 5-meter length provided the best fit ( $r^2 = 0.27$ ). The variable length scale for the restored reach ranged between 7-35 meters, with a mean length of 19 meters. There were no significant relationships in the restored reach in June or August using any length scale of bed slope. Deep flow paths (20-50 cm), which were predominantly downwelling, showed no significant relationships at any time or length scale with the exception of September base flow at the variable length-scale in the restored reach.

Despite the two reaches having similar vertical hydraulic gradients, when we evaluated specific discharge, the degraded reach had a higher exchange flux due to its higher hydraulic conductivity (Figure 7b). The median upward flux in the degraded reach at 20 cm and 50 cm respectively was  $33.2 \text{ cm hr}^{-1}$  and  $42.4 \text{ cm hr}^{-1}$  while the degraded downward flux was  $-33.6 \text{ cm hr}^{-1}$  and  $-16.8 \text{ cm hr}^{-1}$  at either depth. In the restored reach the flux values were substantially reduced with upward gradients of  $2.9 \text{ cm hr}^{-1}$  and  $10.1 \text{ cm hr}^{-1}$  and downward gradients of  $-9.9$  and  $-2.2$  at 20 and 50 cm respectively.

#### 4.3.3 Specific Conductance

Mean specific conductance in groundwater seeps was  $247 \text{ uS cm}^{-1}$  (minimum:  $167 \text{ uS cm}^{-1}$  maximum:  $322 \text{ uS cm}^{-1}$ ) while streamwater ranged from a minimum of 154 in May to a maximum of 180 in June. Baseflow SC was 172 in September. SC from subsurface water samples in the restored reach were consistently higher (20 cm depth: median=  $218 \text{ uS cm}^{-1}$ ; 50 cm depth: median =  $261 \text{ uS cm}^{-1}$ ) than the degraded reach (20 cm depth: median= $178 \text{ uS cm}^{-1}$ ; 50 cm depth: median =  $185 \text{ uS cm}^{-1}$ ) (Figure 7c). In both reaches, median SC values increased with subsurface depth.

#### 4.3.4 Lateral exchange

We analyzed lateral gradients of exchange between shallow groundwater wells and the stream to evaluate the direction of flow toward (positive gradient) or away from (negative gradient) the stream. Figure 8 presents hourly gradients at each of the twelve wells over time. The restored reach exhibited neutral to losing (negative) gradients, becoming more negative with the decline in stream stage. The degraded reach, in contrast, consistently gained (positive gradients) in the lateral direction.

#### 4.4 Temporal trends in Groundwater Recharge-Discharge

##### 4.4.1. Base flow discharge modeling using <sup>222</sup>Radon

In-stream radon concentrations ranged from a minimum of 146 Bq m<sup>-3</sup> in May to a maximum of 663 Bq m<sup>-3</sup> in November. We selected a groundwater radon concentration of 26,250 Bq m<sup>-3</sup> for our model, which was the maximum radon concentration measured at the site, thus our groundwater discharge estimates represent minimum values.

Based on our sensitivity analyses, instrument counting error of radon concentration ( $c$ ) produced the broadest range of model outcomes, followed by gas exchange velocity ( $k$ ). Our final model of groundwater inflows (Figure 9a) presents modeled inflows plus or minus one standard deviation of instrument counting error of  $c$ . Results are normalized by valley length to represent the valley-scale impact of restoration. The  $k$  value used in this model is the mean of the four gas exchange velocity equations. The restored reach demonstrated continuous groundwater inflows to the stream throughout the season (mean restored inflows: 1.70, 1.65, 0.78, 1.80 m<sup>3</sup> day<sup>-1</sup> m valley<sup>-1</sup> for June, July, August and November samples), with 88-100% higher inflows than the degraded reach in July-November. The clear exception to this trend is in June, when the degraded reach shows a 17% higher inflow rate, which rapidly declines towards zero inflows by August (mean degraded inflows: 2.05, 0.20, 0.00, 0.10 m<sup>3</sup> day<sup>-1</sup> m valley<sup>-1</sup> for June, July, August and November samples). In August, at lowest sampled streamflow, the restored reach had an inflow flux of 0.78 m<sup>3</sup> day<sup>-1</sup> m valley<sup>-1</sup> while the degraded reach had 0.00 m<sup>3</sup> day<sup>-1</sup> m valley<sup>-1</sup>.

##### 4.4.2 Net change in discharge

We also used net change in discharge from upstream to downstream to evaluate recharge and discharge dynamics over time (Figure 9b). Similar to the radon model, the degraded reach showed gains in June, declining throughout the season until September base flow when the net change in discharge was slightly negative (losses) (13.7, 15.3, 8.5, -0.4, 6.5 m<sup>3</sup> day<sup>-1</sup> m valley<sup>-1</sup> in June-November). The restored reach, in contrast, gained in early spring, then lost water during the early summer. As base flow approached in August, this dynamic switched, with the restored reach gaining as flows receded (0.65, -5.6, 6.5, 4.6, 2.0 m<sup>3</sup> day<sup>-1</sup> m valley<sup>-1</sup> in June-November). At September base flow, the degraded reach was losing (-0.4 m<sup>3</sup> day<sup>-1</sup> m valley<sup>-1</sup>), while the restored reach maintained gains of 4.6 m<sup>3</sup> day<sup>-1</sup> m valley<sup>-1</sup>.

## 5. DISCUSSION

Restoration altered hydraulic exchange processes across all spatial scales evaluated. Our results suggest 1) Increased in-stream residence time and transient storage 2) Initiation of feature-scale vertical exchange (though limited by substrate stratification) 3) Reduced vertical flux due to lower hydraulic conductivity and 4) Temporal shifts in lateral exchange dynamics, with more neutral to losing (storing) trends in the restored reach. Cumulatively, these changes in hydraulic exchange processes altered temporal patterns of alluvial aquifer recharge and discharge. These results were consistent with our conceptual model, showing increased early-season storage which later subsidized base flow. In the following sections, we discuss how physical alterations to the restored reach morphology led to differences in hydrologic exchange and reach-scale storage and discharge dynamics.

## **5.1 Effects of Restoration on Hydraulic Exchange**

### *5.1.1 Advective velocity and transient storage*

Restoration decreased average velocity and increased transient storage residence times at nearly all flow stages (Figure 6). Each of the observed changes in channel form (increase bedform complexity, sinuosity and decreased slope) has been previously linked to increased transient storage, slowing and recirculating surface water within the channel and reducing the influence of advection (Gooseff et al., 2007; Harvey et al., 2003; Patil et al., 2013; Salehin et al., 2003; Wondzell, 2006). This type of exchange is crucial for short-term processes like biogeochemical transformations (Boulton et al. 1998; Findlay, 1995) but likely has little effect on seasonal trends in storage and baseflow discharge.

### *5.1.2 Vertical exchange*

Our vertical exchange results highlight the importance of considering substrate hydraulic conductivity in conjunction with streambed topography when attempting to modify hyporheic exchange flows. The addition of larger streambed features (e.g. riffles, pools) did lead to predictable spatial patterns of upwelling and downwelling (Table 4) that were not observed in the degraded reach. However, this exchange was limited to the upper 20 cm of the subsurface. There was no evidence to suggest that the constructed features promoted the deeper flowpaths with longer residence times that have been observed in other field and model simulations (Marzadri et al., 2014; Stonedahl et al. 2010; Tonina & Buffington, 2011). We attribute this to the overall lower, and stratified hydraulic conductivity of the subsurface. Lower hydraulic conductivity was likely a result of compaction from the construction process that reduced median vertical flux in the shallow zone by 93-96%. In the degraded reach, we found no relationship between local bedslope and longitudinal patterns of upwelling and downwelling. This suggests that here, vertical exchange is controlled by features smaller than 50 cm (the resolution limit of our analysis), or by other factors such as heterogeneity in the substrate hydraulic conductivity. Stratification of the subsurface was particularly evident in the degraded reach (Figure 5b), resulting in higher fluxes in the upper 20 cm zone. These results are also supported by our SC data. SC in the degraded reach at 20 cm was similar to streamwater with little variance, indicating rapid flushing and little interaction with the substrate (Figure 7c). In the restored reach, at both 20 and 50 cm depths, SC was higher, more variable, and increased with depth. This suggests that longer subsurface residence times allowed for increased weathering reactions and/or mixing with solute-rich groundwater sources.

### *5.1.3 Lateral Exchange*

The patterns of lateral groundwater-surface water exchange measured by our monitoring wells were consistent with our conceptual model. The degraded reach showed lateral gradient trends typical of an incised channel (Schilling et al. 2004) (Figure 8a). Throughout the year, the alluvial aquifer discharged to the degraded stream due to the gradient produced by an unnaturally low channel elevation. This lowered elevation eliminated bank storage processes at high flows and contributed to more rapid drainage of the alluvial aquifer (similar to results of Schilling et al. 2006). The restored reach, in contrast, had neutral to losing gradients throughout the season

(Figure 8b). Losses from the stream generally indicate alluvial aquifer recharge, while relatively neutral gradients may be indicative of dominant subsurface flow running parallel to the channel (underflow, *sensu* Larkin and Sharp, 1997), rather than in the lateral direction. Our instrumentation design did not directly evaluate the impact of increased sinuosity on parafluvial flow or underflow, but we believe that this was likely a substantial exchange process affected by restoration. This is supported by the generally neutral lateral gradient observed, as well as a wealth of literature showing a positive relationship between the degree of channel curvature and exchange flux through bars and banks (e.g. Boano et al. 2006; Cardenas et al., 2009; Gomez et al., 2012; Stonedahl et al., 2010).

## **5.2 Temporal trends in alluvial aquifer recharge and discharge**

Temporal trends in alluvial aquifer recharge and discharge were markedly different in the restored and degraded settings. Overall, our results support the hypothesis that restoration induced alluvial aquifer storage during spring snowmelt, allowing for more sustained and higher volumetric aquifer discharge at low flows. By comparing seasonal trends in lateral gradients to radon modeling and net change in discharge results, we can begin to elucidate the mechanisms behind the recharge-discharge dynamics observed.

In June, the Ninemile basin was likely contributing a maximum amount of water to the Ninemile valley due to Spring snowmelt and precipitation. Our radon modeling, net change in discharge and lateral gradient results all indicate that in the degraded reach, this water moved rapidly into the stream system, causing high rates of groundwater discharge to the stream which rapidly declined as the season progressed (Figures 8 and 9). In the restored reach, however, our radon model shows a buffered response to hillslope contributions, with lower early-season inflows compared to the degraded reach (Figure 9a). This suggests that contributions from hillslopes and bank storage were stored, producing the more gradual decline in alluvial aquifer discharge through the base flow recession. Net change in discharge results also support this observation, showing in-stream losses (aquifer storage) early in the season, shifting to gains (aquifer discharge) that sustained base flows (Figure 9b). Of particular importance, both metrics show substantially higher volumetric discharge at the lowest measured streamflows (increase of  $0.7 \text{ m}^3 \text{ day}^{-1} \text{ m valley}^{-1}$  of radon-modeled groundwater discharge, and  $5 \text{ m}^3 \text{ day}^{-1} \text{ m valley}^{-1}$  net gains).

These trends generally agree with lateral gradient results, supporting our hypotheses that by reducing the elevation differential between the channel and floodplain, restoration neutralizes lateral gradients and increases the duration of the seasonal storage period. Dominant trends of storage and underflow in the restored reach fit our conceptual model (Figure 1) except at base flow where we would expect to see a reversal in the lateral gradient direction, with stored water discharging into the stream (as indicated by radon and net change in flow results).

## **5.3 Restoration Implications: Transferring results outside of the Ninemile Creek Basin**

Our work presents a case study of restoration impacts on a section of Ninemile Creek, Montana. While our results generally align with the predictions of our conceptual model, we recognize that these results are not directly transferable to all systems. Larger-scale basin characteristics such as

lithology, alluvial aquifer volume, climate and basin topography all control the rate, volume, location and timing of inflow into and out of the alluvial aquifer (Bergstrom et al., 2016; Harvey and Gooseff, 2015; Jencso et al., 2009; Jencso et al., 2010; Ward et al., 2016) and play an important role for a particular valley's response to restoration. Restoration practitioners must be sensitive to this variability when attempting predict natural storage enhancement. To promote natural storage, restoration sites must have enough precipitation and basin retention to raise the water table to match new streambed elevations. Additionally, smaller aquifers will be more responsive to surficial manipulations of topography or increased storage capacity than larger, higher order river systems where the relative increase of exchange and storage is lower.

The relative roles of topography and substrate hydraulic conductivity are also important to consider when transferring concepts between basins. Our vertical exchange results provide a key example. Compaction in the restored reach likely caused the low hydraulic conductivity and reduced vertical flux observed. This impact could be minimized or avoided during construction. However, substrate stratification (also seen in the degraded reach) may be a natural result of fluvial sorting of the bed material. In another system with more conductive, homogeneous alluvial material, construction of variable topography might induce deeper flowpaths. In systems like the Ninemile, the impact of these features is limited. Instead, flowpath length and residence time was strongly influenced by the hydraulic conductivity and the potential for substrate stratification. Heterogeneity in both topography and hydraulic conductivity will likely result in power law residence times distributions with concurrent short, medium and long flowpaths, even though the mechanisms driving these distributions differ.

## **6. CONCLUSION**

In this paper, we quantify the effect of channel restoration on nested scales of hydraulic exchange and temporal patterns of alluvial aquifer recharge and discharge. Using a combination of geomorphic and topographic surveys, hydrometrics, groundwater tracers and discharge measurements, we link changes in the physical form of the channel and valley to hydrologic responses to restoration across spatial and temporal scales. Restoration increased transient storage, likely due to increased sinuosity, bedform complexity and reduced slope. Introduction of larger, more variable bed features (riffles and pools) effectively induced vertical exchange, though the depth and rate of exchange was limited by the lower, stratified hydraulic conductivity. Lateral exchange trends in the restored reach were dominated by storage or underflow processes, in contrast to rapid aquifer drainage (discharge) in the degraded reach.

The cumulative impact of these exchange processes resulted in a longer period of alluvial aquifer recharge early in the season, allowing for higher volumetric discharge to sustain base flow. This is evidenced by net losses in stream discharge (storage) in the restored reach at moderate flows and higher net volumetric gains (discharge) at base flow. Additionally, <sup>222</sup>Radon modeling results reveal a more gradual, prolonged reduction in groundwater discharge from Spring to base flow, with higher rates of discharge at most time periods, most notably at the lowest flows.

Our findings support an assumed, but not well examined theory that stream restoration can prolong the baseflow recession, contributing larger volumes of stored alluvial aquifer water to the stream later in the season. This may have significant impacts on streamflow discharge and temperature, especially at base flow. This approach to restoration could, therefore, be effective in buffering streams from climate change-induced variations in the water cycle. Basin characteristics such as climate, lithology and existing storage capacity must be considered to appropriately characterize how form may influence hydrologic function of disturbed and restored watersheds.

### **Acknowledgements:**

Financial support was provided by grants from the University of Montana grant program #M25379 awarded to Jencso, the Montana Institute on Ecosystems and a fellowship awarded to Brissette by the Montana Water Center. We would like to thank Trout Unlimited for access to the research site and logistical support and Dr. Maury Valett and Dr. Lisa Eby for comments and suggestions during the course of this project

### **References**

Arrigoni, A. S., G. C. Poole, L. A. K. Mertes, S. J. O'Daniel, W. W. Woessner, and S. A. Thomas (2008), Buffered, lagged, or cooled? Disentangling hyporheic influences on temperature cycles in stream channels, *Water Resour. Res.*, 44, W09418, doi:10.1029/2007WR006480.

Barnett, T.P., J.C. Adam and D.P. Lettenmaier (2005), Potential impacts of a warming climate on water availability in snow-dominated regions, *Nature*, 438, 303-309, doi:10.1038/nature04141

Bencala, K. E., M. N. Gooseff, and B. A. Kimball (2011), Rethinking hyporheic flow and transient storage to advance understanding of stream-catchment connections, *Water Resour. Res.*, 47, W00H03, doi:10.1029/2010WR010066.

Bergstrom, A., Jencso, K., & McGlynn, B. (2016). Spatiotemporal processes that contribute to hydrologic exchange between hillslopes, valley bottoms, and streams. *Water Resources Research*, 52(6), 4628-4645

Berkowitz, B., Cortis, A., Dentz, M., & Scher, H. (2006). Modeling non-Fickian transport in geological formations as a continuous time random walk. *Reviews of Geophysics*, 44(2).

Boano, F., Camporeale, C., Revelli, R., & Ridolfi, L. (2006). Sinuosity-driven hyporheic exchange in meandering rivers. *Geophysical Research Letters*, 33(18).

Boulton, A. J., Findlay, S., Marmonier, P., Stanley, E. H., & Valett, H. M. (1998). The functional significance of the hyporheic zone in streams and rivers. *Annual Review of Ecology and Systematics*, 29(1),59-81.

Bourke, S.A. , P.G. Cook, M. Shanafield, S. Dogramaci, J.F. Clark (2014) Characterisation of hyporheic exchange in a losing stream using radon-222, *Journal of Hydrology*, 514(A), 94-105

Brunke, M., & Gonser, T. O. M. (1997). The ecological significance of exchange processes between rivers and groundwater. *Freshwater biology*, 37(1), 1-33.

Buffington, J. M. and Tonina, D. (2009), Hyporheic Exchange in Mountain Rivers II: Effects of Channel Morphology on Mechanics, Scales, and Rates of Exchange. *Geography Compass*, 3: 1038–1062. doi: 10.1111/j.1749-8198.2009.00225

Cardenas, M. B. (2007). Potential contribution of topography-driven regional groundwater flow to fractal stream chemistry: Residence time distribution analysis of Tóth flow. *Geophysical Research Letters*, 34(5).

Cardenas, M. B. (2008). Surface water-groundwater interface geomorphology leads to scaling of residence times. *Geophysical Research Letters*, 35(8).

Cardenas, M. Bayani. (2009) Stream-aquifer interactions and hyporheic exchange in gaining and losing sinuous streams. *Water Resources Research* 45.6

Cook, P. G., Lamontagne, S., Berhane, D., & Clark, J. F. (2006). Quantifying groundwater discharge to Cockburn River, southeastern Australia, using dissolved gas tracers  $^{222}\text{Rn}$  and  $\text{SF}_6$ . *Water Resources Research*, 42(10).

Cook, P.G., & A.L. Herczeg (2000), *Environmental Tracers in Subsurface Hydrology*. Springer US: 2000. Print. 10.1007/978-1-4615-4557-6

Covino, T., McGlynn, B., & Mallard, J. (2011). Stream-groundwater exchange and hydrologic turnover at the network scale. *Water Resources Research*, 47(12).

Day, T. J. (1976). On the precision of salt dilution gauging. *Journal of Hydrology*, 31(3-4), 293-306.

E.P.A. 2015. "Connectivity of Streams & Wetlands to Downstream Waters: A Review & Synthesis of the Scientific Evidence." Washington

Findlay, S. (1995). Importance of surface-subsurface exchange in stream ecosystems: The hyporheic zone. *Limnology and oceanography*, 40(1), 159-164.

Google Inc. (2017). Google Earth (Version 7.1.8.3036). Available from <https://www.google.com/earth/>

Gomez, J. D., Wilson, J. L., & Cardenas, M. B. (2012). Residence time distributions in sinuosity-driven hyporheic zones and their biogeochemical effects. *Water Resources Research*, 48(9).

Gooseff, M. N., Anderson, J. K., Wondzell, S. M., LaNier, J., & Haggerty, R. (2006). A modelling study of hyporheic exchange pattern and the sequence, size, and spacing of stream bedforms in mountain stream networks, Oregon, USA. *Hydrological Processes*, 20(11), 2443-2457.

Gooseff, Michael N., Robert O. Hall, and Jennifer L. Tank. (2007) Relating transient storage to channel complexity in streams of varying land use in Jackson Hole, Wyoming." *Water Resources Research* 43.1.

Green, T.R., M. Taniguchi, H. Kooi, J.J. Gurdak, D.M. Allen, K.M. Hiscock, H. Treidel, A.

- Aureli (2011) Beneath the surface of global change: Impacts of climate change on groundwater, *Journal of Hydrology*, 405, 532-560
- Hammersmark, C.T., M.C. Rains, and J.F. Mount. (2008) Quantifying the hydrological effects of stream restoration in a montane meadow, northern California, USA." *River Research and applications* 24.6: 735-753.
- Harvey J.W. and K.E. Bencala (1993), The effect of streambed topography on surface-subsurface water exchange in mountain catchments, *Water Resour. Res.*, 29(1), doi: 10.1029/92WR01960.
- Harvey, J. W., Conklin, M. H., & Koelsch, R. S. (2003). Predicting changes in hydrologic retention in an evolving semi-arid alluvial stream. *Advances in Water Resources*, 26(9), 939-950.
- Harvey, J., and M. Gooseff (2015), River corridor science: Hydrologic exchange and ecological consequences from bedforms to basins, *Water Resour. Res.*, 51, 6893–6922,
- Harvey, J. W., B. J. Wagner, and K. E. Bencala (1996), Evaluating the reliability of the stream tracer approach to characterize stream-subsurface water exchange, *Water Resour. Res.*, 32(8), 2441–2451
- Hauer, F. Richard, et al. (2016) Gravel-bed river floodplains are the ecological nexus of glaciated mountain landscapes. *Science Advances* 2.6
- Helton, A. M., Poole, G. C., Payn, R. A., Izurieta, C., & Stanford, J. A. (2014). Relative influences of the river channel, floodplain surface, and alluvial aquifer on simulated hydrologic residence time in a montane river floodplain. *Geomorphology*, 205, 17-26.
- Hester, E. T. and Gooseff, M. N. (2011) Hyporheic Restoration in Streams and Rivers, in *Stream Restoration in Dynamic Fluvial Systems* (eds A. Simon, S. J. Bennett and J. M. Castro), American Geophysical Union, Washington, D. C.
- Hoeg, S., Uhlenbrook, S., & Leibundgut, C. (2000). Hydrograph separation in a mountainous catchment—combining hydrochemical and isotopic tracers. *Hydrological Processes*, 14(7), 1199-1216
- Hooper, R., B. Aulenbach, D. Burns, J. J. McDonnell, J. Freer, C. Kendall, and K. Beven (1997), Riparian control of streamwater chemistry: Implications for hydrochemical basin models, *IAHS Redbook*, 248, 451–458.
- Hvorslev, M. J. (1951). Time lag and soil permeability in ground-water observations.
- Hill, A. R. (1996), Nitrate removal in stream riparian zones, *J. Environ. Qual.*, 25, 743–755.
- Huntington, J. L., & Niswonger, R. G. (2012). Role of surface-water and groundwater interactions on projected summertime streamflow in snow dominated regions: An integrated modeling approach. *Water Resources Research*, 48(11).

IPCC, 2014: Climate Change 2014: Synthesis Report. Contribution of Working Groups I, II and III to the Fifth Assessment Report of the Intergovernmental Panel on Climate Change [Core Writing Team, R.K. Pachauri and L.A. Meyer (eds.)]. IPCC, Geneva, Switzerland,

Jencso, K., B. McGlynn, M. Gooseff, S. Wondzell, K. Bencala, and L. Marshall (2009), Hydrologic connectivity between landscapes and streams: Transferring reach-and plot-scale understanding to the catchment scale, *Water Resour. Res.*, 45, W04428,

Jencso K.G., B.L. McGlynn, M.N. Gooseff, K.E. Bencala and S.M. Wondzell (2010), Hillslope hydrologic connectivity controls riparian groundwater turnover: Implications of catchment structure for riparian buffering and stream water sources, *Water Resour. Res.*, 46,

Kasahara, T., Wondzell, S.M. (2003) Geomorphic controls on hyporheic exchange flow in mountain streams. *Water Resour. Res.*, 39(1)

Kasahara, T., Mutz, M., and Boulton, A. J. (2009) Treating causes not symptoms: restoration of surface-groundwater interactions in rivers. *Marine and Freshwater Research* 60, 976–981.

Kondolf, G. M., A. J. Boulton, S. O'Daniel, G. C. Poole, F. J. Rahel, E. H. Stanley, E. Wohl, A. Bång, J. Carlstrom, C. Cristoni, H. Huber, S. Koljonen, P. Louhi, and K. Nakamura (2006) Process-based ecological river restoration: visualizing three-dimensional connectivity and dynamic vectors to recover lost linkages. *Ecology and Society* 11(2): 5.

Kim, J. S., & Jain, S. (2010). High-resolution streamflow trend analysis applicable to annual decision calendars: A western United States case study. *Climatic change*, 102(3), 699-707.

Larkin and Sharp (1992) On the relationship between river-basin geomorphology, aquifer hydraulics, and ground-water flow direction in alluvial aquifers. *GSA Bulletin* Dec 1992, 104 (12) 1608-1620

Luce, C. H., & Holden, Z. A. (2009). Declining annual streamflow distributions in the Pacific Northwest United States, 1948–2006. *Geophysical Research Letters*, 36(16).

Marzadri, A., Tonina, D., McKean, J. A., Tiedemann, M. G., & Benjankar, R. M. (2014). Multi-scale streambed topographic and discharge effects on hyporheic exchange at the stream network scale in confined streams. *Journal of Hydrology*, 519, 1997-2011.

Montana Bureau of Mines and Geology, Montana Tech, University of Montana  
Available online at <http://mbmg.mtech.edu/mbmgcat/public/ListArchives.asp>. Accessed [01/14/2016]

Montgomery, D.R. and J.M. Buffington (1997), Channel-reach morphology in mountain drainage basins, *GSA Bulletin*, 109(5), 596-611.

Moore, J. N., Harper, J. T., & Greenwood, M. C. (2007). Significance of trends toward earlier snowmelt runoff, Columbia and Missouri Basin headwaters, western United States. *Geophysical Research Letters*, 34(16).

Natural Resources Conservation Service, United States Department of Agriculture. Web Soil Survey. Available online at <https://websoilsurvey.sc.egov.usda.gov/>. Accessed [11/06/2015].

Negulescu, M., and V. Rojanski. (1969) Recent research to determine reaeration coefficient. *Water Research* 3.3: 189IN3193-192IN6202.

O'Connor, D. and W. Dobbins. 1958. Mechanism of reaeration in natural streams. *Transactions of the American Society of Civil Engineers* 123:641–684.

Patil, S., Covino, T. P., Packman, A. I., McGlynn, B. L., Drummond, J. D., Payn, R. A., & Schumer, R. (2013). Instream variability in solute transport: Hydrologic and geomorphic controls on solute retention. *Journal of Geophysical Research: Earth Surface*, 118(2), 413-422.

Payn, R. A., Gooseff, M. N., McGlynn, B. L., Bencala, K. E., & Wondzell, S. M. (2012). Exploring changes in the spatial distribution of stream baseflow generation during a seasonal recession. *Water Resources Research*, 48(4).

Pilgrim, D. H., Huff, D. D., & Steele, T. D. (1979). Use of specific conductance and contact time relations for separating flow components in storm runoff. *Water Resources Research*, 15(2), 329-339.

Poole, G. C., Stanford, J. A., Running, S. W., & Frissell, C. A. (2006). Multiscale geomorphic drivers of groundwater flow paths: subsurface hydrologic dynamics and hyporheic habitat diversity. *Journal of the North American Benthological Society*, 25(2), 288-303.

Poole, G. C., O'Daniel, S. J., Jones, K. L., Woessner, W. W., Bernhardt, E. S., Helton, A. M., & Beechie, T. J. (2008). Hydrologic spiralling: the role of multiple interactive flow paths in stream ecosystems. *River Research and Applications*, 24(7), 1018-1031.

Puckett, L. J., Zamora, C., Essaid, H., Wilson, J. T., Johnson, H. M., Brayton, M. J., & Vogel, J. R. (2008). Transport and fate of nitrate at the ground-water/surface-water interface. *Journal of environmental quality*, 37(3), 1034-1050.

Raymond, P.A., C.J. Zappa, D. Butman, T.L Bott., J. Potter, P. Mulholland, A.E. Laursen., W.H. McDowell, D. Newbold (2012), Scaling the gas transfer velocity and hydraulic geometry in streams and small rivers. *Limnology and Oceanography: Fluids and Environments*, 2, 10.1215/21573689-1597669.

Rice, K. C., & Hornberger, G. M. (1998). Comparison of hydrochemical tracers to estimate source contributions to peak flow in a small, forested, headwater catchment. *Water Resources Research*, 34(7), 1755-1766.

Salehin, M., Packman, A. I., & Wörman, A. (2003). Comparison of transient storage in vegetated and unvegetated reaches of a small agricultural stream in Sweden: seasonal variation and anthropogenic manipulation. *Advances in Water Resources*, 26(9), 951-964.

Schilling, K. E., Zhang, Y. K., & Drobney, P. (2004). Water table fluctuations near an incised stream, Walnut Creek, Iowa. *Journal of Hydrology*, 286(1), 236-248.

- Schilling, K. E., Li, Z., & Zhang, Y. K. (2006). Groundwater–surface water interaction in the riparian zone of an incised channel, Walnut Creek, Iowa. *Journal of Hydrology*, 327(1), 140-150
- Schwartz, F. W., & Zhang, H. (2003). *Fundamentals of ground water*. New York: Wiley.
- Sheets, R. A., Darner, R. A., & Whitteberry, B. L. (2002). Lag times of bank filtration at a well field, Cincinnati, Ohio, USA. *Journal of Hydrology*, 266(3), 162-174.
- Stanford, J.A., J.V. Ward (1993), An ecosystem perspective of alluvial rivers: connectivity and the hyporheic corridor, *J. N. Am. Benthol. Soc.*, 12(1), 48-60.
- Stonedahl, S. H., Harvey, J. W., Wörman, A., Salehin, M., & Packman, A. I. (2010). A multiscale model for integrating hyporheic exchange from ripples to meanders. *Water Resources Research*, 46(12).
- Todd, D. K. (1956). Ground-water flow in relation to a flooding stream. In *Proceedings of the American Society of Civil Engineers* (Vol. 81, No. 2, pp. 1-20). ASCE.
- Tonina, D. and Buffington, J. M. (2009), Hyporheic Exchange in Mountain Rivers I: Mechanics and Environmental Effects. *Geography Compass*, 3: 1063–1086. doi: 10.1111/j.1749-8198.2009.00226
- Tonina, D., & Buffington, J. M. (2011). Effects of stream discharge, alluvial depth and bar amplitude on hyporheic flow in pool-riffle channels. *Water resources research*, 47(8).
- Tonina, D., de Barros, F. P., Marzadri, A., & Bellin, A. (2016). Does streambed heterogeneity matter for hyporheic residence time distribution in sand-bedded streams?. *Advances in Water Resources*, 96, 120-126.
- Valett, H. M., Dahm, C. N., Campana, M. E., Morrice, J. A., Baker, M. A., & Fellows, C. S. (1997). Hydrologic influences on groundwater-surface water ecotones: heterogeneity in nutrient composition and retention. *Journal of the North American Benthological Society*, 16(1), 239-247.
- Ward, A. S., Schmadel, N. M., Wondzell, S. M., Harman, C., Gooseff, M. N., & Singha, K. (2016). Hydrogeomorphic controls on hyporheic and riparian transport in two headwater mountain streams during base flow recession. *Water Resources Research*.
- Walters et al (2003) Geomorphology and Fish Assemblages in a Piedmont River Basin, USA, *Freshwater Biology* 48(11):1950-1970 · November 2003
- Wett, B., Jarosch, H., & Ingerle, K. (2002). Flood induced infiltration affecting a bank filtrate well at the River Enns, Austria. *Journal of Hydrology*, 266(3), 222-234.
- Whiting, P. J., & Pomeranets, M. (1997). A numerical study of bank storage and its contribution to streamflow. *Journal of Hydrology*, 202(1), 121-136
- Woessner, W. W. (2000). Stream and fluvial plain ground water interactions: Rescaling hydrogeologic thought. *Ground Water*, 38(3), 423-429.

Wondzell S.M. (2006), Effect of morphology and discharge on hyporheic exchange flows in two small streams in the Cascade Mountains of Oregon, USA, *Hydrol. Process.*, 20:267-287  
doi:10.1002/hyp.5902.

Wolman, M. G. (1954). A method of sampling coarse riverbed material. *EOS, Transactions American Geophysical Union*, 35(6), 951-956.

## Appendix A: Tables and Figures

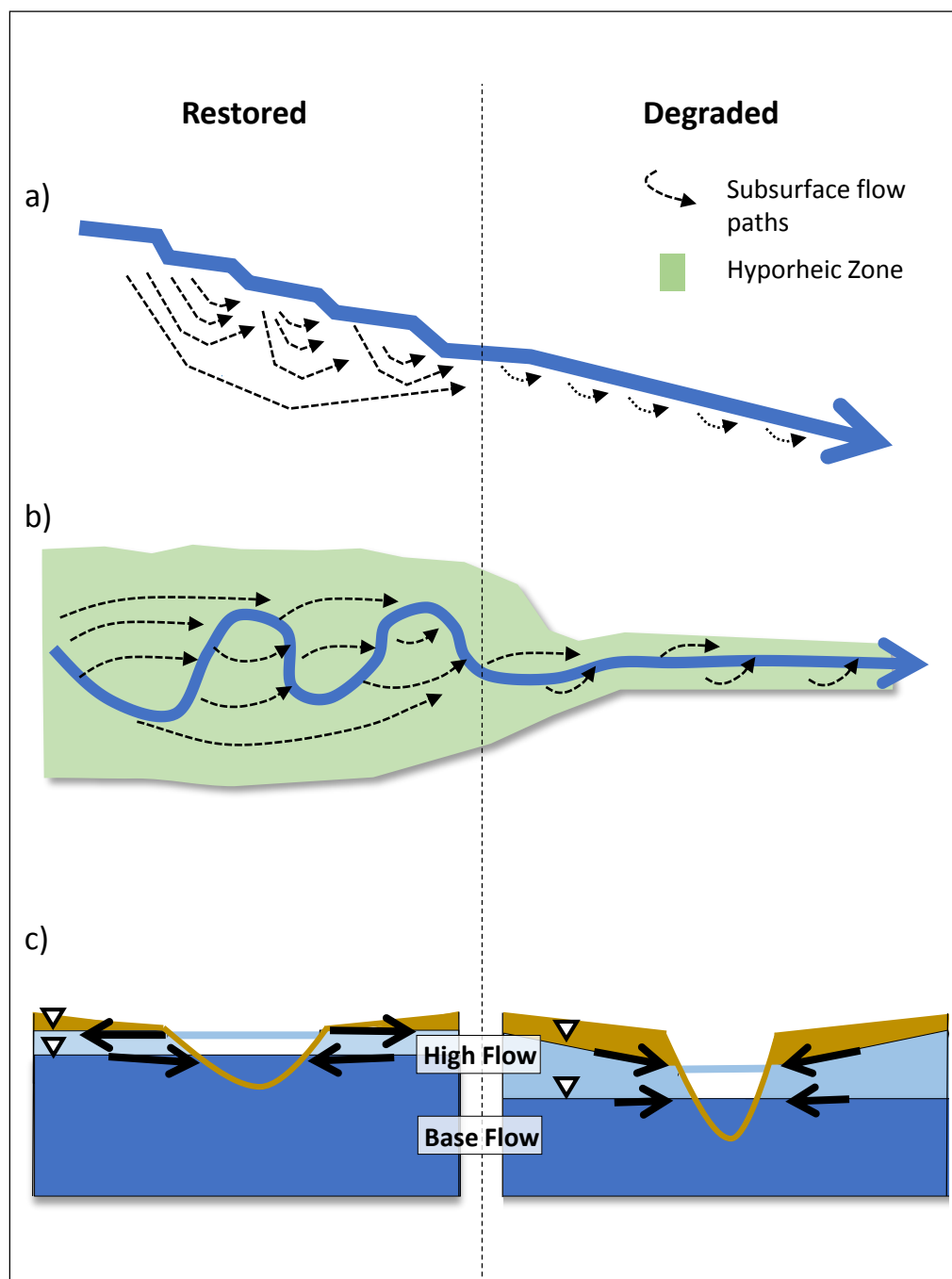


**Figure 1:** Conceptual model of restoration impacts on exchange. Adding geomorphic complexity in the **(a)** longitudinal and **(b)** planform profiles results in longer, more variable flow paths and a larger hyporheic zone. **(c)** Raising the channel bed elevation increases water table height and prolongs the bank storage period at high flows (light blue) contributing to alluvial aquifer recharge. This results in higher volumetric storage and discharge at base flow (dark blue).

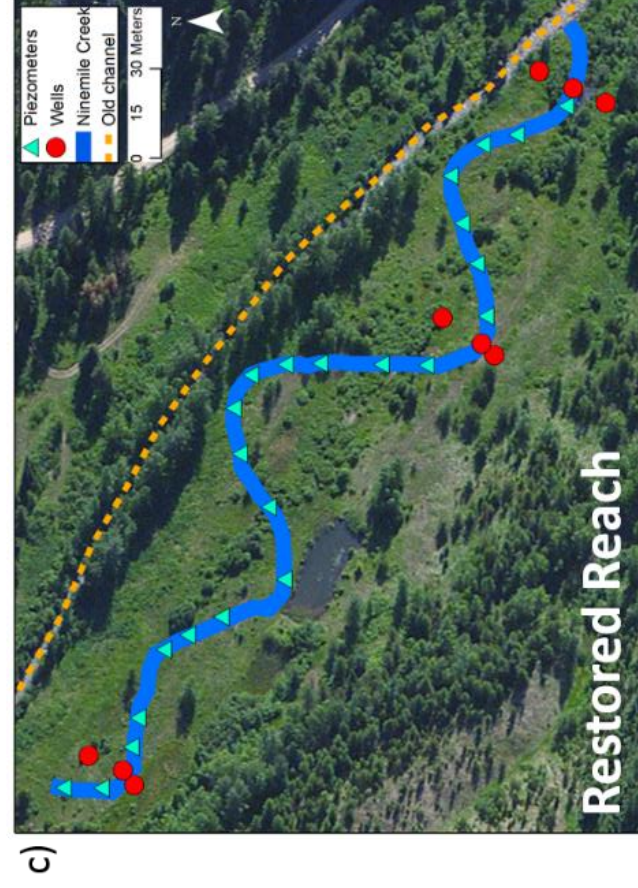
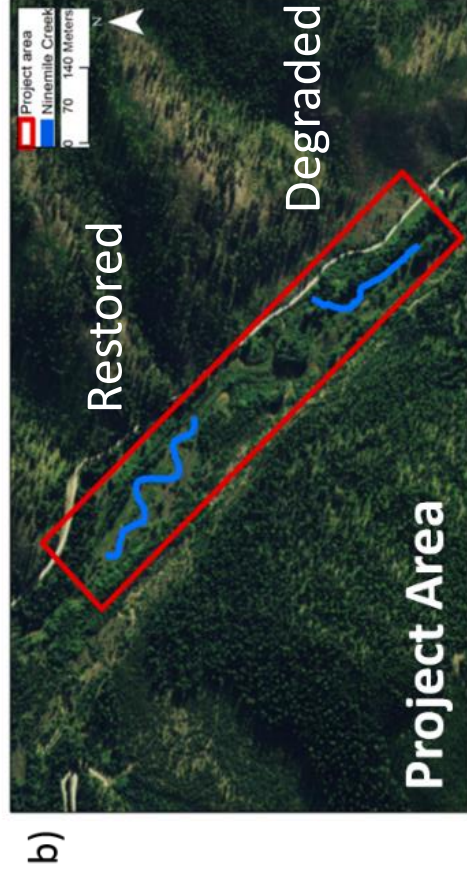
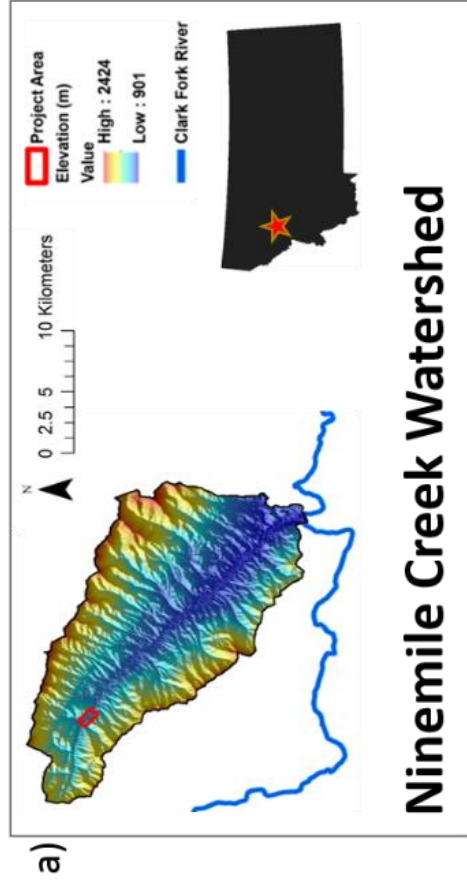


**Figure 2.** Site map **a)** Regional location of the Ninemile Creek project site **b)** Relative locations of restored and degraded reaches **c-d)** Restored and degraded reaches with piezometers (blue triangles) wells (red circles). The restored reach map also denotes the location of the pre-restoration channel (orange dashed line, not evaluated in this study). Flow direction is to the southeast.

**Table 1.** Radon model parameter values and methods of estimation.

Parameter	Units	Values	Method for Parameter Estimation	
Stream discharge	Q [m <sup>3</sup> day <sup>-1</sup> ]	12,874 - 57,542	Field measurement (synoptic flow gauging). Mean of upstream and downstream measurements at each time period.	
<sup>222</sup> Rn concentration in stream	c [Bq m <sup>-3</sup> ]	Restored 150 - 663	Degraded 146 - 383	Field sample collection. Analyzed using the RAD7.
Distance downstream	x [m]	Restored 351	Degraded 224	Field measurement
<sup>222</sup> Rn concentration in groundwater (Equilibrium radon concentration)	c <sub>i</sub> [Bq m <sup>-3</sup> ]	26,250		Highest measured seep/shallow well radon concentration. All water samples were analyzed using the RAD7.
Stream width	w [m]	Restored 7.0	Degraded 5.5	Mean of field measurements.
Evaporation rate	E [m day <sup>-1</sup> ]	0		Assumed to be negligible (Cook et al., 2006)
Gas transfer velocity across water surface	k [m day <sup>-1</sup> ]	5.5 - 21.6	6.0 - 27.7	See Table 2
Stream depth	d [m]	Restored 0.28 - 0.45	Degraded 0.15 - 0.35	Mean of field measurements.
Decay constant	λ [d <sup>-1</sup> ]	0.18		Constant
Production in HZ	γ [Bq m <sup>-3</sup> day <sup>-1</sup> ]	4,725		γ = λ × c <sub>i</sub> (from Bourke et al., 2014) where c <sub>i</sub> =26,250 Bq/m <sup>3</sup> (highest measured concentration)
Depth of HZ	h [m]	1		Radon concentrations at 0.5m depth were consistently lower than secular equilibrium values, inferring that hyporheic exchange is present at this depth.
Porosity of HZ	θ [--]	0.3		Estimated based on subsurface texture.
Mean residence time in HZ	t <sub>h</sub> [day]	0.25	0.4	t <sub>h</sub> = $\frac{c - c_h}{\lambda c_h - \gamma}$ From Bourke et al. (2014) where c <sub>h</sub> is the average radon concentration within the hyporheic zone.

**Table 2.** Equations used to estimate gas transfer velocity (k) for radon modeling based on field measurements of velocity (V), slope (S), depth (D) and temperature (included in k<sub>600</sub> calculation of Raymond et al., 2012 equations)

Equation Citation	Equation
Raymond et al. (2012)	$k_{600} = (VS)^{0.89 \pm 0.02} \times D^{0.54 \pm 0.03} \times 5037 \pm 604$
Raymond et al. (2012)	$k_{600} = (VS)^{0.76 \pm 0.027} \times 951.5 \pm 144$
O'Connor and Dobbins (1958)	$k = 9.301 \times 10^{-3} \left(\frac{v}{d^{1.5}}\right)^{0.5}$
Negulescu and Rojanski (1969)	$k = 4.87 \times 10^{-4} \left(\frac{v}{d}\right)^{0.85}$

### Hydrograph and hietograph of study period Ninemile Creek, 2016

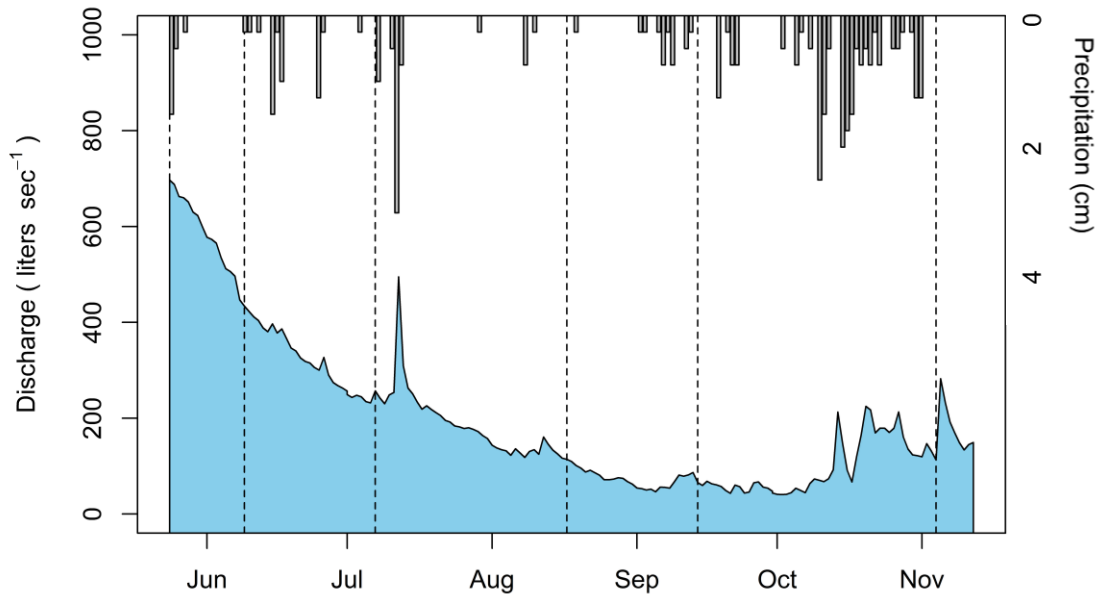


**Figure 3.** Hydrograph and hietograph of the study period. Vertical dashed lines represent synoptic sampling dates. The hydrograph was created using a rating curve developed with six dilution gauging discharge measurements and stilling well stage measurements. Precipitation was measured at the Sleeping Woman (#783) SNOTEL site, located 25 kilometers southeast and 600 meters above the study site. Precipitation data are presented to represent the timing, not magnitude, of precipitation at the project site.

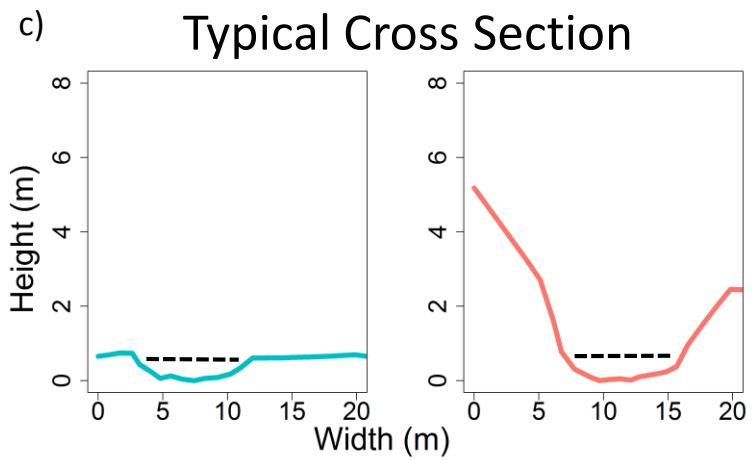
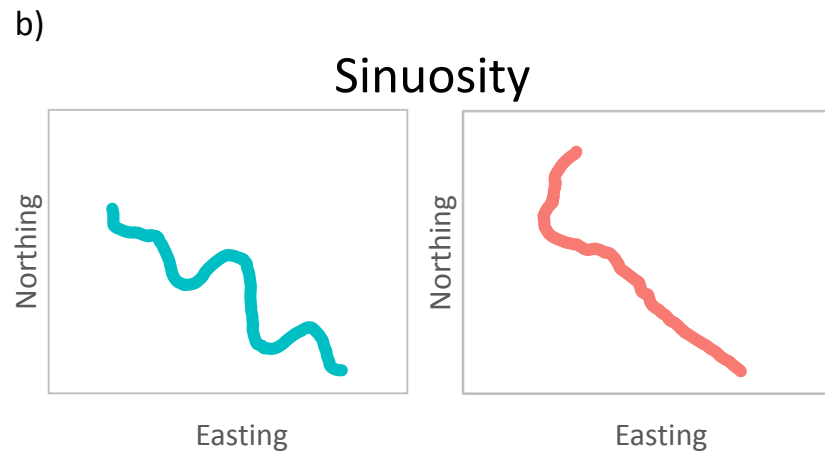
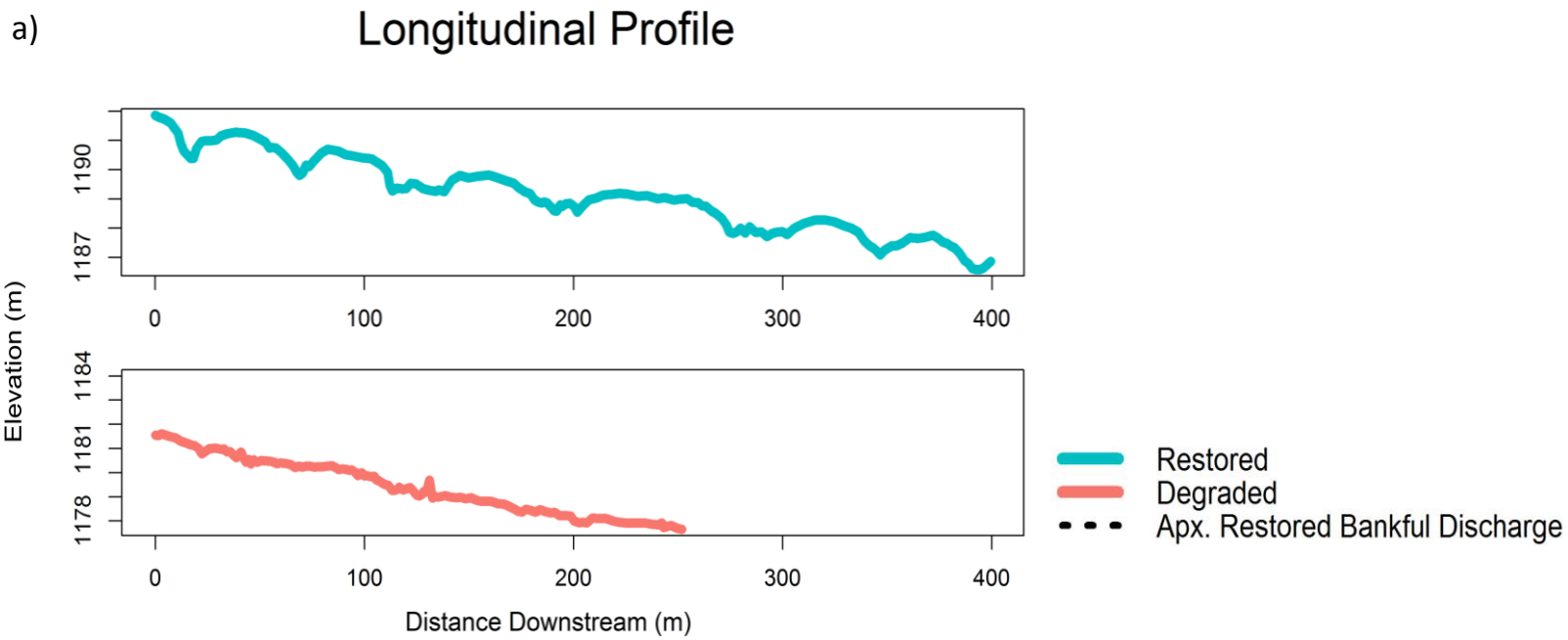


**Figure 4.** Topographic surveys completed in restored (blue) and degraded (red) reaches **a)** longitudinal profile of bed geometry with points collected at apx. 1-meter resolution along the thalweg **b)** sinuosity with points taken at apx. 1-meter resolution along the thalweg **c)** average channel cross-section with approximate bankfull stage (dashed line).

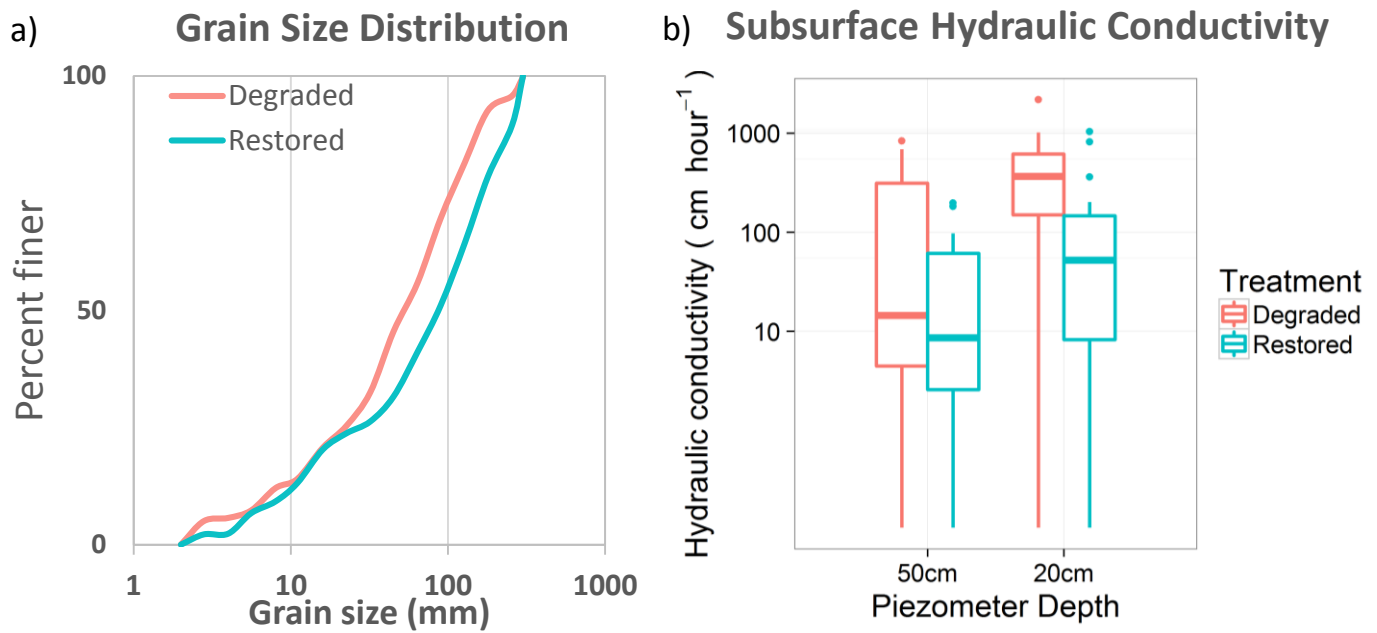


**Figure 5** a) Surface grain size distribution measured using Wolman pebble count methods in restored (red) and degraded (blue) reaches b) Boxplot of subsurface hydraulic conductivity using Horslev slug test analysis in deep (50cm) and shallow (20 cm) piezometers (n=41 at each depth). Boxplots present median values (line), interquartile range (box) and 1.5x the IQR (whiskers).

**Table 3.** Summary of topographic and geomorphic surveys

a) Topographic survey results. All metrics are unitless

	Restored	Degraded
<b>Average Width-to-Depth Ratio</b>	18	12
<b>Stream Slope</b>	0.010	0.015
<b>Sinuosity</b>	1.33	1.05
<b>Thalweg variation: r<sup>2</sup></b>	0.927	0.978
<b>Thalweg variation: SD of residuals</b>	32.4	10.3

b) Summary of Subsurface hydraulic conductivities (units are cm hr<sup>-1</sup>)

	Restored		Degraded	
	50 cm	20 cm	50 cm	20 cm
<b>Median</b>	8.6	52.2	14.5	367.6
<b>Upper Quartile</b>	61.3	146.5	312.7	613.8
<b>Lower Quartile</b>	2.6	8.9	4.5	150.2
<b>IQR</b>	58.7	137.6	308.2	462.8

# Mean transient storage residence time

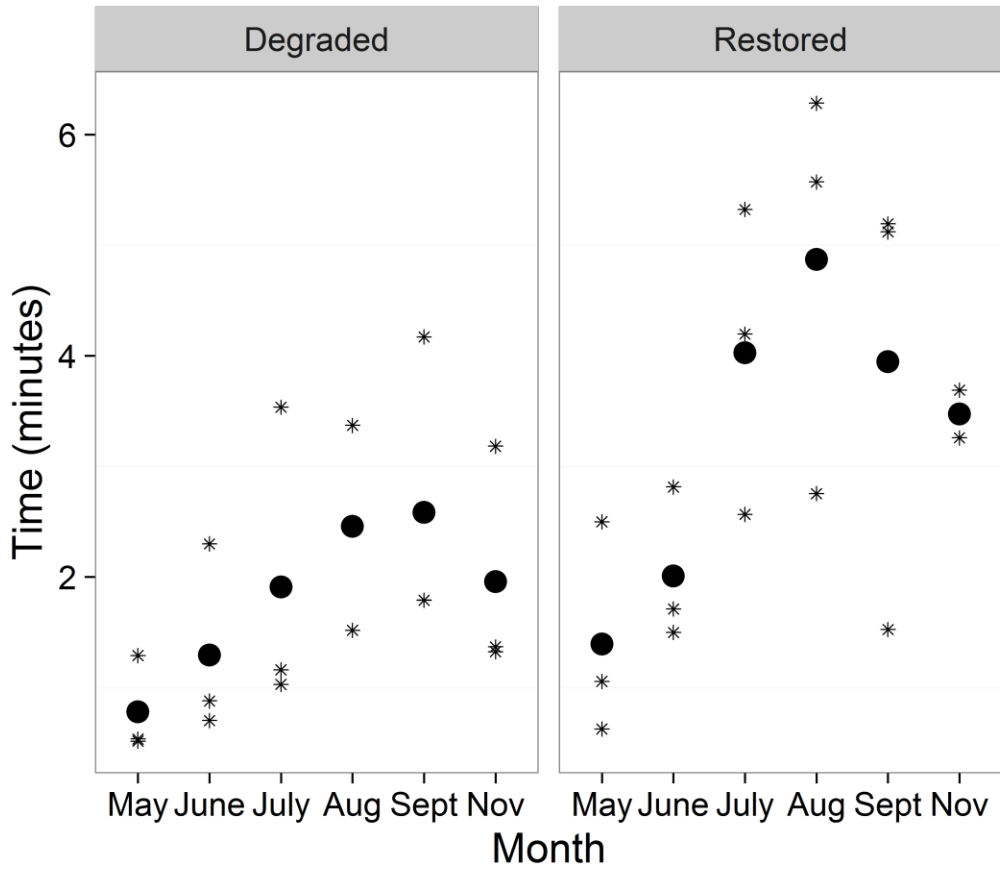


**Figure 6.** Mean transient storage residence time ( $1/r$ ) was evaluated in restored and degraded reaches six times through the hydrograph recession. Measurements were taken along three sub-reaches per treatment reach(stars). Circles represent the mean of the three sub-reach values.

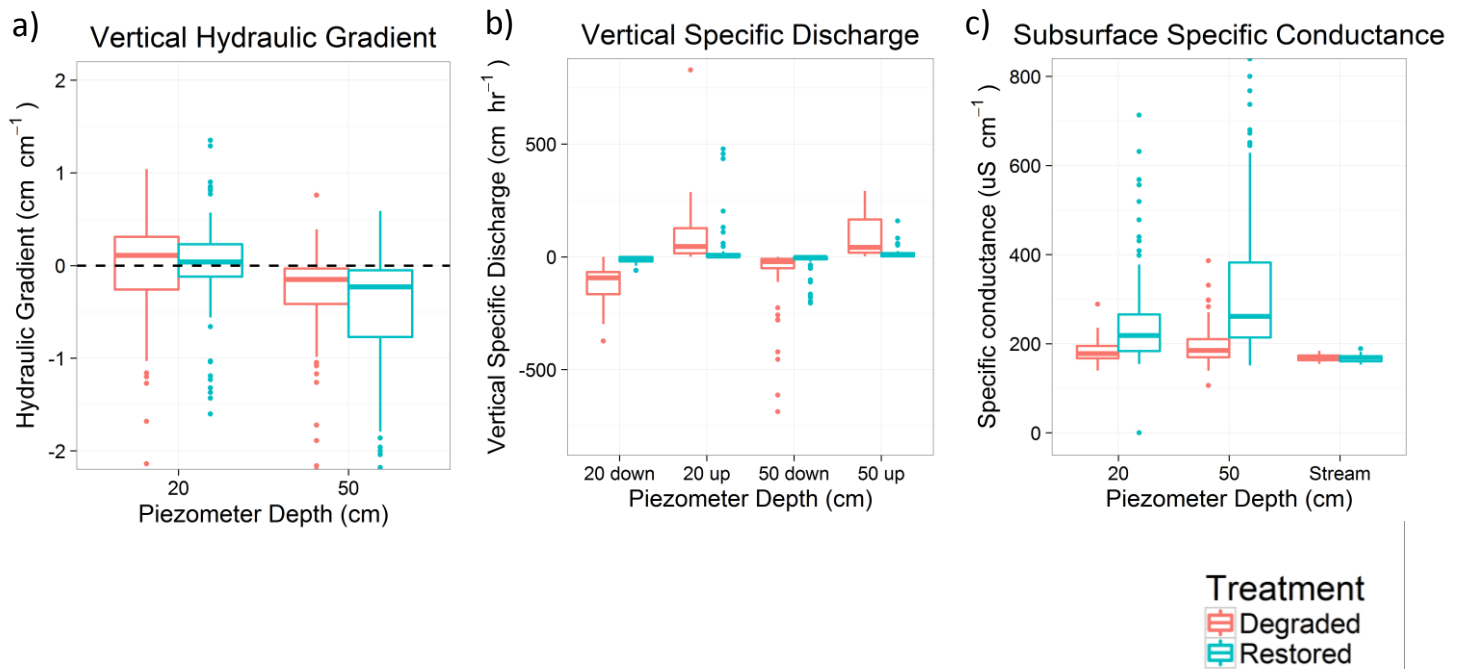


**Figure 7.** Box plots of piezometer measurements taken at 20 cm and 50 cm subsurface (n=18 degraded; n=23 restored for each depth). Measurements were taken six times over the hydrograph recession, but were combined for clarity as no obvious temporal trends existed. **a)** Vertical hydraulic gradients represent upwelling (positive values) and downwelling (negative values). **b)** Vertical specific discharge calculated as the product of the hydraulic gradient and saturated hydraulic conductivity. **c)** Specific conductance measured at 20 cm, 50 cm and within the stream.

**Table 4.** R<sup>2</sup> values of significant relationships between shallow vertical hydraulic gradient and local bed slope at different length scales in the restored reach. Slope was calculated as the average slope across a range of distances upstream of the piezometer where the hydraulic gradient was measured. The variable length scale accounts for the variable length of bed features and was calculated as the average slope between two sequential piezometers. All significant relationships evaluated are shown, with the best fit (highest r<sup>2</sup>) shaded in grey. There were no significant relationships in the degraded reach.

Distance upstream of piezometer (m)	May	June	July	August	September	November
0.5						0.17
1						0.14
2						
5			0.17		0.13	0.27
7						
9	0.19		0.19			0.15
10	0.17		0.21		0.15	0.17
11			0.17			0.16
13						
Variable	0.20		0.26		0.21	0.19

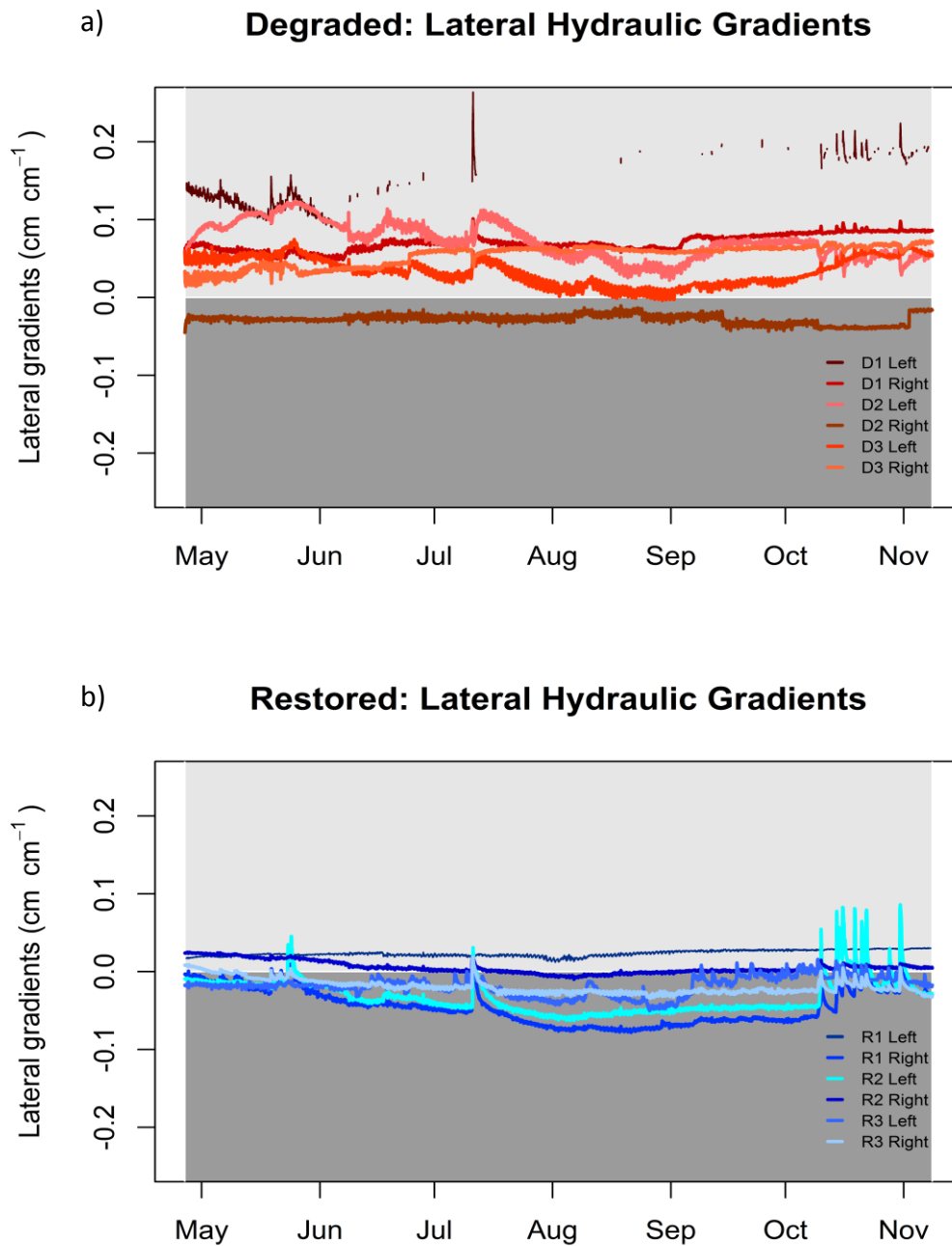
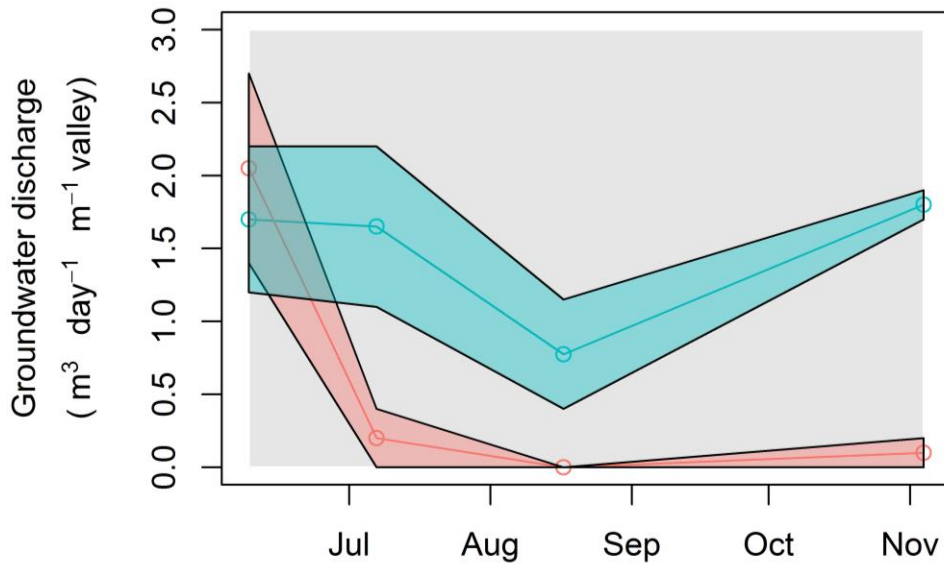


**Figure 8.** Lateral hydraulic gradients calculated between shallow groundwater wells and in-stream stilling wells in **a)** degraded and **b)** restored reaches. Plots present gradients over time for all wells ( $n=6$  per treatment). Positive gradients represent gains to the stream while negative gradients represent losses. Water levels occasionally dropped below the well extent in degraded reach well D1 left (no line).

a)

### Groundwater discharge



b)

### Net change in Discharge

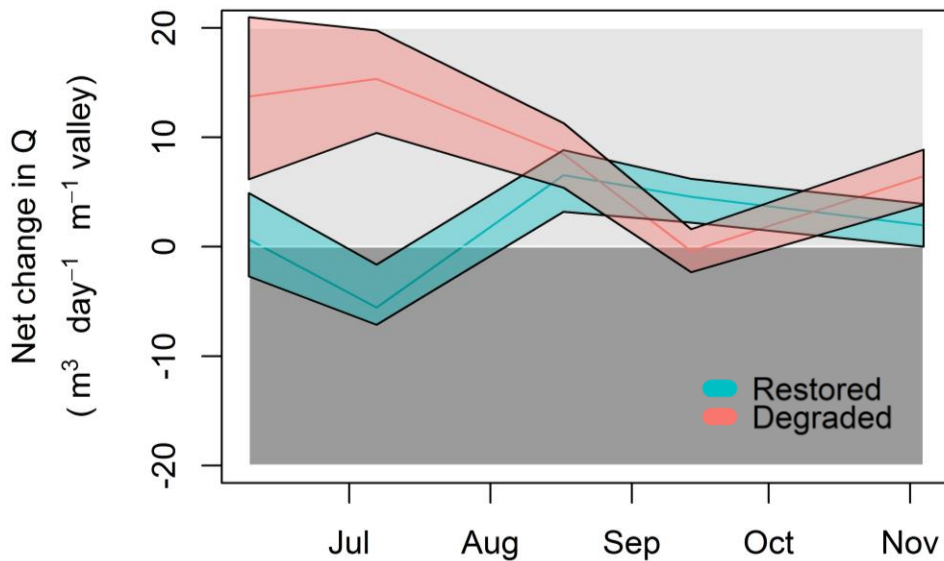
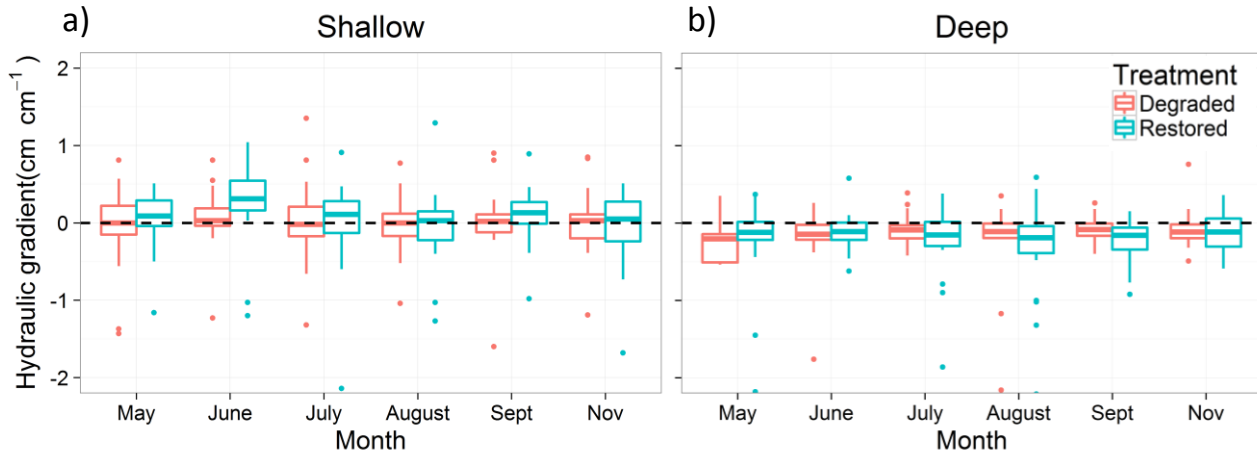
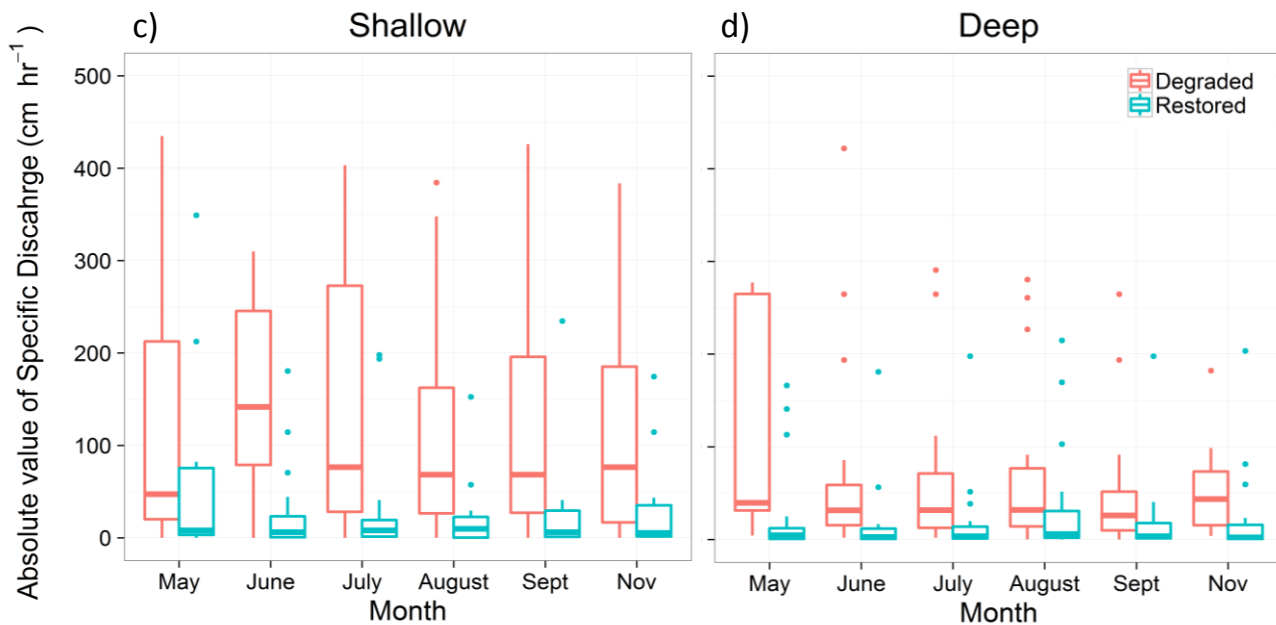


**Figure 9.** Temporal trends in alluvial aquifer recharge and discharge. All measurements are normalized by valley length to represent the valley-scale impact of restoration. **a)** Radon-modeled groundwater discharge over time. Center line represents mean modeled discharge. Shaded areas illustrate model results with  $\pm 1$  standard deviation of radon concentration measurement error. **b)** Net change in discharge over time. Positive values represent a net gaining reach and negative values net losing. Shaded areas represent discharge measurement error.

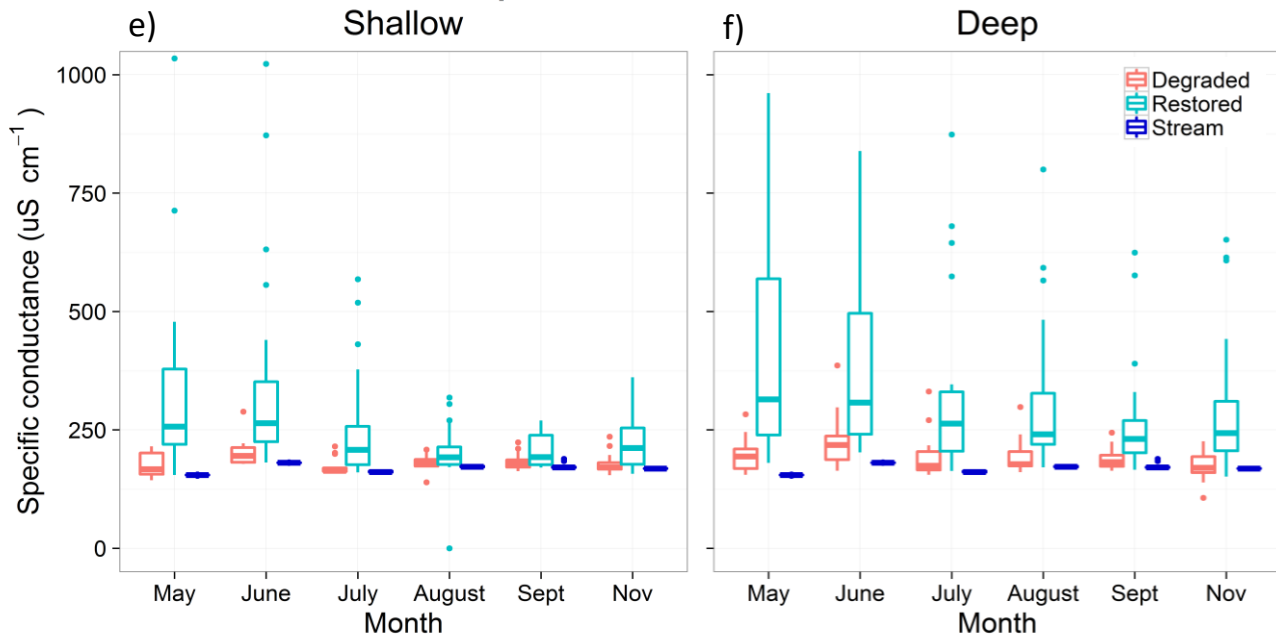
# Vertical Hydraulic Gradients



# Vertical Specific Discharge



# Specific Conductance



# Student Fellowship Project: Remote Sensing of Snowpack in the Bitterroot Mountains of Montana Using Unmanned Aircraft Systems (UAS)

## Basic Information

<b>Title:</b>	Student Fellowship Project: Remote Sensing of Snowpack in the Bitterroot Mountains of Montana Using Unmanned Aircraft Systems (UAS)
<b>Project Number:</b>	2017MT315B
<b>Start Date:</b>	3/1/2017
<b>End Date:</b>	2/28/2018
<b>Funding Source:</b>	104B
<b>Congressional District:</b>	1
<b>Research Category:</b>	Climate and Hydrologic Processes
<b>Focus Categories:</b>	Climatological Processes, Hydrology, Water Quantity
<b>Descriptors:</b>	None
<b>Principal Investigators:</b>	Jonathan Byers

## Publications

There are no publications.

# Remote Sensing of Snowpack in the Bitterroot Mountains of Montana Using Unmanned Aircraft Systems (UAS)

*Montana Water Center Graduate Student Fellowship Project Report*

*Jonathan Byers*

*May 10<sup>th</sup>, 2018*

## **Problem: Assessing Snow Water Equivalent in Mountainous Terrain**

“Estimating the spatial distribution of snow water equivalent (SWE) in mountainous terrain, characterized by high elevation and spatially varying topography, is currently the most important unsolved problem in snow hydrology.” [1] The ability to accurately map and measure snow cover is critical in understanding and adapting to changes in precipitation patterns that supply water for 20% of Earth’s population and support vital aquatic ecosystems [2]. Even with the broad snowpack research network in the U.S., SWE measurements that inform runoff models and water management plans remain poorly quantified. This project uses an Unmanned Aircraft System (UAS) sensor platform and photogrammetry SWE measurements to increase the spatial density of high elevation snowpack measurements, with applications for basin scale SWE modeling improvement [3].

## **Background:**

In the Western U.S., *in situ* snowpack data primarily comes from the Natural Resources Conservation Service (NRCS) SNOW TELEmetry (SNOTEL) stations. These sites have been found to preferentially represent densely forested lower elevation areas and underrepresent higher elevation and complex terrain [4].

Remote sensing snow cover monitoring approaches have used satellite platforms including MODIS, Landsat, and AVHRR, which provide good temporal coverage however their two-dimensional nature prevents snow depth and SWE calculations, and their low spatial resolution prohibits the detection of small-scale variations in snow depth in forests or complex terrain.

The NOAA National Weather Service’s National Operational Hydrologic Remote Sensing Center (NOHRSC) Snow Data Assimilation Systems (SNODAS) model assimilates satellite-derived, airborne, and ground-based observations. Because of biased SNOTEL data and low spatial resolution from satellite remote sensing, it has the tendency to underestimate basinwide SWE [5].

The most effective tools for snowpack monitoring are a combination of airborne LiDAR and hyperspectral imaging as proven by the NASA/JPL Airborne Snow Observatory [6]. The disadvantages of this system are the high cost and very limited spatial coverage, currently only covering three basins in the Sierra Nevada regularly.

UAS photogrammetry has been proven to accurately reconstruct surfaces, including snow however, it has never been evaluated in mixed alpine/forested landscapes [7]. This project will use UAS photogrammetry snow depth reconstructions to investigate the spatial representativeness of SNOTEL measurements. This data will additionally be compared to SWE reconstruction models such as iSnobal, and SNODAS. The additional UAS data for high elevations could be used to

improve the accuracy of these models, providing a much needed improvement in our ability to understand and predict changing water patterns.

### **Methods:**

*Research Location:* Fieldwork was conducted at Lolo Pass in the Bitterroot Mountains, Montana. This site provides easy access to a variety of open and forested slopes, and is the site of the Lolo Pass SNOTEL station (ID: 588). The research area encompasses the heavily trafficked road corridor, and has significant winter recreational use from snowmobilers and skiers. This provides an interesting and dynamic location to visualize the impacts of winter recreation on snowpack.

*UAS platform & Data collection:* With additional support from the University of Montana Autonomous Aerial Systems Office, a fixed wing UAS was designed, built, and flown. This aircraft is capable of covering ~1,600 acres/flight and carries a 24.2 MP Sony a600. However, because of regulatory challenges, this aircraft was not approved for operations on this project. This postponed snow free data collection during the summer of 2017. To accommodate regulatory changes, a multicopter DJI Mavic Pro with a 12MP camera was used for imagery collection. Automated flights were controlled by MapPilot and were flown at a constant 400ft AGL using terrain following with a 80% front and 70% side overlap. A circular polarizing filter was used to darken the image and reduce glare from snow for correct image exposure. Five GPS ground control points were established across the study area and 50 manually measured snow depth points in representative open and forested areas will be used to determine the accuracy of the snow DSM.

*Data Processing & Analysis:* Raw RGB imagery was processed using Agisoft Photoscan and Pix4D Mapper to compare processing methods. Both programs were successful in correctly outputting surface models, however Photoscan appeared to be more resistant to lower overlap between images. Pointcloud files are processed in LAStools to remove trees and ArcMap is used for visualization. Differential correction of surfaces will be done in ArcMap once snow free data is collected.

### **Results:**

A geodatabase of manual snow sampling locations, ground control points, the location and snow depth of the SNOTEL site, and SNODAS model outputs was constructed. The photogrammetry mapping effort resulted in 198 images covering 84 acres with an average ground sampling distance of 3.81 cm. The snow surfaces were correctly reconstructed from RGB imagery (Figure 1). A Digital Elevation Model (DEM) shows the fine scale identification of recreational impacts and the successful creation of snow surfaces even in the densely forested parts of the landscape (Figure 2). Complete results will be available after the snow free data is collected and processed.

### **Discussion:**

This project faced numerous technical, regulatory, and administrative challenges which prevented the collection of snow-free data during the summer of 2017. Despite these challenges,

significant progress and collaboration with both the FAA and the US Forest Service was achieved. There is a large amount of interest in UAS for data collection and navigating the regulations has proved challenging to many other projects. By continuing to develop these relationships, and operating within the bounds of regulations it helps establish a knowledge and experience base at the University of Montana that will aid future operations.

Many valuable lessons about aircraft, sensors, operations, and data processing were learned throughout this process. The use of polarizing filters allowed the successful creation of snow surfaces, a process that had proved challenging during early testing because of the extreme contrast between sunny open slopes and densely tree covered areas. Implementation of terrain following tools allowed for correct overlap to be maintained throughout the data collection flights, and also prevented unwanted controlled flight into terrain.

Because of delayed data collection, no conclusions can be made about the ability of this technique to accurately measure snow depth until snow-free data is collected during the summer of 2018. The authors will publish a full report upon the completion of the project.

**Figures:**

**Lolo Pass SNOTEL Study Area - Snow On**

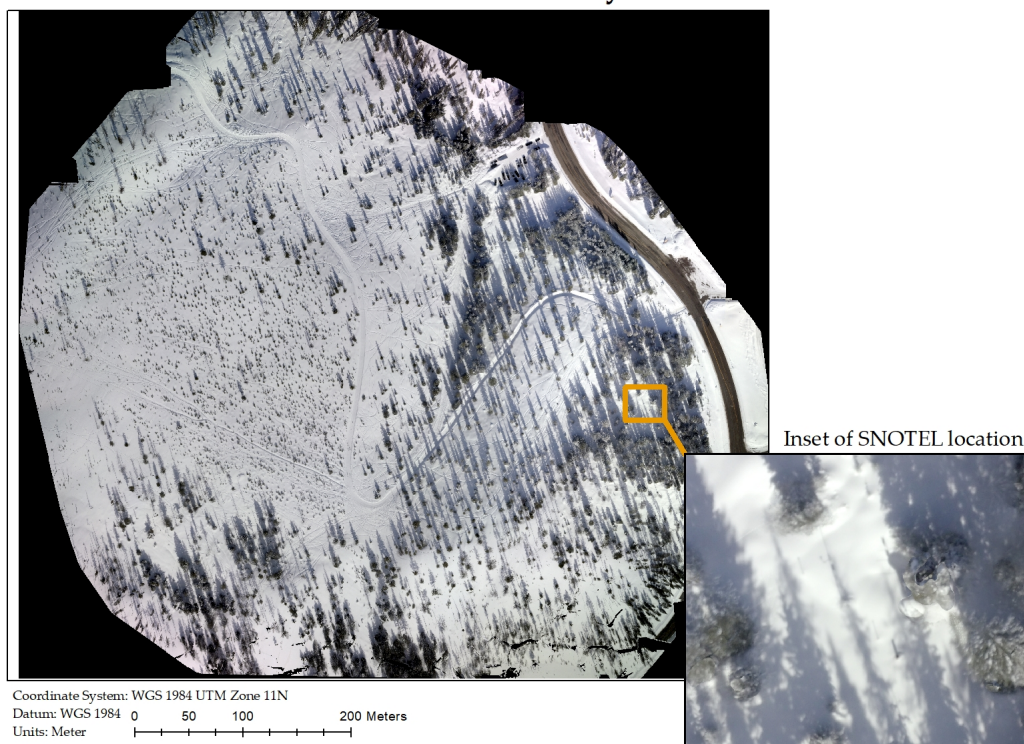


**Figure 1. RGB Orthoimage of the study area**

## Lolo Pass SNOTEL Study Area - Snow On

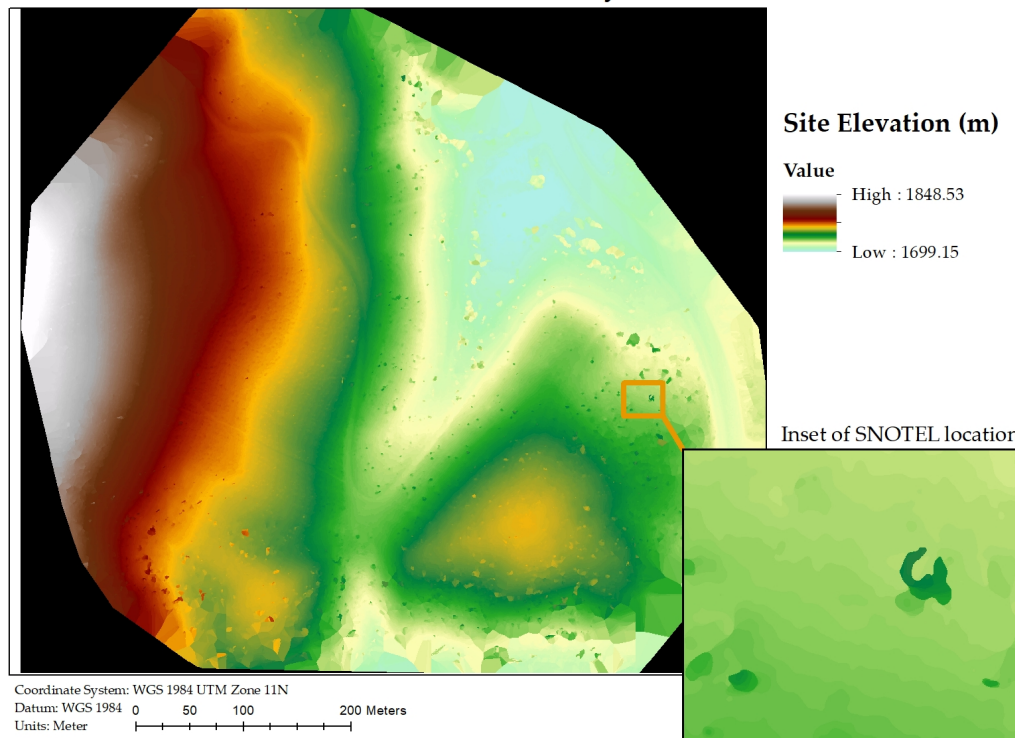


**Figure 2. Photogrammetric Digital Elevation Model of the Study Area**

### **Bibliography:**

- [1] Dozier, J., Bair, E. H., and Davis, R. E. (2016). Estimating the Spatial Distribution of Snow Water Equivalent in the World's Mountains. *Wiley Interdisciplinary Reviews: Water* 3(3):461-474.
- [2] IPCC (2013). *Climate Change 2013: The Physical Science Basis*. Contribution of Working Group 1 to the Fifth Assessment Report of the Intergovernmental Panel on Climate Change. Cambridge University Press, Cambridge, United Kingdom and New York, NY, USA.
- [3] Molotch, N. P., and Bales, R. C. (2006). SNOTEL representativeness in the Rio Grande headwaters on the basis of physiographics and remotely sensed snow cover persistence. *Hydrological Processes*, 20(4), 723-739.
- [4] Silverman, N. L., and Maneta, M. P., (2016), Detectability of change in winter precipitation within mountain landscapes: Spatial patterns and uncertainty, *Water Resour. Res.*, 52, 4301–4320.
- [5] Rittger, K., Kahl, A., & Dozier, J. (2011, April). Topographic distribution of snow water equivalent in the Sierra Nevada. In *Proceedings of the 79th Annual Western Snow Conference, Stateline, NV* (pp. 37-46).
- [6] Bair, E. H., Rittger, K., Dozier, J., & Davis, R. E. (2015). Comparison and error analysis of reconstructed SWE to Airborne Snow Observatory measurements in the Upper Tuolumne Basin. In *Proceedings of Western Snow Conference*.

- [7] Michele, C. D., Avanzi, F., Passoni, D., Barzaghi, R., Pinto, L., Dosso, P., ... & Vedova, G. D. (2016). Using a fixed-wing UAS to map snow depth distribution: an evaluation at peak accumulation. *The Cryosphere*, 10(2), 511-522.

## Student Fellowship Project: Microbially induced metal precipitation and co precipitation in mine influenced water

### Basic Information

<b>Title:</b>	Student Fellowship Project: Microbially induced metal precipitation and co precipitation in mine influenced water
<b>Project Number:</b>	2017MT316B
<b>Start Date:</b>	3/1/2017
<b>End Date:</b>	2/28/2018
<b>Funding Source:</b>	104B
<b>Congressional District:</b>	1
<b>Research Category:</b>	Water Quality
<b>Focus Categories:</b>	Water Quality, Acid Deposition, Hydrogeochemistry
<b>Descriptors:</b>	None
<b>Principal Investigators:</b>	Emily Stoick

### Publications

There are no publications.

**Microbially induced mineral precipitation in mixed constituent mine influenced water  
using an enriched bacterial community native to mine land sediments**

Research Report Submitted to the Montana Water Center

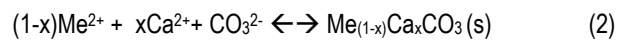
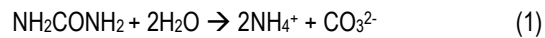
May 11, 2018

Prepared by: Emily Stoick

# 1 Introduction

Heavy metal contamination of surface and groundwater results from a number of resource extraction activities, including mining. In particular, the discharge of mine influenced water (MIW) with elevated levels of dissolved metals contributes to environmental contamination across the globe. Additionally, industrial wastewater with dissolved metal contaminants may require pretreatment prior to discharge into public treatment systems. Chemical precipitation is a prevalent method for dissolved metal removal from these waste streams [1], though not appropriate in all contaminated environments, including porous media or sediments where control of rate and distribution of precipitation is required. Over the past two decades, the process of microbially driven carbonate precipitation has gained interest for a number of environmental applications where mineral formation is controlled by a biological reaction, including strengthening of unconsolidated soils, fracture sealing and remediation of metal cations via co-precipitation [2]. This research investigated the use of microbially induced carbonate precipitation (MICP) as a technique for immobilizing trace metals using environmentally sampled alkaline MIW as a representative solution with multiple metal contaminants.

MICP is promoted by the microbially catalyzed hydrolysis of urea (equation 1) by the urease enzyme, common in soil microorganisms. The reaction produces alkalinity and increases both pH and carbonate concentration. Dissolved metals can precipitate as carbonate minerals as a result of MICP (equation 2) [3]:



Calcium carbonate is the primary precipitate in MICP systems saturated with calcium [4]. The precipitation of  $\text{CaCO}_3$  allows for the co-precipitation of other dissolved metals via adsorption, inclusion, and occlusion [5]. Fujita et al. surmised the addition of nucleation sites due to bacterial cell presence could increase the rate of nucleation and lead to the formation of many small crystals, which increased the partitioning of Sr into calcite [6]. Biogenic mineralization could be favored due to this increased partitioning of trace metals into calcite. Other metal carbonate minerals (i.e.  $\text{MnCO}_3$ ,  $\text{ZnCO}_3$ ) can become supersaturated and precipitate as well, or metals sorbed to microbial cells can be coated and sequestered by newly formed biogenic precipitates, providing mechanisms for metals removal in addition to co-precipitation. Co-precipitation in biogenic calcite has been shown for strontium [7], cadmium [8,9,10,11], nickel [9], copper [8,9], lead [8,9], arsenic [12], cobalt [9], and zinc [13].

The co-precipitation of metals via MICP has been studied by various groups with . Urease positive bacteria have been isolated from mine contaminated soils and used to perform MICP for removal of cadmium, lead, copper, and arsenic[8,11,13]. Zhao, et al.

investigated the removal of cadmium with initial concentration of 10 mg/L and urea concentration of 404 g/L using an isolated strain GZ-22 of *Bacillus sp* [11]. Kang, et al. employed a mixture of urease positive bacteria to induce removal of lead, copper, and cadmium at initial concentrations of 414, 127, and 224 mg/L respectively, with an initial urea concentration of 0.3 g/L [8]. The authors concluded bacterial mixtures supported higher growth rates, urease activity, and heavy metal resistance [8]. Li, et al. achieved 90-99% removal rates of nickel, copper, lead, cobalt, zinc, and cadmium with initial concentrations ranging from 280-750 mg/L and 30 g/L of urea [14].

These past experiments have used synthetic solutions with a single metal, high concentrations of urea and/or additional calcium to achieve high removal rates. However, such high concentrations of metals are not typically found in the environment and drinking water or aquatic life standards for trace metals are often on the order of micrograms per liter. For this technology to be potentially viable in real-world settings, the viability of MICP must be tested with field relevant concentrations of metals, and urea concentrations feasible for field-scale deployment. The goals of this research are to (1) determine the ability of an environmental enriched ureolytic consortium and a model bacterium to grow and hydrolyze urea in a MIW containing a mixture of metals and sampled from an NPL site, and (2) determine the removal efficiency of heavy metal contaminants from the MIW to co-precipitation efficiency under batch and continuous flow conditions. To address the research objectives, sediment enrichments from a contaminated mining site and a model bacterium (*S. pasteurii*) were cultivated in batch experiments with collected MIW (batch data not presented in this report). Then, continuous flow column studies were performed to evaluate whether bacterial viability and metals removal were sustainable over several months. This research used environmentally sampled mine drainage (MIW) continuously discharging from an abandoned mine adit in Central Montana and urea concentrations in the range of 0.5-2 mg/L, several orders of magnitude lower than other metal co-precipitation studies employing MICP [8,9,11,14]. Metal concentrations in this MIW are present in micrograms per liter, constitute a mixture of elements, and vary temporally at the discharge site. Measurement techniques used in this study were unable to detect some of the metals of interest present in very low concentrations, including nickel, copper, and cadmium. Although the MIW is a relevant contaminated water source and contains a cocktail of metals that can influence MICP, this study focused on zinc, which was present in the highest concentration and detectable by ICP-MS methods.

## **2. Methods**

### **2.1 Site Characterization**

MIW was collected from the Evening Star adit at the Carpenter Snow Creek Mining District (CSCMD) EPA Superfund Site in central Montana. The soil, sediment, surface water, and groundwater are still heavily influenced by the 19<sup>th</sup> and 20<sup>th</sup> century mining activity in this area. The MIW discharged at the Evening Star adit is characterized with the following metal concentrations exceeding the Montana Department of Environmental Quality Chronic Exposure Standard for Aquatic Life [15]:

*Table 1: Average annual metal concentrations in Evening Star MIW with one standard deviation above and below the mean. Concentrations vary temporally due to Spring runoff. Metals shown exceed MT DEQ Chronic Exposure Standard for Aquatic Life.*

Metal	Average Discharge [16] (µg/L)	MT DEQ Chronic Exposure Standard for Aquatic Life [15] (µg/L)	Percent Removal for Treatment to Standard
Zinc	674 ± 115	37	95%
Cadmium	0.634±0.525	0.097	85%
Copper	2.4 ± 3.9	2.85	36%
Nickel	26.1 ± 2.7	16.1	37%

The average pH of Evening Star MIW is 6.7; the average temperature is 7.4 °C [16].

## 2.2 Sediment Enrichments

Sediments samples near surface discharge of the Evening Star, Moulton, and Compromise adits were collected and enriched for microbial growth using three different treatments: (1) 0.5 g/L yeast extract, 10 g/L urea, 10 mL/L trace element solution SL-4 (see Appendix Table 3 for recipe) [17], 10 mL/L vitamin solution (see Appendix Table 2 for recipe)[17], and 10 mg/L phenol red in DI water, (2) same as (1) except in MIW and without SL-4, and (3) 3 g/L nutrient broth, 10 g/L urea, 10 g/L ammonium chloride, and 10 mg/L phenol red in DI water. Urea consumption and pH were monitored over the course of 30 days while shaking at 60 rpm at 22±0.5°C. Urea consumption was measured using the Jung Assay [18]. Three grams of sediment were added to 50mL of the respective solution. Phenol red generated a color change to pink as pH increased above 8. After 30 days, 1 mL of the enrichment solution was transferred into 49mL of fresh solution. After another 30 days, this solution was spread plated onto agar with 2% urea and 37 g/L brain-heart infusion (BHI). Ureolytic communities were observed in the MIW enrichments from all three adits and samples were stored at -80°C for DNA analysis. The enrichment from the Evening Star sediments had the most robust growth and ammonia production on the agar plates, so an isolate was attempted using streak plating methods. This attempted isolate, ES enrichment, was also grown in 37 g/L BHI and 2% urea for 48 hours then made into frozen stocks and stored at -80°C.

The environmental enrichments and attempted isolate then underwent DNA extraction and sequencing via MiSeq. PCR was set up to amplify the V1-V3 region of the 16S rRNA gene using primer pairs 8F (5'-AGAGTTTGATCCTGGCTCAG-3') and 529R (5' CGC GGC TGC TGG CAC 3') linked with Illumina adaptors. Each 25- $\mu$ l PCR contained approximately 5–10 ng  $\mu$ l<sup>-1</sup> of DNA, 200 nM of each primer, 12.5  $\mu$ l of Bulls Eye Taq DNA polymerase 2.0 mix (Midwest Scientific, St Louis, MO, USA) and an adjusted volume of sterilized water. The lowest number of PCR cycles was determined for each sample to minimize PCR-induced artifacts. PCR conditions were as follows: denaturation at 94 °C for 2 min, the number of optimal cycles of 94 °C for 30 s, annealing at 58 °C for 1 min, extension at 72 °C for 1 min and a final extension at 72 °C for 7 min. Negative PCR controls without DNA template were run concurrently for each sample. Triplicate PCRs were set up for each sample and combined prior to proceeding with Illumina's 16S Metagenomic Sequencing Library Preparation Guide (Illumina, San Diego, CA) for setting up a 16S rRNA gene sequencing run with the MiSeq® System. The raw data was processed using MOTHUR's MiSeq® SOP [19] for quality check and downstream sequence analysis. The enriched Evening Star community, now referred to as ES enrichment, was then used to perform MICP in some batch and all flow-through column experiments.

### **2.3 Growth Study**

A study comparing the growth of the ES enrichment to *S. pasteurii* (ATCC 11859) was conducted under batch conditions at 21 $\pm$ 0.5°C. Two growth conditions were applied: (1) 100 mL of Artificial Ground Water (See Appendix Table 1 for recipe) with 1 mg/L as zinc ZnSO<sub>4</sub> and 3 g/L yeast extract and (2) 100 mL of deionized water with 1 g/L NH<sub>4</sub>Cl and 3 g/L yeast extract. These two treatments were intended to demonstrate the effect of higher heavy metal concentrations on microbial growth. Zinc was used as the representative heavy metal contaminant as it is present in the mining site at higher concentrations than all other metals (Table 1). One mL of inoculum with an optical density of 0.5 at 600 nm was added to each treatment. OD<sub>600</sub> and pH were measured throughout the course of the experiment.

### **2.4 Column Experiments**

Three flow-through packed bed columns were constructed at the lab-scale. Two-inch schedule 40 PVC pipe was cut to 40 cm and filled with 33 cm of fine gravel. Sampling ports were placed along the tubing at 1 cm below the column inlet and 24 cm at the effluent. Size 14 Masterflex® tubing was attached to the inlet port and fed through a Cole-Parmer® peristaltic pump. The tubing was attached to a flow break to prevent contamination from the reactors into the media. The pump speed was set for a 30-hour residence time after performing tracer studies, with one pore volume equal to approximately 350 mL. The columns were sterilized by pumping the following solutions through them for 60 hours, or the equivalence of two pore volumes: (1) 1% Bleach plus Tween

80 (5 mL and 3.5 g per 500 mL solution, respectively); (2) Sodium chloride (10 g/L); (3) Sodium thiosulfate (2.52 g/L); (4) 70% Ethanol; (5) Ammonium chloride (10 g/L).

After sterilization, the columns were each inoculated at the inlet sampling port with 350 mL of ES enrichment culture using syringes. Two days prior to inoculation, a frozen stock of the ES enrichment was grown in 37 g/L BHI and 20 g/L urea at  $22 \pm 0.5^\circ\text{C}$ . After 24 hours, 10 mL of culture was transferred to 1990 mL of 37 g/L BHI and 20 g/L urea in Evening Star MIW. The culture was grown for another 24 hours at  $22 \pm 0.5^\circ\text{C}$  before inoculating into columns. The culture was incubated in the columns without flow for 16 hours to allow attachment to gravel. After this attachment period, 3g/L yeast extract and 2 g/L of urea in DI water was pumped for 18 hours to allow growth without potential bacteria encapsulation by mineral precipitate. After this initial growth period, 3 g/L yeast extract and 2 g/L of urea in filtered Evening Star MIW was continuously pumped through the columns for 74 days at  $22 \pm 0.5^\circ\text{C}$ .

### 3 Results and Discussion

#### 3.1 Sediment Enrichments

The results from 16S DNA sequencing of the enrichments indicated that each enrichment consisted of a variety of microbial species. Evening Star B had the least variation, consisting of 95.16% *Sporosarcina* and 2.75% *Acidovorax* in relative abundance. The following *Sporosarcina* species are known to be urease positive: *S. ureae*, *S. aquimarina*, *S. globispora*, *S. koreensis*, *S. pasteurii*, *S. psychrophila*, *S. saromensis*, and *S. soli* [22]. A study evaluating metal toxicity determined *S. pasteurii* live cells were viable in the

presence of cadmium, zinc, copper, and lead at levels orders of magnitude greater than the Evening Star MIW [23]. The same study concluded that zinc could be removed via MICP using *S. pasteurii* at concentrations

up to 0.5 mM with live cells present [23]. Zinc is present in the Evening Star MIW at 48.5x less this concentration; thus, it is not

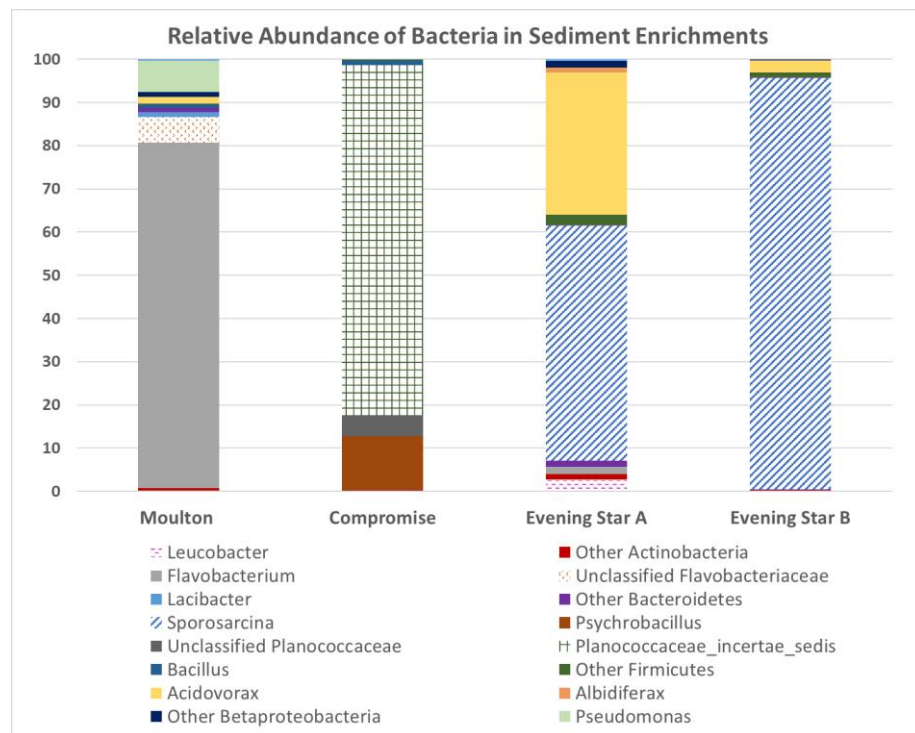


Figure 1: Relative Abundance of Bacteria in Sediment Enrichments. Moulton, Compromise, and Evening Star A are bacterial pellets from enrichment solutions after 3 months. Evening Star B is the attempted colony isolate after spread plating enrichment solution, referred to as ES enrichment in this paper.

unreasonable to assume that various *Sporosarcina* species could viably live and perform MICP at metal concentrations in the MIW for this study.

### 3.2 Growth Study

The growth rates of *S. pasteurii* were compared to the growth rates of the enriched native community to evaluate their behavior under zinc concentrations reflecting MIW. Evening Star B enrichment was used because it had a higher purity and more robust urease activity than the other enrichments. The specific growth rates ( $\mu$ ) were calculated for each treatment by integrating the following exponential growth phase equation [24]:

$$\frac{dX}{dt} = \mu * X$$

In order to yield:

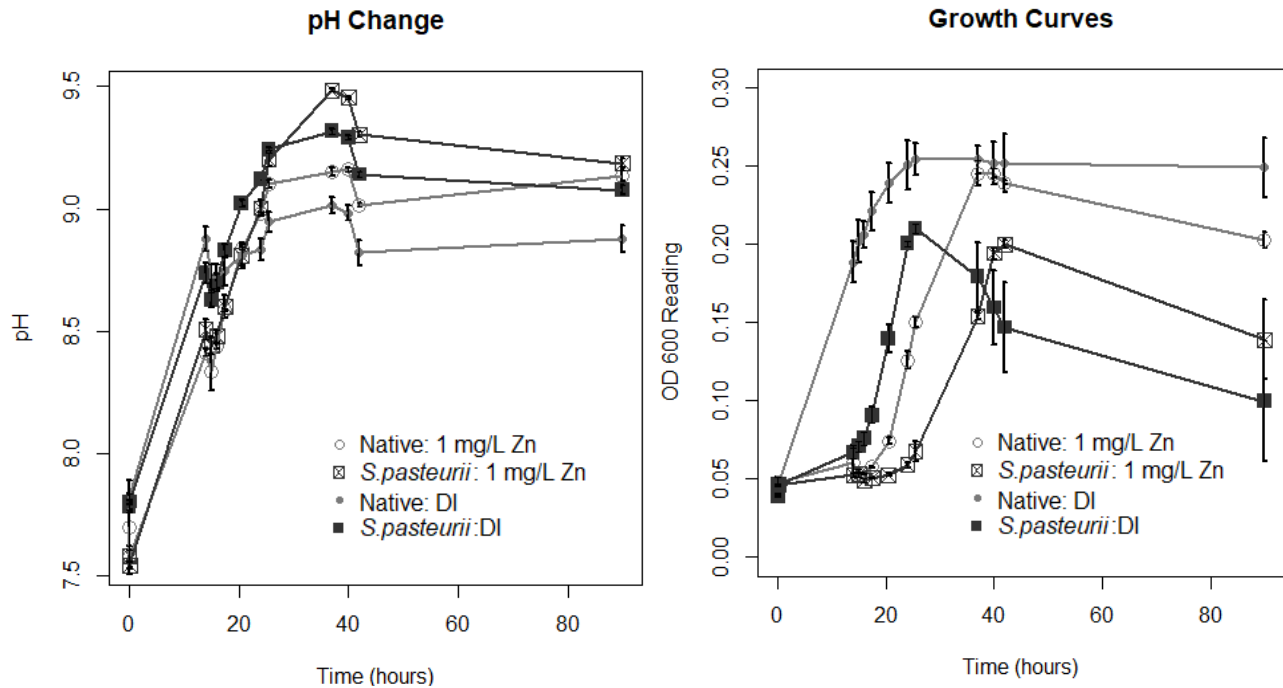
$$\mu = \frac{\ln\left(\frac{X}{X_0}\right)}{t}$$

Where  $\mu$  is the specific growth rate in  $\text{hr}^{-1}$ ,  $X$  is concentration of bacteria, and  $t$  is time in hours. Table 3 summarizes the maximum specific growth rates calculated for each treatment.

Table 2: Average maximum experimental growth rates with one standard deviation from the mean.

Treatment	$\mu_{\text{max}} (\text{hr}^{-1})$
Native Community in AGW + Zn +YE	0.154 ± 0.012
<i>S. pasteurii</i> in AGW + Zn +YE	0.099 ± 0.034
Native Community in DI + NH <sub>4</sub> Cl +YE	0.111 ± 0.005
<i>S. pasteurii</i> in DI +NH <sub>4</sub> Cl +YE	0.144 ± 0.004

The experimental growth rates among all treatments and bacteria ranged from 0.074-0.141 hr<sup>-1</sup>. The enriched native community grew at a faster rate and to a higher maximum cell density than *S. pasteurii* in the artificial groundwater with 1 mg/L zinc. These results indicate that the native community tolerated zinc better than *S. pasteurii*, though bacteria in all growth tests exhibited

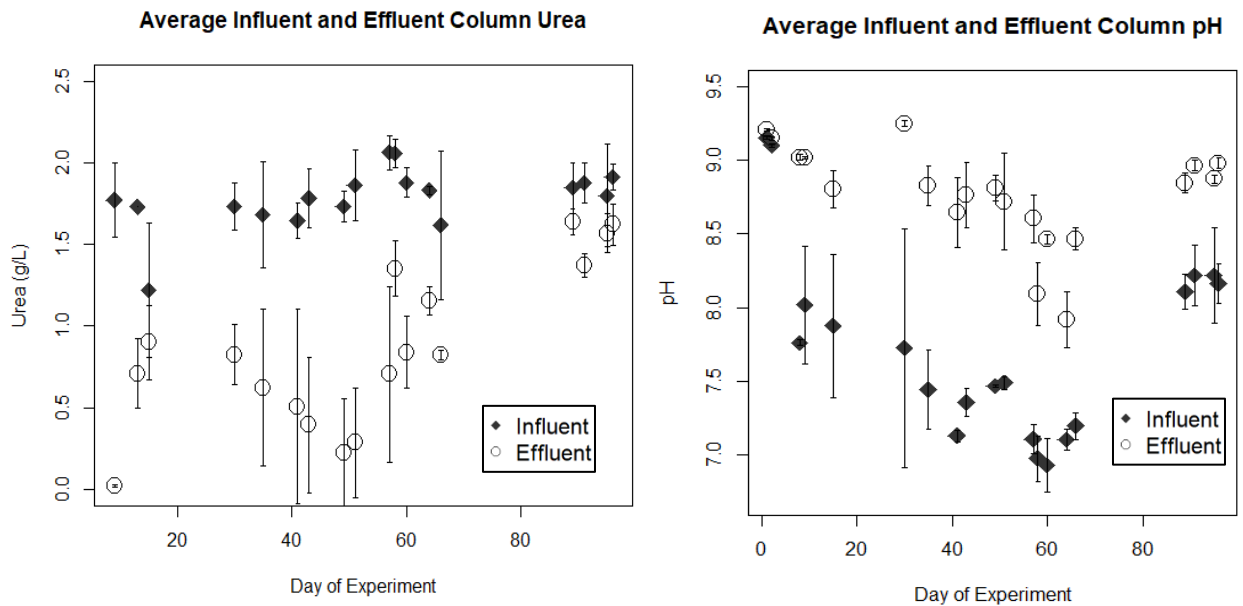


Figures 2(a) & 2(b): pH and OD<sub>600</sub> results from the growth study are presented with error bars representing one standard deviation of triplicate tests.

growth and ureolysis. Figure 2(b) visualizes the delay in growth for *S. pasteurii* compared to the native community. The pH of treatments with *S. pasteurii* reached a higher value than those with the native community, potentially indicating that ureolysis occurs at a higher rate in those treatments. This was later confirmed in the comparative batch experiments. Lower maximum pH values could indicate that urease negative species in the native community grow well and contributed to the cell density without facilitating the pH increase under the experimental conditions.

### 3.4 Column Experiments

The flow-through column reactors were sampled for pH, urea concentrations, and total metals at both the influent and effluent. Although the chemical properties of the influent MIW changed over time due to storage and variation in adit flows, pH was consistently higher exiting the reactor, as is demonstrated in Figure 3b. The pH leaving the reactor had a 95% confidence interval of (.92, 1.2) higher than the pH entering the reactor based on the paired Student's t-test.



Figures 3(a) & 3(b): Temporal influent and effluent urea and pH concentrations observed in the columns. Error bars indicate one standard deviation above or below the mean for triplicate columns.

Urea was consistently degraded in the reactor throughout the course of the experiment; matched-pairs two-sided Student's t-test revealed that 53.5-62% of urea entering the reactor was hydrolyzed from 0-96 days with only the initial inoculation of ES enrichment. This result suggests longevity in urease activity, though less ureolysis appears to be occurring in the later days of the experiment (days 89-96).

Based on the results of the batch studies, zinc and calcium were the main constituents of interest for ICP-MS analysis. Removal of both elements was significant using the matched-pairs two-sided Student's t-test for at least six different sampling days across all three columns. With influent concentrations of zinc averaging at  $278 \pm 27 \mu\text{g/L}$  and exiting at  $70 \pm 26 \mu\text{g/L}$ , the concentrations of zinc leaving the reactors had a 95% confidence interval of 190-226  $\mu\text{g/L}$  less than the initial zinc concentrations (Appendix Figure 1). Similarly, decreased calcium concentrations were observed: average influent concentrations were  $100 \pm 22 \text{ mg/L}$  and average effluent concentrations were  $43 \pm 29 \text{ mg/L}$ . For 51-66 days past inoculation of the system, ureolysis and calcium/zinc removal were still occurring at significant rates. Although the number of sampling dates are limited for ICP-MS analysis, they

indicate this activity is not only long-lived but consistent among the three columns. Modeling Evening Star MIW in equilibrium speciation software Visual MINTEQ 3.1 revealed that at a pH of 8.5, zinc carbonate along with calcium carbonate minerals are supersaturated and thus would be expected to precipitate (see Appendix Table 5 for calculated saturation indices). Partitioning coefficients were calculated for the columns using the following equation modified from Curti [28]:

$$D_{Zn} = \frac{([Zn]_i - [Zn]_f) * [Ca]}{([Ca]_i - [Ca]_f) * [Zn]}$$

It was assumed that the change in concentration of zinc and calcium was precipitated into solid form within the reactor. The median  $D_{Zn}$  is 1.1 with an inter-quartile range of 0.6-5.9, within the range of values previously reported for abiotic co-precipitation (Crocket & Winchester, 1966). These results suggest most of the zinc removal was likely due to co-precipitation into calcium carbonate minerals, validating MICP as the primary treatment technology in the flow-through columns.

## 4 Conclusions

In general, ureolysis and subsequent metal precipitation, particularly zinc, was observed in the treated MIW. Calcium concentrations decreased, pH increased to values near 9, urea was removed, and some metals precipitated over the course of batch and column experiments. The results from the sediment enrichments and subsequent microbial community isolation, in conjunction with column experiments support the assertion that microbially induced calcite precipitation and metal co-precipitation is a viable treatment strategy for toxic trace concentrations of zinc in MIW. Zinc was removed at a significant percentage, nearly to aquatic life standards in some instances. Column studies showed that the ureolytic ES enrichment was capable of growing in MIW with added nutrients and catalyzing MICP and zinc removal over a three-month period. This initial study indicates potential for this process as a passive treatment strategy in appropriate applications. Such applications for this trace metal removal strategy include industrial waste streams upstream of a municipal wastewater treatment plant capable of nitrogen removal, mine land settings with nitrifying/denitrifying polishing steps, or in contaminated groundwaters not required to maintain strict nitrogen standards.

## References

- [1] U.S. EPA. (2014). *Reference Guide for Treatment Technologies for Mining-Influenced Water*. Retrieved from [https://www.epa.gov/sites/production/files/2015-08/documents/reference\\_guide\\_to\\_treatment\\_technologies\\_for\\_miw.pdf](https://www.epa.gov/sites/production/files/2015-08/documents/reference_guide_to_treatment_technologies_for_miw.pdf)
- [2] Phillips, A. J., Gerlach, R., Lauchnor, E., Mitchell, A. C., Cunningham, A. B., & Spangler, L. (2013). Engineered applications of ureolytic biomineralization: a review. *The Journal of Bioadhesion and Biofilm Research*, 29(6), 715-733.
- [3] Warren, L. A., Maurice, P. A., Parmar, N., & Ferris, F. G. (2001). Microbially Mediated Calcium Carbonate Precipitation: Implications for Interpreting Calcite Precipitation and for Dolid-Phase Capture of Inorganic Contaminants. *Geomicrobiology Journal*, 93-115.
- [4] Stocks-Fischer, S., Galinat, J. K., & Bang, S. S. (1999). Microbiological precipitation of CaCO<sub>3</sub>. *Soil Biology & Biochemistry*, 1563-1571.
- [5] Harvey, D. (2000). *Modern Analytical Chemistry*. McGraw-Hill.
- [6] Fujita, Y., Redden, G. D., Ingram, J. C., Cortez, M. M., Ferris, F. G., & Smith, R. W. (2004). Strontium incorporation into calcite generated by bacterial ureolysis. *Geochimica et Cosmochimica Acta*, 68, 3261-3270.
- [7] Lauchnor, E. G., Schultz, L. N., Bugni, S., Mitchell, A. C., Cunningham, A. B., & Gerlach, R. (2013). Bacterially Induced Calcium Carbonate Precipitation and Strontium Coprecipitation in a Porous Media Flow System. *Environmental Science & Technology*, 1557-1564.
- [8] Kang, C.-H., Kwon, Y.-J., & So, J.-S. (2016). Bioremediation of heavy metals by using bacterial mixtures. *Ecological Engineering*, 64-69.
- [9] Li, M., Cheng, X., Guo, H., & Yang, Z. (2016, September). Biomineralization of Carbonate by *Terrabacter Tumescens* for Heavy Metal Removal and Biogrouting Applications. *Journal of Environmental Engineering*, 142(9).
- [10] Kumari, D., Pan, X., Lee, D.-J., & Achal, V. (2014). Immobilization of cadmium in soil by microbially induced carbonate precipitation with *Exiguobacterium undae* at low temperature. *International Biodeterioration & Biodegradation*, 98-102.
- [11] Zhao, Y., Yao, J., Yuan, Z., Wang, T., Zhang, Y., & Wang, F. (2017). Bioremediation of Cd by strain GZ-22 isolated from mine soil based on biosorption and microbially induced carbonate precipitation. *Environmental Science and Pollution Research*, 372-380.
- [12] Achal, V., Pan, X., Fu, Q., & Zhang, D. (2012). Biomineralization based remediation of As(III) contaminated soil by *Sporosarcina ginsengisoli*. *Journal of Hazardous Materials*, 178-184.
- [13] Limcharoensuk, T., Sooksawat, N., Sumarnrote, A., Awutpet, T., Kruatrachue, M., Pokethitiyook, P., & Auesukaree, C. (2015). Bioaccumulation and biosorption of Cd<sup>2+</sup> and Zn<sup>2+</sup> by bacteria isolated from a zinc mine in Thailand. *Ecotoxicology and Environmental Safety*, 322-330.
- [14] Li, M., Cheng, Z., & Guo, H. (2012). Heavy metal removal by biomineralization of urease producing bacteria isolated from soil. *International Biodeterioration & Biodegradation*, 1-5. Retrieved from <http://dx.doi.org/10.1016/j.ibiod.2012.06.016>
- [15] Montana DEQ, Water Quality Division, Water Quality Planning Bureau, Water Quality Standards and Modeling Section. (2017). *DEQ-7 Montana Numeric Water Quality Standards*. Helena: Montana Dept. of Environmental Quality.
- [16] Tetra Tech, Inc. (EMI Unit). (2016). *Final Adit Discharge Monitoring Technical Memorandum*. Helena.
- [17] Atlas, R. M. (2005). *Handbook of Media for Environmental Microbiology* (Second ed.). Boca Raton: CRC Press.
- [18] Jung, D., Biggs, H., Erikson, J., & Ledyard, P. U. (1975). new Colorimetric Reaction for End-Point, Continuous-Flow, and Kinetic Measurement of Urea. *Clinical Chemistry*, 1136-1140.

- [19] Kozich, J., Westcott, S., Baxter, N., & Schloss, P. (2013). Development of a dual-index sequencing strategy and curation pipeline for analyzing amplicon sequence data on the MiSeq Illumina sequencing platform. *Applied and Environmental Microbiology*, 79(17), 5112-5120.
- [20] Herigstad, B., Hamilton, M., & Heersink, J. (2001, March 1). How to optimize the drop plate method for enumerating bacteria. *Journal of Microbiological Methods*, 44(2), 121-129.
- [21] Croghan, C. W., & Egeghy, P. P. (2003, September 26). *Methods of Dealing with Values Below the Limit of Detection using SAS*. Retrieved from United States Environmental Protection Agency: [https://cfpub.epa.gov/si/si\\_public\\_record\\_report.cfm?dirEntryId=64046](https://cfpub.epa.gov/si/si_public_record_report.cfm?dirEntryId=64046)
- [22] Kwon, S.-W., Kim, B.-Y., Song, J., Weon, H.-Y., Schumann, P., Tindall, B. J., . . . Fritze, D. (2007). *Sporosarcina koreensis* sp. nov. and *Sporosarcina soli* sp. nov., isolated from soil in Korea. *International Journal of Systematic and Evolutionary Microbiology*, 57, 1694-1698. doi:10.1099/ijs.0.64352
- [23] Mugwar, A. J., & Harbottle, M. J. (2016). Toxicity effects on metal sequestration by microbially-induced carbonate precipitation. *Journal of Hazardous Materials*, 237-248.
- [24] Maier, R., Pepper, I., & Gerba, C. (2000). *Environmental Microbiology*. San Diego: Academic Press.
- [25] Ferris, F., Fyfe, W., & Beveridge, T. (1987). Bacteria as nucleation sites for authigenic minerals in a metal-contaminated lake sediment. *Chemical Geology*, 225-232.
- [26] Doerner, H., & Hoskins, W. M. (1925). Co-precipitation of radium and barium sulfates. *Journal of the American Chemical Society*, 47(3), 662-675.
- [27] Crocket, J. H., & Winchester, J. W. (1966). Coprecipitation of zinc with calcium carbonate. *Geochimica et Cosmochimica Acta*, 30, 1093-1109.
- [28] Curti, E. (1999, June). Coprecipitation of radionuclides with calcite: estimation of partition coefficients based on a review of laboratory investigations and geochemical data. *Applied Geochemistry*, 14(4), 433-445.

APPENDIX for

**Microbially induced mineral precipitation in mixed constituent mine influenced water  
using an enriched bacterial community native to mine land sediments**

*Emily K. Stoick*

Additional recipes for artificial groundwater, vitamin solution, SL-4 trace element solution, and SL-6 trace element solution. Additional graphs for zinc and calcium removal in column studies, and minerals with saturation indices above 1 for treated Evening Star MIW are also presented.

Table 1: Artificial Groundwater Recipe

Constituent	Concentration (mM)
KNO <sub>3</sub>	0.403
MgSO <sub>4</sub>	0.448
CaCl <sub>2</sub>	36
NaNO <sub>3</sub>	0.044
NaHCO <sub>3</sub>	1.1
KHCO <sub>3</sub>	0.0623

Table 2: Recipe for vitamin solution [17]

Vitamin	Quantity per 1 L solution
Biotin	2 mg
Folic Acid	2 mg
Pyridoxine hydrochloride	10 mg
Thiamine•HCl	5 mg
Riboflavin	5 mg
Nicotinic Acid	5 mg
Calcium D- (+) –pantothenate	5 mg
Vitamin B12	0.1 mg
p-Aminobenzoic Acid	5 mg
Thioctic Acid	5 mg
Distilled Water	1 L

Table 3: Recipe for SL-4 Trace Element Solution [17]

Component	Concentration (g/L)
EDTA	0.5
FeSO <sub>4</sub> *7H <sub>2</sub> O	0.2
SL-6 Trace Element Solution (see below)	100mL

Table 4: Recipe for SL-6 Trace Element Solution [17]

Component	Concentration (g/L)
H <sub>3</sub> BO <sub>3</sub>	0.3
CoCl <sub>2</sub> *6H <sub>2</sub> O	0.2
ZnSO <sub>4</sub> *7H <sub>2</sub> O	0.1
MnCl <sub>2</sub> *4H <sub>2</sub> O	0.03
Na <sub>2</sub> MoO <sub>4</sub> *H <sub>2</sub> O	0.03
NiCl <sub>2</sub> *6H <sub>2</sub> O	0.02
CuCl <sub>2</sub> *2H <sub>2</sub> O	0.01
-Adjust pH to 3.4	

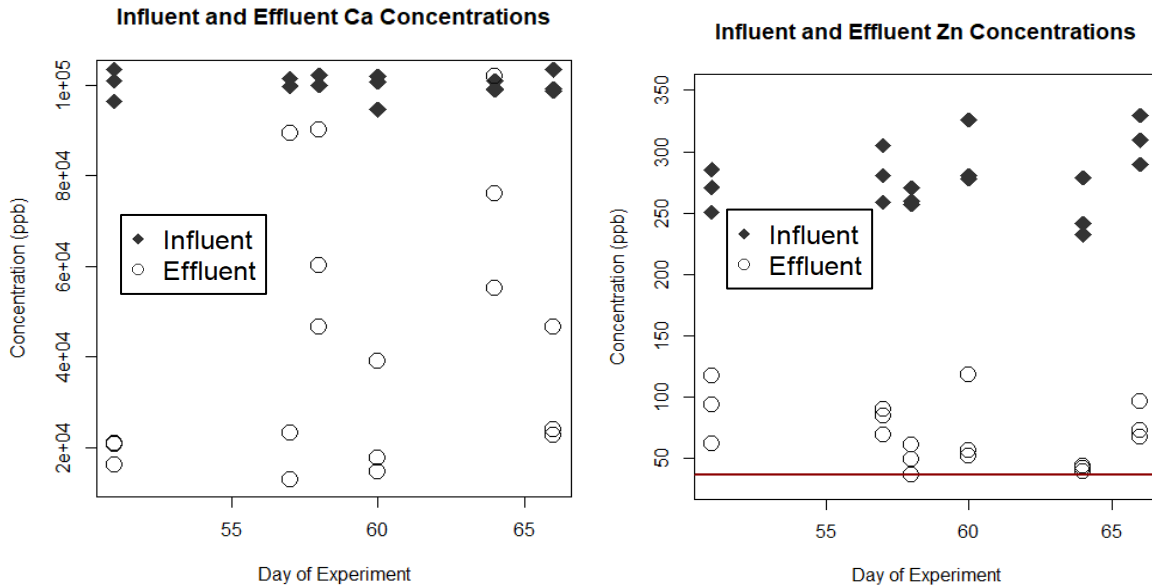


Figure 1: Influent and effluent calcium and zinc concentrations for all three columns from days 51-66. The red line on zinc graph indicates the Montana DEQ zinc standard for aquatic life.

Table5: Saturation indices produced using Visual MINTEQ 3.1 for treated Evening Star MIW at 10°C and 22°C. Carbonate concentration in the MIW was approximated by conservatively assuming 1g/L of urea was hydrolyzed, producing 1000 mg/L of carbonate species.

Mineral	Equation	22°C Saturation Index	10°C Saturation Index
Aragonite	CaCO <sub>3</sub>	1.552	1.398
CaCO <sub>3</sub> xH <sub>2</sub> O(s)	CaCO <sub>3</sub> x H <sub>2</sub> O	0.357	0.214
Calcite	CaCO <sub>3</sub>	1.698	1.553
Dolomite (disordered)	CaMg(CO <sub>3</sub> ) <sub>2</sub>	2.959	2.412
Dolomite (ordered)	CaMg(CO <sub>3</sub> ) <sub>2</sub>	3.521	3.026
Hausmannite	Mn <sup>2+</sup> Mn <sup>3+</sup> <sub>2</sub> O <sub>4</sub>	16.378	15.797
Huntite	Mg <sub>3</sub> Ca(CO <sub>3</sub> ) <sub>4</sub>	2.811	1.59
Hydrozincite	Zn <sub>5</sub> (CO <sub>3</sub> ) <sub>2</sub> (OH) <sub>6</sub>	3.487	2.01
Magnesite	MgCO <sub>3</sub>	0.763	0.806
MnCO <sub>3</sub> (am)	MnCO <sub>3</sub>	1.98	1.994
NiCO <sub>3</sub> (s)	NiCO <sub>3</sub>	0.019	N/A
Pyrolusite	MnO <sub>2</sub>	11.877	12.134
Rhodochrosite	MnCO <sub>3</sub>	2.477	2.477
Siderite	FeCO <sub>3</sub>	1.068	0.92
Smithsonite	ZnCO <sub>3</sub>	0.978	0.934
Vaterite	CaCO <sub>3</sub>	1.123	0.945
ZnCO <sub>3</sub> (s)	ZnCO <sub>3</sub>	0.885	0.869
ZnCO <sub>3</sub> xH <sub>2</sub> O (s)	ZnCO <sub>3</sub> x H <sub>2</sub> O	0.344	0.329

## Student Fellowship Project: Estimate Mountain Front Recharge in a Basin and Range Province in Southwest Montana.

### Basic Information

<b>Title:</b>	Student Fellowship Project: Estimate Mountain Front Recharge in a Basin and Range Province in Southwest Montana.
<b>Project Number:</b>	2017MT317B
<b>Start Date:</b>	3/1/2017
<b>End Date:</b>	2/28/2018
<b>Funding Source:</b>	104B
<b>Congressional District:</b>	1
<b>Research Category:</b>	Ground-water Flow and Transport
<b>Focus Categories:</b>	Groundwater, Hydrology, Agriculture
<b>Descriptors:</b>	None
<b>Principal Investigators:</b>	Charles Shama

### Publication

1. Shama, Charles, 2018, MOUNTAIN FRONT RECHARGE IN A SEMI-ARID CLIMATE, SOUTHWEST MONTANA, Department of Geosciences, Montana Tech of the University of Montana, Butte, MT, 97pp.

**2017MT317B**

**Student Fellowship Project: Estimate Mountain Front Recharge in a Basin and Range Province in Southwest Montana**

**Report for Montana Water Center, May 2018**

**By Charles Shama**

**INTRODUCTION**

Groundwater recharge to regional valley benches originates largely from adjacent Mountain Front Recharge (MFR). The Madison Valley in Southwest Montana is a semi-arid cold climate that receives 31.75cm annual valley precipitation. In this study, two drainages are characterized and compared, looking at the hydrological processes between the stream and groundwater. North Meadow Creek is a high elevation stream dominated by snowmelt and contains reaches of gaining and losing surface water to groundwater. Daylight Creek is a spring fed disconnected stream. Methods used a surface water balance, temperature as an environmental tracer and two and three component mixing models to investigate groundwater underflow, stream and groundwater fluxes, and source waters for streams. The smaller Daylight Creek watershed is a disconnected stream with a range of specific vertical discharge at 2-5m/s to 8-10m/s. The larger North Meadow Creek watershed contains three unique zones. The upper mountainous reach is a gaining stream, the middle reach is a transition from gaining to losing, and the lower zone is a losing reach. Specific vertical discharge has a range of 5.0-5m/s to 8.0-6m/s. A two and three component mixing model was utilized to fractionate soil water and groundwater. North Meadow Creek has a soil water pulse during the spring melt and a fluctuating fraction groundwater contribution of 10% to 75% throughout the study period. Daylight Creek has no seasonal trend and a constant 40%-50% groundwater contribution during the study period.

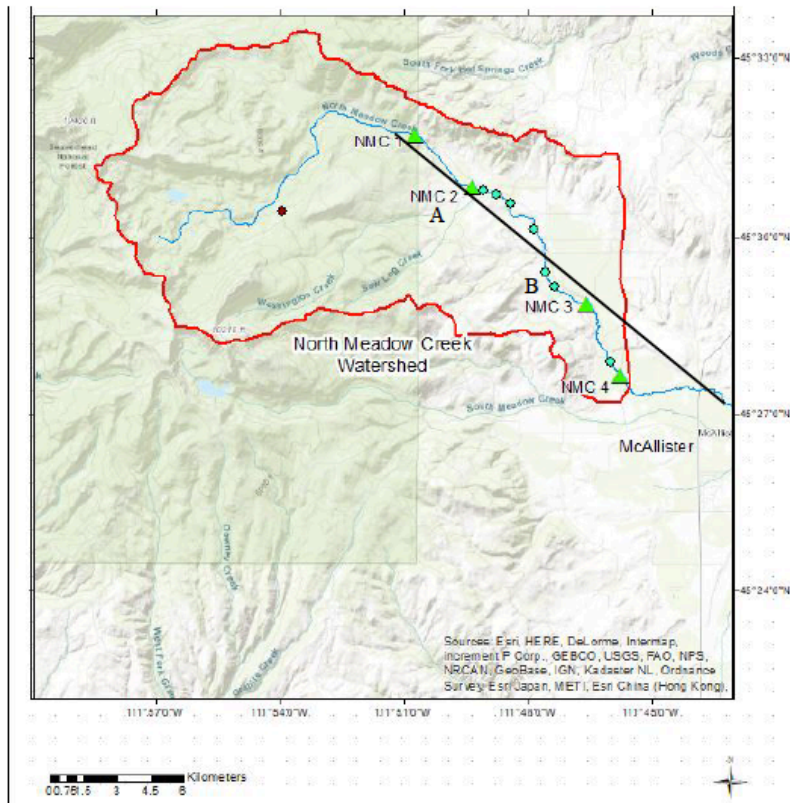
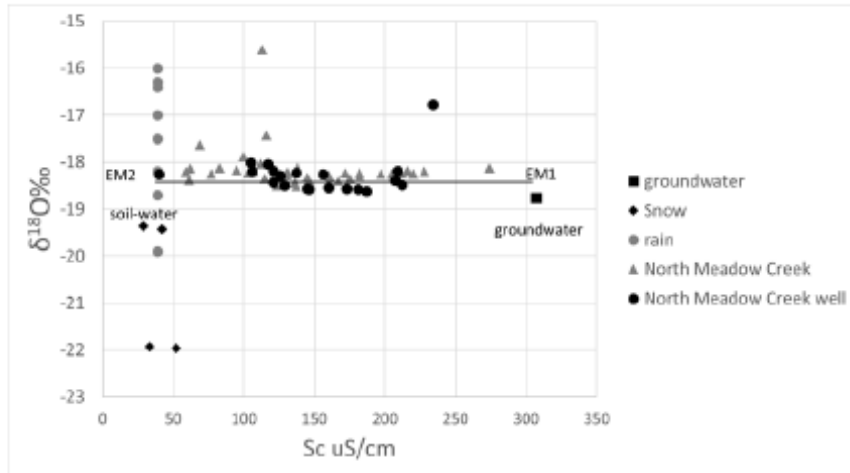


**Figure 3: North Meadow Creek Watershed. NMC1 and NMC2 are located in the upper watershed while NMC3 and NMC4 are located in the lower watershed. Red outline represents watershed boundaries. Cross section and elevation profile is shown with line. Red marker is the location of SNOTEL site 603. Green triangles are study locations. Blue marks are location of irrigation diversions.**

## **SELECTED RESULTS**

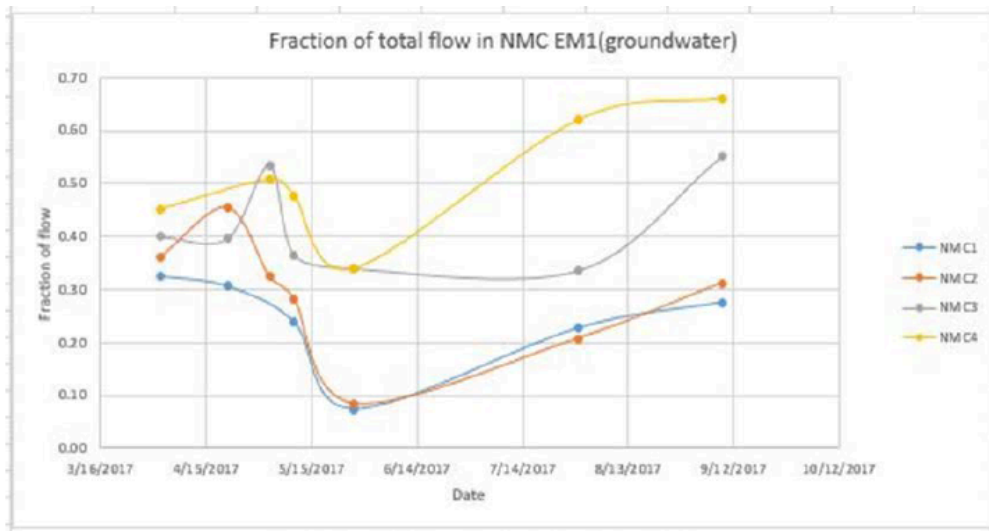
### **Mixing Models**

A three-component mixing model (Figures 26 and 27) separates groundwater, snow, and rain end-members. Rain and snow end-members were chosen based on the furthest value out on the triangle. Groundwater end-member was chosen from a single deep well sample. After reviewing the mixing model data, it has come to the attention that the rain and snow are not the true end-members. The  $\delta^{18}\text{O}$  for rain and snow are different but the  $S_c$  is similar indicating a different end-member. All the surface and groundwater samples trend to be a line. When the rain and snow end-member  $\delta^{18}\text{O}$  samples are averaged, they fall along the trend line. A simpler approach would be a two-member mixing model (Figures 28 and 29) where the end-members rain and snow are combined and averaged to become soil water as one end-member and groundwater as the other end-member. The  $\delta^{18}\text{O}$  data for the stream and well samples are close together between  $-18\text{‰}$  and  $-19\text{‰}$  while the  $S_c$  is a range from 250 – 800  $\mu\text{S}/\text{cm}$ . Rain and snow may not be true end-members, but shallow soil water consisting of mixtures of rain and snow. This would make a two-component mixing model based on  $S_c$  since the  $S_c$  of rain and snow is essentially the same. This study will present results of both three and two component mixing models.



**Figure 28: North Meadow Creek  $\delta^{18}\text{O}$  vs Sc two-component model groundwater and soil water. The soil-water endmember is an average of the rain and snow samples.**

Sc and  $\delta^{18}\text{O}$  were used in three-member and two-member mixing analysis to determine source waters of North Meadow Creek and Daylight Creek. Equations 8-18 results in fractions of each end-member plotted in Figures 31 and 33. Rain and snow  $\delta^{18}\text{O}$  and Sc were averaged to create the soil water end-member. At NMC, the stream and well samples plot closer to the soil water end-member than the groundwater end-member. At DC the stream plots closer to the soil water end-member while the well samples range from groundwater to soil water.



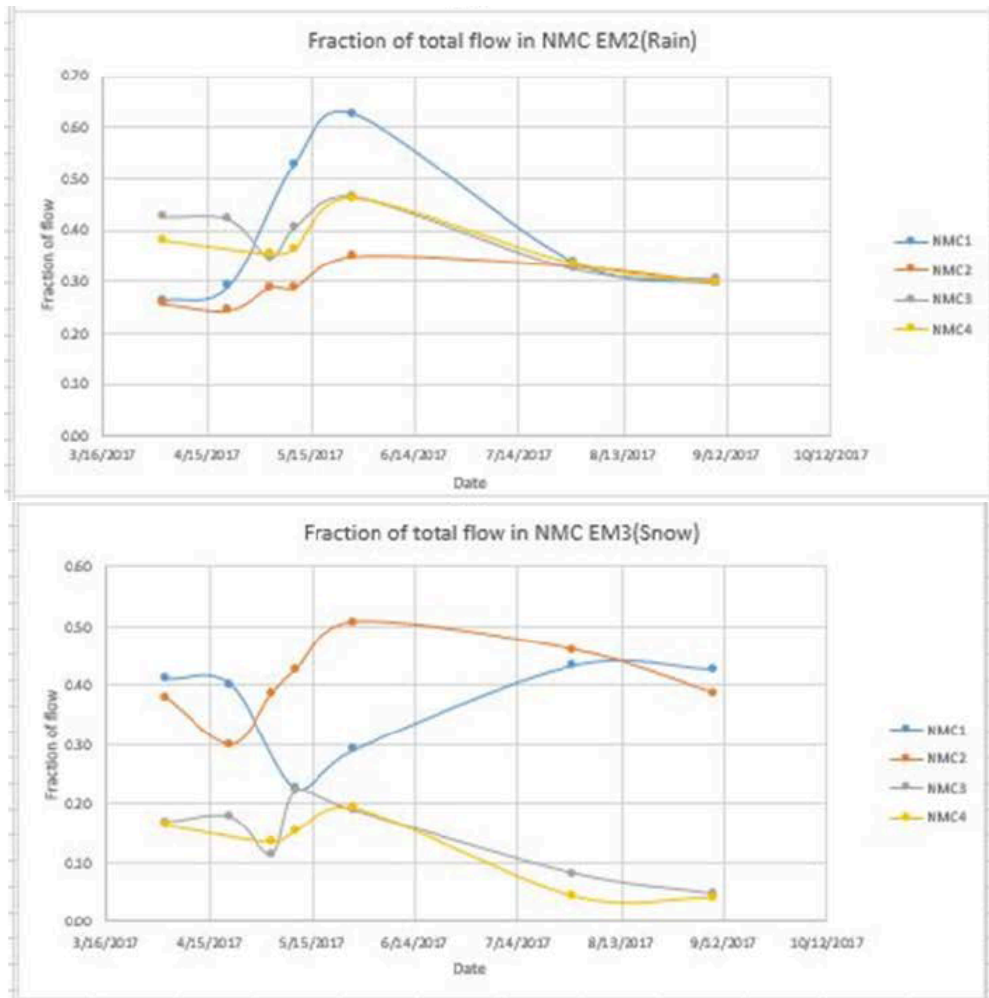


**Figure 30: Fractionation of three end-members groundwater (EM1), rain (EM2), and snow (EM3) at North Meadow Creek. The fraction of the end-members is on the y-axis and the date is on the x-axis.**

The three-component mixing model shows the groundwater end-member with a decline during the spring and steadily increases through the summer and fall (Figure 30). The downstream locations (NMC3, NMC4) have a much larger fraction of groundwater than the upstream locations (NMC1, NMC2). The rain end-member shows an increase during the spring, than all locations converge at about 30% by late summer (Figure 30). The snow end-member has a consistent high fraction in the upstream locations and a low fraction in the downstream locations (Figure 30). See appendix H for complete end-member mixing data. There was little to no precipitation in the form of rain or snow during July and August, yet the three member mixing model shows 30%-40% fraction of rain and upwards of 45% snow during those months. Shallow subsurface residence time could explain the snow-like signature shown in upstream locations NMC1 and NMC2 during late summer.

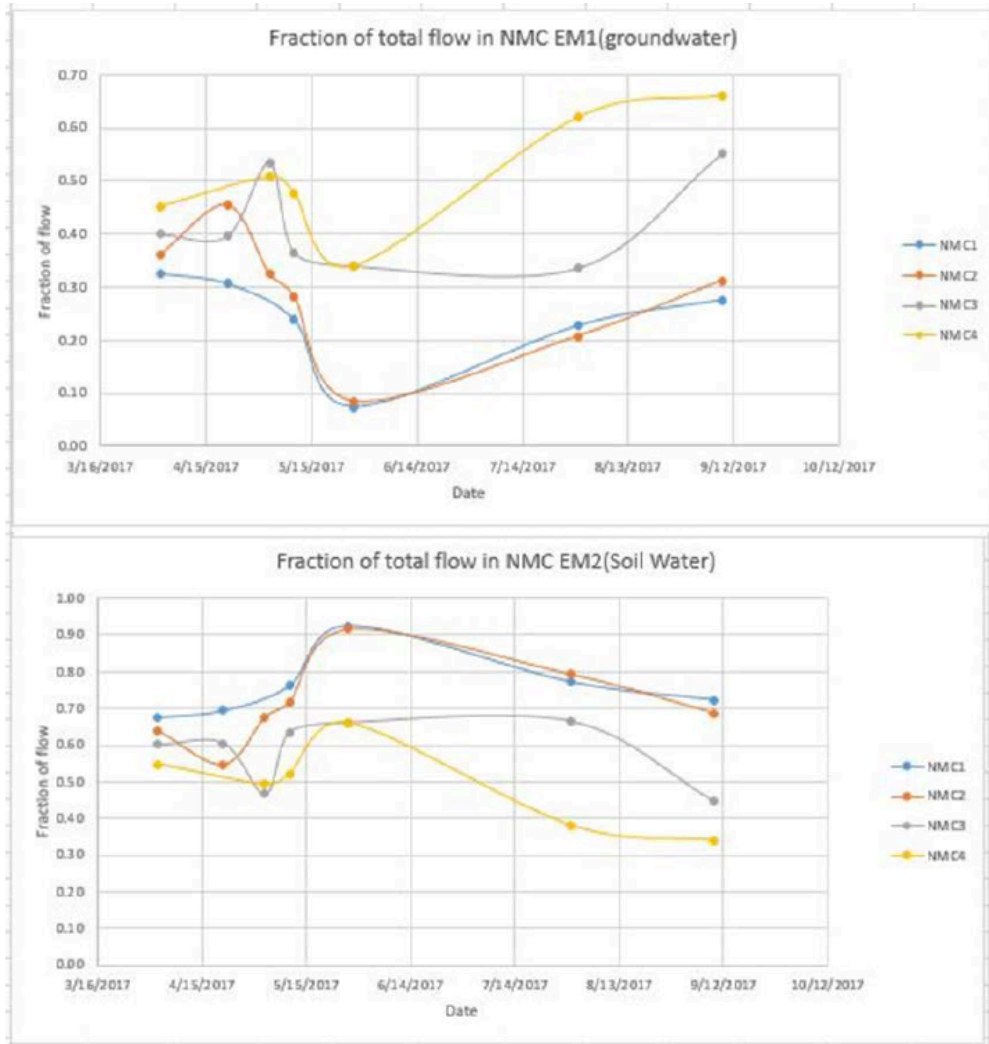


**Figure 31: Fractionation of two end-members groundwater (EM1) and soil water (EM2) at North Meadow Creek. The fraction of the end-members is on the y-axis and the date is on the x-axis.**

The two-component mixing model (Figure 31) has the groundwater end-member at 30%-50% during early spring. During the spring melt, there is a small fraction of groundwater and a large fraction of soil water, which is the previous winters snowpack entering the stream (Figure 31). The soil water fraction stays at about 70% or more in the upstream locations. The downstream locations have a higher groundwater fraction 35-65% than the upstream locations 10-30% during the late summer months. This two-component model shows a similar trend as the three-component model.

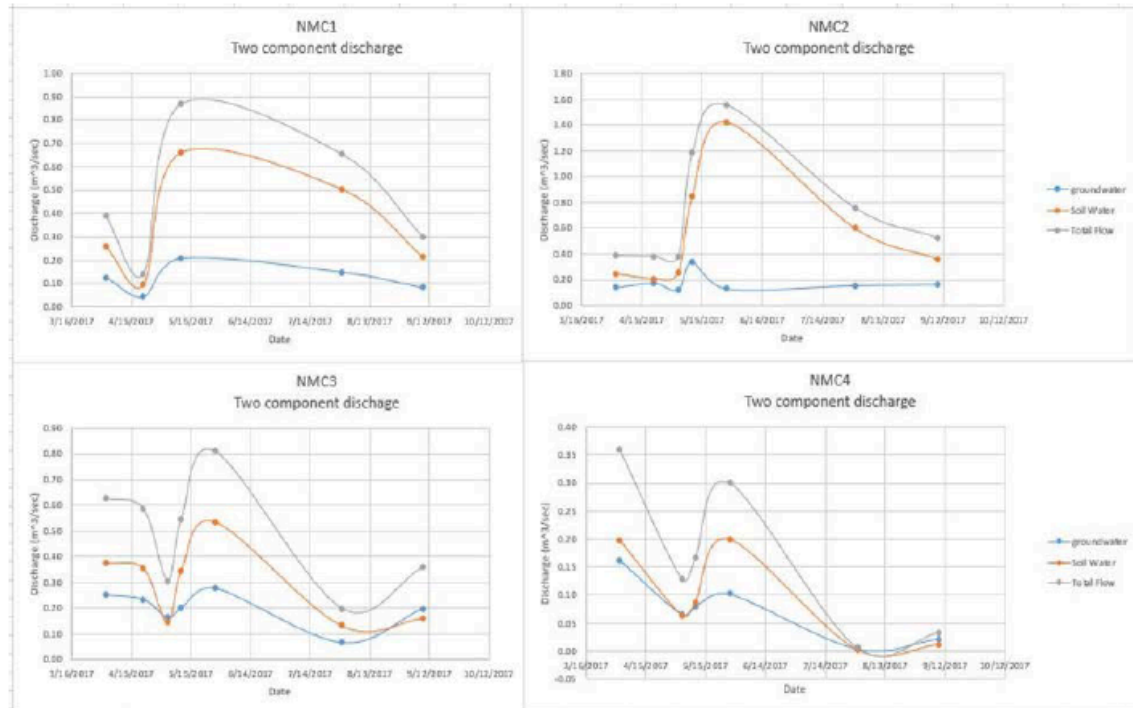


**Figure 35: Two-component discharge at North Meadow Creek. The fractionation of the end-members soil-water (EM1) and groundwater (EM2) are multiplied by the monthly stream discharge.**

The two-component discharge at North Meadow Creek (Figure 35) shows that groundwater is a steady contributor throughout the year. The soil water has a spring melt pulse that gradually tapers off in the summer months, indicating a 1-3 month travel time and a slower melt of high elevation snowfields. Similar to the three-component discharge (Figure 34), the two-component discharge (Figure 35) has a soil water discharge in the upper reaches and a groundwater discharge in the lower reaches.

## **SUMMARY**

### **Vertical GW/SW fluxes for recharge/discharge (RS).**

The physical hydraulic properties of the streams, wells, and sediments permit groundwater flux estimates using the Darcy equation (equation 4). North Meadow Creek has a high hydraulic conductivity (Table II) and groundwater fluxes vary through the season (Table III & IV). At NMC2 the stream transitions from point A to point B (Figure 3). This reach has groundwater gaining until after B where the stream transitions to a constant losing reach. Daylight Creek has a low hydraulic conductivity (Table II) and groundwater fluxes stay relatively constant (Table III & IV).

Observations of changes in groundwater temperature profiles enabled an estimate of downward and upward fluxes (Table IV). The Darcy fluxes also provide estimates of groundwater fluxes and compliment the temperature results (Table III). The temperature profiles reveal that North Meadow Creek is a stream that has a snowmelt runoff with gaining and losing segments transitioning throughout the study. In April, the gaining section of the stream ends at NMC2 and transitions to a losing stream by NMC3. During snowmelt runoff, May through June, the gaining section pulses downstream to NMC3. In July through October,

the gaining reaches recedes upstream to NMC2, and NMC3 transitions back to a losing stream. At Daylight Creek the flux estimates are small magnitude and do not change through the season. Daylight Creek is a losing stream throughout the study.

The specific vertical discharge estimates from the temperature profiles (Table 4) match close to the estimates from the Darcy equation (Table 3). The flux estimates are within one to two orders of magnitude and agree on direction of either upward or downward groundwater flow.

The surface water balance reveals that North Meadow Creek is a gaining stream between NMC1 and NMC3 and a losing stream between NMC3 and NMC4 (Table V). At NMC3, this location is not losing during the entire study and the reach above NMC3 may be only partially gaining during the wet months of May and June and losing during the dry months of July, August, and September. This reinforces the GW/SW fluxes the Darcy and temperature profile methods.

### **Mixing models to determine source waters for catchment GW/SW.**

The relative fraction of groundwater in North Meadow Creek is 10-30% during the snowmelt runoff and 25-65% during the late summer months when the creek is near base flow (Figure 31). Identification and characterization of water sources to North Meadow Creek and Daylight Creek and water mixing in these watersheds are addressed by examining variations of specific conductivity (Figures 26-29). These mixing fractions show that groundwater is similar in both three-member and two-member mixing models (Figures 30-33). In the months of July and August a precipitation signature is seen even though there was very little rain events during those months (Figures 30 & 32). This signature may be incorrectly assigned to precipitation end-members (rain and snow). Soil water is the shallow near-surface water entering the streams. This soil water has a short residence time and is younger than the groundwater end-member. The water samples do not show a variation with  $\delta^{18}O$  as much as Sc between precipitation and groundwater (Figures 31 & 33). The soil water is water directly flowing from the spring into the creek, not collecting many salts from the soils and having a low specific conductivity. The groundwater is underground seeps that are in contact with the soils and are increasing specific conductivity.

### **Stream Processes**

North Meadow Creek is a stream with gaining and losing segments that cycle through the year. Early spring the gaining section of the stream ends at NMC2 and transitions to a losing stream by NMC3. During spring runoff the gaining section pulses downstream to NMC3. After the spring runoff and through the summer the gaining section recedes upstream to NMC2 and NMC3 transitions back to a losing stream. The relative fraction of groundwater in North Meadow Creek is low during the spring runoff and high during the late summer months. In the months of July and August shallow near-surface water dominates the upstream sections at NMC2 and NMC1 while groundwater dominates the lower stream sections of NMC3 and NMC4. The bedrock is fractured and has weathered to sandy/gravelly alluvium in the stream valley resulting in a good connection between groundwater and surface water. This enhanced groundwater underflow and stream connectivity is shown with a gaining reach in the high elevations. As the stream flows out of the mountains it becomes a losing reach as seen in both the Darcy and temperature flux estimates (Tables 3 and 4).

NMC1 and NMC2 show a constantly gaining stream throughout the study period. NMC3 shows a transition from a gaining stream during the spring runoff months and a losing stream during the dry summer months. NMC4 shows a losing stream during the summer. Shallow

subsurface residence time could explain the snow-like signature shown in upstream locations NMC1 and NMC2 during late summer. The source of the water is from high elevation mountains and is mostly meteoric and does not have an evaporation signal (Figure 20). Daylight Creek is a spring creek with little to no variation in stream flow or stream chemistry. The surface geology of Daylight Creek is volcanic tuff weathered to clays; this clay has poor hydraulic conductivity 2-7m/s (Table II) and may be a losing and disconnected stream.

Isotope samples show the source of the spring is snowmelt from high elevations. At the high elevation there is a permeable layer of bedrock (Table 1), where the source water enters the ground. At lower elevations, the volcanic tuff weathers into clay and becomes unstable resulting in landslides that dominate the topography. Groundwater flow must be blocked and springs emerge from past landslides that form Daylight Creek.

During the summer months there is no snowpack or much rainfall, therefore all of the stream flow originates from springs. The source of water for the springs comes from a higher elevation than the lower elevation watershed (Figure 21). The soil water could be the water directly flowing from the spring into the creek, collecting many salts from the soils and having a low specific conductivity, while the groundwater can be underground seeps that are in contact with the soils and are collecting more dissolved constituents while moving through the soil profile.

## **CONCLUSION**

Isotope and water chemistry analysis indicate that direct infiltration by precipitation and mountain front recharge are the two main recharge sources in the study area. End-member mixing analysis using stable isotopes and specific conductivity as tracers was shown useful for estimating the contribution of the different recharge sources.

Local and regional geology of the catchment might have the largest control on the timing and amount of groundwater that contributes to streamflow in North Meadow Creek and Daylight Creek. The use of  $\delta^{18}\text{O}$ ,  $\delta\text{D}$ ,  $\text{Sc}$ , and temperature as environmental tracers in groundwater and surface water in North Meadow Creek and Daylight Creek drainages provide a good method for characterizing how precipitation and groundwater partitions through mountain catchments. These tracers reveal complex spatial and temporal mixing between recent precipitation and deeper groundwater.

## **FUTURE RESEARCH**

Further research would include water sampling at spring locations and along both mountain ranges to the south and north of Daylight Creek to determine source waters for the springs. Water sampling at smaller tributaries and more rain and snow sampling within the higher elevations at North Meadow Creek would establish a more accurate mixing model.

Geophysical methods to determine the cross sections of the stream valleys such as electrical resistivity can better estimate the surface to bedrock depth and can be used with the Darcy equation to determine groundwater underflow (FS). Residential wells within each drainage should be sampled and have their water level monitored to get a better understanding of the groundwater processes.

These methods are inexpensive, easy to implement and can be reproduced in other mountain

catchments providing a useful contribution by demonstrating methods to improve the understanding of groundwater dynamics within the mountain front.

Mountain Front Recharge is an important component of the basin groundwater balance in a semi-arid area. Improving the understanding and estimation of MFR is critical for effective basin water management.

### **REFERENCES CITED**

Anderson, J., (2015) Geochemical Assessment and Separation of Source Waters in the Upper Boulder River Watershed Near Boulder, MT. Graduate Theses & Non-Theses.

Clark, I., Fritz, P., (1997) Environmental Isotopes in Hydrogeology, CRC Press

Craig, H., (1961) Isotopic Variations in Meteoric Water, Science, vol. 133 No. 3465, 1702-1703.

Constantz, J., A. E. Stewart, R. Niswonger, and L. Sarma, (2002) Analysis of temperature profiles for investigating stream losses beneath ephemeral channels, Water Resour. Res., 38(12), 1316, doi:10.1029/2001WR001221.

Constantz, J. (2008), Heat as a tracer to determine streambed water exchanges, Water Resour. Res., 44, W00D10, doi:10.1029/2008WR006996.

Earman, S., Campbell, A. R., Phillips, F. M., & Newman, B. D. (2006). Isotopic exchange between snow and atmospheric water vapor: Estimation of the snowmelt component of groundwater recharge in the southwestern United States. Journal of Geophysical Research: Atmospheres, 111(D9).

Fetter, C. W., (2014). Applied Hydrogeology (4th), Pearson Education Limited.

Frisbee, M. D., Phillips, F. M., Campbell, A. R., Liu, F., & Sanchez, S. A. (2011). Streamflow generation in a large, alpine watershed in the southern Rocky Mountains of Colorado: Is streamflow generation simply the aggregation of hillslope runoff responses? Water Resources Research, 47(6).

Gammons, C. H., Poulson, S. R., Pellicori, D. A., Reed, P. R., Roesler, A. J., Petrescu, E. M. (2006) The hydrogen and oxygen isotopic composition of precipitation, evaporated mine water, and river water in Montana, USA, Journal of Hydrology, Volume 328, Issues 1–2

Gleeson, T., & Manning, A. H. (2008). Regional groundwater flow in mountainous terrain: Three - dimensional simulations of topographic and hydrogeologic controls. Water Resources Research, 44(10).

Liu, F., M. W. Williams, and N. Caine (2004), Source waters and flow paths in an alpine catchment, Colorado Front Range, United States, Water Resour. Res., 40, W09401, doi:10.1029/2004WR003076

Magruder, I. A., Woessner, W. W. and Running, S. W. (2009), Ecohydrologic Process

Modeling of Mountain Block Groundwater Recharge. *Ground Water*, 47: 774–785.  
doi:10.1111/j.1745-6584.2009.00615.x

59

Manning, A. H., & Solomon, D. K. (2003). Using noble gases to investigate mountain-front recharge. *Journal of Hydrology*, 275(3), 194-207.

Madison Stream Team (MST), (2018). Water Quality Information  
<http://waterquality.montana.edu/madison/streamteam/pages/NorthMeadow.html> (Accessed March 2018)

Natural Resources Conservation Service National Water And Climate Center,  
[www.wcc.nrcs.usda.gov](http://www.wcc.nrcs.usda.gov) <https://wcc.sc.egov.usda.gov/nwcc/site?sitenum=603> (Accessed January 2018)

Shaw, G. D., M. H. Conklin, G. J. Nimz, and F. Liu (2014), Ground water and surface water flow to the Merced River, Yosemite Valley, California:  $^{36}\text{Cl}$  and  $\text{Cl}^-$  evidence, *Water Resour. Res.*, 50, 1943–1959, doi:10.1002/2013WR014222.

USGS 500k wmas\_02282013 <https://mbmg.mtech.edu/storymaps/GeologicMaps.html>  
(Accessed January 2018)

Voytek, E.B.; Drenkelfuss, Anja; Day-Lewis, F.D.; Healy, Richard; Lane, J.W., Jr.; and Werkema, Dale, 2013, 1DTempPro: Analyzing Temperature Profiles for Groundwater/Surface-water Exchange: *Ground Water*.

Wilson, J. L., & Guan, H. (2004). Mountain - Block Hydrology and Mountain - Front Recharge. *Groundwater recharge in a desert environment: The Southwestern United States*, 113-137.

Western Regional Climate Center, Ennis Montana (242793) <https://wrcc.dri.edu/cgi-bin/cliMAIN.pl?mt2793> (accessed 1/17/2018)

1DTempPro – Version 2.0, 7/23/2015  
<http://water.usgs.gov/ogw/bgas/1dtemppro/>

## Student Fellowship Project: Leaf Water Potential as an Improved Predictor of Drought Induced Conifer Stress

### Basic Information

<b>Title:</b>	Student Fellowship Project: Leaf Water Potential as an Improved Predictor of Drought Induced Conifer Stress
<b>Project Number:</b>	2017MT318B
<b>Start Date:</b>	3/1/2017
<b>End Date:</b>	2/28/2018
<b>Funding Source:</b>	104B
<b>Congressional District:</b>	1
<b>Research Category:</b>	Biological Sciences
<b>Focus Categories:</b>	Drought, Ecology, Climatological Processes
<b>Descriptors:</b>	None
<b>Principal Investigators:</b>	Caelan Simeone

### Publication

1. Simeone, Caelan, 2018, COUPLED ECOHYDROLOGY AND PLANT HYDRAULICS MODEL PREDICTS PONDEROSA SEEDLING MORTALITY AND LOWER TREELINE IN THE US NORTHERN ROCKY MOUNTAINS, MS Thesis, Department of Geosciences, University of Montana, Missoula, Montana, 54pp.

## USGS 104g Report

Caelan Simeone

Coupled ecohydrology and plant hydraulics modeling predicts ponderosa pine seedling mortality and lower treeline in the U.S. Northern Rocky Mountains.

### **Abstract**

Drought influences the extent of forests through large-scale die-offs and reductions of seedling recruitment and survival. We examined the spatial distribution of drought stress in seedlings to evaluate its influence on regeneration at the lower treeline in the northern Rockies. We used a novel ecohydrologic model (Ech2o-SPAC) combined with a vegetation dynamic stress index that incorporates intensity, duration, and frequency of stress, to examine mortality from loss of hydraulic conductivity in *Pinus ponderosa* seedlings. We calibrated our model using a glasshouse drought experiment; tested our model using *in situ* monitoring data on seedling mortality from reforestation efforts; and simulated high-resolution drought stress in seedlings within the Bitterroot River watershed of western Montana. Our model successfully simulated drought responses and mortality of seedlings in the glasshouse and within monitored stands. Low elevation, south-facing, non-convergent locations with high atmospheric demand and limited upslope water subsidies experienced the highest rates of modeled mortality in our study watershed. Modeled drought mortality in seedlings from 2001-2015 correlated tightly with the current distribution of forest cover near the lower treeline, suggesting that drought limits recruitment and ultimately constrains the low elevation extent of conifer forests within the region.

### **Introduction**

Evergreen forest cover is predicted to decline in the western U.S. in the next century, due in part to increased drought stress associated with climate change (Van Mantgem et al., 2009; Jiang et al., 2013; Hartmann et al., 2015; McDowell et al., 2016). These predictions concur with observed shifts in ecosystem composition over regions of complex terrain (Walther et al., 2002; Parmesan & Yohe, 2003) and with the global increase in the frequency and magnitude of drought-induced forest mortality events over the last two decades (Allen et al., 2010; Allen et al., 2015). Increasing air temperatures are extensively documented over much of the western U.S (Christensen et al., 2007; IPCC, 2014) and compound the effects of droughts through increased evaporative demand (Weiss et al., 2009, Williams et al., 2013). More frequent, drier and warmer periods are expected to impact the distribution of common low-elevation species in the western U.S, such as ponderosa pine (*Pinus ponderosa*) (Coops et al., 2005, Rehfeldt et al., 2014). These impacts will occur not only through more extensive mature tree die-off events (Allen & Breshears, 1998) but also through a decline in the frequency of climatic conditions favorable for seedling establishment, especially along the low elevation, drier margin of these species' ranges (Rother et al., 2015; Petrie et al., 2016). While recruitment dynamics have been studied extensively at the upper treeline (e.g. Smith et al., 2009; Kueppers et al., 2017), less is known about lower treeline (the forest boundary dictated by water limitations). Loss of seedling recruitment at the lower treeline could dramatically decrease the distribution of forest cover, given the high edge-area ratios of low elevation forest boundaries.

Forest demography, composition, and distribution are sensitive to recruitment and establishment success rates of different tree species (Petrie et al., 2016) which in turn are sensitive to drought pressures (Savage et al., 1996; Dobrowski et al., 2015). Furthermore, although the same physical principles drive water transport in seedlings and adult trees, seedlings and saplings are more vulnerable to drought-induced mortality than older trees (Harcombe, 1987; Bell et al., 2014). Understanding seedling response to drought and water stress is therefore essential to accurately assessing the stability of current forest boundaries and to identify forested regions that are vulnerable to ecosystem transitions (Bell et al., 2014;

Petrie et al., 2017).

Soil supply and atmospheric demand constrain the balance of energy in the soil-plant-atmosphere continuum (SPAC), generating sufficient lift within plants to sustain transpiration. Drought increases atmospheric demand and decreases soil water supply, leading to more negative water potentials in plant vascular systems. Low water potentials drive cavitation-induced embolism, reducing plant hydraulic conductivity and impairing a plant's ability to transport water (Tyree & Sperry, 1988; Tyree, 1997; Sperry et al., 1998; Venturas et al., 2017). Large losses of conductivity have been ubiquitously linked with drought-induced mortality (Adams et al., 2017; Martínez-Vilalta & Garcia-Forner, 2017). Severe losses of conductivity cause hydraulic failure (McDowell et al., 2008; Sevanto et al., 2014). More prolonged, less severe droughts cause both hydraulic impairment and carbohydrate depletion (shown to be important in c. 60% of cases, Adams et al., 2017) leading to cascading system failures (Anderegg et al., 2012) as a function of intensity, duration, and frequency of drought (Porporato et al., 2001). Seedlings have minimal nonstructural carbohydrate storage and as a result may be more directly responsive to hydraulic dysfunction.

Despite advances in understanding of the relationships between drought and tree mortality (e.g. Sperry et al., 1998; McDowell, 2011; Martínez-Vilalta & Garcia-Forner, 2017; Venturas et al., 2017), our ability to predict landscape-scale drought-induced forest mortality remains limited. The linkages between landscape-scale plant water stress and forest mortality are complex and vary between species and growth stages. These linkages also depend heavily on climate and physical processes that vary at fine spatial scales in regions of complex topography (Anderegg, LDL et al., 2013). While the inclusion of static terrain indices can improve forest mortality predictions (Tai et al., 2017), most hydrologic models used in forest mortality studies omit lateral redistribution of water and are forced with gridded meteorological data that are too coarse to resolve aspect-scale variations in radiation and temperature (e.g. McDowell et al., 2016).

Experimental research at the plant level has identified species-specific water potential thresholds in the soil and within the plant below which, hydraulic function is compromised affecting plant survival (Choat et al., 2012). These thresholds have been used to map forest mortality risk using landscape-scale water stress metrics based on climatic and hydrologic variables. Some of these metrics are statistical or correlative in nature (Williams et al., 2013; Anderegg et al., 2015a). While these metrics capture observed spatial patterns of drought-related forest stress and mortality with varying degrees of success, they are correlative rather than mechanistic. This decreases the opportunity for process insight and reduces our ability to transfer predictions from models to novel spatial and temporal domains. Alternative approaches with a stronger mechanistic foundation use plant water potential, loss of xylem conductivity, and plant carbon status to predict plant response to drought and mortality (e.g. Mackay et al., 2003; Ogee et al., 2003; McDowell et al., 2013; Tai et al., 2017). While detailed physiologically, these approaches have not yet fully integrated 3D hydrologic and climatic controls on vegetation dynamics (Vico, 2009).

Physiological and modeling studies commonly use percent loss of conductivity (PLC) to quantify water stress. PLC reflects hydraulic impairment, which Adams et al. (2017) note as a ubiquitous driver of drought-induced plant mortality. Tai et al. (2017) found that using plant hydraulics improved predictions of mortality by 40% compared to using soil moisture, emphasizing the importance of integrating plant physiological responses to modeling approaches of plant mortality. PLC reflects the resistance of the xylem to cavitation under varying drivers of drought, including available soil water and atmospheric water demand (Sevanto et al., 2014). Varying intensity, duration, and frequency of drought have been shown to be important in drought-induced mortality (Porporato et al., 2001, Anderegg, WRL, 2013; Mitchell et al. 2013). However, approaches based on PLC accounting for these factors have not been fully developed.

We present a modeling study to understand potential instabilities in low elevation forest boundaries in the

western U.S. We developed a mechanistic ecohydrologic model to simulate landscape-scale water and energy exchanges and plant hydraulic function. We used the model in conjunction with a glasshouse experiment of ponderosa pine seedling mortality to (1) calibrate plant hydraulic parameters, and (2) to determine the functional dependence of seedling mortality risk on declining xylem hydraulic function during droughts. This functional form uses statistics on the mechanistically derived measures of plant stress under the assumption that a sequence of events (periods of stress) of different duration and intensities which accumulate damage in the plant cause drought-induced mortality. We tested the model on seedling mortality data from U.S. Forest Service (USFS) reforestation efforts. We then ran the model in a semiarid watershed in western Montana and compared the spatial distribution of simulated seedling water stress to remotely-sensed forest cover with the goal of predicting the current distribution of lower tree line.

## Materials and Methods

### Ecohydrologic Model

Our modeling framework extends an ecohydrologic model, Ech2o (Maneta & Silverman, 2013), to investigate the impact of the redistribution of water and energy at the landscape scale on plant vascular hydraulic stress. Ech2o is a spatially distributed, mechanistic model that couples a two-layer vertical solution of the energy balance, a water balance with lateral and vertical water redistribution in the landscape, and a dynamic vegetation growth scheme. Ech2o has an intermediate level of complexity compared to other ecohydrologic models, bridging a gap between catchment hydrology models and comprehensive land surface models that simulate energy, water and biotic interactions within the critical zone. Because of its relatively parsimonious design, Ech2o can run efficiently over large domains at relatively high spatial and temporal resolutions. We coupled Ech2o with a plant hydraulics model (Sperry et al., 1998) (Ech2o-SPAC) to simulate dynamic SPAC processes in a fully integrated manner across landscape gradients of energy and water.

Maneta & Silverman (2013), Lozano-Parra et al. (2014), and Kuppel et al. (2018) comprehensively describe the model.

### Plant Hydraulics Component

Water transport through the SPAC is a function of water potential gradients within the plant vascular system according to the cohesion-tension theory (Sperry et al., 1998). Cavitation-induced embolisms occur when steep tension gradients between soil and the atmosphere along the SPAC overcome the strength of the water column at nucleation points (Tyree, 1997; Venturas et al., 2017). These events reduce the plant's capacity to transport water and at high enough rates lead to hydraulic failure and death. Our model simulates the tension gradient driving water lift by solving a system of four equations that incorporate interactions with the energy balance, soil water balance, soil-plant water balance, and soil-plant water potential balance (Eqn. S1). Loss of conductivity depends on leaf water potential (LWP) and is used as a proxy for stress. The fraction of conductivity lost to embolism (referred to as PLC to resemble common nomenclature) is:

$$PLC = 1 - e^{-(-\psi_{leaf}/b)^c} \quad (1)$$

where  $\psi_{leaf}$  is LWP and  $b$  and  $c$  are experimental values from a Weibull vulnerability curve:  $b$  is the LWP value mathematically corresponding to 63% PLC, and  $c$  controls the shape and slope of the function (Sperry et al., 1998; Hubbard et al., 2001).

### Dynamic Stress Index

To transition from an instantaneous measurement of stress (PLC) to a probabilistic prediction of mortality, we adapt a statistical framework based on the dynamic stress index (DSI, $\theta$ ) presented by Porporato et al.

(2001). The original framework assumes that static vegetation water stress begins at the volumetric water content (VWC) in the soil at which incipient stomatal closure occurs. Static stress reaches a maximum at the VWC at which stomata completely close. This static stress is the basis for a dynamic measurement of vegetation stress that incorporates the mean intensity, duration, and frequency of periods of soil moisture deficit. In our implementation, we substitute PLC for VWC to calculate DSI. PLC subsumes tension dynamics in the soil and xylem and includes variable hydraulic architecture and response to the onset of water deficit. We interpret DSI as the integrated probability of tree mortality at a location.

To calculate DSI we first calculate a static stress index,  $\zeta(t)$ . When PLC surpasses an initial threshold ( $PLC_{init}$ ) stress increases until a maximum threshold of stress ( $PLC_{crit}$ ). A piecewise function calculates the static stress index:

$$\zeta(t) = \begin{cases} 0, & \text{if } PLC(t) < PLC_{init} \\ \frac{PLC_{init} - PLC(t)}{PLC_{init} - PLC_{crit}}, & \text{if } PLC_{init} < PLC(t) < PLC_{crit} \\ 1, & \text{if } PLC(t) > PLC_{crit} \end{cases} \quad (2)$$

We calculate the mean weighted stress ( $\bar{\zeta}$ ) during the growing season as the accumulated static stress during the growing season:

$$\bar{\zeta} = \frac{\int_0^1 (\zeta_z(D) dD) + F_z(1)}{P(PLC_{init})} \quad (3)$$

where  $F_z(1)$  is the probability that static stress exceeds the maximum threshold ( $PLC_{crit}$ ). The integral accounts for periods when stress is between the initial ( $PLC_{init}$ ) and maximum ( $PLC_{crit}$ ) thresholds.  $P(PLC_{init})$  is the probability of exceeding the minimum threshold.

The mean weighted water stress ( $\bar{\zeta}$ ) accounts for the mean intensity of stress during periods of stress but lacks direct information on either duration or frequency of stress, both of which impact plant response. Once  $\bar{\zeta}$  is calculated, information on the frequency and duration of events is included in the Dynamic Stress Index ( $\bar{\theta}$ ), which is constrained between zero and one and represents the probability of mortality:

$$\bar{\theta} = \begin{cases} \left( \frac{\bar{\zeta} \bar{T}_{PLC}}{k T_{seas}} \right)^{\bar{n}_{PLC}^r}, & \text{if } \bar{\zeta} \bar{T}_{PLC} < k T_{seas} \\ 1, & \text{otherwise} \end{cases} \quad (4)$$

where  $T_{seas}$  is the length of the growing season, determined by the number of days with modeled soil temperature above five °C (Bailey & Harrington, 2006; Beedlow et al., 2013), using the average temperature modeled through the full soil column.  $T_{PLC}$  and  $n_{PLC}$  are respectively the average length and frequency of drought events where hydraulic impairment over the level of  $PLC_{init}$  occurs. Parameter  $k$  is a constant for plant resistance to drought. The parameter  $r$  is a constant that estimates plant legacy effect (Porporato et al., 2001 uses resilience) from drought. It ranges from zero (no drought memory; plants fully recover after a drought) to increasing values as damage from prior drought stress accumulates.

### Glasshouse Dataset Used for Calibration

We used data from a glasshouse experiment conducted at the University of Montana to calibrate our model parameters for predictions of both physiological signals of stress and seedling mortality rates under drought stress (Martínez-Vilalta et al. unpublished; Sapes & Sala unpublished). This experiment exposed 250 one-year-old ponderosa pine seedlings of the genetically distinct Northern Rocky Mountain race (Potter et al. 2013) to three successive dry-down cycles followed by re-watering to pre-condition seedlings before a final dry-down leading to death. Periodically during the dry-down, subsets of 30 randomly selected seedlings were re-watered to and their mortality determined after at least one month based on foliage browning, completely desiccated phloem, and no signs of recovery. At each time seedlings were removed to re-water and assess mortality, we randomly selected five seedlings to assess physiological

status (including transpiration and LWP) followed by destructive measurements to determine PLC. Such a design allowed us to estimate the point of no return (when seedlings can no longer recover) at the population level and relate it to the mean physiological status of seedlings at that point. LWP and PLC values were used to fit a Weibull vulnerability curve for the seedlings. A few conductance values that increased during the three conditioning dry-downs due to growth were set to zero PLC and assumed to have sustained limited cavitation. We measured soil VWC with a 30-minute sampling resolution using three randomly selected pots per race instrumented with 5TE soil sensors (Meter Inc.) placed at the same soil depth.

### **Calibration Approach**

The model represented the glasshouse as a 3X3 pixel flat domain where we simulated all four dry-downs. Atmospheric boundary conditions were provided by hourly measurements of temperature (Vaisala HMP35C), solar radiation (Licor 200X), and relative humidity (Vaisala HMP35C). We estimated longwave radiation based on measured air temperature using the Stefan-Boltzmann equation with an emissivity of 0.95. To prevent zero transpiration from occurring during measured periods of zero windspeed we increased measured windspeed from the glasshouse by 0.25(m/s). Plant watering schedules and amounts were simulated as precipitation inputs.

We used a Monte Carlo Markov Chain approach for calibration using both Metropolis-Hastings and Gibbs-Step-Slice Sampler algorithms. We divided the calibration into two steps. In the first step, we calibrated Ech2o-SPAC to simulate the physiological response to the drought induced within the glasshouse. We included a group of the most sensitive parameters in the calibration. We performed 5,500 model runs within the Monte Carlo framework to sample the parameter space. We matched measured VWC, transpiration, and LWP with multiple objective calibration. In the second step, we calibrated three variables in the DSI framework ( $PLC_{init}$ ,  $PLC_{crit}$ , and  $k$ ) against the observed probability of mortality from the glasshouse. For each of our 5,500 model executions, we took the LWP time series from an Ech2o-SPAC run with the mean calibrated parameters and applied the DSI framework to that time series. We held  $r$  at 0.5 (see Porporato et al., 2001) during this calibration because there was only one stress-inducing drought event in the glasshouse, which prevented us from examining plant memory effects of drought.

### **Application to Northern Rockies seedling survival data**

To step to the landscape scale we used data on seedling survival rates from the USFS Region 1 reforestation program. Following timber harvest or disturbance, one to three-year-old nursery-grown seedlings were planted to facilitate reforestation. At these sites, stake rows of seedlings were monitored at one and three years after planting to assess the fraction of seedlings that experienced mortality. The majority of the stake row data represented two to three-year-old seedlings. Consequently, from the full dataset, we extracted data for 29 sites in which one-year-old bare-root seedlings were planted (the closest stock type to our glasshouse calibration) for ponderosa pine, Douglas-fir (*Pseudotsuga menziesii*) and western larch (*Larix occidentalis*) (Fig. 1). Each of these sites had 30 or more seedlings in their stake row (mean = 71, std = 38). These stake row sites span a range of elevations (mean=1534m, std=341m), annual precipitations (mean=0.72m, std=0.19m), and mean annual temperatures (mean=9.8° C, std=2.5° C).

We ran Ech2o-SPAC at a three-hour timestep at each reforestation site from 2001-2015, simulating a center target cell with a one cell wide buffer (9 total cells) to facilitate lateral routing of water. Ech2o-SPAC requires five highly heterogeneous soil properties as spatial input; soil depth, porosity, saturated hydrologic conductivity, Brook-Corey pore size distribution index and albedo. These values were extracted from the U.S. Department of Agriculture Soil Survey Geographic Database (SSURGO). For areas where SSURGO data were unavailable, we developed models for each soil property layer to estimate missing soil values following methods described in Landguth et al. (2017). Changes in parameters from the glasshouse are presented in Supporting Information Tables S1 & S2. Weather inputs required to run Ech2o-SPAC include minimum and maximum temperature and relative humidity,

shortwave and longwave radiation, precipitation and wind speed. Daily gridded temperature inputs for simulations at each stake row point were extracted from 250-m grids (Holden et al. 2016). Minimum and maximum daily humidity data were extracted from grids described in Holden et al. (unpublished). Daily precipitation data were extracted from 4 km PRISM data and resampled to 250-m resolution by bilinear interpolation (Daly et al. 2008) and daily wind speed data were extracted from the North American regional reanalysis data (Mesinger et al. 2006). Daily weather data values were converted to three-hour values using time of sunrise and sunset and sine functions adapted from the Interpol.T library in R (R Core Development Team 2010). We converted the Ech2o-SPAC time series of LWP to PLC using Eqn. 1, then calculated the probability of mortality using the DSI framework (equations 2-4).

### **Watershed-level evaluation of low elevation treeline**

To evaluate whether model predictions of seedling drought-induced mortality correspond to the current distribution of lower tree line, we ran Ech2o-SPAC in the Bitterroot River watershed (8<sup>th</sup> code HUC 17010205) in western Montana, USA at a three-hour timestep from 2001-2015 (Fig. 1). Forest managers report widespread seedling mortality in this area following reforestation efforts (Shelagh Fox USFS, personal communication). The simulation domain covers 4,728 km<sup>2</sup> (75,642 250-m grid cells) and spans elevations from 1,000-3,000 m. The watershed encompasses the southern portion of the Bitterroot Mountains to the west; this range is the easternmost portion of the Idaho Batholith and is formerly glaciated (Alden, 1953). The lower-elevation Sapphire range (part of the Sapphire Block) is on the east side of the Bitterroot watershed and is primarily underlain by Belt Supergroup lithology. The Sapphire Range has lower overall slopes and thicker and more extensive soil cover than the steeper, more bedrock-dominated Bitterroot Mountains. Weather systems primarily move from west to east, resulting in higher precipitation in the highest-elevation portions of the Bitterroot Mountains and progressively lower moisture to the east. Grasslands transitioning into low-elevation ponderosa pine-dominated forests make up drier low elevation portions of the watershed. Mid-elevation regions are primarily composed of Douglas-fir, western larch, and lodgepole pine (*Pinus contorta*) forests, while cottonwood (*Populus trichocarpa*) dominate riparian areas.

We ran Ech2o-SPAC in the watershed using vegetation parameters derived from the glasshouse calibration experiment. For vegetation inputs into the model, we assumed a uniform planting of seedlings with a leaf area index of 0.27 m<sup>2</sup>/m<sup>2</sup> (value from the glasshouse) to examine the potential DSI of newly recruited seedlings assuming unforested terrain. Inputs were the same as for the stake row analysis, with increased effective soil conductivity to better reflect regional hydrology.

We evaluate landscape topographic patterns of DSI using terrain indices derived from the U.S. Geological Survey National Elevation Dataset. We focus on examining how elevation, aspect, and topographic convergence, three metrics demonstrated to influence ecohydrology, impact the spatial distributions of drought stress (e.g. Allen & Breshears, 1998; Worrall et al., 2008; Hawthorne & Miniati, 2018). To measure convergence, we calculated topographic position index (TPI, Weiss, 2001), where zero is planar, more negative values are more convergent, and more positive values are more divergent. We extracted maps of climate for mean solar radiation (W/m<sup>2</sup>, indicative of aspect), mean daily maximum temperature (°C), mean annual precipitation (m), and peak snow depth (m). Finally, we extracted maps of key ecohydrologic variables across the watershed, including VPD, VWC, and DSI. VPD (KPa, indicative of atmospheric demand) is the summer mean daily maximum value. VWC (m<sup>3</sup>/m<sup>3</sup>, indicative of water supply) is the mean summer value in the rooting zone (top 40 cm of soil). DSI is the mean annual probability of mortality from 2001-2015.

We compared spatial maps of simulated drought stress with two existing forest vegetation products to examine the relationship between drought stress and forest distribution. Forest vegetation products were the 250-m Moderate Resolution Imaging Spectroradiometer (MODIS) vegetation continuous field percent canopy cover product for the year 2015 (DiMiceli et al., 2011) and the LANDFIRE program canopy height product (Landfire, aggregated from 30m to 250m) derived percent forest cover maps for 2015

(Rollins, 2009). All maps were initially analyzed visually to assess trends in the distribution of drought stress across the landscape. DSI was then matched to each variable and split into 100 bins based on the mapped variable value. The median DSI value of each bin was plotted along with an envelope of the 10th and 90th percentiles. We examined the highly interdependent relationships between DSI, TPI, elevation, solar radiation, VWC, and VPD graphically.

To measure the impact of DSI on forest distribution we classified MODIS forest cover as forest/no forest at a threshold of 10%, below which an area was deemed non-forested. Landfire locations with measured canopy were classified as forested. We classified forest cover predicted from DSI on a threshold basis where locations below the value were forested and those above the value were not forested. To determine the proper threshold we calculated minimum, median, mean, and maximum DSI between 2001 and 2015 and sampled a range of DSI values (0-1) examining how well different thresholds predicted forest cover. We then evaluated the agreement between classified DSI and current forest cover maps by calculating the Area Under the Receiver-Operator Curve (Hanley & McNeil, 1982) and Cohen's Kappa statistics (Cohen, 1960) for the full watershed and for the Skalkaho Creek catchment, a subbasin in the Sapphire Range. Across the entire Bitterroot prescribed and wildfire disturbances, as well as topographic features such as talus slopes and cliffs (common in the Bitterroot Range), can confound model predictions. We calculate statistics in the Skalkaho catchment in addition to the entire Bitterroot because there are relatively fewer of these confounding factors in the Skalkaho catchment. The Skalkaho catchment additionally spans steep gradients of energy and water in a small enough space to allow for higher-resolution visualization of important processes. Biotic effects such as seedling predation by herbivores and dispersal limitation (i.e. distance from seed sources) that we cannot account for may cause a certain degree of disagreement between our models and MODIS/Landfire maps.

## Results

### Calibration of SPAC response to glasshouse drought

Ech2o-SPAC effectively simulated the observed VWC, transpiration, LWP, and mortality response of ponderosa seedlings in our glasshouse drought experiment (Fig. 2). Predicted VWC matched the observations for the three initial soil dry-downs and the major mortality-inducing drought event (Fig. 2a). Ech2o-SPAC slightly underestimated VWC at or above field capacity, but, the match was precise at low VWC, which is most important for predicting stress (Fig. 2a). Transpiration suppression and a steep decline in LWP were observed only after VWC declined in the final dry-down period leading to death (Fig. 2bc), indicating that Ech2o-SPAC properly captured the onset of high hydraulic stress. Increases in mortality lagged behind indicators of increased stress (Fig. 2d). Drought conditions exemplified by low VWC first reduced levels of transpiration, followed by lowering LWP. Low values of LWP were accumulated for a period before plant mortality began, demonstrating the nonlinear threshold behavior captured by Eqn. 2. Through calibration of the DSI framework, we found that stress began to accumulate at a PLC ( $PLC_{init}$ ) of 0.26. The critical level of PLC ( $PLC_{crit}$ ) and the parameter  $k$  were found to be 0.55 and 0.17, respectively. This indicates that 100% mortality would occur in a population of similar ponderosa pine seedlings exposed to a PLC of 0.55 during 17% of the growing season.

### Stake row seedling analysis.

Based on the glasshouse calibration, Ech2o-SPAC effectively simulated mortality of one-year-old bare-root seedlings of ponderosa pine, Douglas-fir and western larch planted in previously disturbed areas (Fig. 3;  $r^2=0.69$ ,  $p<0.01$ ). There is a relatively high amount of variance, as expected from the uncertainty in landscape characteristics and landscape heterogeneity below the 250-m model resolution that impacts individual growth and survival. The trend of the best fit has a slope of 1.20, and an intercept of 0.02 making it close to the 1:1 line, with a slight underestimation of mortality (modeled mean mortality=0.11, observed mean mortality=0.16). This underestimation may be because observed mortality includes all forms of mortality, while modeled mortality is only from PLC drought stress. The good fit demonstrates

the model's skill moving from the glasshouse to the landscape while incorporating heterogeneous physical and climatic processes.

### **Drought-induced mortality at the landscape scale**

When Ech2o-SPAC was fully distributed across the Bitterroot watershed, topography (Fig. 4ab) strongly influenced the distribution of energetic demand (Fig. 4cdg) and water supply (Fig. 4efh). Energy inputs were dominated by elevation (Fig. 4d) and aspect (Fig. 4c), where atmospheric demands decreased with elevation and increased on south-facing slopes (Fig. 4g). Precipitation also increased with elevation (Fig. 4e), however, this pattern differed from plant-available soil moisture (Fig. 4h). Elevation and terrain convergence both controlled the plant available soil moisture (Fig. 4bh). Hydrologic routing concentrated water in convergent locations while draining other positions. Forests were concentrated at locations with sufficient energy and water for growth resulting in high canopy cover at mid-elevation locations, and a preference for north-facing and convergent slopes.

The distribution of dynamic stress (Fig. 5) depended on topography (Fig. 6ab) through the controls that the latter exerts on energetic demand and water supply (Fig. 6c-h). In general, DSI decreased with elevation (Fig. 6a) but varied with convergence and aspect, which distribute lateral routing of water and incoming solar radiation inputs, respectively (Fig. 6bc, 7ab). Median DSI was near zero in highly convergent zones and increased sharply beyond a TPI convergence threshold (c.-50) (Fig. 6b, 7a). DSI increased with solar radiation, although the relationship varied significantly (Fig. 6c, 7b). VWC appeared to be the dominant influence on DSI (Fig. 6h, 7c) but atmospheric demand influenced DSI at sites with low water availability (Fig. 6g, 7c). Additionally, soil VWC did not reach extremely low values (corresponding to high DSI values) without co-occurring large values of VPD (high atmospheric demand for water). Forest cover showed a clear inverse relationship with DSI in regions with sparse forest coverage, but the strength of this relationship decreased once forest cover exceeded 10% (Fig. 6i).

### **DSI predicts the presence and absence of low elevation forest**

Our simulations of DSI for ponderosa seedlings from 2001-2015 correlated with current forest cover (Fig. 8), supporting the hypothesis that drought-induced seedling recruitment failure is a major determinant of the lower treeline. Minimum DSI with a threshold of 0.28 probability of mortality best-predicted presence/absence of forest cover, with high accuracy (kappa of 0.47 for the entire Bitterroot and 0.65 for the Skalkaho subbasin as compared to Landfire presence of canopy). In some cases, places where modeled predictions differed from observations, resulted from scaling and aggregation issues, reflecting local influences on forest extent, rather than model error.

## **Discussion**

### **ECH2O-SPAC captures measured drought response and predicts seedling mortality in the field**

ECH2O-SPAC accurately simulated plant hydraulics in the glasshouse experiment. These results indicate that the physical and biological representation of the SPAC as implemented in the model was adequate for simulating soil moisture depletion, ponderosa pine seedling physiological state, and mortality. Ech2o-SPAC performed comparably to other physiological models (TREES, Tai et al. 2017; MuSICA & ED(X), McDowell et al. 2013). Ech2o-SPAC simulates SPAC dynamics and xylem tensions at sub-daily timescales, necessary to capture critical diurnal demand cycles driving the different stresses experienced by vegetation between predawn and midday (Jackson and Grace 1994).

An important aspect of this research was to provide a functional form relating instantaneous plant hydraulic stress to drought-induced mortality, including duration and frequency of stress events. McDowell et al. (2013) found that time over a threshold of drought stress predicted mortality more effectively than maximum stress levels alone. They also found that pinyon pine (*Pinus edulis*) surviving drought had a mean of 41% PLC, while those that died had a mean PLC of 63%. Adams et al. (2017) found 60% or higher PLC in drought-induced mortality events across species. These values are

comparable to our finding that stress initiates at a PLC of 26% and that the critical threshold for mortality is 55% PLC. Based on our calibration 17% of the growing season had to surpass the PLC<sub>crit</sub> threshold for total (100%) mortality in a seedling population. In contrast, but consistent with greater drought vulnerability in seedlings, Anderegg (2015a) found that adult aspen (*Populus tremuloides*) experienced exacerbated mortality after c. 30 months of extreme PLC. Rates of mortality were sensitive to legacy effects supporting work by Anderegg (2015b) highlighting the importance of better quantification of plant legacy effect in predictions of mortality, especially in drier environments (Dorman et al., 2013) and near species range limits (Camarero et al., 2018). These results combined with empirical evidence (Hacke et al., 2001; Anderegg, WRL et al., 2013; Anderegg et al., 2015b) indicate that intensity and duration of drought stress interact along with prior drought legacy effects to drive mortality (Anderegg et al., 2012) and should be included in simulations of drought-induced mortality.

Our integrated ecohydrologic and plant hydraulic model combined with a framework that incorporates intensity, duration, and frequency of stress into predictions of mortality effectively simulated plant mortality from the glasshouse experiment (Fig. 2) concurrent with the physiological point of no return (Anderegg et al., 2012) rather than a less constrained metric of mortality such as canopy loss or browning. This framework performed well when scaled from the greenhouse to point simulations across the landscape (Fig. 3) capturing population-level mortality as measured on individuals. This demonstrates that Ech2o-SPAC is robust under multiple conditions. We note that in this application of the model we refrained from additional calibration or adjustments to the parameters, using values from the glasshouse. These two independent applications illustrate the capacity of the model to simulate seedling mortality at multiple spatial scales while accounting for the influence of heterogeneous environmental settings using singly calibrated parameters.

### **Modeling drought impacts in complex terrain**

Past studies examining relationships between drought and tree mortality often use gridded weather inputs at resolutions (>4mk) that do not resolve either fine-scaled variations in temperature and radiation or lateral water routing in complex mountainous terrain (e.g. McDowell et al., 2016). Questions related to the stability of the lower tree line in complex terrain, however, demand climatic inputs at higher spatiotemporal resolutions and insights on the benefits of potential water subsidies from upslope regions. Tai et al. (2017) advanced the simulation of mortality across complex terrain, using a statistical relationship based on topographic attributes to address the influence of lateral redistribution of water. We build on these advances by integrating the simulation of the SPAC in a spatially-distributed, physically-based model that simulates the lateral redistribution of water and uses gridded datasets that account for climatic variations in aspect position at sub-daily time steps. The higher radiation loads and 3-4 °C differences on south versus north facing aspects (Holden et al., 2016) translate into observable differences in DSI with aspect position (Fig. 5). Accounting for topographic variations in energy and moisture resolved at fine resolutions is important to explain observed spatial patterns of mortality and delineate areas with high probability of future die-offs, which is useful to inform forest management. Reforestation specialists understand this and use topography to select the most favorable locations and to increase seedling survival. Our study demonstrates the potential to integrate complex, mechanistic modeling at a scale that resolves important sources of topographic variations that can support localized decision making.

### **Landscape patterns of stress and mortality**

Patterns of energy, water availability, and physiological stress vary significantly across the landscape, highlighting the importance of considering both moisture supply and atmospheric demand when simulating plant stress. An exclusive focus on energy and atmospheric demand for water (VPD) as a proxy for plant stress (e.g. Williams et al., 2013) may result in overestimates of stress in valley bottoms and convergent zones. Similarly, focusing only on precipitation or VWC as a proxy for water supply and plant stress (e.g. Porporato et al., 2001) may result in overestimates of stress in higher elevation regions. These areas tend to be drier during the summer months because they typically have shallower soils and

strong drainage. However, atmospheric demand is lower in these areas, reducing plant hydrologic stress and water usage.

DSI from Ech2o-SPAC integrates the balance between water supply and demand on plant hydrologic stress as mediated by their vascular system (Fig. 6). Energy increases DSI (Fig 6cdg) while water decreases DSI (Fig 6efh). Low elevation, south-facing, non-convergent locations with high atmospheric demand and limited upslope water subsidies had the highest rates of modeled mortality. This coheres with the topographic positions of documented drought-induced mortality events (e.g. Allen & Breshears, 1998; Frey et al., 2004; Worrall et al., 2008). Soil moisture in the rooting zone appeared to be the dominant control on drought stress (Fig. 6h, 7c), supporting findings that water availability drives species distributions more than temperature (Crimmines et al., 2011). Topographic convergence increases water availability across elevations (Fig. 7a), thereby reducing the risk of drought mortality in areas where it would otherwise be high. Increased convergence limits the coupling between plant-hydraulic-stress and climate variables and buffers these areas from the impacts of drought. Hydrologic processes in these convergent locations introduce additional heterogeneity in the spatial distribution of plant stress and mortality that is not captured by models that lack topographic controls on water redistribution at fine scales.

### **Drought controls on forest distribution through recruitment suppression**

Our modeled seedling mortality at the lower tree line when accounting for elevation, aspect, and convergence consists with the actual distribution of forests near the lower treeline (Fig. 8). Observed forest cover is higher at middle to high elevations in the Bitterroot watershed, where simulated seedling mortality is lower. Likewise, seedling mortality is higher and forest cover lower on south-facing slopes than on north-facing slopes, while the reverse is true in riparian corridors and convergent locations. We therefore empirically demonstrate that the distribution of forest cover in our study area corresponds with the simulated distribution of drought-induced mortality of one-year-old ponderosa pine seedlings. These results concur with the consensus that one-year-old seedlings are the most vulnerable stage for successful recruitment (Johnson et al. 2011) and that in the absence of other disturbances such as fire, drought is the major factor limiting recruitment at the lower tree line in montane forests of the western U.S. (e.g. Barton, 1993; Kroiss & HilleRisLambers, 2015). Minimum stress predicted forest cover better than mean, max, or median stress. This suggests that the least stressful years are the most important for seedling establishment and survival, and that recruitment will be less likely in areas lacking these low-stress years. This consists with research showing that ponderosa pine recruitment occurs episodically during cool and wet years (Savage et al., 1996; League and Veblen, 2006).

As drought pressures increase, forest mortality is expected to accelerate (Allen et al., 2015; McDowell et al., 2016). Our results suggest that increases in drought will cause an upslope retraction of the lower treeline away from south-facing and non-convergent areas at moderate drought risk (Bell et al., 2014). Increases in temperature associated with climate change will likely drive these patterns to some extent, relegating forest to higher elevations and north-facing aspects. Uncertainty of precipitation response to climate change may complicate this pattern. In western Montana, precipitation is projected to increase in fall, winter, and spring, but decrease during the summer (Whitlock et al., 2017). However, the uncertainty in these predictions (Silverman et al., 2013; Silverman & Maneta, 2016; Whitlock et al., 2017) is far greater than the uncertainty of projections of increased temperature. Given that VWC had the strongest relationship with DSI (Fig. 6h, Fig. 7c), changes in precipitation during the 21<sup>st</sup>-century impact forest distribution. Regardless of the direction of precipitation changes, topographic convergence and lateral routing of water will strongly mediate distributions of drought stress at the lower treeline, particularly in the context of expected temperature increases. Highly convergent areas may increasingly act as zones of climate refugia buffering forests from climate change (Dobrowski, 2011; Mclaughlin et al., 2017). Biodiversity both in structure and species traits has been shown to buffer ecosystem response to drought (Dobrowski et al., 2015; Anderegg et al., 2017). Here we build on research showing that abiotic diversity

(topographic position and hydrologic routing) also buffers ecosystem response to drought. This bringing up the possibility that biotic diversity and abiotic diversity (e.g. topography, lateral routing, lithology, groundwater, soil dynamics, and nutrient availability) will act interdependently to mitigate some impacts of climate change-induced drought.

### Concluding remarks

We show that a fully integrated ecohydrologic and plant hydraulics model that accounts for spatial heterogeneity and drought memory effects effectively captured the physiology and mortality of one-year-old ponderosa pine seedlings in a glasshouse drought experiment. We reasonably simulated observed seedling mortality at sites across western Montana and northern Idaho using an independent data set. Atmospheric and hydrologic controls concentrated simulated seedling mortality at low elevation, south-facing, non-convergent locations in the Bitterroot Valley of western Montana. The pattern of this mortality captured current forest cover observations (high simulated seedling mortality correspond to low forest cover). Our results indicate that increasing drought as a result of global warming may limit seedling recruitment at the lower tree line and reduce the capacity of low elevation forests to regenerate.

### Acknowledgements

This material is based upon work supported by the National Science Foundation under grant no. GSS-1461576. Support to attend the American Geophysical Union 2017 Fall Meeting and present this work was granted from by the USGS 104g grant program through the Montana Water Center. This work was additionally contributed to and authored by Marco Maneta, Solomon Dobrowski, Zachary Holden, Gerard Sapes, and Anna Sala.

### Figures

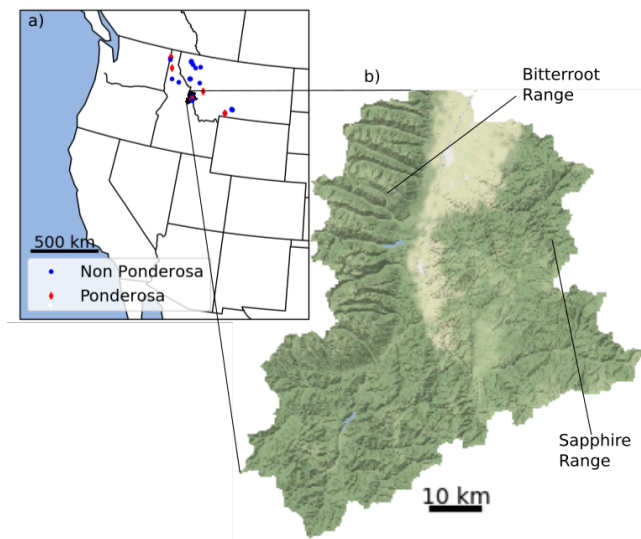


*Figure 1: Map of the southern Bitterroot watershed and locations of USFS stake row sites. a) The black outline in the larger map is the location of the Bitterroot watershed. Red markers are locations of ponderosa stake rows, while blue markers are other species. b) The Bitterroot mountain range is on the west side. The Sapphire mountain range is on the east.*

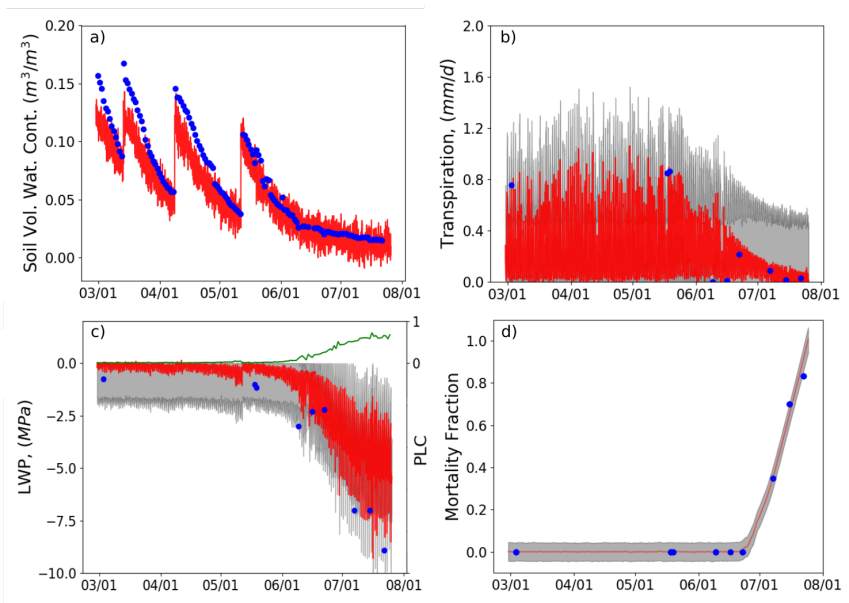


Figure 2: Modeled and observed fits for the glasshouse experiment: a) soil volumetric water content (VWC) ( $R^2=0.94$ ,  $p<0.01$ , slope=0.79), b) transpiration ( $R^2=0.74$ ,  $p<0.01$ , slope=0.74), c) leaf water potential (LWP) ( $R^2=0.94$ ,  $p<0.01$ , slope=0.98), and d) fraction of mortality ( $R^2=0.99$ ,  $p<0.01$ , slope=1.04). Modeled values (red) are timeseries values with intervals of 1 hour. Observed values (blue) are point measurements. For VWC the interval is once per day. For other variables, the samples are taken throughout the experiment when destructive sampling occurred. Gray shaded areas represent the central 60% of the modeled distribution. In c) the green line shows the modeled percent loss of conductivity (PLC) values that result from the corresponding LWP values. The calibrated fits for the DSI calibration (panel d) were 0.26 PLC for the onset of stress ( $PLC_{init}$ ), 0.55 PLC for critical stress ( $PLC_{crit}$ ), and a resistance value ( $k$ ) of 0.17.

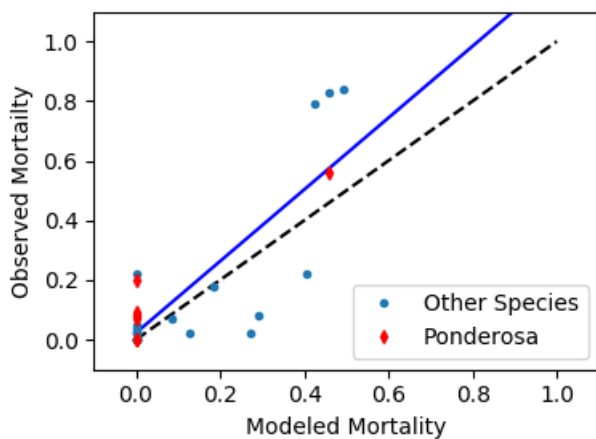


Figure 3: Modeled versus observed mortality for one-year-old bare-root seedlings from USFS stake row data.  $R^2 = 0.69$ . For the best fit line: slope= 1.20, intercept= 0.02.  $p < 0.01$ .  $n = 29$ . The dashed line represents the 1:1 line between both variables.

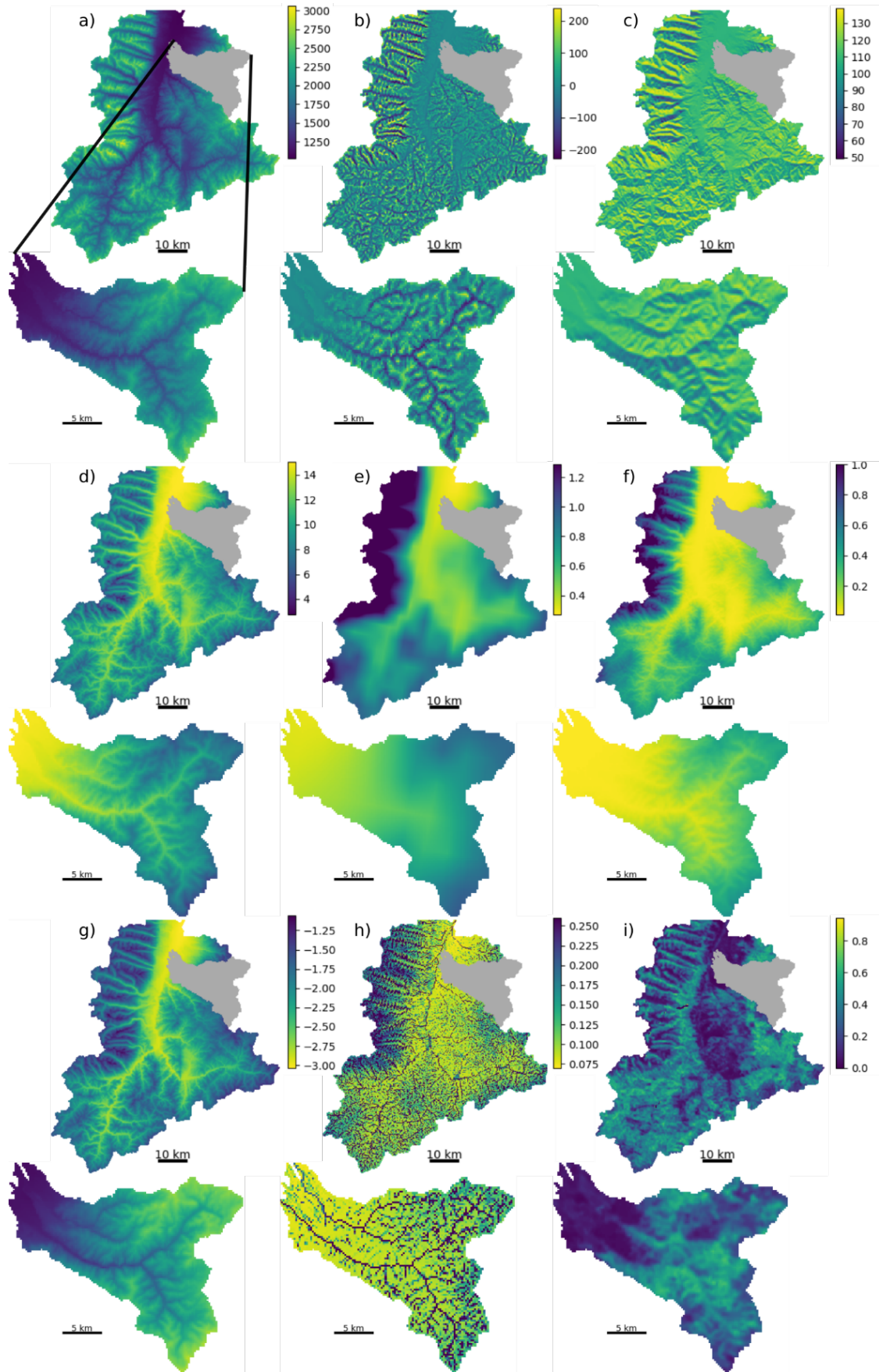


Figure 4: Maps of physical, climate, and ecohydrologic variables in the Bitterroot watershed and the Skalkaho Sub-basin: a) elevation in the watershed, b) topographic position index, c) mean solar radiation, d) mean maximum daily temperature ( $^{\circ}\text{C}$ ), e) total annual precipitation (m), f) peak annual snow water equivalent (m), g) summer mean maximum daily vapor pressure deficit (KPa), h) summer mean volumetric water content in the rooting zone, i) percent forest cover derived from MODIS. Panels f and h were simulated by Ech2o-SPAC.

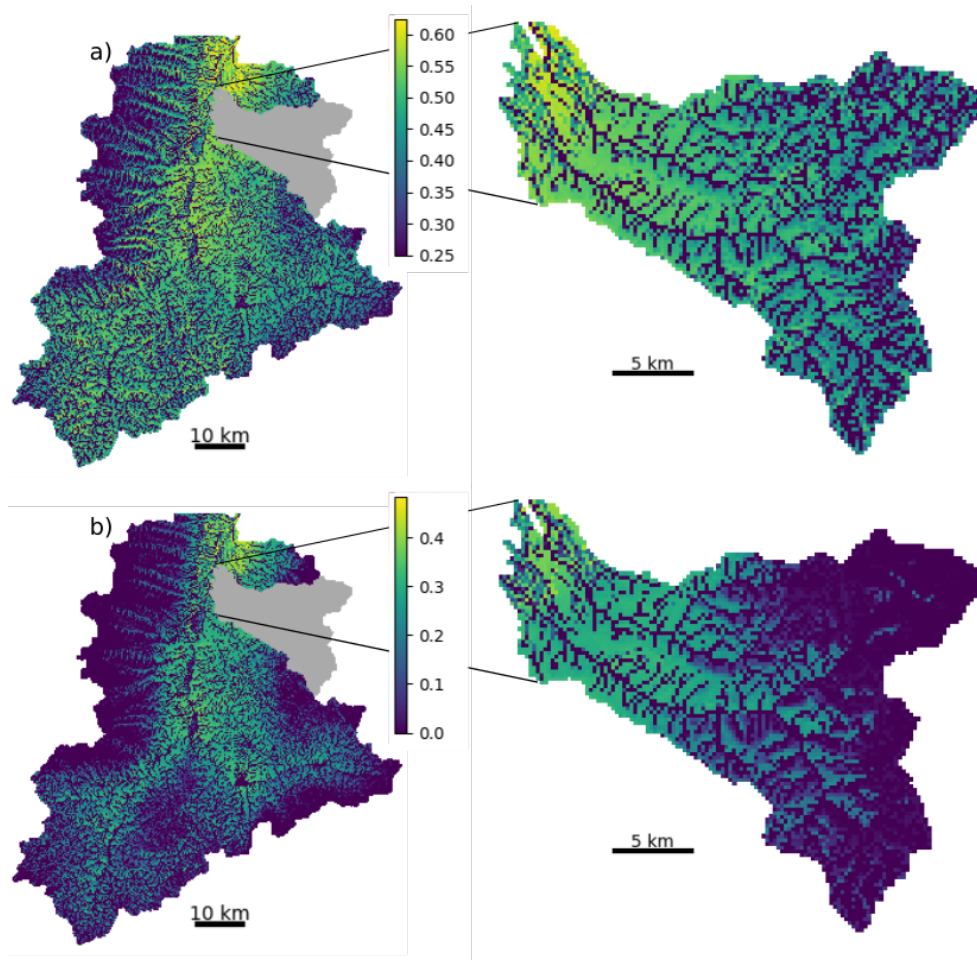


Figure 5: Dynamic stress index (DSI) for the Bitterroot watershed and the Skalkaho catchment. a) Mean DSI between 2001 and 2015. b) Minimum DSI from 2001 – 2015. Warm and cold colors represent higher and lower stresses respectively.

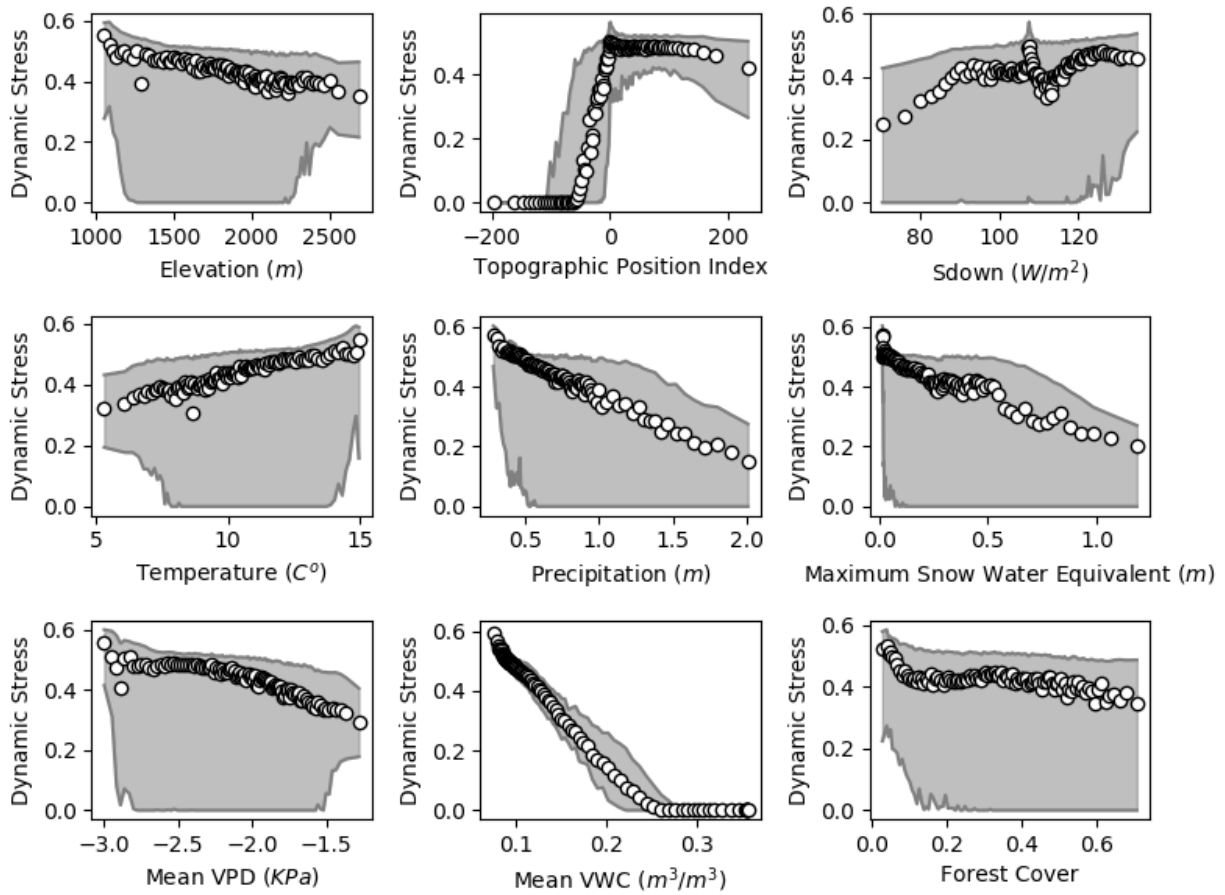


Figure 6: Relationships between dynamic stress index (DSI) and physical, climatic, and ecohydrologic variables. The points are the median DSI values and the envelope are the 10<sup>th</sup> and 90<sup>th</sup> percentile ranges for DSI split into 100 bins based on: a) elevation, b) topographic position index, c) mean solar radiation, d) mean maximum daily temperature (°C), e) total annual precipitation (m), f) peak annual snow water equivalent (m), g) summer mean maximum daily vapor pressure deficit (KPa), h) summer mean volumetric water content in the rooting zone, and i) percent forest cover derived from MODIS. VWC had the strongest correlation with seedling mortality.

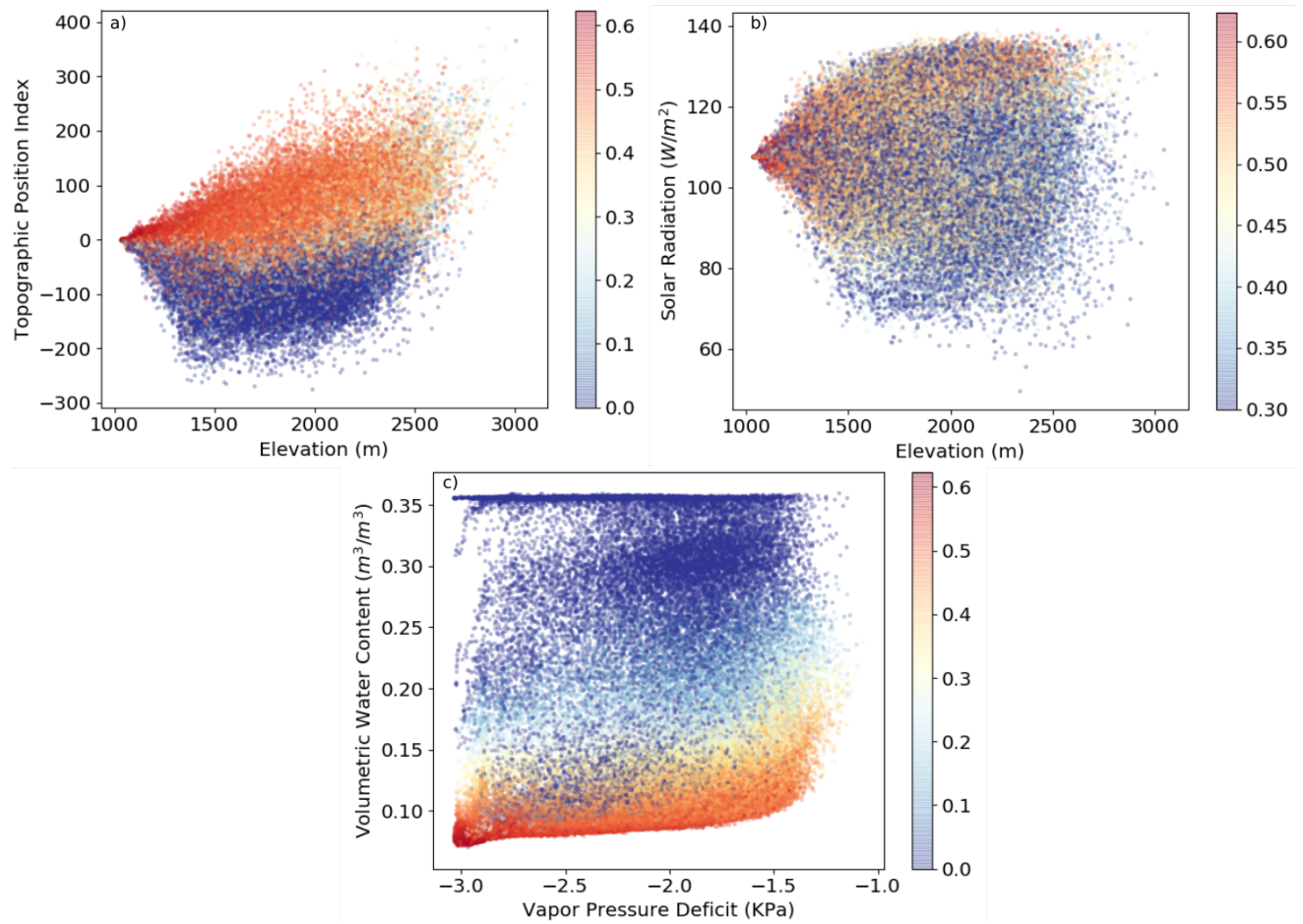


Figure 7: A, B) Scatter plots examining how elevation and either topographic position index (TPI) or solar radiation influence dynamic stress index (DSI). Color corresponds with the DSI value according with the color bar on the right side of each figure. For solar radiation this trend is only present at high DSI values (in this case the DSI color scale starts at 0.3). C) Scatter plot examining the combined influence of vapor pressure deficit and volumetric water content on DSI.

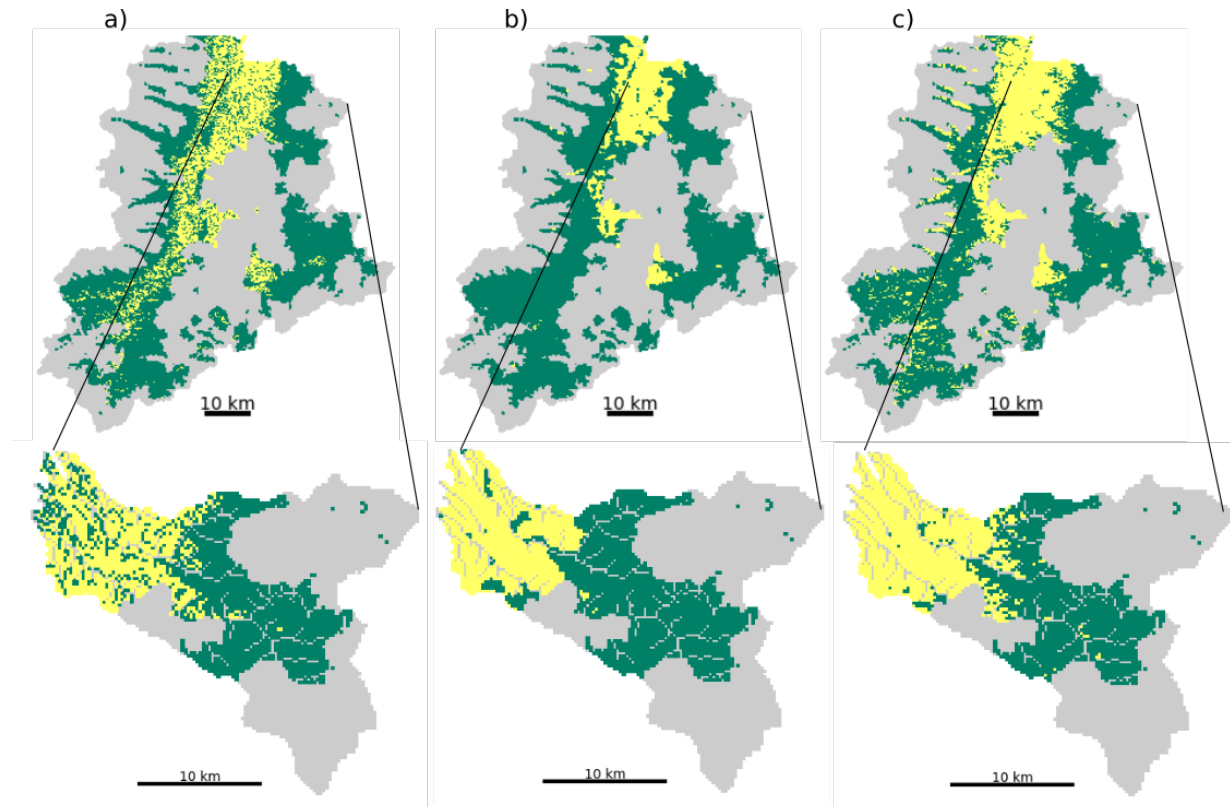


Figure 8: Maps of forest cover (green) and no forest cover (yellow) in the southern Bitterroot watershed (top) and the Skalkaho catchment (bottom). Gray areas represent streams, locations with less than 140 days of growing season (measured by soil temperature over 5 °C) to account for the upper treeline, and areas that have been disturbed by fire since 1984. A) Forest cover predicted from the minimum dynamic stress index (DSI) value at each pixel from 2001-2015. Minimum DSI predicted forest cover better than mean, maximum, Q25, median, or Q75 (As measured by Cohen's Kappa). Forest cover is predicted where minimum DSI is under 0.28. B) Actual forest cover from 2015 MODIS percent cover maps. Actual forest cover is mapped where cover is greater than 10%. Cohen's Kappa between A and B is 0.44 for the entire Bitterroot watershed and 0.62 for the Skalkaho. AUC is 0.79 for the Bitterroot and 0.80 for Skalkaho. C) 2015 Forest Cover measured by Landfire. Cohen's Kappa between A and C is 0.47 for the entire Bitterroot and 0.65 for the Skalkaho. AUC is 0.75 for the Bitterroot and 0.81 for Skalkaho. Cohen's Kappa between B and C, two independent remote sensed measures of forest cover was 0.60 for the entire Bitterroot and 0.79 for the Skalkaho.

## References

- Adams HD, Zeppel MJB, Anderegg WRL, Hartmann H, Landhäusser SM, Tissue DT, Huxman TE, Hudson PJ, Franz TE, Allen CD, et al. 2017. A multi-species synthesis of physiological mechanisms in drought-induced tree mortality. *Nature Ecology and Evolution* 1: 1285–1291.
- Alden, W.C., 1953, Physiography and glacial geology of western Montana and adjacent areas: U.S. Geological Survey Professional Paper 231, pp. 200.
- Allen CD, Breshears DD. 1998. Drought-induced shift of a forest-woodland ecotone: Rapid landscape response to climate variation. *Proceedings of the National Academy of Sciences* 95: 14839–

14842.

- Allen CD, Macalady AK, Chenchouni H, Bachelet D, McDowell N, Vennetier M, Kitzberger T, Rigling A, Breshears DD, Hogg EH., et al. 2010. A global overview of drought and heat-induced tree mortality reveals emerging climate change risks for forests. *Forest Ecology and Management* 259: 660–684.
- Allen CD, Breshears DD, McDowell NG. 2015. On underestimation of global vulnerability to tree mortality and forest die-off from hotter drought in the Anthropocene. *Ecosphere* 6: 292–297.
- Anderegg LDL, Anderegg WRL, Berry JA. 2013. Not all droughts are created equal: Translating meteorological drought into woody plant mortality. *Tree Physiology* 33: 701–712.
- Anderegg WRL, Berry JA, Field CB. 2012. Linking definitions, mechanisms, and modeling of drought-induced tree death. *Trends in Plant Science* 17: 693–700.
- Anderegg WRL, Plavcová L, Anderegg LDL, Hacke UG, Berry JA, Field CB. 2013. Drought's legacy: Multiyear hydraulic deterioration underlies widespread aspen forest die-off and portends increased future risk. *Global Change Biology* 19: 1188–1196.
- Anderegg WRL, Flint A, Huang CY, Flint L, Berry JA, Davis FW, Sperry JS, Field CB. 2015a. Tree mortality predicted from drought-induced vascular damage. *Nature Geoscience* 8: 367–371.
- Anderegg WRL, Schwalm C, Biondi F, Camarero JJ, Koch G, Litvak M, Ogle K, Shaw JD, Shevliakova E, Williams AP, et al. 2015b. Pervasive drought legacies in forest ecosystems and their implications for carbon cycle models. *Science* 349: 528–532.
- Anderegg WRL, Konings A, Trugman A, Pacala S, Yu K, Sulman B, Sperry J, Bowling D. 2017. Plant hydraulic diversity buffers forest ecosystem responses to drought. Abstract B44A-04 presented at 2017 Fall Meeting, AGU, New Orleans, LA., 11-15 Dec.
- Bailey JD, Harrington C. 2006. Temperature regulation of bud-burst phenology within and among years in a young Douglas-fir (*Pseudotsuga menziesii*) plantation in western Washington, USA. *Tree Physiology* 26: 421–430.
- Barton AM. 1993. Factors Controlling Plant Distributions: Drought, Competition, and Fire in Montane Pines in Arizona. *Ecological Monographs* 63: 367–397.
- Beedlow PA, Lee EH, Tingey DT, Waschmann RS, Burdick CA. 2013. The importance of seasonal temperature and moisture patterns on growth of Douglas-fir in western Oregon, USA. *Agricultural and Forest Meteorology* 169: 174–185.
- Bell DM, Bradford JB, Lauenroth WK. 2014. Early indicators of change: Divergent climate envelopes between tree life stages imply range shifts in the western United States. *Global Ecology and Biogeography* 23: 168–180.
- Camarero J, Gazol A, Sangüesa-Barreda G, Cantero A, Sánchez-Salguero R, Sánchez-Miranda A, Granda E, Serra-Maluquer X, Ibáñez R. 2018. Forest Growth Responses to Drought at Short- and Long-Term Scales in Spain: Squeezing the Stress Memory from Tree Rings. *Frontiers in Ecology and Evolution* 6: 1–11.
- Choat B, Jansen S, Brodribb TJ, Cochard H, Delzon S, Bhaskar R, Bucci SJ, Feild TS, Gleason SM, Hacke UG, et al. 2012. Global convergence in the vulnerability of forests to drought. *Nature* 491: 752–755.
- Christensen JH, Hewitson, B., Busuioc, A., Chen, A., Gao, X., Held, R., Jones, R., Kolli, R. K., Kwon, W. K., Laprise, R. et al. 2007. Regional Climate Projections. *Climate Change: The Physical*

- Science Basis 27: 847–940.
- Cohen J. 1960. A Coefficient of agreement for nominal scales. *Educational and Psychological Measurement* 20: 37–46.
- Coops NC, Waring RH, Law BE. 2005. Assessing the past and future distribution and productivity of ponderosa pine in the Pacific Northwest using a process model, 3-PG. *Ecological Modelling* 183: 107–124.
- Crimmins SM, Dobrowski SZ, Greenberg JA, Abatzoglou JT, Mynsberge AR. 2011. Changes in Climatic Water Balance Drive Downhill Shifts in Plant Species' Optimal Elevations. *Science* 331.
- Daly C, Halbleib M, Smith J, Gibson W, Doggett M, Taylor G, Curtis J, Pasteris P. 2008. Physiographically sensitive mapping of climatological temperature and precipitation across conterminous United States. *International Journal of Climatology*.
- DiMiceli, C.M., M.L. Carroll, R.A. Sohlberg, C. Huang, M.C. Hansen, and J.R.G. Townshend (2011), Annual Global Automated MODIS Vegetation Continuous Fields (MOD44B) at 250 m Spatial Resolution for Data Years Beginning Day 65, 2000 - 2010, Collection 5 Percent Tree Cover, University of Maryland, College Park, MD, USA.
- Dobrowski SZ. 2011. A climatic basis for microrefugia: The influence of terrain on climate. *Global Change Biology* 17: 1022–1035.
- Dobrowski SZ, Swanson AK, Abatzoglou JT, Holden ZA, Safford HD, Schwartz MK, Gavin DG. 2015. Forest structure and species traits mediate projected recruitment declines in western US tree species. *Global Ecology and Biogeography* 24: 917–927.
- Dorman M, Svoray T, Perevolotsky A, Sarris D. 2013. Forest performance during two consecutive drought periods: Diverging long-term trends and short-term responses along a climatic gradient. *Forest Ecology and Management*.
- Frey BR, Lieffers VJ, Hogg EHT, Landhäusser SM. 2004. Predicting landscape patterns of aspen dieback: mechanisms and knowledge gaps. *1390: 1379–1390*.
- Hacke UG, Stiller V, Sperry JS, Pittermann J, McCulloh KA. 2001. Xylem Linked references are available on JSTOR for this article: Cavitation Fatigue, Embolism and Refilling Cycles Can Weaken the Cavitation Resistance of Xylem. *Plant Physiology* 125: 779–786.
- Hanley AJ, McNeil JB. 1982. The Meaning and Use of the Area under a Receiver Operating Characteristic (ROC) Curve. *Radiology* 143: 29–36.
- Harcombe P. 1987. Tree Life Tables. *BioScience* 37: 557–568.
- Hartmann H, Adams HD, Anderegg WRL, Jansen S, Zeppel MJB. 2015. Research frontiers in drought-induced tree mortality: Crossing scales and disciplines. *New Phytologist* 205: 965–969.
- Hawthorne S, Miniati CF. 2018. Topography may mitigate drought effects on vegetation along a hillslope gradient. *Ecohydrology* 11.
- Holden ZA, Swanson A, Klene AE, Abatzoglou JT, Dobrowski SZ, Cushman SA, Squires J, Moisen GG, Oyler JW. 2016. Development of high-resolution (250 m) historical daily gridded air temperature data using reanalysis and distributed sensor networks for the US Northern Rocky Mountains. *International Journal of Climatology* 36: 3620–3632.
- Holden Z. Unpublished.
- Hubbard RM, Ryan MG, Stiller V, Sperry JS. 2001. Stomatal conductance and photosynthesis vary

- linearly with plant hydraulic conductance in ponderosa pine. *Plant, Cell and Environment* 24: 113–121.
- IPCC, 2014: Climate Change 2014: Synthesis Report. Contribution of Working Groups I, II and III to the Fifth Assessment Report of the Intergovernmental Panel on Climate Change [Core Writing Team, R.K. Pachauri and L.A. Meyer (eds.)]. IPCC, Geneva, Switzer.
- Jackson G, Grace J. 1994. Cavitation and water transport in trees. *Endeavour* 18: 50–54.
- Jiang X, Rauscher SA, Ringler TD, Lawrence DM, Park Williams A, Allen CD, Steiner AL, Michael Cai D, McDowell NG. 2013. Projected future changes in vegetation in western north America in the twenty-first century. *Journal of Climate* 26: 3671–3687.
- Johnson DM, Mcculloh KA, Reinhardt K. 2011. The Earliest Stages of Tree Growth: Development, Physiology and Impacts of Microclimate. In: *Size- and Age-Related Changes in Tree Structure and Function*. Springer, 65–90.
- Kroiss S, HilleRisLambers J. 2015. Recruitment limitation of long-lived conifers: implications for climate change responses. *Ecological Society of America* 96: 1286–1297.
- Kueppers LM, Conlisk E, Castanha C, Andrew B. 2017. Warming and provenance limit tree recruitment across and beyond the elevation range of subalpine forest. *Global Change Biology*: 2383–2395.
- Kuppel S, Tetzlaff D, Maneta MP, Soulsby C. 2018. What can we learn from multi-data calibration of a process-based ecohydrological model? *Environmental Modelling and Software* 101: 301–316.
- LANDFIRE, 2008, Existing canopy height layer, LANDFIRE 1.1.0, U.S. Department of the Interior, Geological Survey. <http://landfire.cr.usgs.gov/viewer/>.
- Landguth EL, Holden ZA, Mahalovich MF, Cushman SA. 2017. Using landscape genetics simulations for planting blister rust resistant whitebark pine in the US Northern Rocky Mountains. *Frontiers in Genetics* 8: 1–12.
- League K, Veblen T. 2006. Climatic variability and episodic *Pinus ponderosa* establishment along the forest-grassland ecotones of Colorado. 228: 98–107.
- Lozano-Parra J, Maneta MP, Schnabel S. 2014. Climate and topographic controls on simulated pasture production in a semiarid Mediterranean watershed with scattered tree cover. *Hydrology and Earth System Sciences* 18: 1439–1456.
- Mackay DS, Ahl DE, Ewers BE, Samanta S, Gower ST, Burrows SN. 2003. Physiological tradeoffs in the parameterization of a model of canopy transpiration. *Advances in Water Resources* 26: 179–194.
- Maneta MP, Silverman NL, Maneta MP, Silverman NL. 2013. A Spatially Distributed Model to Simulate Water, Energy, and Vegetation Dynamics Using Information from Regional Climate Models. *Earth Interactions* 17: 1–44.
- Martínez-Vilalta J, García-Forner N. 2017. Water potential regulation, stomatal behavior and hydraulic transport under drought: deconstructing the iso/anisohydric concept. *Plant Cell and Environment* 40: 962–976.
- Martínez-Vilalta et al. Unpublished
- McDowell N, Pockman WT, Allen CD, Breshears DD, Cobb N, Kolb T, Plaut J, Sperry J, West A, Williams DG, et al. 2008. Mechanisms of plant survival and mortality during drought: Why do some plants survive while others succumb to drought? *New Phytologist* 178: 719–739.
- McDowell NG. 2011. Mechanisms Linking Drought, Hydraulics, Carbon Metabolism, and Vegetation

- Mortality. *PLANT PHYSIOLOGY* 155: 1051–1059.
- McDowell NG, Fisher RA, Xu C, Domec JC, Hölttä T, Mackay DS, Sperry JS, Boutz A, Dickman L, Gehres N, et al. 2013. Evaluating theories of drought-induced vegetation mortality using a multimodel-experiment framework. *New Phytologist* 200: 304–321.
- McDowell NG, Williams AP, Xu C, Pockman WT, Dickman LT, Sevanto S, Pangle R, Limousin J, Plaut J, Mackay DS, et al. 2016. Multi-scale predictions of massive conifer mortality due to chronic temperature rise. *Nature Climate Change* 6: 295–300.
- McLaughlin BC, Ackerly DD, Klos PZ, Natali J. 2017. Hydrologic refugia, plants, and climate change. : 2941–2961.
- Mesinger F, DiMego G, Kalnay E, Mitchell K, Shafran PC, Ebisuzaki W, Jović D, Woollen J, Rogers E, Berbery EH, et al. 2006. North American regional reanalysis. *Bulletin of the American Meteorological Society* 87: 343–360.
- Mitchell PJ, O’Grady AP, Tissue DT, White DA, Ottenschlaeger ML, Pinkard EA. 2013. Drought response strategies define the relative contributions of hydraulic dysfunction and carbohydrate depletion during tree mortality. *New Phytologist* 197: 862–872.
- Ogée J, Brunet Y, Loustau D, Berbigier P, Delzon S. 2003. MuSICA, a CO<sub>2</sub>, water and energy multilayer, multileaf pine forest model: Evaluation from hourly to yearly time scales and sensitivity analysis. *Global Change Biology* 9: 697–717.
- Parmesan C, Yohe G. 2003. A globally coherent fingerprint of climate change impacts across natural systems. *Nature* 421: 37–42.
- Petrie MD, Wildeman AM, Bradford JB, Hubbard RM, Lauenroth WK. 2016. A review of precipitation and temperature control on seedling emergence and establishment for ponderosa and lodgepole pine forest regeneration. *Forest Ecology and Management* 361: 328–338.
- Petrie MD, Bradford JB, Hubbard RM, Lauenroth WK, Andrews CM, Schlaepfer DR. 2017. Climate change may restrict dryland forest regeneration in the 21st century. *Ecology* 98: 1548–1559.
- Porporato A, Laio F, Ridolfi L, Rodriguez-Iturbe I. 2001. Plants in water-controlled ecosystems: active role in hydrologic processes and response to water stress III. *Vegetation water stress. Advances in Water Resources* 24: 707–723.
- Potter KM, Hipkins VD, Mahalovich MF, Means RE. 2013. Mitochondrial DNA haplotype distribution patterns in *Pinus ponderosa* (Pinaceae): Range-wide evolutionary history and implications for conservation. *American Journal of Botany* 100: 1562–1579.
- Rehfeldt GE, Jaquish BC, Sáenz-Romero C, Joyce DG, Leites LP, Bradley St Clair J, López-Upton J. 2014. Comparative genetic responses to climate in the varieties of *Pinus ponderosa* and *Pseudotsuga menziesii*: Reforestation. *Forest Ecology and Management* 324: 147–157.
- Rollins, M.G., 2009. LANDFIRE: a nationally consistent vegetation, wildland fire, and fuel assessment. *Int. J. Wildland Fire* 18, 235–249. <http://dx.doi.org/10.1071/WF08088>.
- Rother MT, Veblen TT, Furman LG. 2015. A field experiment informs expected patterns of conifer regeneration after disturbance under changing climate conditions. *Canadian Journal of Forest Research* 45: 1607–1616.
- Savage M, Brown PM, Feddema J. 1996. The role of climate in a pine forest regeneration pulse in the southwestern United States. *Écoscience* 3: 310–318.

Sapes & Sala, Unpublished

- Sevanto S, McDowell NG, Dickman LT, Pangle R, Pockman WT. 2014. How do trees die? A test of the hydraulic failure and carbon starvation hypotheses. *Plant, Cell and Environment* 37: 153–161.
- Silverman NL, Maneta MP, Chen SH, Harper JT. 2013. Dynamically downscaled winter precipitation over complex terrain of the Central Rockies of Western Montana, USA. *Water Resources Research* 49: 458–470.
- Silverman NL, Maneta MP. 2016. Detectability of change in winter precipitation within mountain landscapes: Spatial patterns and uncertainty. *Water Resources Research* 52: 4301–4320.
- Smith WK, Germino MJ, Johnson DM, Reinhardt K. 2009. The altitude of alpine treeline: A bellwether of climate change effects. *Botanical Review* 75: 163–190.
- Sperry JS, Adler FR, Campbell GS, Comstock JP. 1998. Limitation of plant water use by rhizosphere and xylem conductance: Results from a model. *Plant, Cell and Environment* 21: 347–359.
- Tai X, Mackay DS, Anderegg WRL, Sperry JS, Brooks PD. 2017. Plant hydraulics improves and topography mediates prediction of aspen mortality in southwestern USA. *New Phytologist* 213: 113–127.
- Tyree MT, Sperry JS. 1988. Do Woody Plants Operate Near the Point of Catastrophic Xylem Dysfunction Caused by Dynamic Water Stress?: Answers from a Model. *PLANT PHYSIOLOGY* 88: 574–580.
- Tyree MT. 1997. The Cohesion-Tension theory of sap ascent: current controversies. *Journal of Experimental Botany* 48: 1753–1765.
- Van Mantgem PJ, Stephenson NL, Byrne JC, Daniels LD, Franklin JF, Fulé PZ, Harmon ME, Larson AJ, Smith JM, Taylor AH, et al. 2009. Widespread increase of tree mortality rates in the Western United States. *Science* 323: 521–524.
- Venturas MD, Sperry JS, Hacke UG. 2017. Plant xylem hydraulics: What we understand, current research, and future challenges. *Journal of Integrative Plant Biology* 59: 356–389.
- Vico G, Porporato A. 2009. Hydrologic controls on vegetation: From leaf to landscape. Ph.D.
- Walther GR, Post E, Convey P, Menzel A, Parmesan C, Beebee TJC, Fromentin JM, Hoegh-Guldberg O, Bairlein F. 2002. Ecological responses to recent climate change. *Nature* 416: 389–395.
- Weiss A. 2001. Topographic position and landforms analysis. Poster presentation, ESRI User Conference, San Diego, CA 64: 227–245.
- Weiss JL, Castro CL, Overpeck JT. 2009. Distinguishing pronounced droughts in the southwestern united states: Seasonality and effects of warmer temperatures. *Journal of Climate* 22: 5918–5932.
- Whitlock C, Cross W, Maxwell B, Silverman N, Wade A. 2017. 2017 Montana Climate Assessment Executive Summary. <http://montanaclimate.org/chapter/executive-summary>.
- Williams AP, Allen CD, Macalady AK, Griffin D, Woodhouse CA, Meko DM, Swetnam TW, Rauscher SA, Seager R, Grissino-Mayer HD, et al. 2013. Temperature as a potent driver of regional forest drought stress and tree mortality. *Nature Climate Change* 3: 292–297.
- Worrall JJ, Egeland L, Eager T, Mask RA, Johnson EW, Kemp PA, Shepperd WD. 2008. Rapid mortality of *Populus tremuloides* in southwestern Colorado, USA. *Forest Ecology and*

## Student Fellowship Project: Influence of wood on sediment storage in a low order stream in the northern Rocky Mountains

### Basic Information

<b>Title:</b>	Student Fellowship Project: Influence of wood on sediment storage in a low order stream in the northern Rocky Mountains
<b>Project Number:</b>	2017MT319B
<b>Start Date:</b>	3/1/2017
<b>End Date:</b>	2/28/2018
<b>Funding Source:</b>	104B
<b>Congressional District:</b>	1
<b>Research Category:</b>	Climate and Hydrologic Processes
<b>Focus Categories:</b>	Sediments, None, None
<b>Descriptors:</b>	None
<b>Principal Investigators:</b>	Robin Welling

### Publications

There are no publications.

Robin Welling  
2017 Montana Water Center Student Fellow  
May 8, 2018

## Project Report

### **1. Introduction**

Sediment connectivity, or the set of processes by which sediment is transported from its source to the outlet of a basin, varies through space and time. It includes lateral, vertical, and longitudinal linkages, and the relative strength of these depends on the spatial and temporal scales at which they are considered (Fryirs, 2013). Several modeling approaches and metrics have been proposed to address the challenge of quantifying sediment connectivity (Wohl, 2017). For example, the sediment delivery ratio (SDR) relates downstream sediment output to input from basin erosion (Walling, 1983). The SDR declines with increasing basin size (Walling, 1983) and is thought to approach one in the long-term (Hoffmann, 2015). Over time scales up to hundreds of thousands of years, the SDR may be well above or below one, indicating that the basin is in disequilibrium with respect to production and transport of sediment (Hoffmann, 2015).

Sediment connectivity tends to be high in low-order mountain streams. Steep hillslopes and narrow valleys result in high lateral sediment connectivity (Montgomery and Buffington, 1997). Mountain streams effectively convey sediment downstream and thus also have strong longitudinal connectivity (Walling, 1983; Fryirs, 2013). Higher-order channels are sensitive to sediment input from low-order tributaries due to their lower transport capacity, resulting in sediment deposition and morphological changes at confluences (Benda and Dunne, 1997; Imhoff and Wilcox, 2016). The balance of sediment supply and transport capacity in alluvial streams controls channel morphology, which influences reservoir storage capacity, susceptibility to flooding, and aquatic habitat (Lane et al., 2008; Goode et al., 2012; Elosegi et al., 2017).

The size and residence time of sediment stores affect downstream sediment flux and mediate sediment connectivity in channel networks. Wood obstructions are the most common sites of sediment storage in some low-order streams, although sediment may also be present in bars and trapped behind boulders (Megahan, 1982; May and Gresswell, 2003; Fisher et al., 2010). The influence of wood on pool formation and other aspects of stream morphology and aquatic habitat is widely recognized (Bisson et al., 1987; Montgomery et al., 1995; Gurnell et al., 2002). Recent emphasis on river connectivity, or the ability of matter and organisms to move among spatially distinct units, highlights the broader importance of wood (Wohl, 2017). For example, wood and sediment in riverine corridors represent a sink within the global carbon cycle (Wohl et al., 2012; Wohl et al., 2017). Despite advances in understanding of the influence of instream wood on river connectivity in general, and sediment connectivity in particular (Wohl and Scott, 2016), key questions persist about the effect of instream wood on sediment routing through time and across different types of mountain streams.

### **2. Research Questions**

Channel-spanning log jams are particularly effective at storing sediment. Nevertheless, few reach-scale studies in forested mountain streams have considered the

relative magnitude of sediment stored by individual large wood pieces and jams of various size. Furthermore, most intensive studies of sediment stored in association with large wood have been conducted in gravel-bed streams in coastal environments, especially the Pacific Northwest. Compared to the Pacific Northwest, mountain streams in the interior west contain smaller and more mobile wood due to lower forest stand density and average tree diameter, and long-duration, snowmelt-driven peak streamflows (Wohl and Jaeger, 2009). I am considering the role of large wood on sediment routing in a mixed bedrock-alluvial stream in a semi-arid landscape. My research addresses the following questions and hypotheses:

Q1: How does the distribution of large wood in a mixed bedrock-alluvial stream impact sediment storage?

H1: Large wood stores more sediment per unit wood volume where it forms channel-spanning jams compared with small jams and individual pieces, which produce less form drag than jams and thus have lower sediment-storage potential.

Q2: How does large wood affect sediment residence time?

H2: The residence time of coarse and fine sediment stored in association with instream wood is greater than for sediment that is not wood-influenced.

### **3. Methods**

I am addressing my study questions and hypotheses using a combination of field surveys, remote sensing, and modeling applied to Lost Horse Creek, an intermediate-sized stream in the Bitterroot Mountains (Figure 1). The volume of wood and associated sediment was determined through a field survey. I am using bed material tracers and fallout radionuclide analysis to estimate the residence time of sediment stored by wood. To provide context for field data, I will use measurements of channel geometry, discharge, and bed material to model hydraulics and sediment transport. Finally, I will calibrate an amended version of a stochastic model of instream wood and sediment storage. By comparing model predictions to my field measurements, I can assess whether this model captures key processes driving wood and sediment load.

#### **3.1 Study Site**

The Bitterroots are part of the northern Rocky Mountains, which lie in the continental climate transition zone between the Pacific Northwest and eastern Rocky Mountains (Brunelle et al., 2005). The range is oriented north-to-south and consists of a series of west-to-east trending canyons, which were occupied by valley glaciers during multiple Pleistocene glaciations (Alden, 1953). The Bitterroot's bedrock dominance and coarse valley fill are consistent with other post-glacial landscapes (Hoffmann, 2015). Where soil-mantled hillslopes occur, they support mixed coniferous forests dominated by Douglas fir (*Pseudotsuga menziesii*), ponderosa pine (*Pinus ponderosa*), and Engelmann spruce (*Picea engelmannii*). Most precipitation falls as snow, and summer drought and convective storms can trigger fires (Brunelle et al., 2005). Streams on the eastern side of the Bitterroot Mountains flow into the Bitterroot River, which is in the headwaters of the Columbia River Basin.

My study site is a 750 m, third-order reach with an elevation of about 1650 m and drainage area of 37 km<sup>2</sup> (Figure 2). Forest density and extent are greatest in the valley bottom. Hillslope cover includes sparse montane and sub-alpine forests, talus slopes, boulder fields, and exposed bedrock. Average annual precipitation ranges from 1130 mm to 2300 mm (PRISM, 2018). Data from the nearby Twelvemile Creek snow telemetry (SNOTEL) site (elevation 1707 m) indicate that precipitation is greatest from November to January, and July to September are the driest months. Lost Horse Creek is ungaged but has a snowmelt-driven flow regime, with peak flows occurring in May and June and reaching baseflow by September. The upper 370 m of the study reach is predominantly alluvial, and it transitions from a riffle-pool to a plane-bed channel type. Below this, it is a mixed bedrock-alluvial stream with cascade and step-pool channels. The full reach contains individual pieces of wood, dozens of small jams, and two channel-spanning jams.

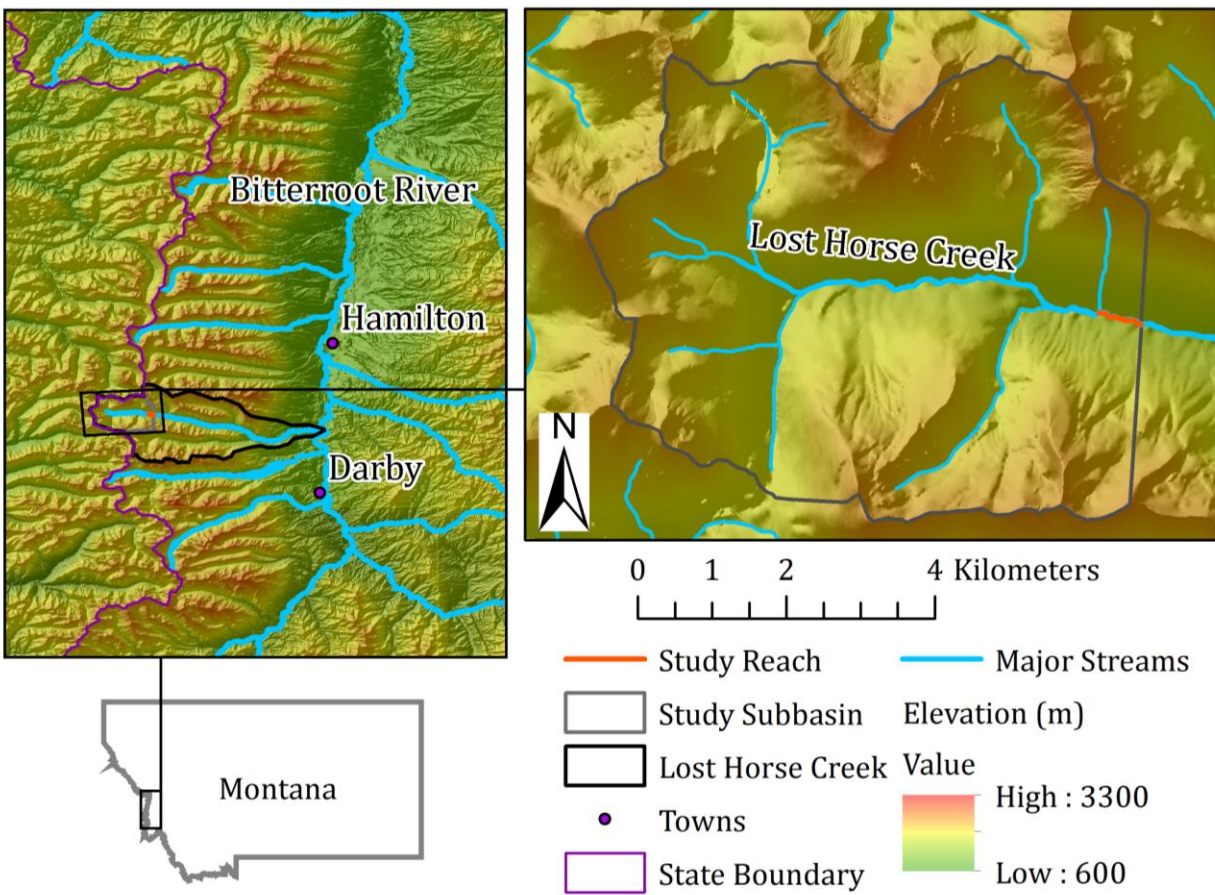


**Figure 1:** Study site on Lost Horse Creek in the Bitterroot Mountains, southwestern MT.

### 3.2 Remote Sensing

I am using aerial photographs, a drone survey, and an airborne LiDAR survey to characterize instream wood and channel morphology in my study reach. Within Google Earth, I inspected air photos from July 2013 and September 2016 to evaluate the persistence of individual logs and jams. The National Center for Landscape Fire Analysis

(Fire Center) at the University of Montana completed a drone survey of a 1km segment of Lost Horse Creek, including my study reach, in November 2016. I am using the resulting orthomosaic to construct a geomorphic map of the reach following guidance in Wheaton et al. (2015). I am incorporating field measurements of sediment stored in association with wood to illustrate how these stores relate to general patterns of erosion and deposition within the reach.

To understand valley constraints on channel form and process, I am using a bare earth DEM from an airborne LiDAR survey completed in September 2016 (NCALM, 2016). I extracted a longitudinal profile of my study reach from the resulting bare earth DEM, to which I am comparing field and drone-surveyed profiles. To identify and determine the degree to which side channels are connected with the main channel, I obtained multiple floodplain cross sections and am comparing the elevations of side channels with the main channel. Lastly, I am investigating the shape of the long profile in the context of valley and hillslope topography and the influence of landscape forcings including glaciation and tectonics.

### 3.3 Fieldwork

To understand how large wood and sediment relate to channel morphology and hydraulics, I conducted a field survey of Lost Horse Creek during summer 2017. To precisely distinguish between and characterize the alluvial and mixed bedrock-alluvial subreaches, I surveyed the channel dimensions, slope, and size of bed material throughout my study reach. I used a Leica TS06 Total Station to survey a longitudinal profile along the thalweg. From this, the two channel types can be distinguished based on slope and bedform. To determine channel width and depth, I surveyed 11 equally spaced cross sections. The surface grain size was characterized by modified Wolman pebble counts. At every other cross section, I measured the median diameter of 200 particles using a gravelometer. Because Lost Horse Creek is ungaged, I am using a combination of field measurements, analysis of nearby gage data, and USGS regression relations (StreamStats, 2017) to estimate flow magnitudes and frequencies.

To determine how large wood load and distribution relates to channel type, I measured and characterized instream wood. I surveyed large wood that extended at least 1 m into the bankfull channel and had a diameter greater than or equal to 0.1 m. I measured the length and mid-length diameter of each piece of wood with a tape and a tree caliper, respectively. From these measurements, I calculated the volume of each piece by treating each log as a cylinder. I classified each piece as single or part of a jam (three or more pieces of wood that are in contact). I estimated the total volume of each jam from the sum of individual piece volumes. Where it was impractical to survey individual pieces within a jam, I used the porosity method to estimate the total volume (Livers et al., 2015).

I am quantifying sediment in wood-forced riffles, bars, and pools within the active channel. I surveyed sediment in riffles and bars with a surface area  $> 1 \text{ m}^2$  during summer 2017. To estimate the volume of coarse bed material stored by log bed-steps and jams, I treated each sediment deposit as a wedge defined by breaks in channel gradient and bed material size. I calculated the volume of each bar from the surface area and average height. The volume of fine bed material stored in each pool will be determined by probing

sediment depth in a gridded pattern (Lisle and Hilton 1992); these surveys are planned for summer 2018.

To compare the geomorphic influence of individual pieces, small jams, and channel-spanning jams, I relate the average volume of each type of wood-forced sediment store to the average volume of corresponding wood. Specifically, I will divide the volume of sediment by the volume of wood for each feature, calculate the average sediment to wood volume for each type of wood-forced sediment store, and compare the results using analysis of variance. I will also address my first research question at the reach scale by comparing the total volume of sediment to the cumulative volume of wood in individual pieces, small jams, and channel-spanning jams. Pfeiffer and Wohl (2017) refer to this metric as the large wood particulate storage index (LWPSI).

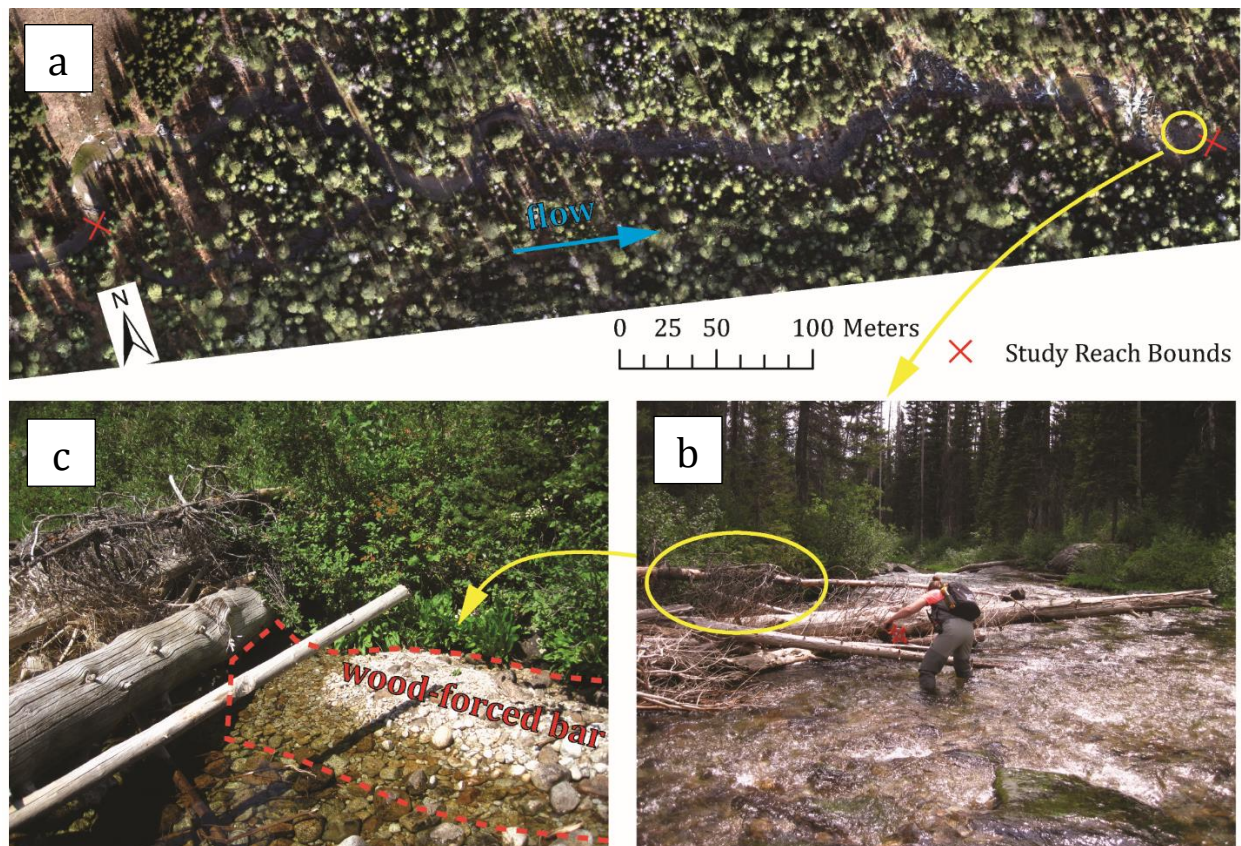


**Figure 2:** Field site on Lost Horse Creek, where channel dimensions, bed material size, and distribution of wood and wood-forced sediment were surveyed in 2017. Orthomosaic of study reach from drone-based aerial imagery (a). Measurement of first large wood jam (b) and associated bar (c).

To assess the influence of large wood on the transport of coarse bed material, I am monitoring the movement of painted tracers through a wood jam. In late fall 2017, I seeded 90 painted and numbered tracers, with sizes within the D16 and D84 of the mobile fraction of the bed material, in three transects. One transect was within 10 m of the downstream end of the jam, the second was within the measured sediment deposit, and the third was about 10 m upstream of the upper edge of the deposit. During baseflow in summer 2018, I will survey the position of all recovered tracers. Particle mobility will be analyzed using

generalized linear regression of recovery rate and normalized transport distance as function of initial position with respect to the jam. I will calculate the magnitude and duration of competent flows for context. Finally, residence time can be inferred by relating particle mobilization to the estimated recurrence interval of peak flows.

I will gain insight into the residence time of fine sediment by fallout radionuclide analysis (See also Appendix A1). I will compare activities of the radionuclides  $^7\text{Be}$  ( $t_{1/2} = 53.4$  days),  $^{210}\text{Pb}$  ( $t_{1/2} = 20.4$  years), and  $^{137}\text{Cs}$  ( $t_{1/2} = 30.1$  years) in sediment stored in association with large wood to potential upstream sources. In fall 2017, I collected the following test samples: two samples within a channel-spanning jam, one from an emergent bar 15 m upstream, and one from each of two submerged bars 70 m and 130 m upstream. I used a large shovel to collect similar-sized samples to a depth of 10 cm. During summer 2018, I will collect additional samples at these locations after snowmelt-driven peak streamflow, a period of several weeks without rain, and after a recent storm event. I will use the normalized  $^7\text{Be}$  activity of each sample to calibrate a constant initial activity model, to which subsequent sample activities can be compared. When combined with stage records, the predicted and observed radionuclide activities can provide information about transport dynamics and associated residence time.

### 3.4 Modeling

To complement my field data, I will model hydraulics and sediment transport. I will run the one-dimensional (1D) HEC-RAS (Hydrologic Engineering Center's River Analysis System) model to identify the degree to which side channels adjacent to the alluvial subreach are hydrologically connected to the main channel. Combined with measurements of wood and sediment within a representative side channel, I can then evaluate the extent to which channel-spanning jams contribute to multi-thread channels and enhanced storage of wood and sediment.

To estimate sediment transport rates and annual sediment export, I will use Bedload Assessment for Gravel-bed Streams or BAGS. I will provide the reach-average channel dimensions, the friction slope calculated in HEC-RAS, bed material size distribution, and minimum and maximum recorded discharges to develop a sediment rating curve. When combined with measurements of discharge, I can use this rating curve to estimate annual sediment output during the 2017 and 2018 periods of record. This will enable me to relate the total volume of sediment stored by wood to sediment transport.

I will use my field data to test the generality of a stochastic model of wood loading and sediment storage, the reach-scale channel simulator (RSCS) (Eaton et al., 2012). The RSCS models wood input, modification, transport, and interaction to predict wood and sediment storage (Figure 3). It has a time step of one year, and each year it records the total volume of functional wood in the reach, the volume of sediment stored by this wood, the number of wood jams, the volume of wood and sediment associated with jams, and the age and sediment released by any jams that failed. It was calibrated using data from Fishtrap Creek, a gravel-bed river in coastal British Columbia (Eaton et al., 2012). While the channel dimensions, slope, and discharge of Fishtrap Creek are similar to those of Lost Horse Creek, the average diameter of instream wood is about double that of Lost Horse, and boulders and bedrock do not constitute a significant component of the bed (Eaton et al., 2012).

I will calibrate the RSCS using aerial and field measurements of the channel and

floodplain of Lost Horse Creek. I will complete 100 model runs for the mean length of time necessary to achieve a steady state. My measurements of wood and sediment can then be compared to model results to assess whether the RSCS captures key processes controlling the interaction between instream wood and sediment.

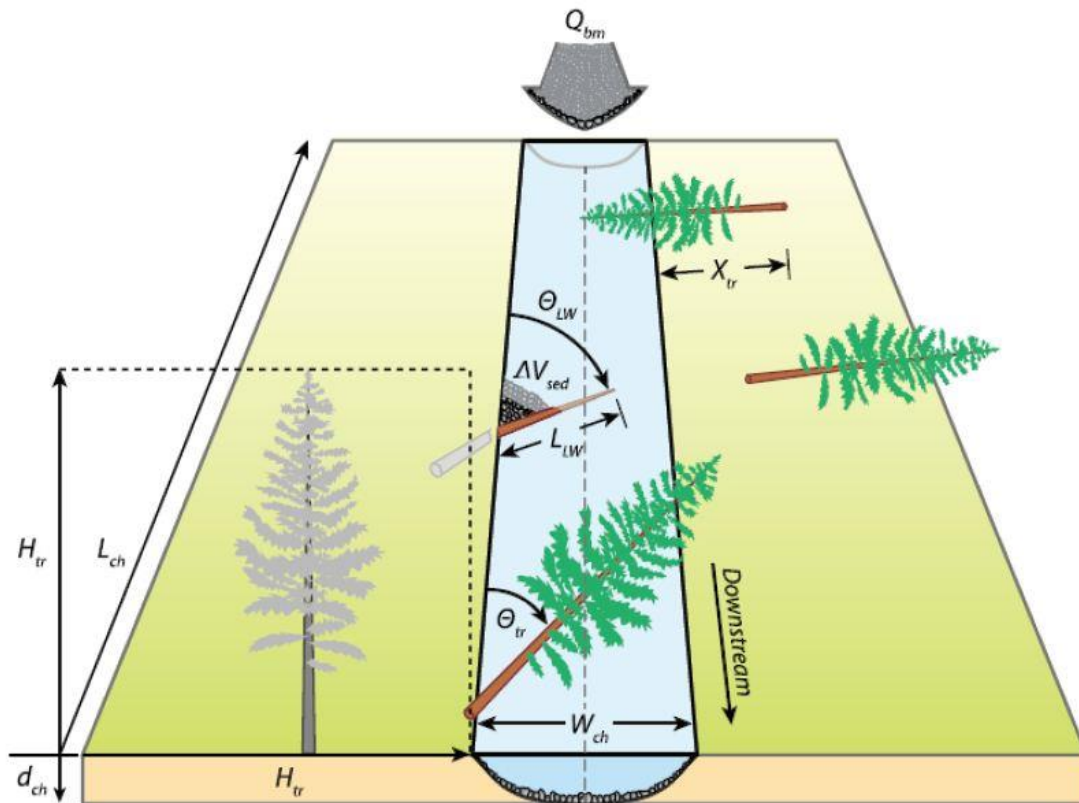


**Figure 3:** Schematic of Reach Scale Channel Simulator (RSCS). Model determines volume of instream wood and sediment within a reach of length  $L_{ch}$ , bankfull width  $W_{ch}$ , bankfull depth  $d_{ch}$ , and sediment transport,  $Q_{bm}$ . The length of newly recruited instream wood,  $L_{LW}$ , depends on tree height,  $H_{tr}$ , its distance from the channel,  $X_{tr}$ , and its fall direction,  $\theta_{tr}$ . Piece dimensions and orientation to the flow,  $\theta_{LW}$ , dictate how much sediment it stores,  $\Delta V_{sed}$ . Figure from Eaton et al. (2012).

## **4. Preliminary Results and Discussion**

### **4.1 Long Profile Shape**

The longitudinal profile of the thalweg displays a major change in slope (Figure 4). The upper portion, which corresponds with the alluvial subreach, has a significantly smaller average slope than does the lower mixed bedrock-alluvial subreach.

Both the LiDAR-derived and field-based longitudinal profiles of the water surface and streambed, respectively, are convex (Figure 6, Figure A1). Under steady state conditions, the balance of uplift and erosion typically produces concave up stream profiles (Burbank and Anderson, 2012). Lithologic changes, faulting, joint spacing differences,

sediment influx from hillslope erosion, bedload cover variation, and human factors including dams can result in convexities that range from  $10^0$  to  $10^3$  m in length (Phillips and Lutz, 2008). The downstream portion that gives the longitudinal profile of my study reach its convex shape is dominated by boulders with only occasional bedrock exposures. Because uplift rates are likely low and the lithology of Lost Horse Creek is relatively uniform (Foster et al., 2008; Lonn and Berg, 1996), I considered how various geomorphic processes related to Pleistocene glaciation might account for the observed profile convexity. Given the upstream location of my study reach, neither glacial deposition nor base level change caused by Glacial Lake Missoula are reasonable explanations (Alden, 1953; Pardee, 1910). Therefore, variable hillslope erosion through rock fall and talus slope production likely result in profile convexity, consistent with previous observations by UM Geosciences graduate students.

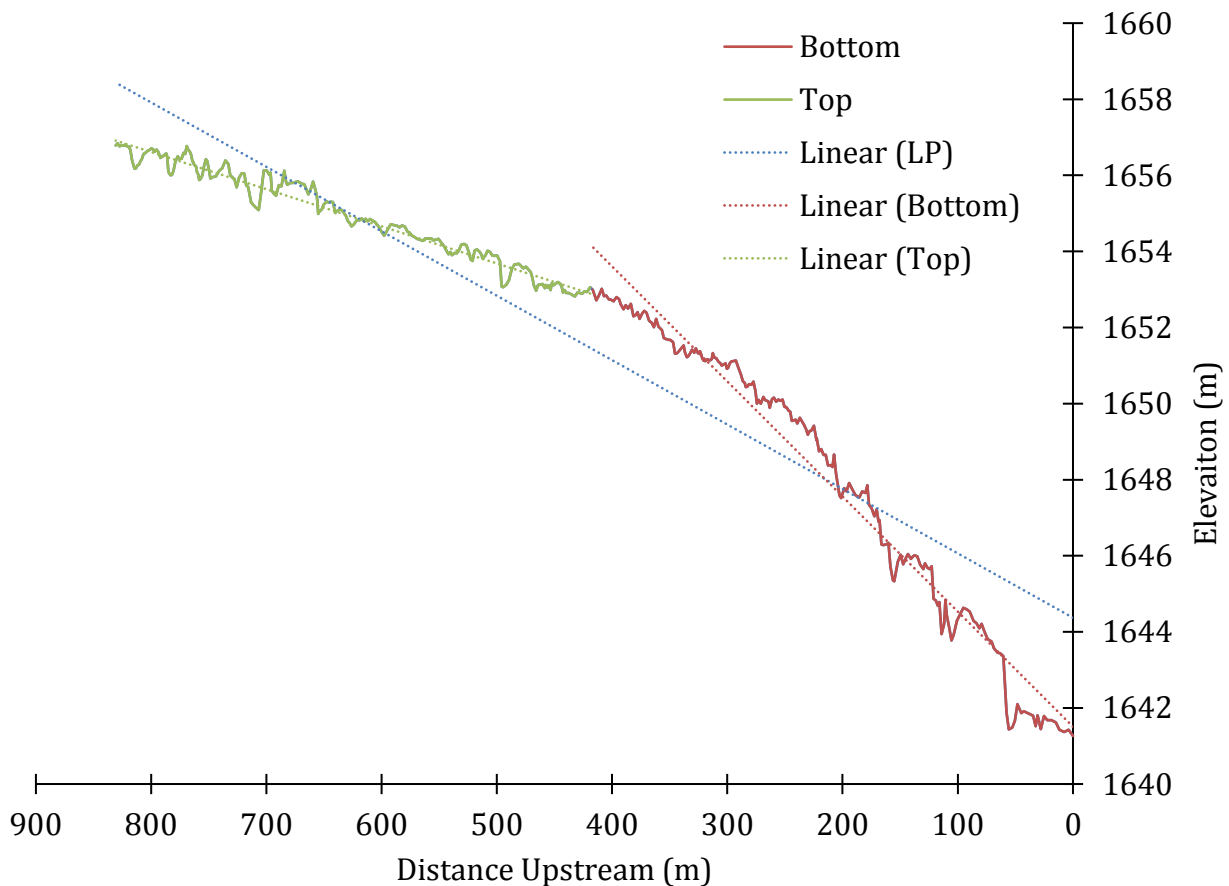


**Figure 4:** Longitudinal profile of the thalweg. The equation of the line of best fit for my entire study reach has a slope of 0.017 and a  $R^2$  of 0.90. The reach was manually split based on shape of the profile (convexities, spikes), and verified by comparison with my field-based determination of channel type. The upper subreach has a slope of 0.010 and a  $R^2$  of 0.97 and the lower subreach has a slope of 0.030 with an  $R^2$  of 0.97.

## 4.2 Bed Material Size

Bed material size increases from the upstream to the downstream end of my study reach (Figure 5). The size distribution also becomes more right-skewed. This reflects the presence of immobile boulders and bedrock, which are more prevalent within the mixed bedrock-alluvial subreach.

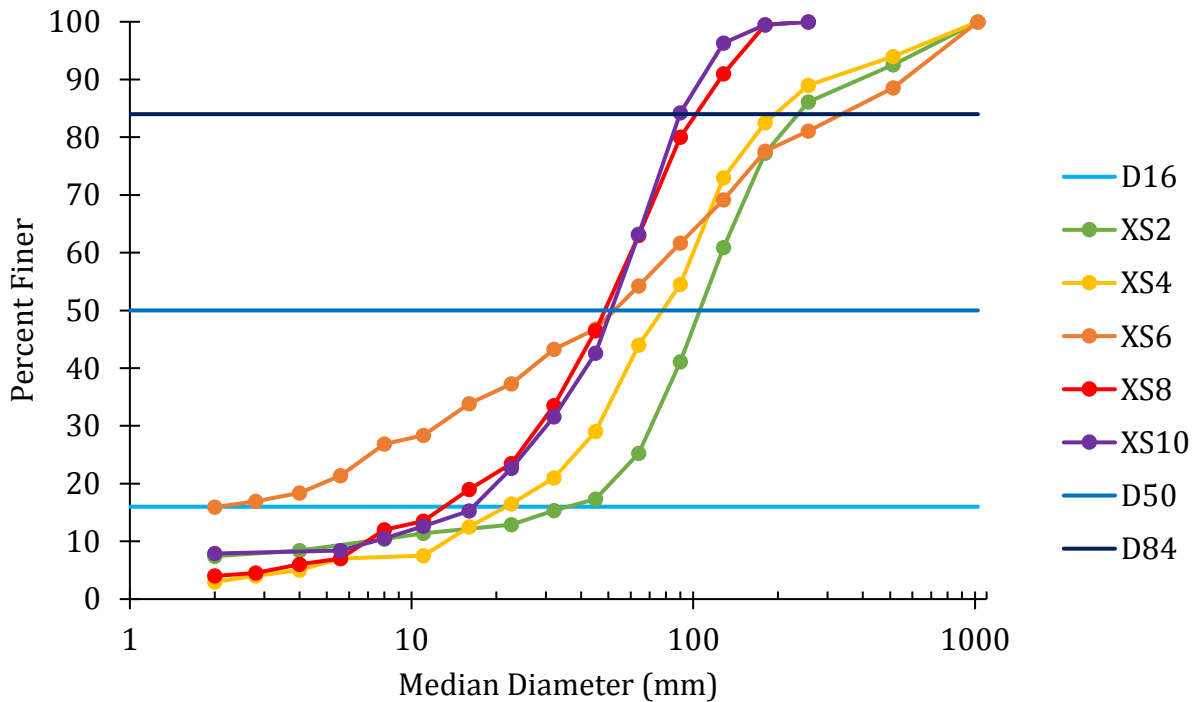


**Figure 5:** Pebble counts of 200 particles at each of five, evenly spaced cross sections. Cross sections are numbered from downstream to upstream. XS6 is just downstream of the break in channel type (Figure A1). Also indicated are the D16, D50, and D84 or the median diameter below which 16, 50, and 84% of the bed material is finer, respectively.

## 4.3 Large Wood and Sediment

Air photos from July 2013 and September 2016 indicate that the majority of large logs and jams in my study reach are stable. Of the logs identified from aerial imagery, 30 were stable, three appeared to be new, one moved downstream, and the position of ten could not be reliably compared between the two photos. Jams also seemed stable. Twenty-one jams remained in place, two formed, and two could not be tracked through time. During this period, the nearest stream gage, which is on the Bitterroot River near Darby, MT, recorded a maximum mean daily discharge with a recurrence interval between four and five years. Thus, the observed mobility of large wood in my study reach is potentially consistent with typical annual streamflows.

Most large wood within the mixed bedrock-alluvial subreach is suspended on boulders or bedrock and/or parallel to the direction of flow, and therefore not actively

storing sediment. In contrast, there are significant changes in stream gradient, bed material size, and channel morphology associated with two channel-spanning large wood jams in the riffle-pool section of the alluvial subreach. More than half of the total volume of wood and sediment stored in the reach is associated with these jams (Figure 6). The large wood particulate storage index mirrors the trend in Figure 6 and further demonstrates that the geomorphic influence of large wood increases with piece interaction (Figure 7).



**Figure 6:** Proportion of the total volume of wood and associated sediment for pieces, small jams, and channel-spanning jams.

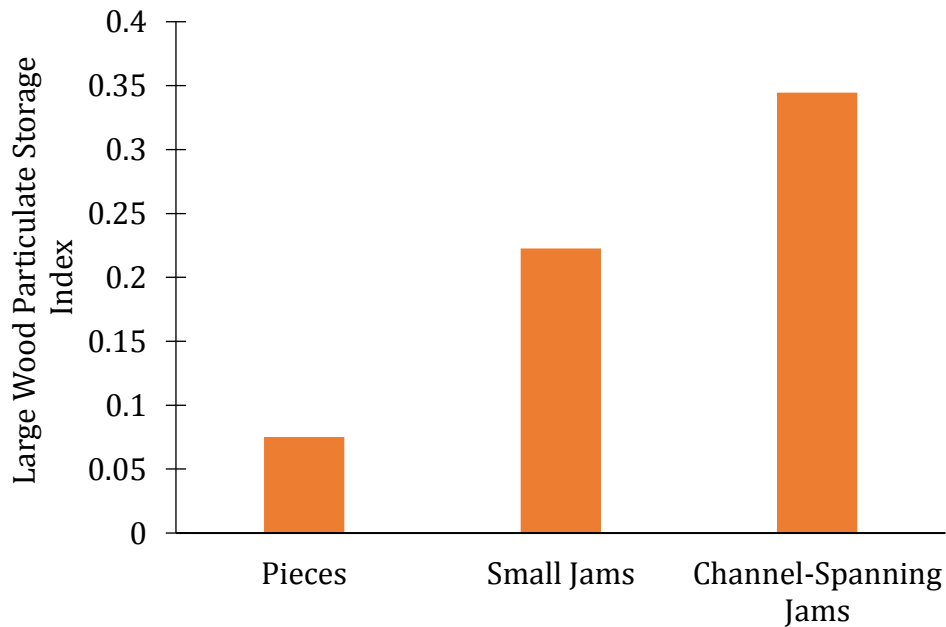


**Figure 7:** Large wood particulate storage index for pieces, small jams, and channel-spanning jams. It represents the volume of sediment stored per m<sup>3</sup> of large wood.

## **5. Summary and Implications**

This project is using field surveys, remote sensing, and modeling to advance understanding of how large wood influences sediment routing in a mixed bedrock-alluvial stream. The inclusion of two distinct channel types facilitates comparison of the geomorphic role of large wood within gravel-bed streams, the site of the majority of research on this topic, and mixed bedrock-alluvial streams, which remain poorly understood. The distribution of large wood was determined by characterizing and measuring all pieces throughout my study reach. Measurements of sediment stored in association with individual pieces and small jams was compared to those of two channel-spanning jams. In this way, their relative importance as a barrier to sediment transport was assessed. The use of painted tracers through a large jam and fallout radionuclide analysis of fine sediment within a channel-spanning jam will enable me to estimate the length of time for which sediment is stored by wood. Hydraulic and sediment transport modeling will illustrate temporal and spatial variations in transport capacity and will generate an estimate of annual sediment export. Field observations can be compared to a stochastic model of wood and sediment storage.

This research has potential implications for forested mountain watersheds at a range of scales. By documenting the distribution of wood and its impact on sediment storage within a mixed bedrock-alluvial stream, it can provide insights on fish habitat. This project may also help us understand a key control – wood load – on the degree of sediment transfer to higher-order streams. It may enhance our understanding of stream sensitivity to climate and land use changes as the efficacy of fluvial sediment routing influences a stream's sensitivity to disturbance and its anticipated response time (Hoffmann, 2015). Lastly, it informs our knowledge of landscape evolution in that streams set the base level for hillslope erosion and control regional denudation.

## **6. Acknowledgments**

I would like to thank the University of Montana's Department of Geosciences, the National Science Foundation, the Montana Institute on Ecosystems, the Montana Water Center, and the Geological Society of America for funding this research. I would also like to thank my advisor, Dr. Andrew Wilcox, other committee members, Dr. Rebecca Bendick and Dr. Bob Hall, and Dr. Jean Dixon for their guidance, enthusiasm, and patience, and the members of the Wilcox lab group, including undergraduate student Haylie Brown, for assisting me with many long days of fieldwork.

## **7. References**

- Alden, W. C. 1953. *Physiography and Glacial Geology of Western Montana and Adjacent Areas*. United States Geological Survey. Vol. 231. Washington: United States Government Printing Office.
- Benda, L. and T. Dunne. 1997. "Stochastic Forcing of Sediment Routing and Storage in Channel Networks." *Water Resources Research* 33 (12): 2865-2880.

- Bisson, P. A., R. E. Bilby, M. D. Bryant, C. A. Dolloff, G. B. Grette, R. A. House, M. L. Murphy, and V. K. Koski. 1987. "Large Woody Debris in Forested Streams in the Pacific Northwest: Past, Present, and Future." In *Streamside Management: Forestry and Fisheries Interactions*, 144-190. University of Washington, Seattle: Institute of Forest Resources.
- Blake, W. H., D. E. Walling, and Q. He. 2002. "Using Cosmogenic Beryllium-7 as a Tracer in Sediment Budget Investigations." *Geografiska Annaler, Series A: Physical Geography* 84 (2): 89-102. doi:10.1111/j.0435-3676.2002.00163.x.
- Bonniwell, E. C., G. Matisoff, and P. J. Whiting. 1999. "Determining the Times and Distances of Particle Transit in a Mountain Stream using Fallout Radionuclides." *Geomorphology* 27 (1): 75-92. doi:10.1016/S0169-555X(98)00091-9.
- Brunelle, A., C. Whitlock, P. Bartlein, and K. Kipfmüller. 2005. "Holocene Fire and Vegetation Along Environmental Gradients in the Northern Rocky Mountains." *Quaternary Science Reviews* 24 (20): 2281-2300. doi:10.1016/j.quascirev.2004.11.010.
- Burbank, D. W. and R. S. Anderson. 2012. *Tectonic Geomorphology*. 2. ed. Chichester: Wiley.
- Eaton, B. C., M. A. Hassan, and S. L. Davidson. 2012. "Modeling Wood Dynamics, Jam Formation, and Sediment Storage in a Gravel-Bed Stream." *Journal of Geophysical Research. Earth Surface* 117: 1-18.
- Wohl, E., R. O. Hall, K. B. Lininger, N. A. Sutfin, and D. M. Walters. 2017. "Carbon dynamics of river corridors and the effects of human alterations." *Ecological Monographs*, 87(3): 379-409. doi: 10.1002/ecm.1261.
- Elosegi, A., J. R. Diez, L. Flores, and J. Molinero. 2017. "Pools, Channel Form, and Sediment Storage in Wood-Restored Streams: Potential Effects on Downstream Reservoirs." *Geomorphology* 279: 165-175.
- Fisher, G. B., F. J. Magilligan, J. M. Kaste, and K. H. Nislow. 2010. "Constraining the Timescales of Sediment Sequestration Associated with Large Woody Debris using Cosmogenic <sup>7</sup>Be." *Journal of Geophysical Research. Earth Surface* 115 (1): 1-19. doi:10.1029/2009JF001352.
- Foster, D., S. H. Brocklehurst, and R. L. Gawthorpe. 2008. "Small Valley Glaciers and the Effectiveness of the Glacial Buzzsaw in the Northern Basin and Range, USA." *Geomorphology* 102: 624-639.
- Fryirs, K. 2013. "(Dis)Connectivity in Catchment Sediment Cascades: A Fresh Look at the Sediment Delivery Problem." *Earth Surface Processes and Landforms* 38 (1): 30-46. doi:10.1002/esp.3242.
- Goode, J. R., C. H. Luce, and J. M. Buffington. 2012. "Enhanced Sediment Delivery in a Changing Climate in Semi-Arid Mountain Basins: Implications for Water Resource Management and Aquatic Habitat in the Northern Rocky Mountains." *Geomorphology* 139-140: 1-15.

- Gurnell, A. M., H. Piegay, F. J. Swanson, and S. V. Gregory. 2002. "Large Wood and Fluvial Processes." *Freshwater Biology* 47 (4): 601-619. doi:10.1046/j.1365-2427.2002.00916.x.
- Hoffmann, T. 2015. "Sediment Residence Time and Connectivity in Non-Equilibrium and Transient Geomorphic Systems." *Earth-Science Review* 150: 609-627.
- Imhoff, K. S. and A. C. Wilcox. 2016. "Coarse Bedload Routing and Dispersion through Tributary Confluences." *Earth Surface Dynamics* 4: 591-605.
- Lane, S. N., S. C. Reid, V. Tayefi, D. Yu, and R. J. Hardy. 2008. "Reconceptualising Coarse Sediment Delivery Problems in Rivers as Catchment-Scale and Diffuse." *Geomorphology* 98 (3): 227-249. doi:10.1016/j.geomorph.2006.12.028.
- Lisle, T. E. and S. Hilton. 1992. "The Volume of Fine Sediment in Pools: An Index of Sediment Supply in Gravel-Bed Streams." *Journal of the American Water Resources Association* 28 (2): 371-383. doi:10.1111/j.1752-1688.1992.tb04003.x.
- Livers, B., K. Lininger, N. Kramer, and E. Wohl. 2015. "Porosity Problems." Poster Session 3. Third international conference of wood in world rivers: Padova, Italy, July 8, 2015.
- Lonn, J. and R. B. Berg., 1996. *Preliminary Geology Map of the Hamilton 30' X 60' Quadrangle*. Butte, MT: Montana Bureau of Mines and Geology, Open File No. 340.
- May, C. L. and R. E. Gresswell. 2003. "Processes and Rates of Sediment and Wood Accumulation in Headwater Streams of the Oregon Coast Range, USA." *Earth Surface Processes and Landforms* 28 (4): 409-424. doi:10.1002/esp.450.
- Megahan, W. 1982. "Channel Sediment Storage Behind Obstructions in Forested Drainage Basins Draining the Granitic Bedrock of the Idaho Batholith." In *Sediment Budgets and Routing in Forested Drainage Basins*, edited by F. J. Swanson, R. J. Janda, T. Dunne, and D. N. Swanston, 114-121. USDA Forest Service General Technical Report PNW-141. Portland, OR: USDA Forest Service.
- Montgomery, D. R. and J. M. Buffington. 1997. "Channel-Reach Morphology in Mountain Drainage Basins." *GSA Bulletin* 109 (5): 596-611. doi:CRMIMD>2.3.CO;2.
- Montgomery, D. R., J. M. Buffington, R. D. Smith, K. M. Schmidt, and G. Pess. 1995. "Pool Spacing in Forest Channels." *Water Resources Research* 31 (4): 1097-1105.
- NCALM. 2016. Northern Rockies, Montana lidar 2016. OpenTopography. <http://opentopo.sdsc.edu/datasetMetadata?otCollectionID=OT.062017.26911.1>
- Pardee, J. T. 1910. "The Glacial Lake Missoula." *Journal of Geology* 18: 376-386.
- Pfeiffer, A. and E. Wohl. 2018. "Where does Wood most Effectively Enhance Storage? Network-Scale Distribution of Sediment and Organic Matter Stored by Instream Wood." *Geophysical Research Letters* 45 (1): 194-200. doi:10.1002/2017GL076057.
- Phillips, J. D. and J. D. Lutz. 2008. "Profile Convexities in Bedrock and Alluvial Streams." *Geomorphology* 102 (3): 554-566. doi:10.1016/j.geomorph.2008.05.042.

- PRISM Climate Group. 2018. 30-Year Normal Precipitation, 1981-2010. Oregon State University: Oregon State University.
- Salant, N. L., C. E. Renshaw, F. J. Magilligan, J. M. Kaste, K. H. Nislow, and A. M. Heimsath. 2007. "The use of Short-lived Radionuclides to Quantify Transitional Bed Material Transport in a Regulated River." *Earth Surface Processes and Landforms* 32 (4): 509-524. doi:10.1002/esp.1414.
- StreamStats. 2017. StreamStats Version 3.0. U.S. Dept. of the Interior, U.S. Geological Survey. <http://water.usgs.gov/osw/streamstats/>
- Walling, D. E. 1983. "The Sediment Delivery Problem." *Journal of Hydrology*: 209-237.
- Wheaton, J. M., K. A. Fryirs, G. Brierly, S. G. Bangen, N. Bouwes, and G. O'Brien. 2015. "Geomorphic Mapping and Taxonomy of Fluvial Landforms." *Geomorphology* 248: 273-295.
- Wohl, E. 2017. "Connectivity in Rivers." *Progress in Physical Geography* 41 (3): 345-362. doi:10.1177/0309133317714972.
- Wohl, E., R. O. Hall, K. B. Lininger, N. A. Sutfin, and D. M. Walters. 2017. "Carbon Dynamics of River Corridors and the Effects of Human Alterations." *Ecological Monographs* 87 (3): 379-409. doi:10.1002/ecm.1261.
- Wohl, E. and K. Jaeger. 2009. "A Conceptual Model for the Longitudinal Distribution of Wood in Mountain Streams." *Earth Surface Processes and Landforms* 34 (3): 329-344. doi:10.1002/esp.1722.
- Wohl, E. and D. N. Scott. 2016. "Wood and Sediment Storage and Dynamics in River Corridors." *Earth Surface Processes and Landforms*: 1-19. doi:10.1002/esp.390

## **8. Appendix**

### **A1. Fallout Radionuclide Analysis**

Fallout radionuclide analysis is a tractable method of estimating sediment residence time. Fallout radionuclides are unstable elements that are delivered from the atmosphere to earth's surface through wet and dry fallout (Bonniwell et al., 1999). Because they bind strongly to soil particles, water in streams and lakes are assumed to have negligible radionuclide concentrations (Bonniwell et al., 1999; Fisher et al., 2012). Thus, when a soil particle becomes submerged, its activity level, which correlates with radionuclide abundance, declines exponentially (Fisher et al., 2012). When its initial activity level is well constrained, the age of fine sediment in streams can be estimated from its current activity level (Fisher et al., 2012). While fallout radionuclide analysis has mainly been applied to suspended sediment (Bonniwell et al., 1999), several studies have used it to evaluate transitional bedload transport (Blake et al., 2002; Salant et al., 2007; Fisher et al., 2010).

All test samples collected in fall 2017 had detectable levels of the longer-lived radionuclides  $^{210}\text{Pb}$  and  $^{137}\text{Cs}$ , and four of five had a detectable level of  $^7\text{Be}$  (Figure A1). Because samples were depth-integrated, I cannot say whether the observed concentrations

reflect uniform sediment age or a mixture of sediment deposited over multiple events. Sample analysis and interpretation is being performed in collaboration with Dr. Jean Dixon at Montana State University.

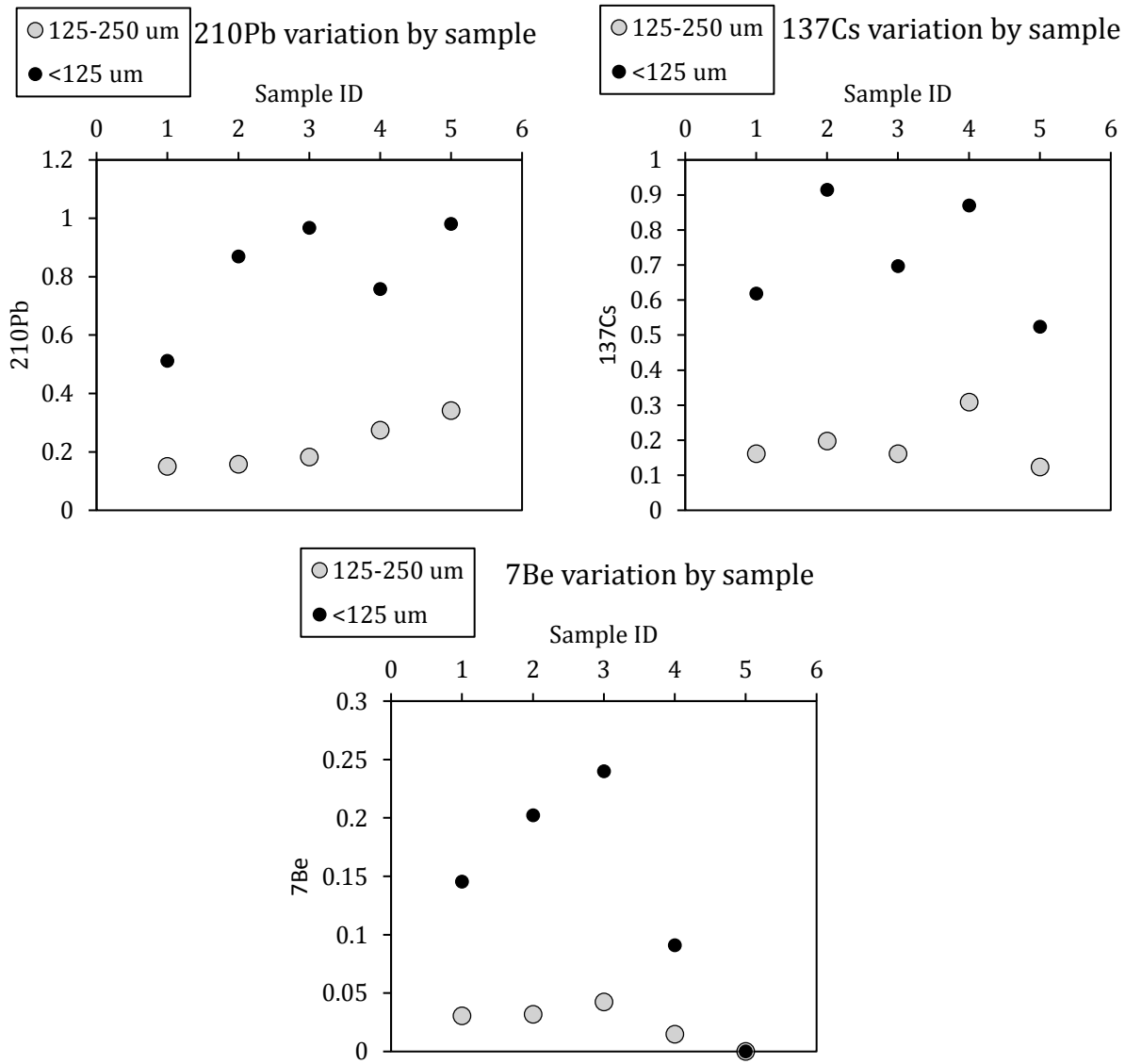


**Figure A1:** Decays per second, which strongly correlates with activity level, of three fallout radionuclides by sample location and size class. Samples 1 and 2 were collected within a channel-spanning jam, Sample 3 was collected from an emergent bar 15 m upstream, and Samples 4 and 5 came from submerged bars 70 m and 130 m upstream, respectively. Note that activity level roughly scales with particle size.

## Information Transfer Program Introduction

Supporting students to become water science professionals is a core mission of the Montana Water Center. The Center continued to work closely with faculty researchers to engage students in water-related research including producing reports and publishing papers. Faculty researchers who received research funding from the Water Center are required to actively mentor students in the research projects.

The Center encouraged students from a wide array of disciplines that are water related to apply for student fellowships. The Water Center also encouraged students engaged in water resource studies to present at regional and national conferences. The presentations, posters and publications of faculty and students listed in their reports attest to the support given to students to both take on research and also present it at local and national meetings as well as follow through to publication in scientific journals.

In addition to working with faculty and students, Water Center programs reached thousands of others interested in water issues in Montana, including water resource professionals, teachers, farmers, ranchers, engineers, drinking water and wastewater system operators.

Specific information transfer activities include the following:

\*The MTWC completed research and writing on the Water Chapter of the Montana Climate Assessment in the fall of 2017. MTWC presented findings at a number of meetings and to a variety of stakeholders in 2017.

- In April 2017, Assistant Director, Whitney Lonsdale, presented to faculty and students at the Rough Cut Series, put on by the Institute on Ecosystems at Montana State University.

- In May 2017, Assistant Director, Whitney Lonsdale, presented at a meeting between Israeli water experts and water professionals in Montana. The meeting was convened by Montana's Lt Governor and aimed to share lessons learned in dealing with water scarcity and climate change.

- In the fall of 2017, Water Chapter findings were shared across Montana in a series of Montana Climate Assessment outreach events. Interim Director, Whitney Lonsdale, presented at three separate events, held in Miles City, Glasgow and Havre, Montana. The two other events were held in Kalispell and Hamilton, MT. Events attracted local agricultural producers, irrigation managers, state and federal agency employees, extension agents, municipal planners, university faculty, and other citizens concerned about the future of Montana's water.

\*In the summer of 2017, MTWC, in conjunction with the MT Department of Natural Resources, the MT Department of Environmental Quality, the MT Bureau of Mines and Geology, and non-profit One Montana, began the planning of the first Montana Water Summit, to be held in March 2018. Planning continued throughout the fall of 2017, with the goal of bringing together academics, water managers, water planners and water users from around the state to discuss the past policy and future challenges around maintaining a sustainable water supply in Montana, focusing on challenges presented by population growth, industry and climate change.

\*Sponsored the 84th Annual School for Water & Wastewater Operators & Managers held in October 2017 at Montana State University. This training was attended by staff members of water and wastewater utilities with the purpose of preparing new system operators to pass the certification exam, and familiarize participants with other resources they may find helpful in the future. Assistant Director Lonsdale gave a welcome address and moderated discussions during the training.

## Information Transfer Program Introduction

\* Grant funded water education programs were delivered by MTWC that focused on the following areas: Project WET curriculum training for primary, secondary and community educators, and a lake ecology graduate course.

\*Helped organize and execute a state water meeting with the Montana Section of the American Water Resources Association in Helena, MT on October 18-20, 2017. The conference theme was “Science, Policy & Communication: The role of science in a changing world.” Approximately 220 people attended the conference. Oral and poster presentations highlighted much of the current water research being conducted throughout Montana by university, federal, state, county and non-profit researchers and resource managers. Associate Director Wilcox gave a welcome address.

\* Responded to information requests on water topics ranging from water rights to water quality to effects of climate change on water supply.

\*Faculty and students supported by 104b funds presented their research at conferences throughout Montana, the U.S., and in Europe. Many of these posters and presentations earned awards and recognition of excellence. Faculty and students also shared research findings at meetings with state and local government, technology fairs, and in university classes and symposiums. In addition, faculty and students disseminated research results through community focus groups and through the creation of websites and newsletters.

# USGS Summer Intern Program

None.

# **Notable Awards and Achievements**

## Publications from Prior Years

1. 2012MT264B ("Thresholds in fluvial systems: Flood-induced channel change on Montana rivers") - Articles in Refereed Scientific Journals - Wilcox, A. C., O'Connor, J. E., & Major, J. J. (2014). Rapid reservoir erosion, hyperconcentrated flow, and downstream deposition triggered by breaching of 38 m tall Condit Dam, White Salmon River, Washington. *Journal of Geophysical Research: Earth Surface*, 119(6), 1376-1394.
2. 2012MT263B ("Assessing Hydrologic, Hyporheic, and Surface Water Temperature Responses to Stream Restoration") - Articles in Refereed Scientific Journals - McCluney, K. E., Poff, N. L., Palmer, M. A., Thorp, J. H., Poole, G. C., Williams, B. S., ... & Baron, J. S. (2014). Riverine macrosystems ecology: sensitivity, resistance, and resilience of whole river basins with human alterations. *Frontiers in Ecology and the Environment*, 12(1), 48-58.
3. 2012MT275B ("Student Research Fellowship: COLUMBIA RIVER TREATY RENEGOTIATION PROCESS: COLLABORATIVE IN WORD OR DEED?") - Articles in Refereed Scientific Journals - Shively, D., & Thompson, A. (2016). Stakeholder collaboration in the Columbia river treaty review process. *International Journal of Water Resources Development*, 32(1), 57-76.
4. 2013MT280B ("Student Fellowship: Rephotography as a tool to Understand the Effects of Resource Use on Rivers of the Greater Yellowstone Region") - Book Chapters - Patten, D. T. (2018). *The Gallatin Way to Yellowstone*. Arcadia Publishing.
5. 2014MT284B ("Improving accessibility to satellite soil moisture measurements: Linking SMOS data retrievals to ground measurements in Montana") - Articles in Refereed Scientific Journals - Gerken, T., Bromley, G. T., & Stoy, P. C. (2018). Surface moistening trends in the northern North American Great Plains increase the likelihood of convective initiation. *Journal of Hydrometeorology*, 19(1), 227-244.
6. 2014MT289B ("Student Fellowship: Estimating Evapotranspiration at the Regional Scale: An Energy Balance Approach") - Dissertations - Johnson, A. V. (2015). *Scaling and uncertainty in landsat remote sensing of biophysical attributes*, MS Thesis, Dept of Land Resources and Environmental Science, Montana State University, Bozeman, Montana, 70 pp.
7. 2015MT294B ("Designing scenarios for hydrologic resilience in the Upper Missouri Headwaters with integrated ecosystem models") - Conference Proceedings - Hoy, J., Poulter, B., Emmett, K., Cross, M., Al-Chokhachy, R., & Maneta, M. (2016, April). From terrestrial to aquatic fluxes: Integrating stream dynamics within a dynamic global vegetation modeling framework. In *EGU General Assembly Conference Abstracts (Vol. 18, p. 5073)*.
8. 2015MT294B ("Designing scenarios for hydrologic resilience in the Upper Missouri Headwaters with integrated ecosystem models") - Conference Proceedings - Poulter, B., Joetzjer, E., Renwick, K., Ogunkoya, G., & Emmett, K. (2015, December). Addressing spatial scales and new mechanisms in climate impact ecosystem modeling. In *AGU Fall Meeting Abstracts*.
9. 2015MT295B ("Student Fellowship: Climatic and geomorphologic influences on soil development and transport in the Bitterroot and Sapphire Mountains, Montana, USA") - Dissertations - Benjaram, S. S. (2017). *Morphologic and climatic controls on soil evolution in the Bitterroot and Sapphire Mountains, Montana*, MS Thesis, College of Letters & Sciences, Montana State University-Bozeman, Montana, 150pp.
10. 2015MT295B ("Student Fellowship: Climatic and geomorphologic influences on soil development and transport in the Bitterroot and Sapphire Mountains, Montana, USA") - Conference Proceedings - Dixon, J., & Benjaram, S. (2017, April). Thresholds for soil cover and weathering in mountainous landscapes. In *EGU General Assembly Conference Abstracts (Vol. 19, p. 10212)*.
11. 2016MT305B ("Student Fellowship: Riparian Ecosystem Succession Following Fire Disturbance on the North Fork Flathead River, Montana") - Dissertations - Powers, R., *Assessing riparian ecosystem condition and monitoring recovery from natural and anthropogenic disturbance*, MS Thesis, Department of Systems Ecology, University of Montana, Missoula, Montana, 147pp.